Convective Heat Transfer from a Rotating Disc in a Transverse Air Stream

by

Anthony Patrick Campbell De Vere

A thesis submitted to the University of Leicester
for the degree of Doctor of Philosophy

June 1975

Abstract

The variation in the local radial heat transfer coefficient is reported for a disc rotating in still air up to 1650 r.p.m. and in a transverse or crossflow air stream of speeds up to 33 m/s. These measurements have been made with the aid of a small sensor, using thermistors as heating elements. It is found that the heat transfer coefficient is governed by the main air flow, the rotation of the disc resulting in a small upward perturbation on this level. Tests with different disc aspect ratios, simulated by the disc protruding from a leading edge shroud, show that the radial distribution is greatly modified, but again the main air stream dominates the process.

A thin film sensor has been developed to monitor the fluctuations in the heat transfer coefficient about the mean level as the disc rotates in the air stream. The local effects of rotation are examined closely. The velocity distributions around the stationary and rotating disc in still air and a transverse flow are presented.

The experimentation is finally extended to the case of a simple train wheel shape, thus attempting to model the convective heat dissipation for the condition of train wheel braking.

Contents

Nomenclature

Symbol	Quantity	Units
A	$A'Y/mC_p\omega$	
A	Arbitrary area.	m^2
A'	Mean level of heat transfer variation h(t).	$W/m^2 deg.C$
$A_{A,B,C}$	Areas in heat flux sensor.	m^2
A_f	Platinum film area.	m^2
A_s	Arbitrary sensing area.	m^2
B	$B'Y/mC_p$	
B'	Amplitude of heat transfer fluctuation.	$W/m^2 deg.C$
C	Constant of integration.	
C_p	Specific heat.	J/kg deg.C
d	Diameter of emitting surface.	m
$\dot{E}$	Ohmic heating rate of Platinum film.	W/m^2
$E(tN)$	Oscilloscope bridge voltage at t = N.	Volts
F	Radial velocity function, where $v_r = r\omega F(\eta)$	
G	Tangential velocity function, $v_\phi = r\omega G(\eta)$	
H	Axial velocity function, $v_z = \sqrt{\nu\omega} H(\eta)$	
h_c	Local heat transfer coefficient.	$W/m^2 deg.C$
$\bar{h}_c$	Average heat transfer coefficient.	$W/m^2 deg.C$
h_R	Local radial heat transfer coefficient.	$W/m^2 deg.C$
h_p	Point heat transfer coefficient.	$W/m^2 deg.C$
$h(t)$	Arbitrary heat transfer coefficient, $A' + B'\sin\omega t$.	$W/m^2 deg.C$
$h_c(t_N)$	Local heat transfer coefficient at time t = N.	$W/m^2 deg.C$
$h_c'(t_N)$	Fluctuating heat transfer coefficient about the mean level.	$W/m^2 deg.C$

I	Current.	amps
I_o	Bridge current.	amps
$I_o I_1$	Bessel functions.	
κ	Thermal conductivity.	W/m deg.C
K	$q/mC_p\omega$	
$K_o K_1$	Bessel functions.	
L	Length of flat plate.	m
ℓ	Length of substrate.	m
ℓ_c	Sensor dimension.	m
m	Mass of copper disc.	kg
n	Integer.	
N	Rotational speed.	r.p.m./rad/s.
Nu	Local Nusselt number $h_R R/k$	
$\overline{Nu}$	Mean Nusselt number $\frac{\bar{h}_c R_o}{\kappa}$	
P_T	Number of steps in periodic time T.	
P	Pressure function $p = -\rho\nu\omega\, P_F(\eta)$.	
P	Laplace transforms.	
Pr	Prandtl number $\mu C_p/k$	
p	$h_c/k_c t_A$.	
q_c	Convective heat transfer.	W
q	Heat supply to copper disc.	W
$\dot{q}_c$	Unit convective heat transfer.	W/m^2
$\dot{q}_c(t)$	Time dependent unit convective heat transfer.	W/m^2
Q_c	Total convective heat transfer.	W
Q_R	Radiation transfer.	W

R	Radius.	m
R_o	Disc radius.	m
R_T	Copper disc tip radius.	m
R_T'	Disc tip approximation = $\sqrt{R_T(R_T + t_A)}$	m
R_1 ..... R_{12}	Sensor thermal resistances.	deg.C/W
R_s	Radius at flow instability.	m
R_T	Radius at transition.	m
R_f	Platinum film resistance.	ohms
ΔR_f	Change in film resistance.	ohms
$R_{1,2,3}$	Bridge resistances.	ohms
Re	Rotational Reynolds number NR^2/ν .	
Re_o	Main stream Reynolds number UR_o/ν .	
$T_{1,2,3,4}$	Heat flux sensor temperatures.	^oC
T_s	Sensing temperature.	^oC
T_∞	Ambient temperature.	^oC
T_w	Disc surface temperature.	^oC
T_f	Film temperature	^oC
ΔT	Temperature difference.	deg.C
$T\upsilon$	Turbulence intensity	
T	Periodic time.	secs
τ	Variable of integration.	
t	Shroud setting.	m
t/R_o	Aspect ratio.	
t	Time.	secs
t	Thickness.	
$\Delta t'$	Time interval.	secs
Δt_1	Time interval over which semi-infinite equation may be applied to finite substrate.	secs

U	Main stream velocity.	m/s
u_1	Velocities as measured by hot wire.	m/s
u_2	Velocities as measured by hot wire.	m/s
V	Voltage.	Volts
ΔV	Out of balance bridge voltage.	Volts
v_r	Radial velocity component.	m/s
v_ϕ	Tangential velocity component.	m/s
v_z	Axial velocity component.	m/s
v_T	Total tangential velocity.	m/s
V_B	Anemometer bridge voltage.	Volts
V_o	Anemometer bridge voltage in still air.	Volts.
z	ωt (in Appendix A2).	
x	Distance from leading edge of flat plate.	m
Y	Face area of copper disc.	m^2
r,z,ϕ	Cylindrical polar coordinates.	m,m,deg.
α	Angle of resultant velocity.	deg.
α	Thermal diffusivity of substrate = $k/\rho C_p$.	
α_R	Film resistance temperature coefficient.	K^{-1}
β	Velocity ratio u_2/u_1.	
ε	Emissivity.	
η	Dimensionless distance $z\sqrt{\frac{\omega}{\nu}}$	
θ	Temperature above ambient.	deg.C
μ	Viscosity.	kg/m s
ν	Kinematic viscosity.	m^2/s
ρ	Density.	kg/m^3
σ	Stefan-Boltzmann constant.	$J/m^2 s(deg.K)^4$
ϕ	Angular position.	deg.
η	Hottel factor.	
τ	Variable of integration	

ω	Rotation.	rpm
δ	Boundary layer thickness.	m
z'	Axial distance from front face of disc.	m
θ	Angle.	degs.

<u>Suffices</u>

s	Substrate.
w	wall.
A,B,C	Sensor components.

Chapter 1

1.1. Introduction

This work arose from an interest in the temperature distribution and consequent stress distribution in train wheels resulting from a continued braking condition.

In its conventional form braking is achieved with a series of pads rubbing on the periphery of the wheel. A large percentage of the heat generated by the friction is imparted through to the wheel with the subsequent rise in temperature throughout its volume. Over a continued period of braking these temperatures rise by several hundreds of degrees. Serious stresses can occur and there is the danger of the wheel seriously distorting and cracks forming.

The temperature distribution is governed by three factors. Firstly by the heat imparted to the rim of the wheel, determined by the size, shape and material used for braking and the braking load. Secondly by the heat conduction through the wheel which will depend upon the geometry and thermal properties of the wheel, and thirdly the heat dissipated away from the surface via convection and radiation.

It is the convective cooling process which is the subject of this thesis. The geometry under investigation, a plane rotating disc in a free jet, is idealized from the train situation. There the wheel shape is not a plane disc and the surrounding suspension gear, the track and the ground cause considerable shrouding around the wheel. Nevertheless the present idealized geometry is an obvious starting off point from which to build experience in this field. The surface temperature is isothermal and heated internally rather than at the rim.

Measurements of heat transfer coefficients from a rotating disc in still air and in an air stream normal to the disc surface have been reported[1,2]. In the case of a rotating disc in an air stream parallel to the disc surface (herein referrred to as transverse flow), the only relevant work that has been done is by Dennis, Newstead and Ede[(21)]. While the size of their apparatus and range of rotational and free stream Reynolds numbers are comparable with the present work, their measurements only involved average heat transfer coefficients over the whole disc. In the problem of calculating the temperature distribution in train wheels,where there are considerable changes in the radial thickness of the wheel, the radial variation of the heat transfer coefficient at the surface is required. This work only become known after the experimentation was completed.

For a disc rotating in still air, the tangential friction drag at the surface imparts a circumferential velocity to the air and, due to the centrifugal forces, an outward radial flow occurs. At high disc speed there is a transition in the resultant spiral flow from laminar to turbulent. For the laminar case analytic solutions have been produced, and with suitable assumptions, predictions have been made for the fully turbulent case. Comprehensive surveys of both experimental and analytical work in this field have been published by Dorfman[1] and Kreith[2] and Refs 22-29.

In the case of a rotating disc in a transverse air flow, the flow pattern is of a complex three dimensional nature giving little hope of an analytical solution at present. Thus the emphasis in this work is experimental.

The thesis reports measurements of heat transfer from a heated isothermal disc rotating in a transverse air flow. To enable local heat transfer coefficients to be measured a small heat flux sensor has been used in which a thermistor provides a localized energy source. The thermal mass of the sensor does not allow transient measurements to be made, average values over the circular paths traversed are obtained.

For a disc rotating in a transverse air flow measurements have been taken over a range of air jet speeds. Air speeds both below and above the disc peripheral speed have been investigated and particular attention paid to the condition where air speed and disc peripheral speed are matched.

In reaching an understanding of the measurements further tests on the disc stationary in the transverse air stream together with flow visualization using smoke have been useful. All the results suggest that the heat transfer process is dominated by the main air flow, the secondary flow caused by the disc rotation having a minor effect. In particular flow separation at the leading edge followed by reattachment to the disc face is important. The extent of the separations and reattachment zones are determined by the aspect ratio of the disc (disc radius/disc thickness). So further measurements have been made for a range of disc aspect ratios. These have been simulated using the simple disc by rotating it within a shroud. By allowing the disc to protrude from the shroud into the transverse air stream any desired aspect ratio is set up. For very large aspect ratios (very little separation) and a range of matched speeds the results have been correlated by a general expression. The process is shown to compare closely with the theoretical prediction for the heat transfer from turbulent flow over a flat stationary plate.

A thin film fast response sensor has been used to measure the instantaneous heat transfer coefficient as the disc rotates in the air stream. For large aspect ratios the heat transfer variation is as anticipated, being significantly greater when the flow is against the rotation than when it is in the same direction. The results are examined qualitatively and the effect of rotation is tentatively assessed by comparison with the stationary tests in air with the previous sensor. For large aspect ratios the dominance of the separation and reattachment on the local coefficient is examined.

The velocity profiles at positions close to the disc surface have been measured with the aid of a hot wire anemometer, for a wide range of air speeds with the disc rotating and stationary. For a stationary disc the effect of the aspect ratio on the velocity profiles has been examined and the results have confirmed the effectiveness of the leading edge shroud. With the disc rotating, measurements of the flow pattern are complicated by the reversal of flow close to the surface. However, for a particular rotational speed over a wide range of air speeds, the results have confirmed the main stream dominance and give a good indication of the flow pattern.

At the request of the British Railway Board, Research and Development Division, a study of the heat transfer coefficient variation from a simple train wheel shape has been undertaken. The wheel is the plain disc with an annular ring attached at the periphery to represent the thickening at the flange and a central boss to represent the hub of the wheel. The effect of the rotation is again assessed and comparisons made with the previous work on plain discs. Flow visualization tests have helped to explain the nature of the coefficient variations and also give a qualitative idea of the flow distribution over the wheel.

1.2. Heat Transfer Coefficients

The numerical value of the heat transfer coefficient at a point in a system depends on the geometry of the surface and the velocity of the fluid, as well as on the physical properties of that fluid and often even the temperature difference, ΔT. As these quantities are rarely constant over a surface, the heat transfer coefficient varies from point to point.

So it is necessary to distinguish between a point, a local and an average heat transfer coefficient. The heat transfer coefficient at a point, h_P, is defined by

$$dq_c = h_P\, dA(T_s - T_\infty) \tag{1.1}$$

In most experiments involved in heat transfer measurement the sensing area A_s is small but finite. The heat transfer determined by the sensor is given as

$$q_c = \iint_{A_s} h_P\, (T_s - T_\infty)dA \tag{1.2}$$

where a local heat transfer coefficient h_c is defined as

$$q_c = h_c A_s(T_s - T_\infty) \tag{1.3}$$

For a rotating disc it is necessary to define a local radial heat transfer coefficient, h_R, which is a measure of the average heat transfer for the path traversed by the sensor, i.e.

$$h_R = \frac{1}{2\pi} \int_0^{2\pi} h_c d\phi \tag{1.4}$$

The average heat transfer coefficient $\bar{h}_c$ for the whole isothermal disc is defined as

$$Q_c = \bar{h}_c \pi R_o^2\, (T_s - T_\infty) \tag{1.5}$$

and is related to the local and radial coefficients by the expressions

$$Q_c = \int_0^{R_o} h_R(T_s - T_\infty)2\pi R dR = \int_0^{R_o}\int_0^{2\pi} h_c(T_s - T_\infty)R d\phi dR \tag{1.6}$$

For future reference, measurements described in Chapters 2 and 3 refer to the determination of the local radial coefficients, h_R. Chapter 4 deals with measurements of the local heat transfer coefficient, h_c.

1.3. Methods of measuring heat transfer coefficients

The heat transfer from the surface of a rotating disc can be measured using a number of experimental techniques. The relative merits of these techniques are discussed. Four methods are considered

1) Direct localized heat transfer measurement.
2) Thermal boundary layer.
3) Internal temperature distribution.
4) Mass transfer Mercury evaporation.

1.3.1. Direct localized heat transfer measurement

Perhaps the most obvious method of measuring local heat transfer coefficients between a surface and a fluid flowing past, is the measurement of the energy transferred across a small area of the surface located at the point of interest, the surface temperature and the ambient temperature. This readily leads to the concept of a small calorimeter insert into the surface carrying a heater and a temperature measuring device.

Fig.(1.1) shows one design of a calorimeter insert. A small electrically heated disc A is surrounded by a guard ring, C , to ensure that all the measured energy input, q , passes through the disc A and is convected away into the neighbouring air. The insert is mounted in the main rotating disc with its surface flush withthe surrounds.

However it is not sufficient just to introduce a heated insert into an otherwise unheated surface. For flow over a heated flat plate, in addition to the velocity boundary layer, a thermal boundary layer can be defined across which the fluid temperature varies from the surface temperature to the free stream temperature. This thermal boundary layer has zero thickness at the start of the heated portion of the surface. In this layer the heat transfer/unit area $\dot{q}_c$ at the wall is

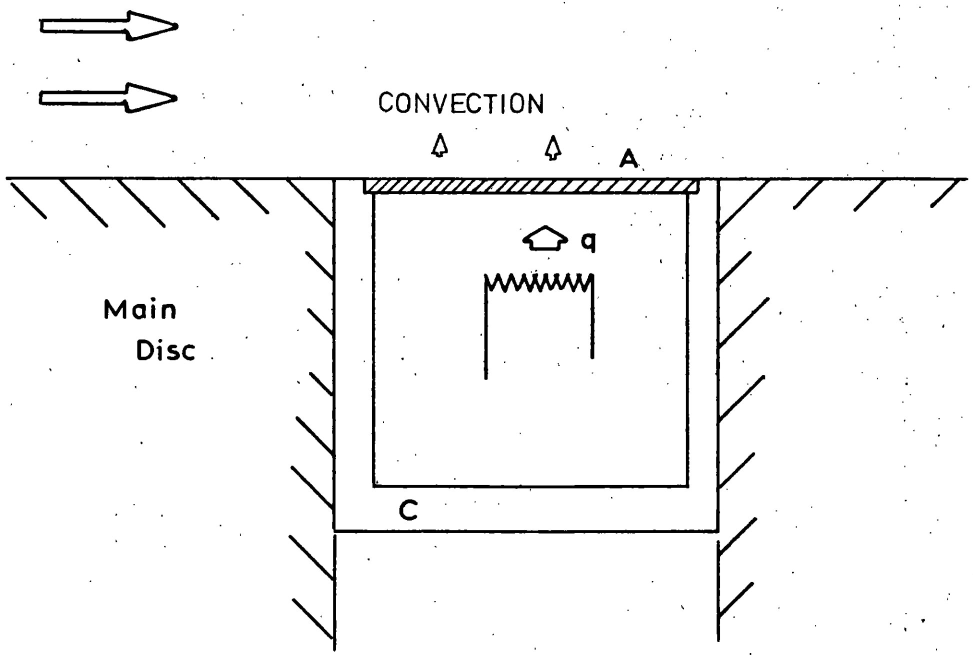

Fig 1·1 Calorimeter Insert

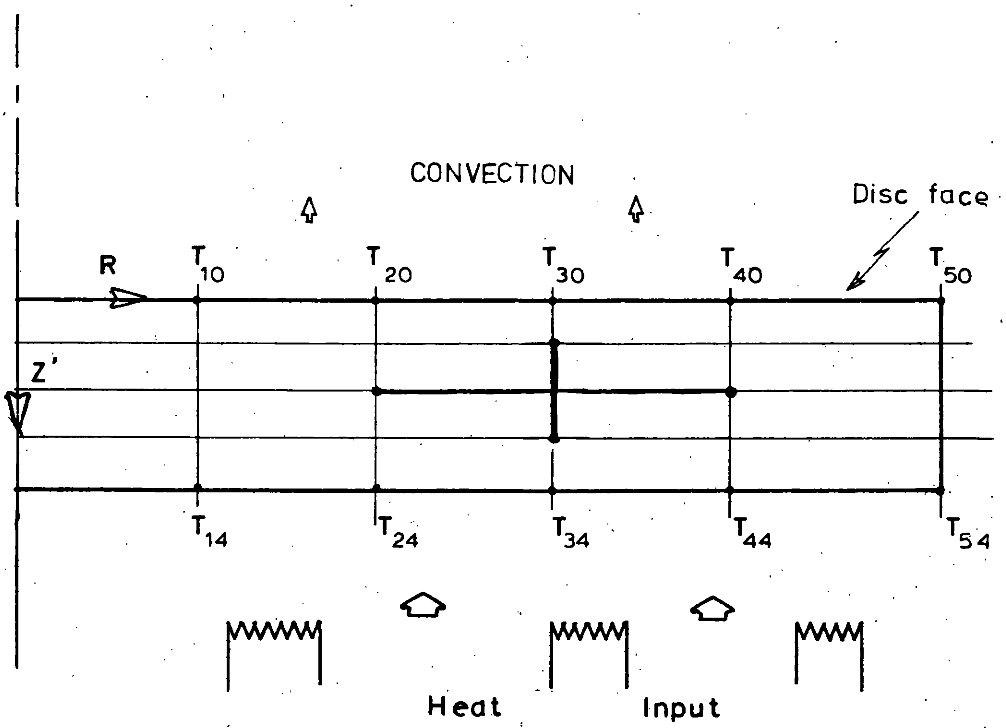

Fig 1·2 Internal Distribution

$$\dot{q}_c = - k\left(\frac{\partial T}{\partial z}\right)_{z=o} \qquad (1.7)$$

where $\left(\frac{\partial T}{\partial z}\right)_{z=o}$ is the value of the temperature gradient at the wall and k the thermal conductivity of the fluid. At the start of the thermal boundary layer the temperature gradient is infinite but rapidly falls off along the heated surface. The heat transfer coefficient defined through the expression

$$\dot{q}_c = h_p(T_s - T_\infty) \qquad (1.8)$$

shows the same variation. Thus a heated insert in an otherwise unheated surface would give a higher heat transfer coefficient than the insert in a surface heated to the same temperature as the insert. In the first case the heat transfer coefficient varies over the insert area falling from infinity at the leading edge. In the second case the heat transfer coefficient is of a lower value and varies only slowly. Thus in setting up an experiment to measure heat transfer coefficients by this manner it is necessary to provide a disc which is heated over its entire surface.

The comparative ease in determining local heat transfer coefficients by such a calorimeter is considered an obvious advantage. Flexibility in positioning, adaption to different situations and the important feature of non-interruption of the velocity and temperature conditions are further advantages.

The disadvantage of this method is that, as power is required to heat the surfaces of the rotating disc and insert and surface temperatures must be monitored, slip rings are needed. This means a complex and expensive rig. Also the method is subject to certain inaccuracies from heat leakage from the insert other than through the surface A into the neighbouring air.

A sensor of this type is relatively massive, so, when the disc is rotating, the sensor will not monitor angular changes in the local heat transfer coefficient. Instead a local radial heat transfer coefficient, h_R, is measured.

1.3.2. Thermal boundary layer measurement

In this method the heat transfer coefficients are determined from direct measurement of the temperature profile in the air stream at any particular location. In any fluid motion a thin layer close to the surface of the wall is postulated where the process of heat transfer is achieved by molecular conduction. Measurements of the temperature at discrete points close to the wall enable the heat transfer from the surface to be determined from

$$\dot{q}_c = -k \left.\frac{dT}{dz}\right|_{z=o} = h_P(T_s - T_\infty) \tag{1.9}$$

This method relies on the accuracy of the measurement of $\left.\frac{dT}{dz}\right|_{z=o}$ and this implies measurement of air temperatures very close to the wall. An estimate of a normal boundary layer thickness suggests that the probe must be positioned within 0.1 mm from the wall. The overall size of the probe is therefore limited. Very thin thermocouple or platinum resistance wires are required.

Apart from these difficulties in positioning and manufacture the flow distribution and hence temperature distribution are affected by the insert of the probe into the boundary layer. Furthermore, heat conduction down the leads of the wires produces considerable errors in the temperatures measured.

Cobb and Saunders[3] overcame some of these problems by stretching a thin Nickel-Constantan thermocouple across a Perspex fork with the junction in the middle. Arranging the wire as nearly as possible along an isothermal with the wire parallel to the surface and across the mean direction of the flow reduced the heat leakage down the leads. In the case of a rotating disc in a transverse air stream, positioning the fork along an isothermal is impossible as the flow direction is unknown and varies from point to point.

The advantage of this method is that heat transfer coefficients, h_p, can be obtained. However for a comprehensive picture of the heat transfer coefficient variation this means the measurement of many temperature profiles. The accuracy of the method does not justify the large amount of work that would be required.

1.3.3. Internal Temperature Distribution

Although termed an internal temperature distribution technique this method requires disc surface temperatures and uses them to predict the internal distribution by Laplace's equation,

$$\frac{\partial^2 T}{\partial R^2} + \frac{1}{R}\frac{\partial T}{\partial R} + \frac{\partial^2 T}{\partial z'^2} \tag{1.10}$$

where z' is the axial distance from the front face of the disc. The surface heat transfer is then obtained by differentiating a polynomial fit of the axial temperature distribution i.e.

$$q_c = -k\left.\frac{dT}{dz'}\right|_{z'=0} = h_c(T_s - T_\infty) \tag{1.11}$$

Owen, Haynes and Bayley[4] measured heat transfer coefficients from a rotating disc in this manner. Fig.(1.2) shows the disc with electric radiant heaters at the back. Thermocouples were embedded in the front and back faces of the disc. The measured surface temperatures T_{10}, T_{20} and T_{14}, T_{24} etc. were then fitted to a cubic spline and the interpolated values used as the boundary conditions in the finite difference solution of equation (1.10).

One disadvantage with a technique of this nature is that a large number of slip-ring channels are needed for monitoring the temperatures.

If local radial values are required over thirty channels must be provided. It is also important that the thermocouples and their respective mountings do not alter the internal temperature distribution within the disc.

1.3.4. Mass Transfer - Mercury evaporation

An alternative to a direct heat transfer measurement is to carry out a mass transfer experiment. Heat transfer coefficients are then predicted using the Chilton Colburn[5] analogy between mass and heat transfer. Fig.(1.3) shows a typical experiment for determining a mass transfer coefficient from a coated surface. For the analogy to be valid the momentum (velocity) profiles must be identical and the mass (concentration) profiles similar to the thermal (temperature) profiles. Furthermore identical upstream conditions must be maintained.

Nash and Maxwell[6,7] reported the use of this analogy and its attractiveness in overcoming problems connected with rotational systems, e.g. the temperature measurement and provision of power through slip rings. Their study employed the Mercury evaporation technique which has the advantage over other mass transfer techniques of providing the means by which existing surfaces are easily coated with Mercury. It does not involve the insertion of plugs or accurate weighings before and after each test as with Napthalene. The low vapour pressure of Mercury ensures low evaporation rates and requires low energy transfer rates of the moving fluid phase. Their experiments measured mass transfer rates in both stationary and rotating cylinders, spheres and discs.

In the context of a rotating disc in still air, the disadvantages of this technique are that only overall mass transfer coefficients are measured with any degree of accuracy. Local radial values may be measured by applying successive coatings as illustrated by Figure (1.4). Applying a coating of Mercury to the area of radius R_1, detecting the

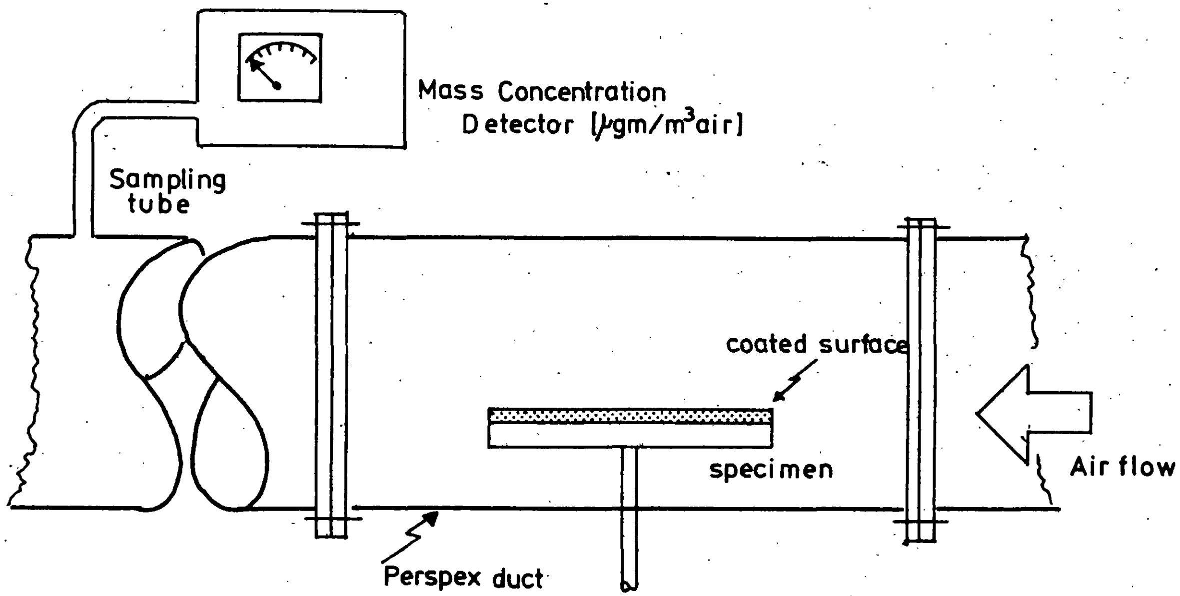

Fig 1·3 Mass transfer measurement

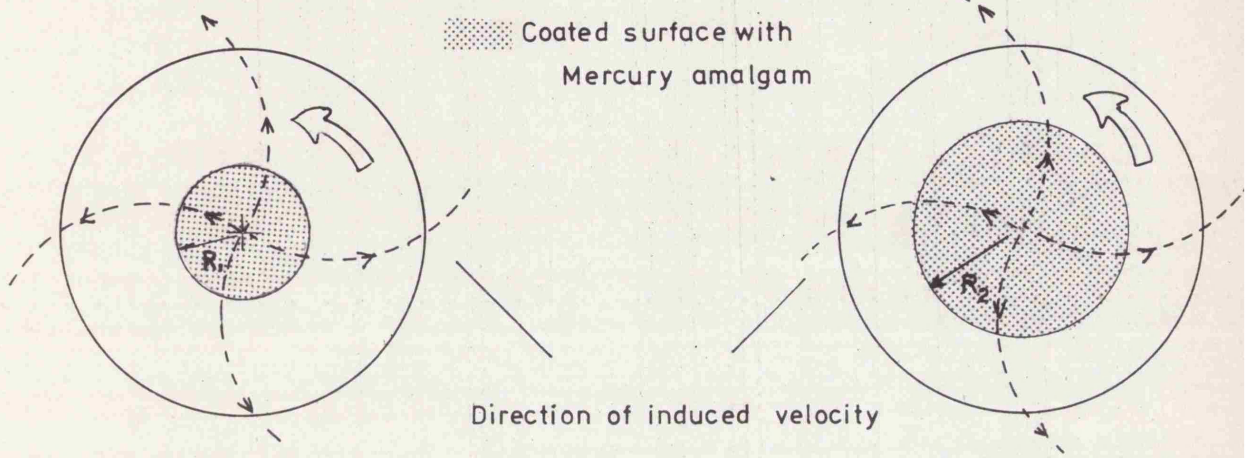

[a] 1st Coating

[b] 2nd Coating

Fig. 1.4 Rotating disc in still air

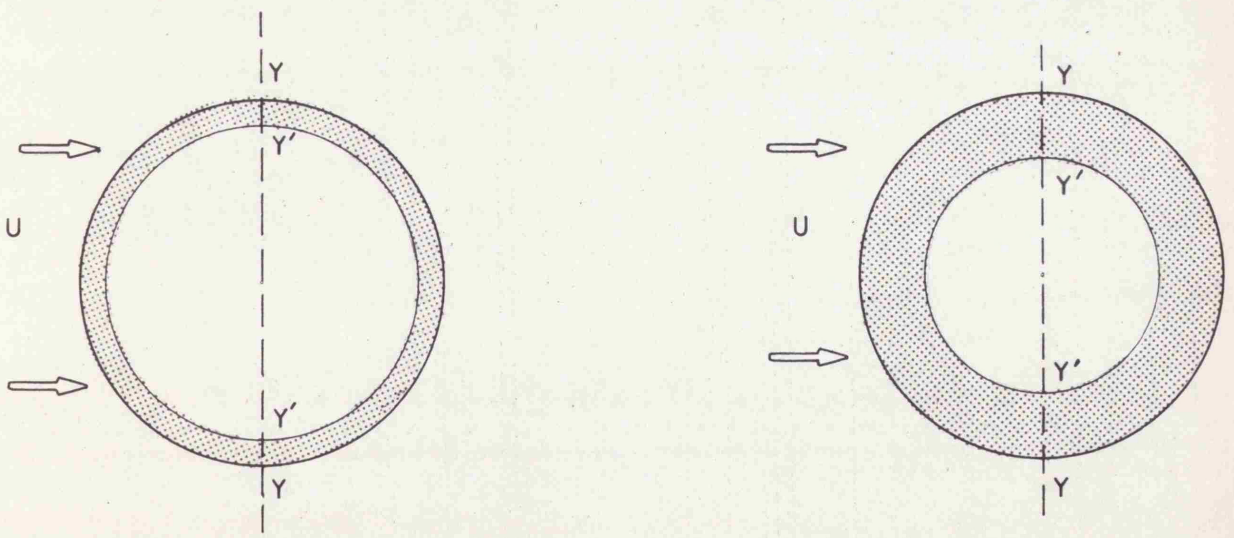

[a]

[b]

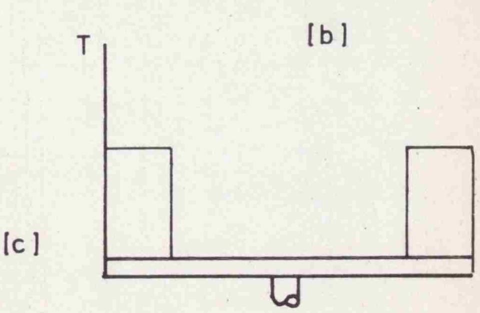

Fig. 1.5 Rotating disc in transverse airstream

resulting concentration C_1, then repeating the test with a larger area of radius R_2 and concentration, C_2, enables the local radial mass transfer coefficient at $(R_1 + R_2)/2$ to be determined from the difference in concentrations, $C_2 - C_1$.

This method is not considered particularly accurate as it involves small differences between comparatively low concentrations. It cannot be applied to the case of a rotating disc in a transverse air stream as illustrated by Figures (1.5 a and b). The upstream condition is satisfied to the left of YY but not to the right of Y′Y′. Essentially the arrangement is analogous to a non-isothermal disc with the surface temperature profile shown in Figure (1.5c).

Specific problems were encountered when this method was fully investigated. Firstly it was found that modelling and scaling down the disc for use in the Maxwell-Nash test rig, a 15 cm x 15 cm duct, produced rotational and air speeds well beyond the facilities available, in addition to very low Mercury concentrations. At sizes where the speeds could be achieved the large volumes of Mercury present were clearly not practical and considered hazardous to health. Secondly, the Mercury detection meter was unreliable and required frequent calibration. This calibration procedure entails boiling Mercury until a saturated mixture of Mercury vapour in air is achieved. This condition is extremely difficult to maintain and results in large errors in the calibration itself. Furthermore, the accuracy of the computed heat transfer coefficients relies on the Chilton-Colburn analogy which is not an exact transform.

1.3.5. Conclusions

On balance the calorimeter is favoured. Although the thermal boundary layer and internal distribution measurements are possible ways of overcoming some of the calorimeter's disadvantages they, themselves, have so many further inherent disadvantages that they offer no real advantage. The

Mercury evaporation method in essence holds out the possibility of overcoming a lot of these disadvantages, for example,the provision of slip rings and disturbing the flow by inserting probes, but it too presents further problems in modelling and is subject to significant inaccuracies.

Chapter 2

Experimental Arrangement

The apparatus used, shown diagrammatically in Figure (2.1), consists of a 51cm. diameter heated composite aluminium-wooden disc carried over-hung at one end of a shaft mounted in self aligning ball bearings. Lead wires from heaters, thermocouples and the heat transfer sensor are brought out through slip rings mounted on the shaft. The shaft also carries pulleys which allow the system to be belt driven from an electric motor at a number of speeds up to 1650 r.p.m.

The structure is placed with the disc central in the neck of an open jet wind tunnel, with disc face aligned with the direction of flow of the air jet. To avoid any vibrations which could affect the laminar-turbulent transition in the boundary layer formed, the system is mechanically balanced.

2.1. The Disc

The disc is a composite structure and is shown schematically in Figure (2.2). An aluminium plate 51cm. diameter and 2.5cm.thick, (made from two plates, because of material availability) contains electrical heaters located in five annular grooves. This metal pair is made massive to even out the energy distribution from the heaters and ensure a uniform surface temperature. The heaters, each rated at 500 watts. are Incoloy sheathed with mineral insulation. They are of circular cross section, 8mm. nominal diameter, and are a push fit against the sides and bottom of the recesses to give good thermal contact with the aluminium. The back face is shown in Fig. (2.4) and is covered by an asbestos board to reduce heat loss from that surface, followed by a wooden backing board. The composite, 5cm. thick is clamped together by twelve bolts.

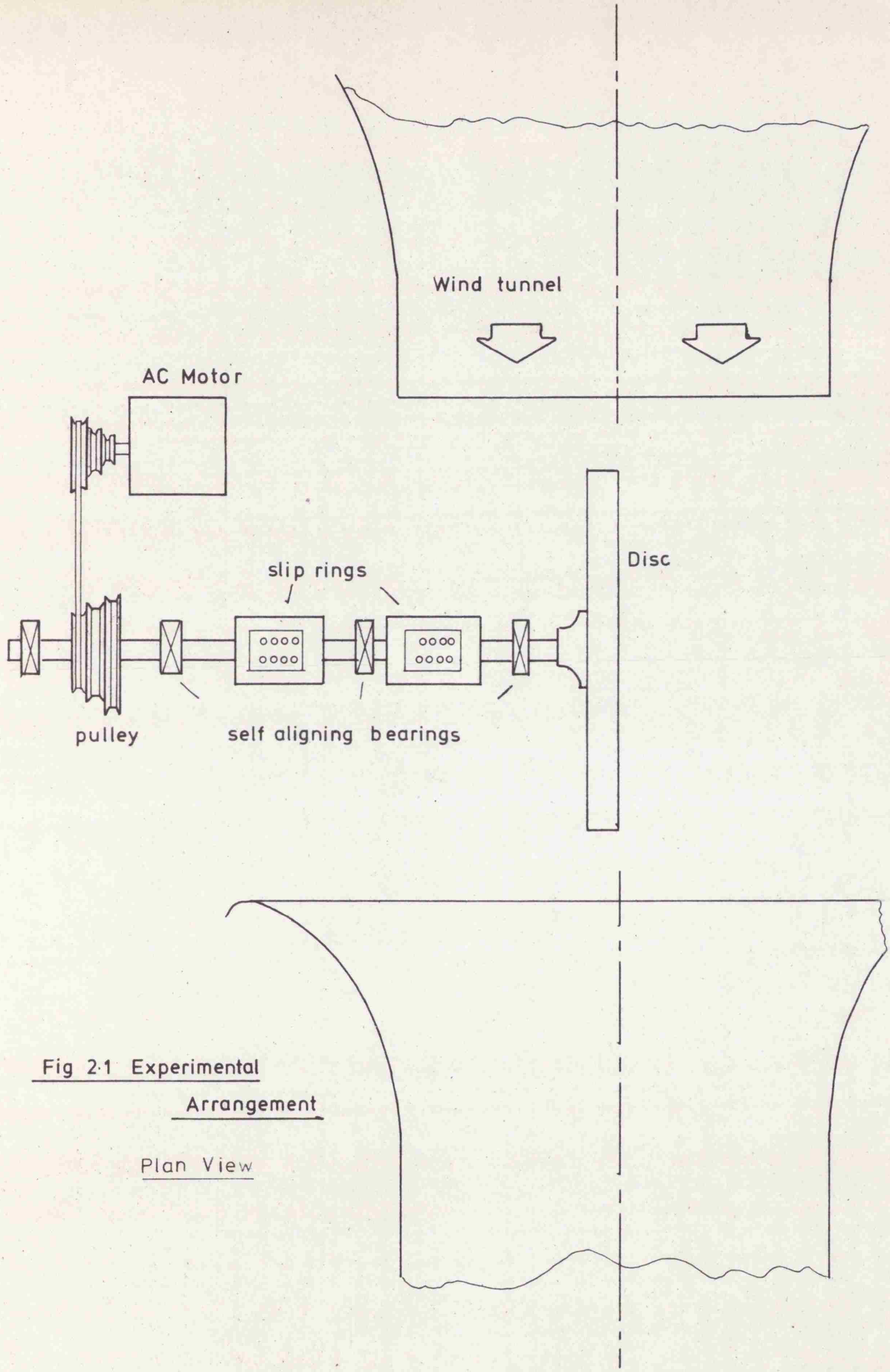

Fig 2·1 Experimental Arrangement

Plan View

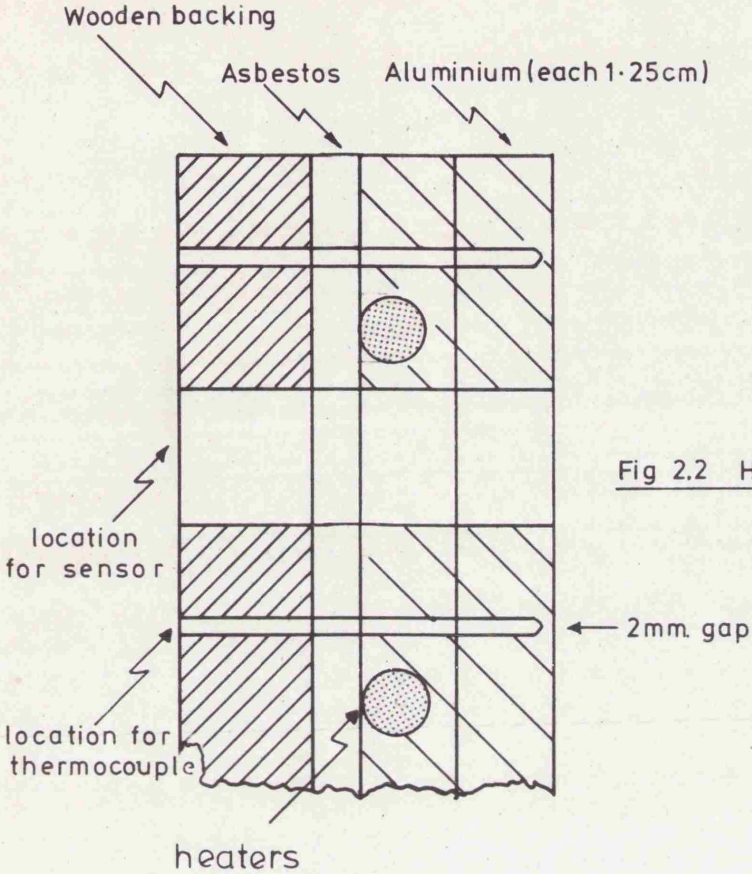

Fig 2.2 Heated Disc

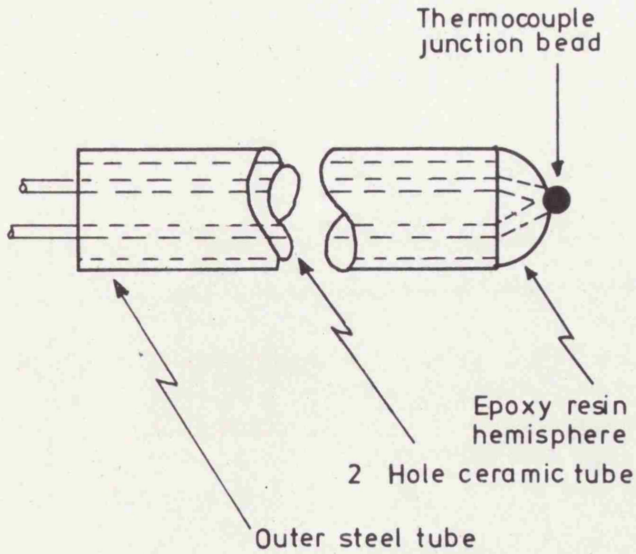

Fig 2·3 Thermocouple probe

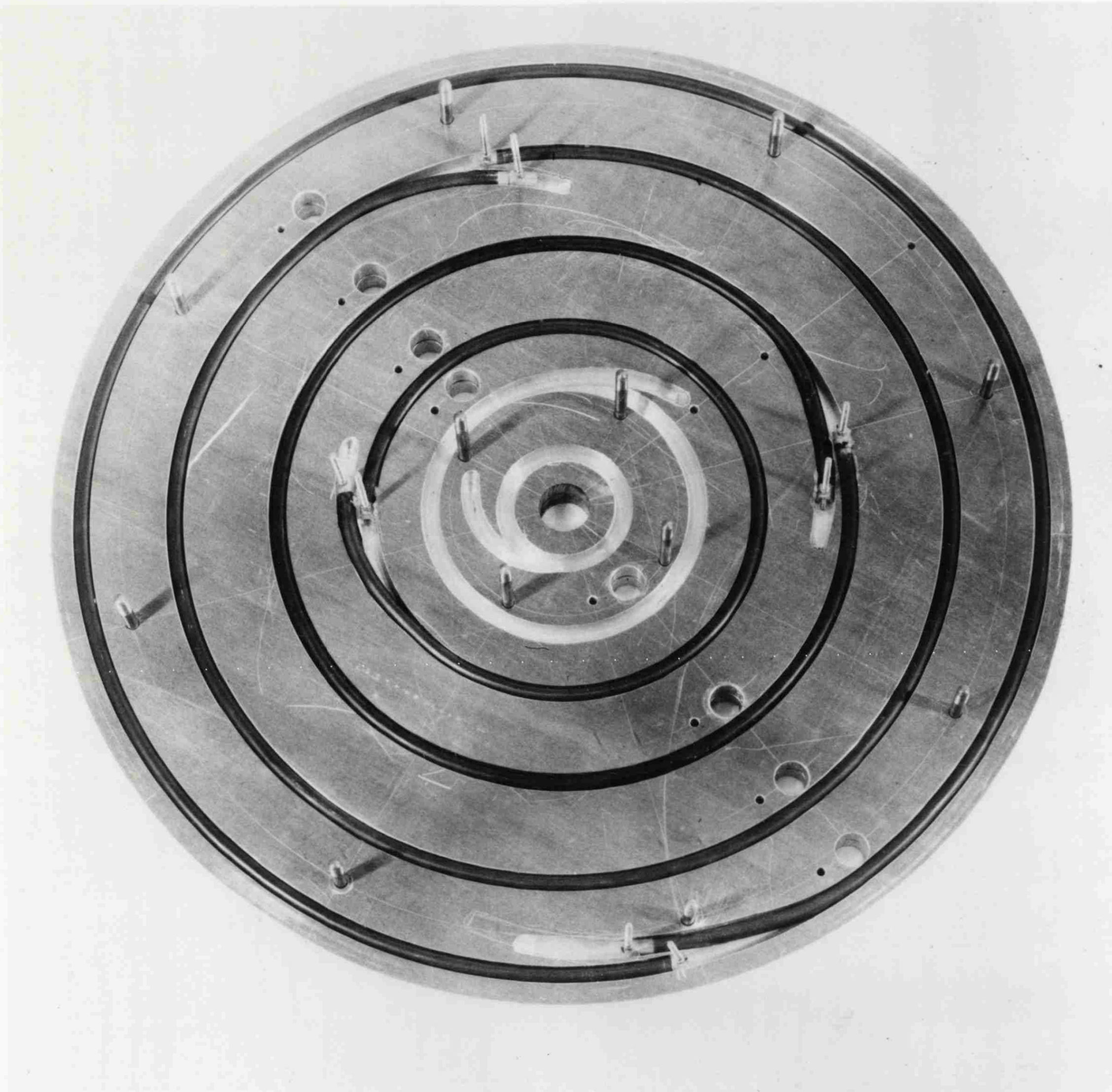

Fig 2.4 Back face of Aluminium disc section showing annular heaters, thermocouple and sensor holes

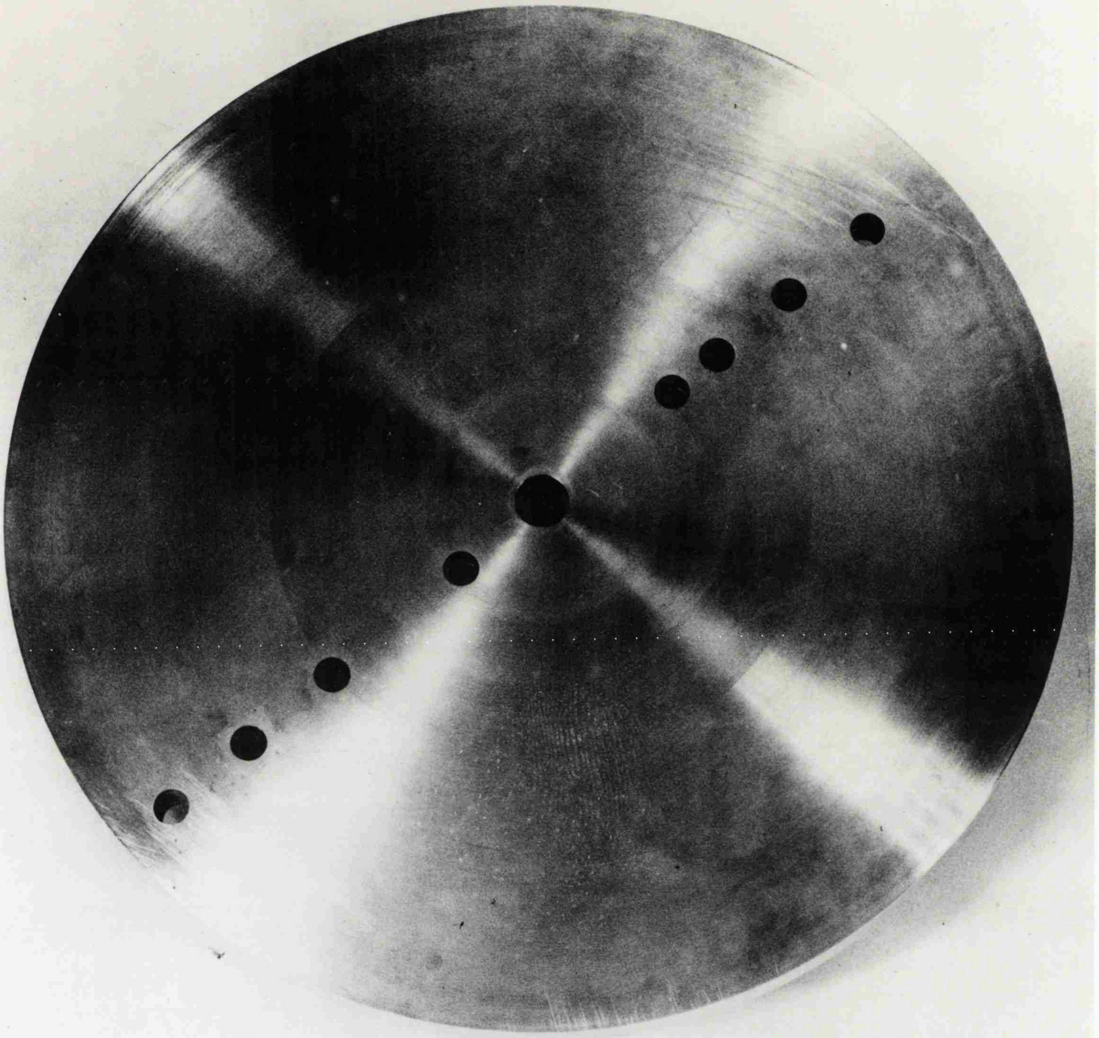

Fig 2·5 Front face of disc

The front surface temperature is measured by seven Chromel/Alumel thermocouples, of the type shown in Figure (2.3), distributed across a diameter. These are pushed into blind holes which locate the thermocouple junctions just below the aluminium surface, the junctions being pressed hard against the metal.

In practice with this construction a uniform surface temperature is achieved. The thermocouples located near the edge and near the centre of the disc show the largest variations but these are within four per cent of the mean temperature difference between the disc face and the ambient air.

The composite disc carries holes to allow mounting the heat flux sensor in any one of seven radial positions, with the sensors face flush with the front face of the aluminium. The holes not in use are filled with dummy aluminium plugs. Figure (2.5) shows the front face of the aluminium disc with the plugs removed.

2.2. Heat Flux Sensor

The heat flux sensor is shown in Figure (2.6). A thin copper disc A is mounted on a Tufnol washer B, which is seated flush inside a hollow copper cylinder C. A small heating element D, is attached to the underside of the disc A, and a similar heater E, to the back of cylinder C. Disc thermistors are ideal for this purpose. They give uniform energy generation throughout their volume and avoid the necessity of winding small heating coils. It was hoped that in addition to providing a heat source, these thermistors would be suitable for measuring the temperatures of copper disc A and cylinder C. Although thermistors are normally used for measuring temperatures this is not possible when they are simultaneously used as heaters. Experiments to calibrate the thermistors under the relatively heavy electrical loading proved unsuccessful. Large errors were caused by the internal thermal gradients within the thermistor.

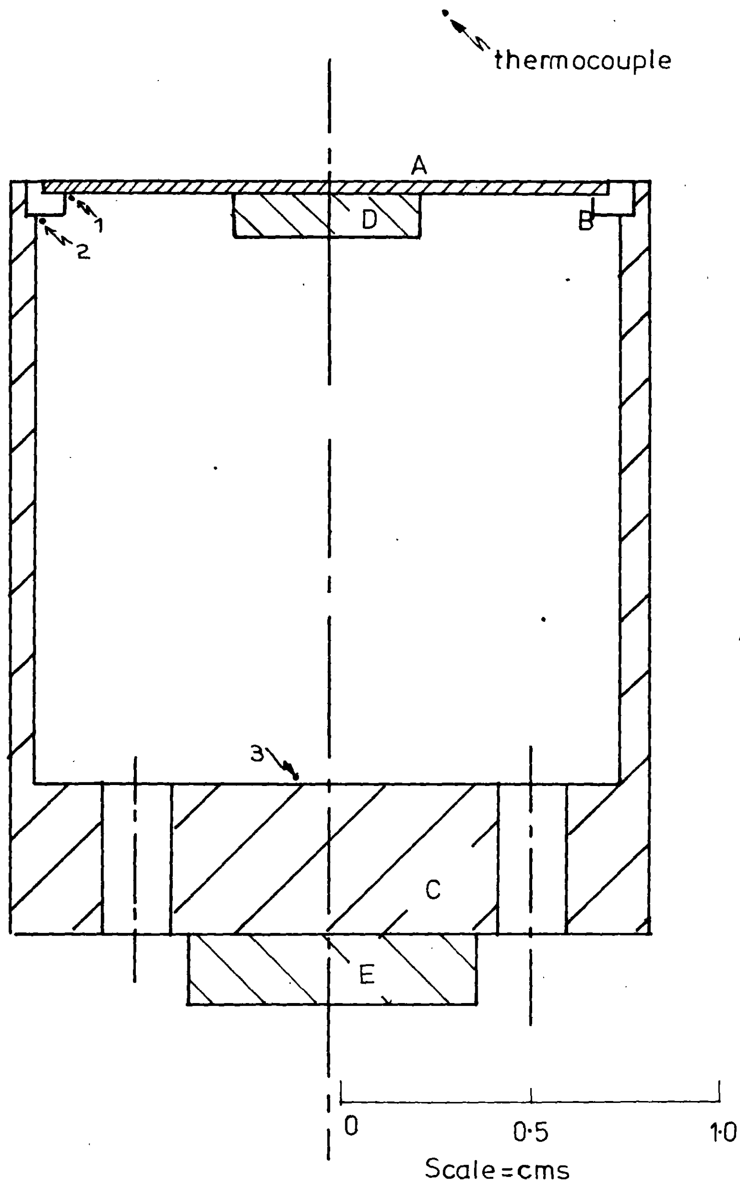

Fig 2·6 The Heat Flux Sensor

Therefore three Chromel-Alumel thermocouples were attached in the positions shown, the junctions being in good thermal contact with the copper. The thermistor E controls the temperature of the guard ring C, whilst D provides the input energy for the heat transfer measurement.

The sizing of the Tufnol washer is a compromise between mechanical strength, minimizing heat loss from the disc A through the washer into the surrounding metal C, and minimizing heat loss through the washer into the surrounding air by convection. The guard ring C also prevents leakage from the back and sides of the thermistor D.

During operation the sensor is positioned inside the main rotating disc with its front surface flush with that of the disc.

2.2.1. Thermal Design

Two types of errors can occur in the value obtained for the heat transfer coefficient measured. Firstly systematic errors occur due to

a) Heat leakage from the copper disc A through the Tufnol washer to the ambient air.

b) Temperature variation across the copper disc A.

c) Radiation from disc A.

see illustration, Figure (2.7).

Secondly random errors may occur. These are caused by heat leakage between the copper disc A and thermistor D combination and the guard ring C due to temperature inequalities at positions 1, 2 and 3, as illustrated by Figure (2.8).

A detailed analysis of these losses is given in Appendix (A1) based upon the thermal resistance values of the constituent parts of the sensor. These resistances are given in Figure (2.9) and Table (1).

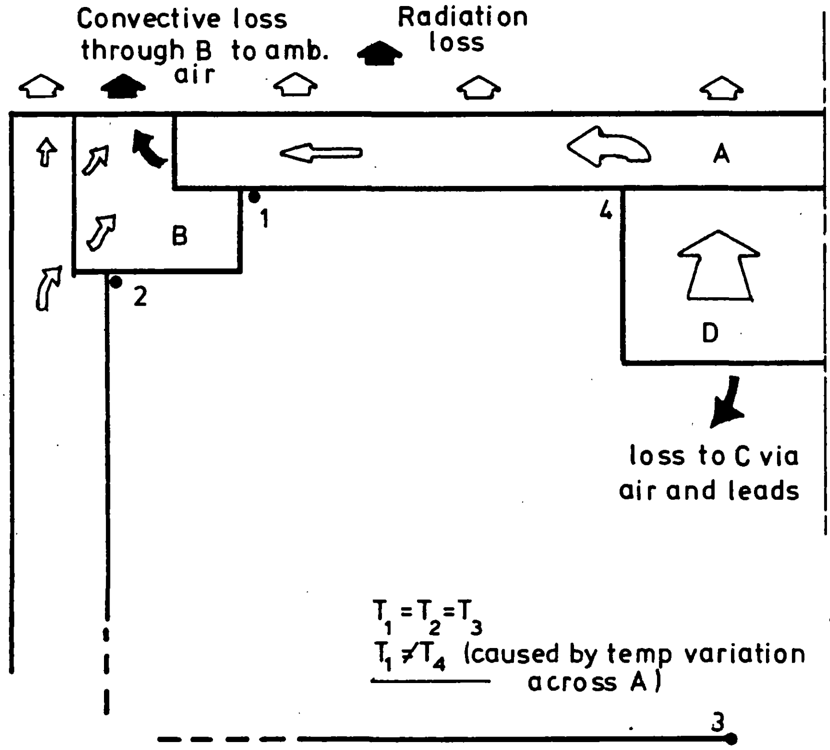

Fig 2.7 Systematic Errors

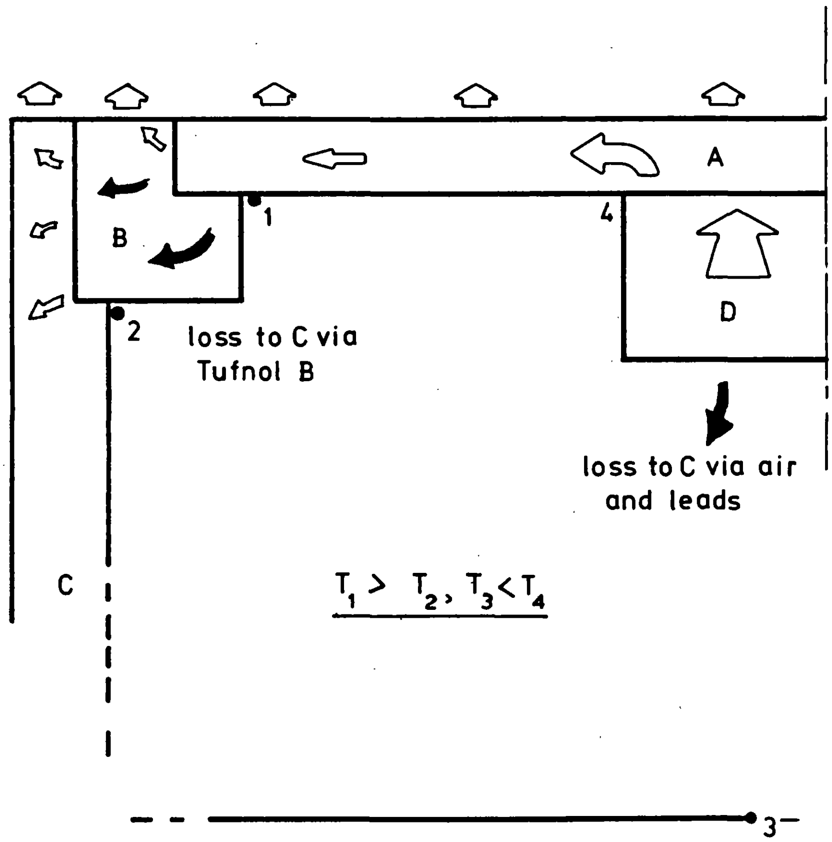

Fig 2.8 Random Errors

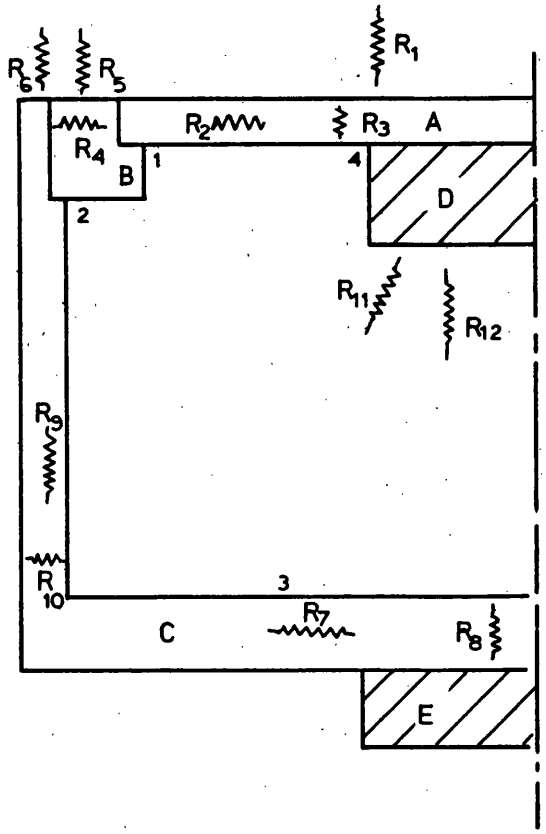

Fig 2·9 Sensors Internal Thermal Resistances

Table 1

R	ΔT/Q deg C/W	Description.
1	390 [39]	Convective transfer from A
2	0·9	Radial conduction through A
3	0·0076	Axial " " "
4	55·4	Radial " " B
5	2850 [285]	Convective transfer from B
6	3880 [388]	" " " C
7	0·0813	Radial cond. through btm. of C
8	0·0482	Axial " " " C
9	1·67	Axial " " wall of C
10	0·0036	Radial " " " C
11	2450	Cond. from D to C through air gap
12	230	" " " " elect. leads

Bracketed quantities refer to $h=150\ W/m^2 deg\,C$

A summary of both the systematic and random errors is given in the Table below where the effects of both high and low heat transfer coefficientsand temperature gradients are considered. The figures given are percentage errors.

Table 1

		ΔT=100deg.C	ΔT=20deg.C
a) Heat leakage	15W/m^{2}deg.C	+ 6.8	+ 6.8
from A to B	150	+ 6.8	+ 6.8
b) Temperature	15	-	-
variation	150	+ 1.2	+ 1.2
c) Radiation	15	+ 3.25	+ 0.4
	150	+ 0.325	-
Total	15	10.05	7.2
	150	8.325	8.0
Temperature	15	± 2.2	±11.2
inequalities	150	± 0.22	± 1.12

1) Systematic errors

2) Random errors

(due to 0.25deg.C in balance in thermocouples 1 and 2 (&3)

In the table above the total systematic and random errors are given. It is seen that when measuring low heat transfer coefficients (15W/m^{2}deg.C) care must be taken to ensure radiation losses remain small by maintaining the surface temperature as low as possible. In contrast random errors, caused by temperature inequalities are more significant at these low temperatures. Careful balancing is necessary when low heat transfer coefficients are being measured. At higher values the sensor is expected to be more accurate in its measurement of heat transfer.

In Chapter 3 practical measurements are made to check the performance of the heat flux sensor by comparison with previous work on rotating discs in still air. The results show good agreement with these works and are within the limits of accuracy as determined from the above analysis.

An estimate of the random errors involved in the measurements place the heat transfer coefficients values accurate within ± 2%. This is borne out by the reproducability of the results obtained from repeat tests.

2.2.2. Transient Response

The heat transfer coefficient from a rotating disc in still air remains constant with angular position. However when a transverse air stream blows across the rotating disc a variation in the heat transfer is expected as the disc rotates through 360 degrees. The point is illustrated in Figure (2.10). Position A is subject to a convective condition caused by a relative air stream velocity $U + 2\pi NR$; whereas at position C a lower heat transfer rate is expected where the relative velocity is $U - 2\pi R$. Intermediate values are expected in the other two positions B and D. A profile similar to that illustrated in Figure (2.11) results.

The sensor was not designed with instantaneous measurements in mind. The thermal mass of the copper disc A is too large to permit sudden changes in heat transfer to be monitored. The input (heat transfer coefficient) is cyclically varying yet the output (temperature) is some mean. The interpretation of this mean is discussed in Appendix(A2). The analysis for a sinusoidal input shows the measured value is a straight average of the input and suggests that other wave forms will produce the same result.

The analysis is extended to a very much faster responding sensor with a thermal mass a thousand times smaller. In such a case it is shown that the output is a sinusoid whose mean does not correspond with the average heat transfer coefficient. The point is illustrated in

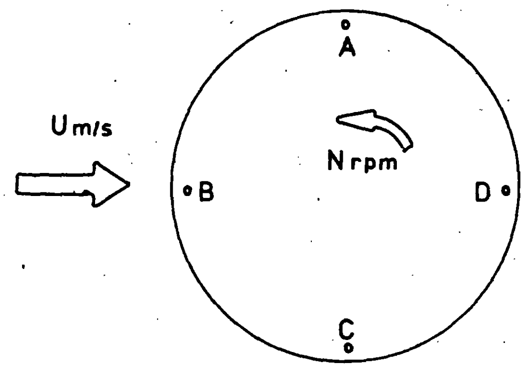

Fig 2·10

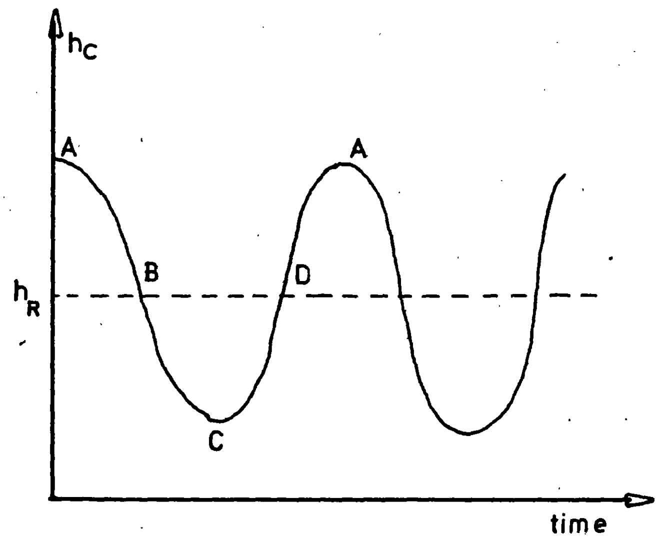

Fig 2·11 Typical heat transfer variation

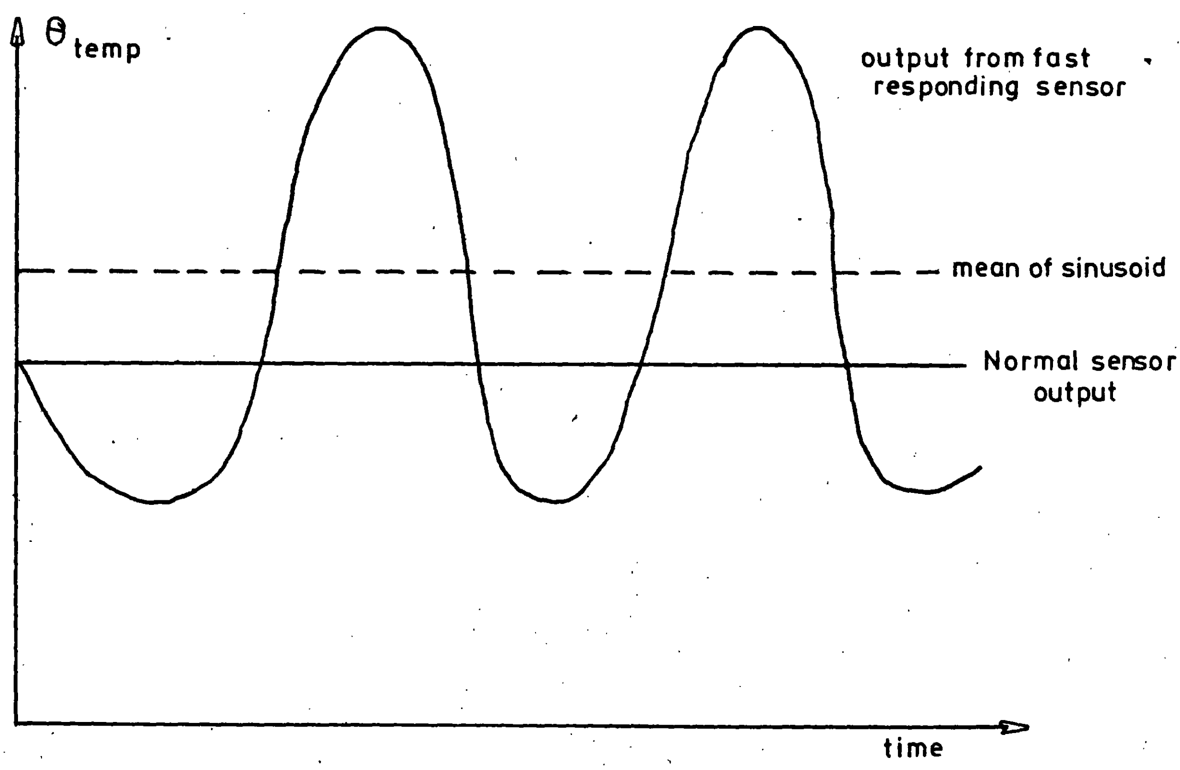

Fig 2·12 Temperature Variation

Figure (2.12). The constant output from the heat flux sensor previously described is shown with the cyclic variation of the output from a faster responding sensor. The mean of this output is greater than that of heat flux sensor. If the measuring device is unable to respond to these temperature fluctuations then the average heat transfer coefficient measured will be in error. However for the measurements taken with the present heat flux sensor it can safely be assumed that the measured values are straight averages of the heat transfer coefficient.

2.3. Slip Rings/Thermocouple Arrangements

Two eight channel slip ring units are used to feed power to the electric heaters and transmit the signals from the thermocouples. Both units, Type PC-08-10 are manufactured by I.D.M. Electronics Ltd. and contain silver rings and silver graphite brushes. They are specifically designed to give a very low noise level (5μV/mA). Although air cooling could be applied to reduce spurious e.m.f's it was found unnecessary in practice. One of the slip ring units is modified to cope with the higher voltage requirement of the electric heaters.

To maximise slip ring usage the Chromel/Alumel thermocouples are paralleled through the assembly and then fed through the same electrical circuit in the 'Comark' temperature recorder via a switch. The ambient temperature is monitored by a similar thermocouple placed in the air jet. Comparative temperature measurements are needed to determine the heat transfer coefficients so the accuracy of the absolute level is not too important. The temperatures can be read to within 0.1 degrees.

2.4. The Wind Tunnel

A recirculating tunnel with an open jet is available in the Aerodynamics Laboratory of the University of Leicester Engineering Department. This wind tunnel gives a circular jet of 61cm. diameter with an air speed up to 33m/s. Pitot static traverses at the mouth show the jet has a square profile. Fig.(2.13) shows three typical profiles in both horizontal and vertical planes. Generally the profile is uniform with slight peaks close to the tunnel wall, the result of a contraction section in the wind tunnel upstream of the jet opening.

With the disc shaft centred on the tunnel axis, the maximum variation in air velocity over the disc diameter is four per cent. Further pitot static traverses around the disc confirm that the disc can be considered to be in a uniform stream, and that there are no wall constraint effects. The blockage ratio of the disc is 8.5%.

2.5. Experimental Procedure

To reach steady state prior to taking measurements from which heat transfer coefficients are determined, the following procedure is adopted.

With the wind tunnel operating at the desired air velocity the power supply to the disc heaters is adjusted to give a uniform face temperature, usually between 20 and 60 deg.C above ambient. The disc is then set in rotation and power applied independently to the sensor thermistors and controlled to match the temperatures registered by the three sensor thermocouples and the temperature of the disc face.

From measurements of the power input to thermistor D, the sensor face temperature and ambient temperature registered by the thermocouple at the edge of the air jet, heat transfer coefficients are calculated from the equation

$$h = \frac{V.I.4}{\pi d^2(T_1 - T_\infty)} \qquad 2.1.$$

where the diameter, d, of the emitting surface was taken from the actual sensor and found to be 1.5 cm.

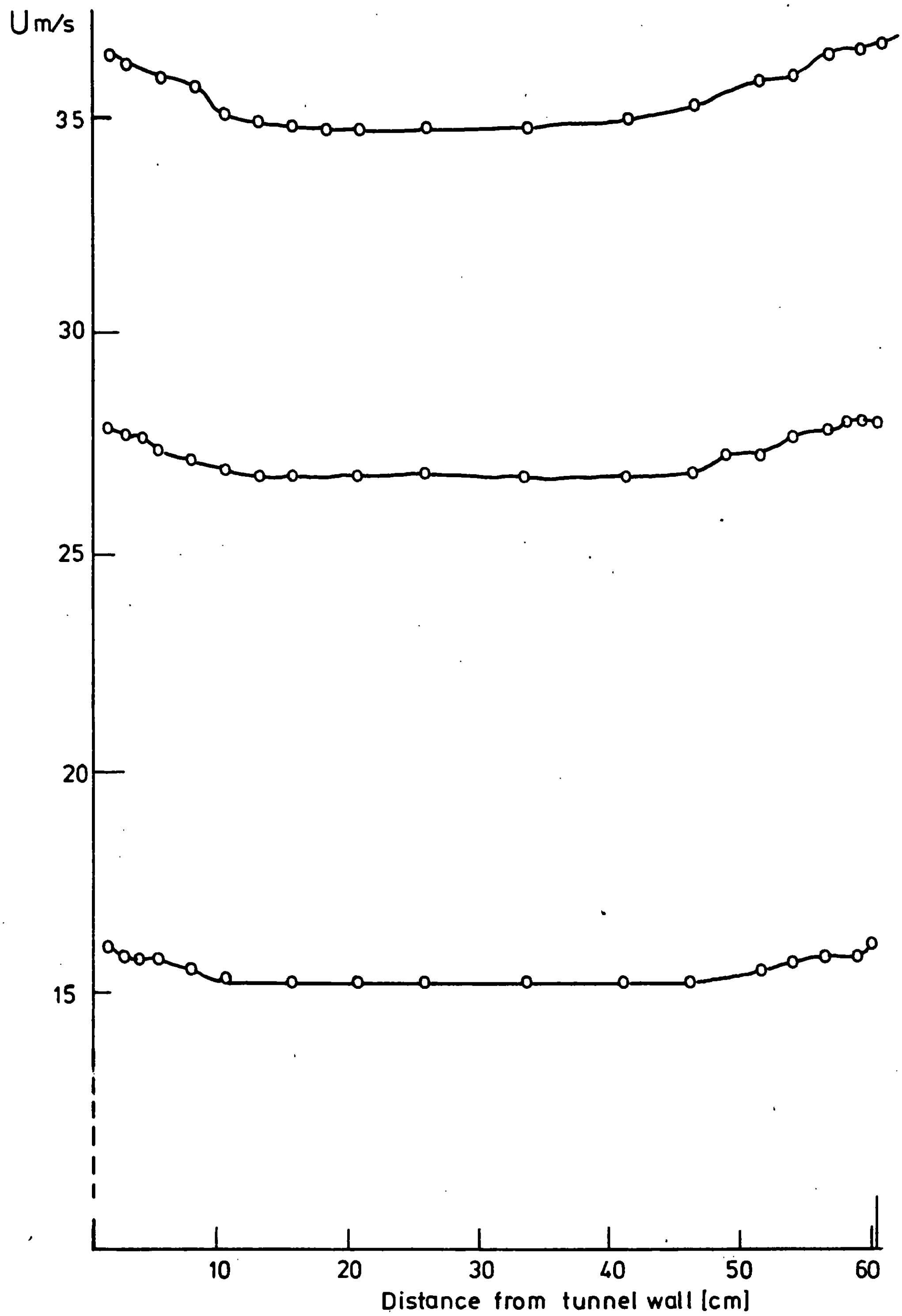

Fig 2·13 Velocity distribution across wind tunnel for three speed settings (vert & horiz profiles identical)

Chapter 3

Heat Transfer Measurements

3.1. Isothermal Disc Rotating in Still Air

These tests over a range of disc speeds, 296 - 1650 r.p.m. were carried out to provide a check on the efficiency of the heat flux sensor in measuring heat transfer coefficients by making comparisons with published data. The disc surface temperature T_w, was varied between 20 and 60 deg.C above ambient with no significant effect on the measured heat transfer coefficient, h_R. The results are presented in tabular form in Appendix (A3) and have been plotted in both dimensional and non-dimensional form in Figures (3.1) and (3.2) respectively. Figure (3.2) is a plot of the local Nusselt number, $Nu = \frac{h_R R}{\kappa}$, versus the rotational Reynolds number, $Re = \frac{NR^2}{\nu}$, the physical properties being evaluated at the film temperature.

The motion, and heat transfer, produced by a rotating disc is divided up into three regimes, laminar, transition and turbulent flow. Various techniques have been used to examine these regimes.

Gregory, Stuart and Walker[8] carried out an investigation into how laminar flow loses its stability in the vicinity of a rotating disc. One side of the disc was coated with china clay and rotated at several speeds to 3000 r.p.m. A typical example of the pattern obtained is shown in Figure (3.3)[8]. Two critical radii were obtained separating the three regimes of flow. Within the inner radius, R_s, the flow is purely laminar and beyond the outer radius wholly turbulent. In between, a series of traces in the form of equiangular spirals were recorded in the china clay. The critical Reynolds Numbers related to these two positions of instability and transition were determined as

$$Re_s = \frac{NR_s^2}{\nu} = 1.82 \times 10^5 \quad \text{(instability)}$$

$$Re_T = \frac{NR_T^2}{\nu} = 2.82 \times 10^5 \quad \text{(transition)}$$

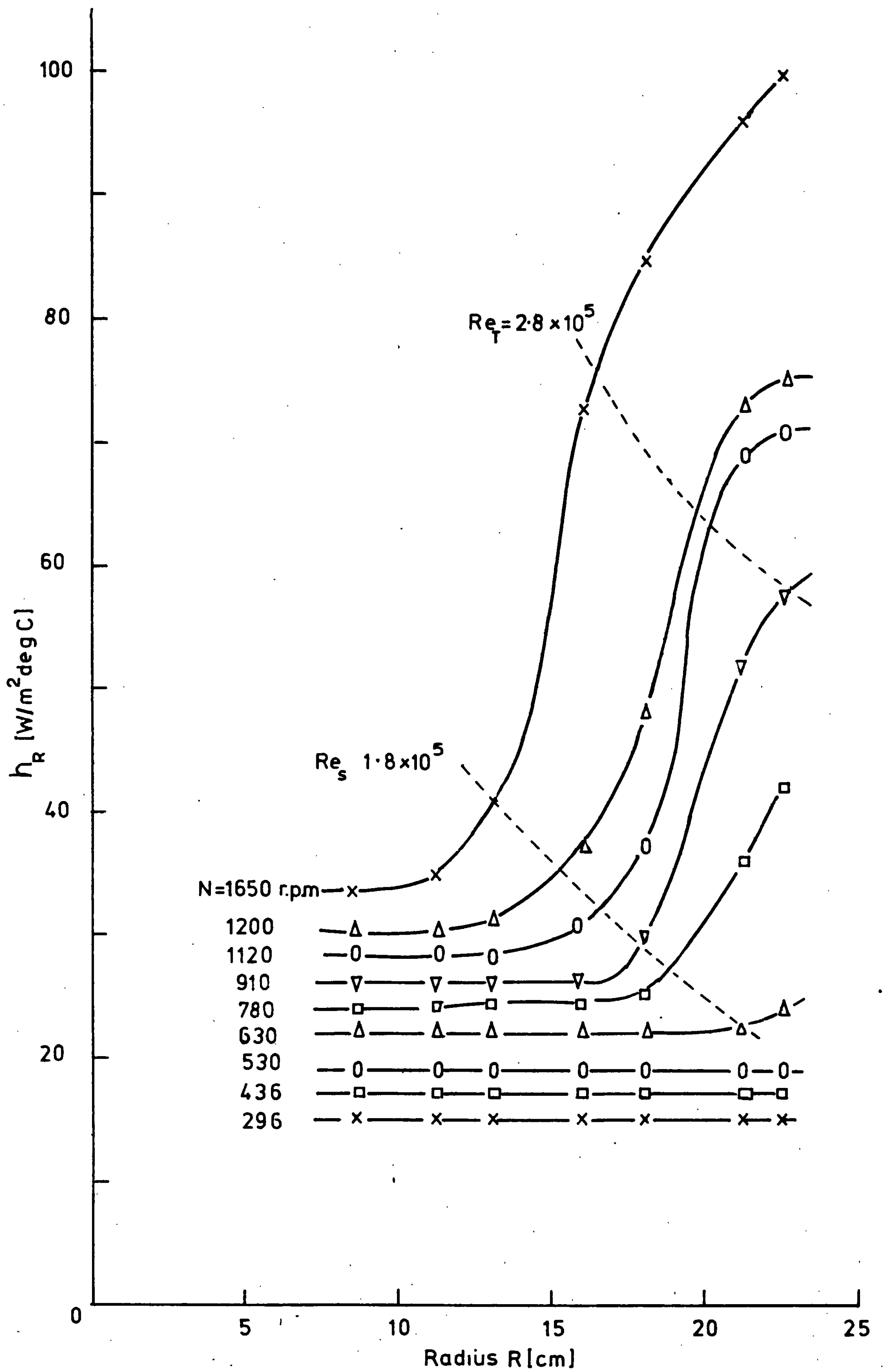

Fig 3·1 Rotating Disc in Still Air – Radial Variation.

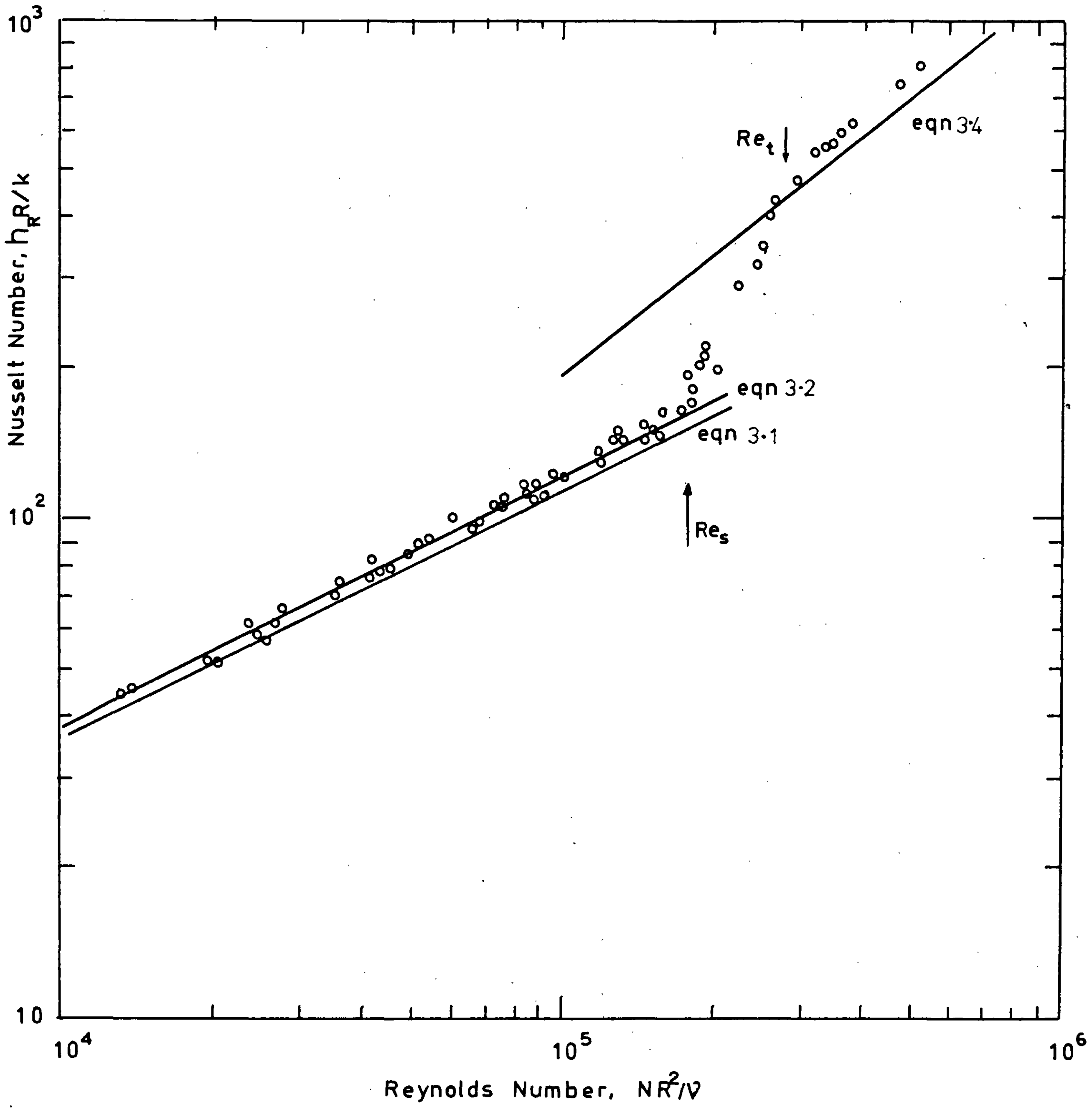

Fig 3·2 Rotating Disc in Still Air - Dimensionless Plot

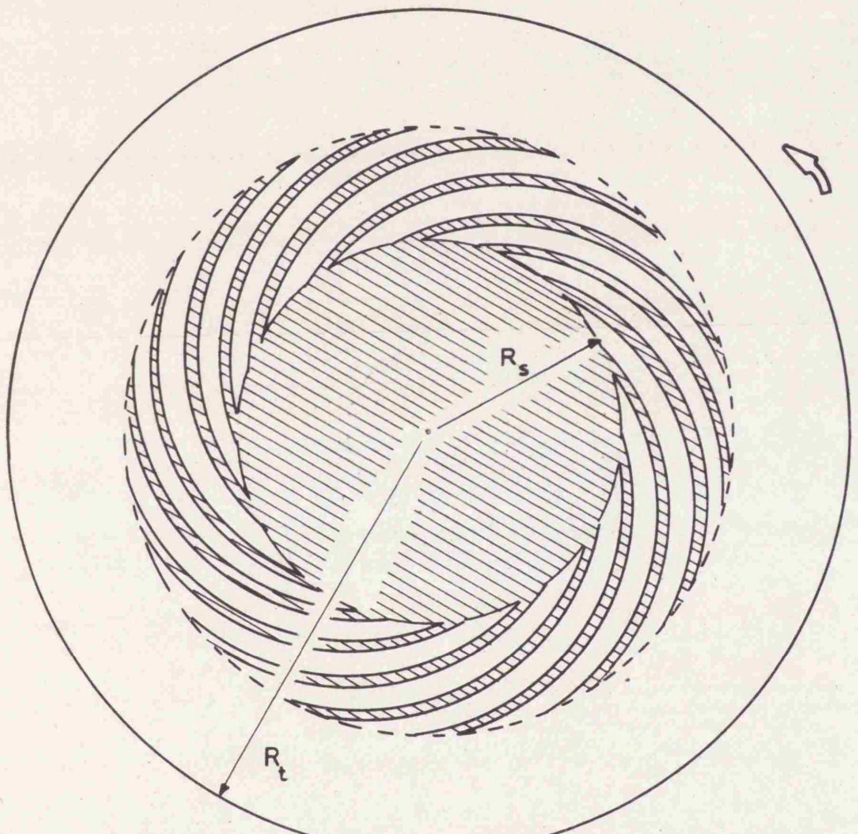

Fig 3·3 Schematic picture of the sweeping off of China Clay in the rotation of a disc in free space

During the present heat transfer measurements these positions of instability and transition were confirmed with the aid of an acoustic stethoscope. The silence in the laminar field was easily distinguishable from the definite pitch in the transition zone and the heavy thumping noise as turbulence was reached. These changes correlated with the above Reynolds numbers.

The experimental data of Cobb and Saunders[9] for laminar flow in air, Pr = 0.72, is correlated by the expression

$$Nu = 0.36\ Re^{0.5} \tag{3.1}$$

and that of Goldstein[10] by

$$Nu = 0.38\ Re^{0.5} \tag{3.2}$$

and recently that of Dennis, Newstead and Ede[21] by

$$Nu = 0.4\ Re^{0.5} \tag{3.3}$$

As yet no single correlation exists for the local turbulent heat transfer variation. Dorfman[1] suggests the results in the turbulent region can be correlated by

$$Nu = 0.0194\ Re^{0.8} \tag{3.4}$$

for a Prandtl Number of 0.7. These correlations are shown by the solid lines in Figure (3.2).

The present work shows good agreement with that of Goldstein, and Dennis, Newstead and Ede, although it is a few per cent higher than that of Cobb and Saunders. In the turbulent regime, $Re > 2.82 \times 10^5$, the measured values are some ten per cent higher than the predictions of Dorfman. In view of the analytical assumptions inherent in this prediction the agreement is considered to be reasonable.

Figure (3.1) shows how the local heat transfer coefficient varies with radius and rotational speed. In the laminar region, $Re_r < 1.82 \times 10^5$ the heat transfer coefficient is seen to be independent of radial position as predicted by the theory[1,2] and evident from equations (3.1) and (3.2). At $N < 530$ r.p.m. the heat transfer remains constant over the whole surface of the disc. At higher speeds the radial variation shows the flow to be laminar near the centre becoming turbulent at larger radii. As the speed increases the points of instability and transition move towards the centre of the disc.

On the evidence of the information presented in Figures (3.1) and (3.2) the heat flux sensor is regarded as a viable instrument.

3.2. Isothermal Disc Rotating in a Transverse Air Stream

Considerable testing was done over a range of disc rotational speeds from 296 - 1120 r.p.m. and at each speed for a range of main stream air speeds 0 - 33 m/s.

Of particular interest from the ideal train wheel point of view is the condition where the air jet speed is matched to the disc peripheral speed, thus attempting to simulate a wheel rolling along a track in still air. The influence of the track on the flow distribution is not considered. For this matched condition the radial variation in heat transfer coefficient, h_R, is shown in Figure (3.4). The results are presented in tabular form in Appendix (A3). In Figures (3.5(a)(b)(c)) the radial variations in heat transfer coefficients are shown for a selection of unmatched flows for three different speeds.

3.3. Discussion

Two main observations can be made from the information so far presented

i) The magnitude of the heat transfer coefficient is dominated by the main air stream flow. For instance at a speed of 1120 r.p.m.

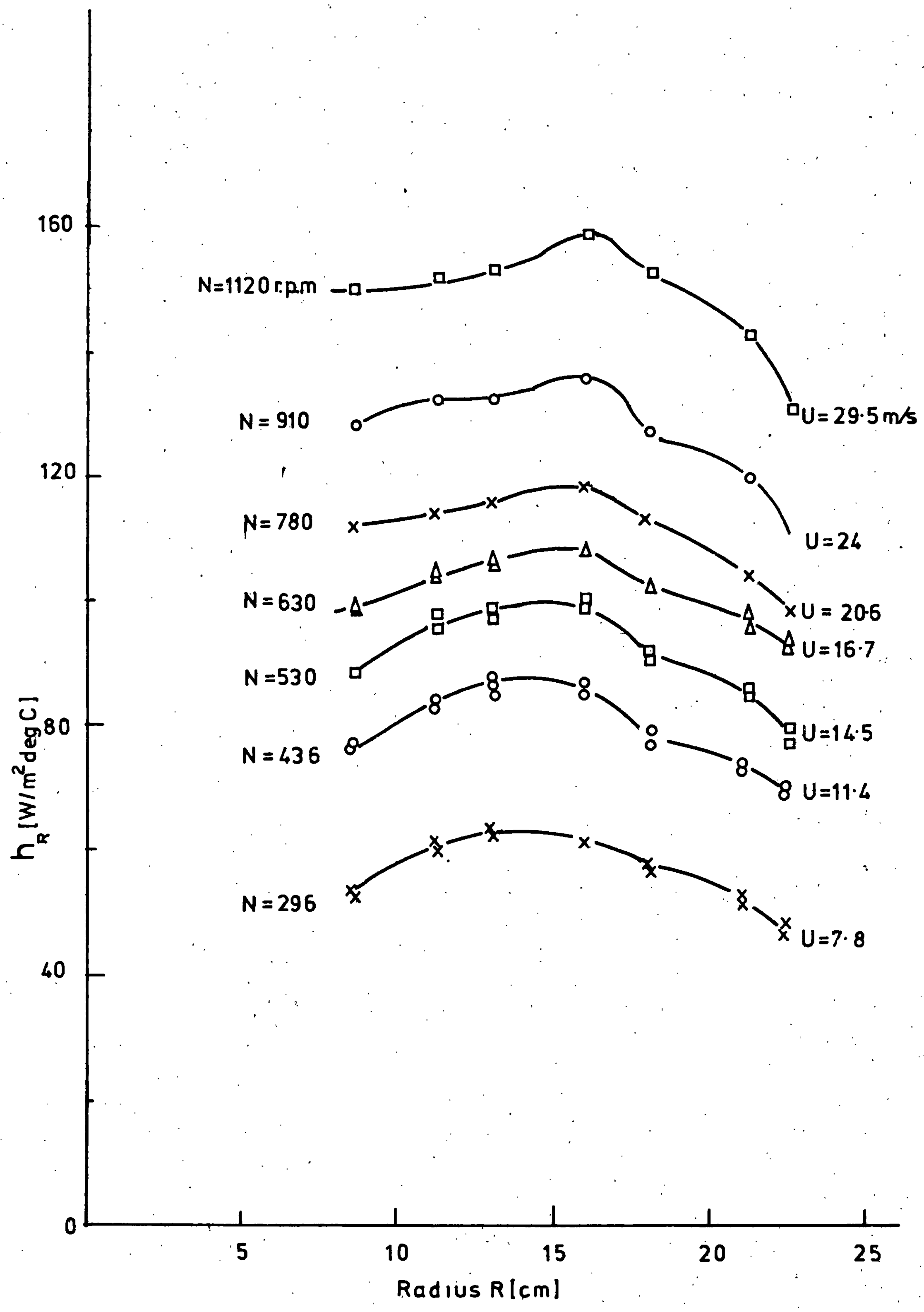

Fig 3·4 Rotating Disc in a Matched Air Stream

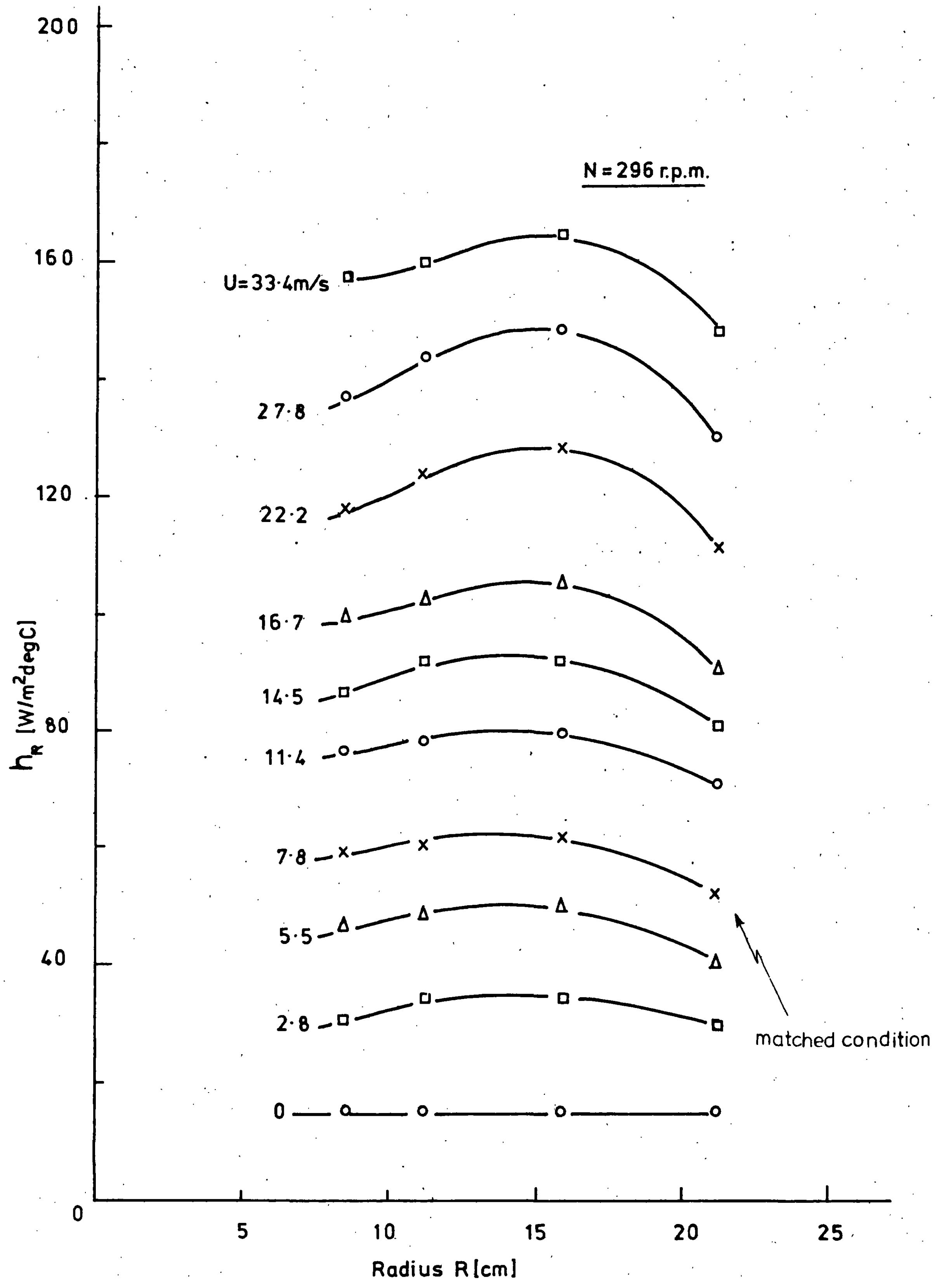

Fig 3·5 a Rotating Disc in Unmatched Air Stream - Disc speed 296 r.p.m.

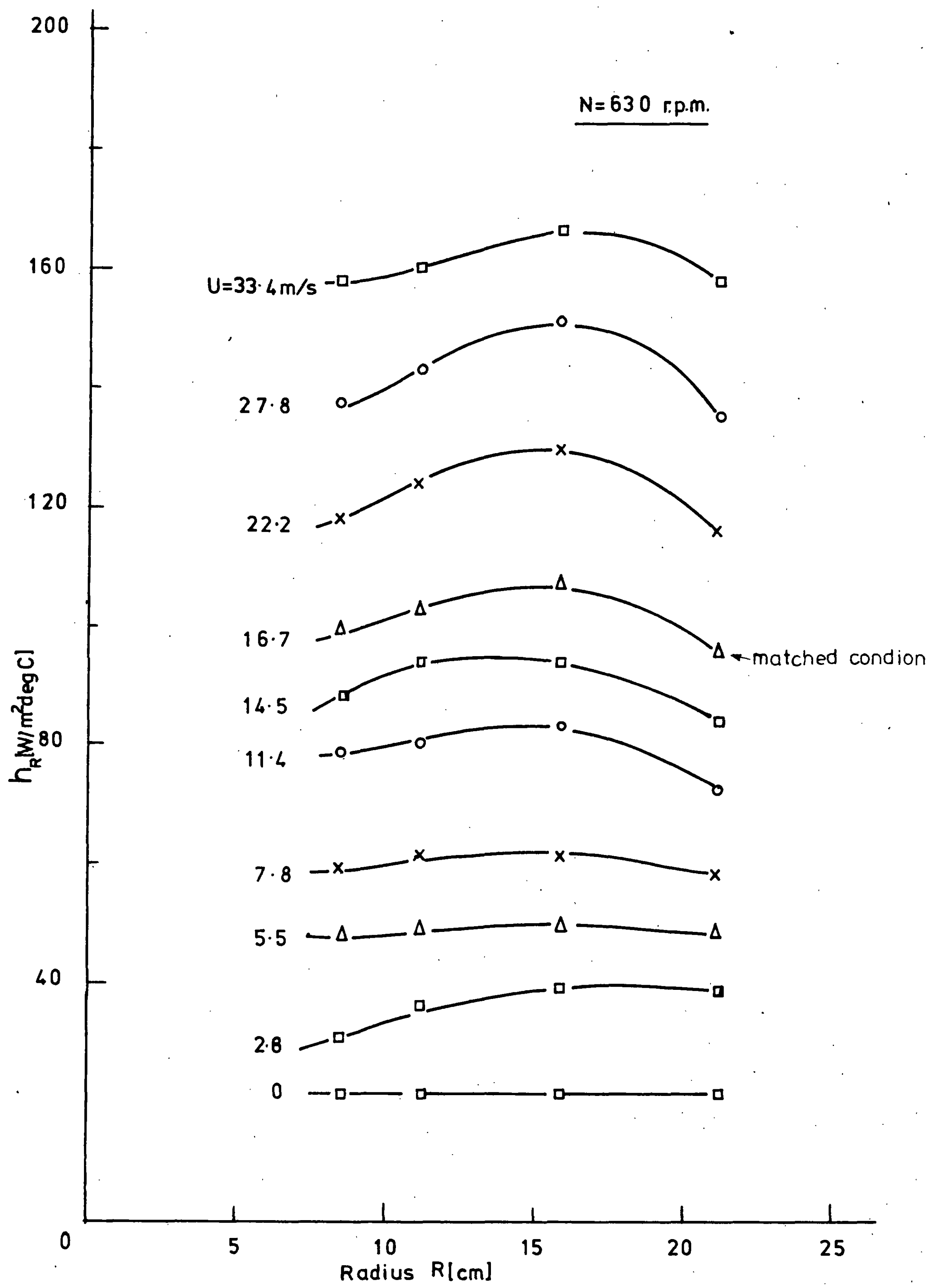

Fig 3·5b Rotating Disc in Unmatched Air Stream - Disc speed 630 r.p.m.

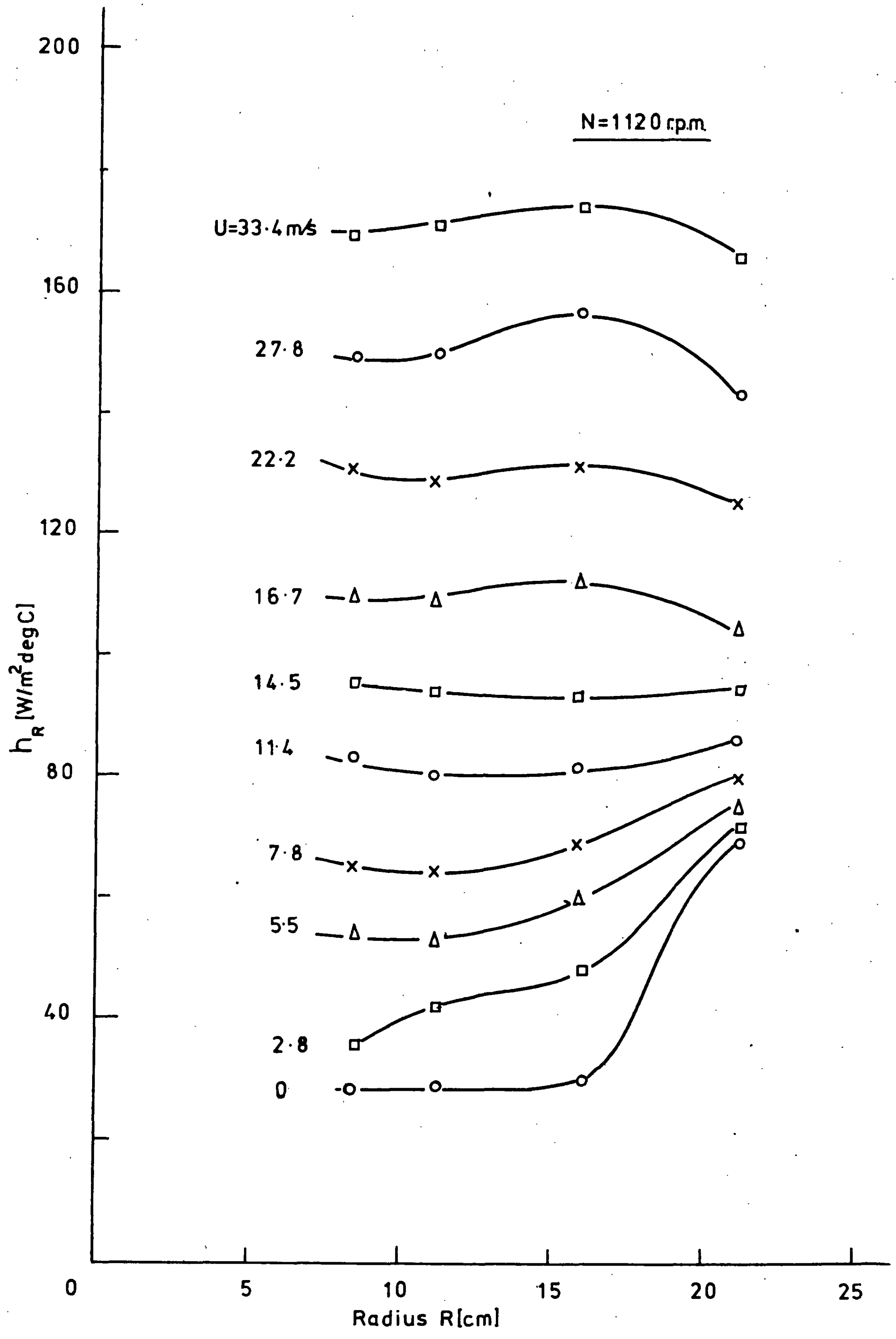

Fig 3·5c Rotating Disc in Unmatched Air Stream - Disc speed 1120 r.p.m.

changes in the air speed from 0-33 m/s cause some four fold increase in the heat transfer coefficient (Figure (3.5(c))). At an air speed of 33 m/s a change in the disc speed from 296 to 1120 r.p.m. only causes a 10 per cent variation (Figures (3.5(a) and (c))).

ii) The radial variation is considerably altered from the still air case. At low rotational speeds the heat transfer coefficient is no longer independent of radius but shows a peak value at approximately half radius, (Figure (3.5(a))). At high rotational speeds the marked radial change in heat transfer coefficient due to the laminar-turbulent transition becomes smoothed out as the wind speed increases, (Figure (3.5(c))). This set of curves again demonstrate how the flow regime and hence the heat transfer process rapidly become dominated by the main strain flow rather than that the secondary rotational flow.

To strengthen this view of main stream dominance a series of tests was made with the disc stationary in the transverse air flow. The sensor, when rotating, gives an average heat transfer coefficient h_R, over the circular path traversed. Thus for the stationary disc local heat transfer coefficients were measured at each radial position for five angular positions, 0, 45, 90, 135 and 180 degrees, 0 corresponding to the leading edge of the disc on the centre line of the wind tunnel. In this case it was found by a number of heat transfer measurements that the flow was symmetrical above and below the centre line of the wind tunnel. Thus only the top half of the disc was examined in any detail.

The results are presented in Figures (3.6(a),(b),(c)). These figures show at a particular location the values of the heat transfer coefficient and list for each radius the average coefficient defined as a straight average of the eight individual values. These average values are plotted

Fig 3.6 Heat Transfer Coefficients for Stationary Disc in Air Stream.

Average values over 360 deg.

R[cm]	U=7·8m/s	16·7	29·5
22·5	37·0	75·2	107·6
21·2	41·3	82·1	117·5
18·0	49·0	89·0	129·6
15·9	53·4	96·6	137·6
13·0	55·5	101·1	139·6
11·2	55·3	99·8	141·0
8·5	50·0	97·0	142·5

[$W/m^2 deg C$]

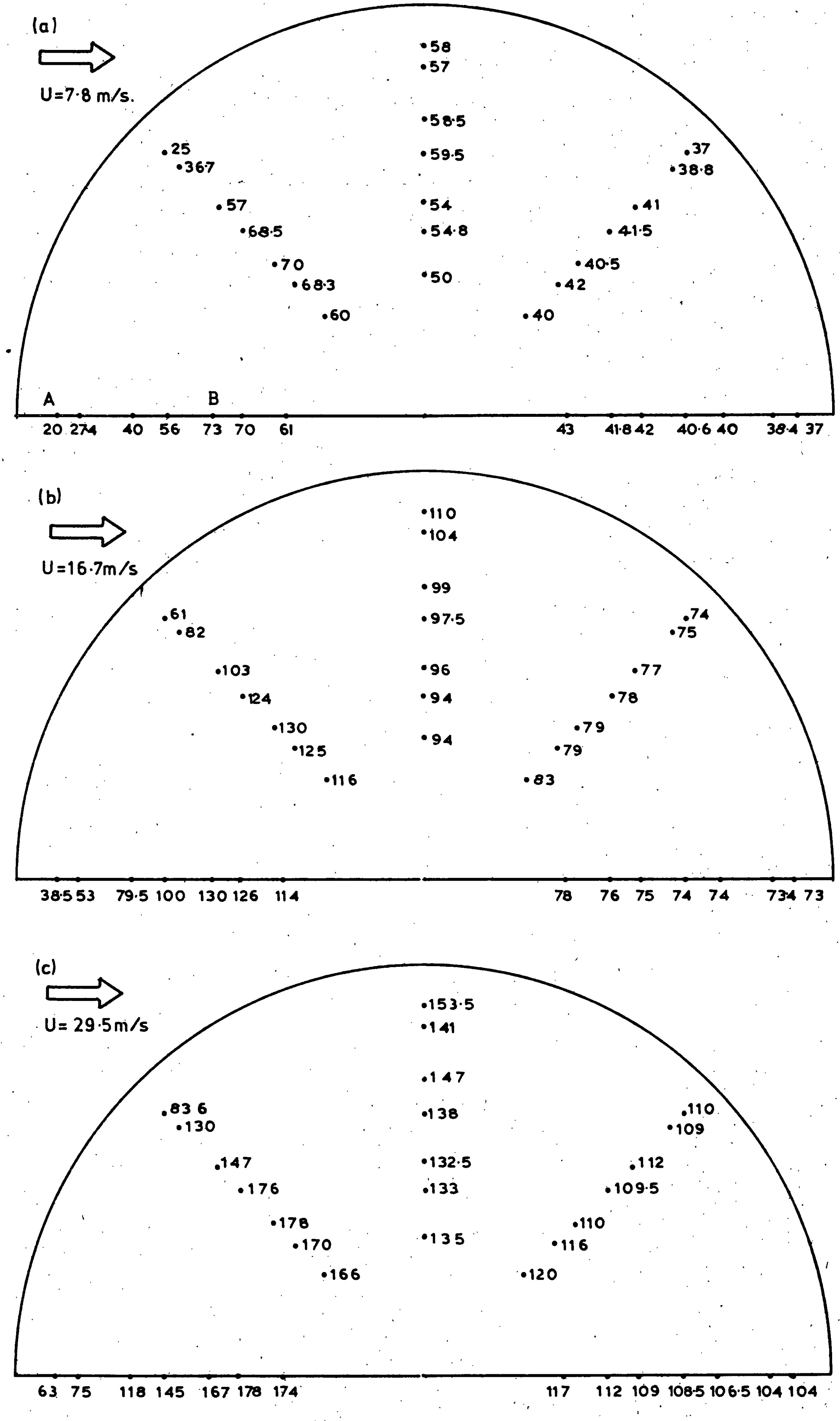

(a)
U=7·8 m/s.
58
57
58·5
59·5
54
54·8
50
25
36·7
57
68·5
70
68·3
60
37
38·8
41
41·5
40·5
42
40
A
B
20 27·4 40 56 73 70 61
43 41·8 42 40·6 40 38·4 37
(b)
U=16·7m/s
110
104
99
97·5
96
94
94
61
82
103
124
130
125
116
74
75
77
78
79
79
83
38·5 53 79·5 100 130 126 114
78 76 75 74 74 73·4 73
(c)
U= 29·5m/s
153·5
141
147
138
132·5
133
135
83 6
130
147
176
178
170
166
110
109
112
109·5
110
116
120
63 75 118 145 167 178 174
117 112 109 108·5 106·5 104 104

in Figure (3.7) and have superimposed the smooth curves taken from Figure (3.4), the rotating disc in a matched transverse air stream. This gives added weight to the view that the level of the heat transfer coefficient is determined by the main air flow with the rotation having a small second order effect.

The distribution of the individual heat transfer coefficients shown in Figures (3.6(a),(b),(c)) provides an explanation of the peak that occurs in the radial variation of the heat transfer coefficient. Referring to Figure (3.6(a)) the variation in h_c across the centre line of the wind tunnel is shown. Slightly downstream from the leading edge at point A , low heat transfer occurs. Proceeding across the disc the heat transfer first increases, reaching a maximum at point B , then slowly falls off towards the trailing edge. A pictorial summary of these areas of high and low heat transfer is shown in Figure (3.8).

The disc is thick, 5 cm., and presents a bluff face to the air stream. Flow separation at the leading edge with reattachment to the disc face at some point downstream is expected as illustrated by Figure (3.9). The heat transfer pattern is consistent with this flow, low heat transfer corresponding to the separation region and high heat transfer over the reattachment area. Beyond this area the decrease in heat transfer corresponds to the normal entry length situation. Referring to the rotating disc, the sensor gives an average value of the path it traverses. At the outer radii, see Figure (3.8), a large proportion of that path lies in the low heat transfer/separation region. At a medium radius a large proportion of the path lies in the first part of the reattachment with consequent high heat transfer. At smaller radii the path lies in regions where the heat transfer changes less rapidly.

3.4. Flow Visualisation Tests 1

To lend weight to the generalisation made earlier that the main flow

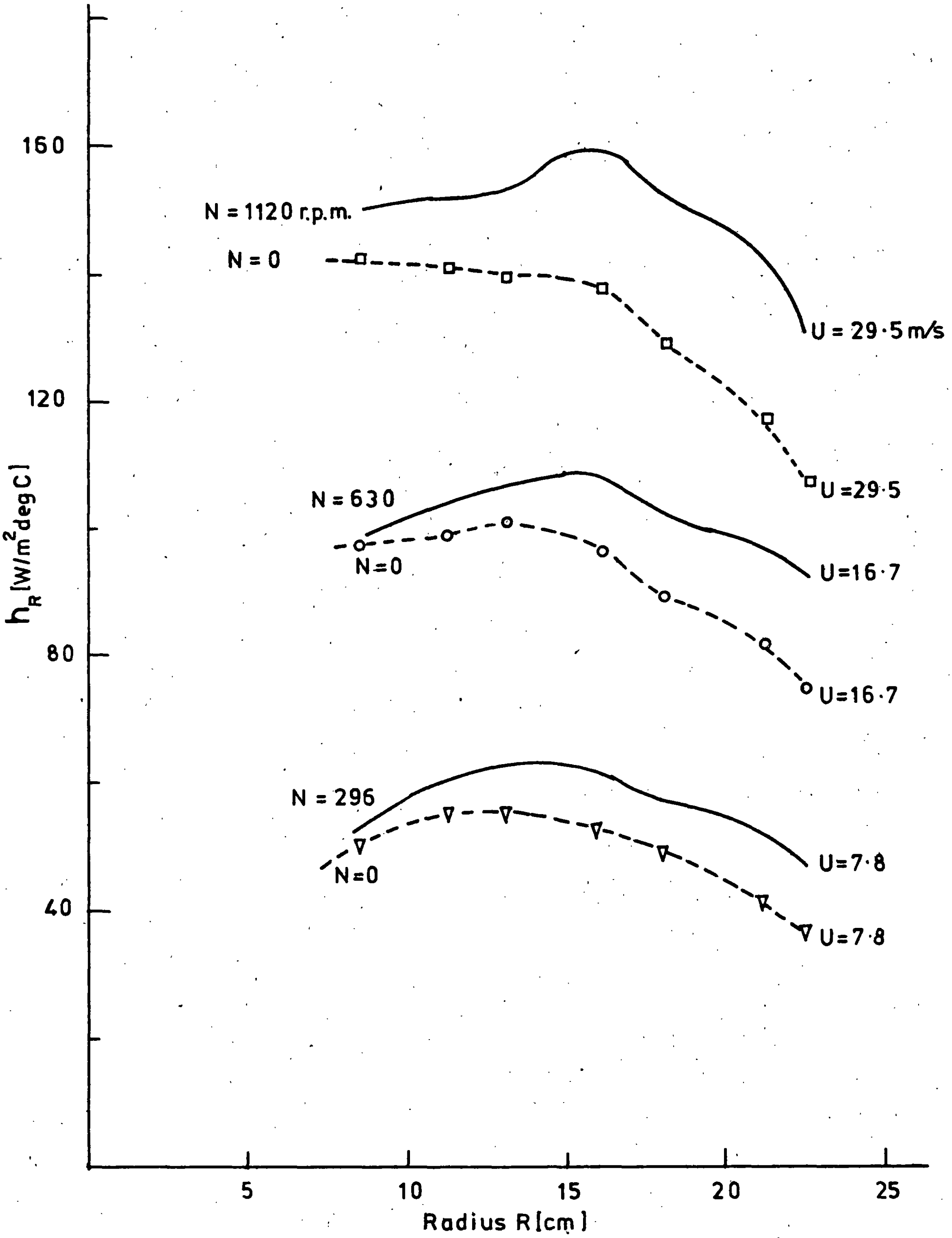

Fig 3·7 Effect of Disc Rotation.

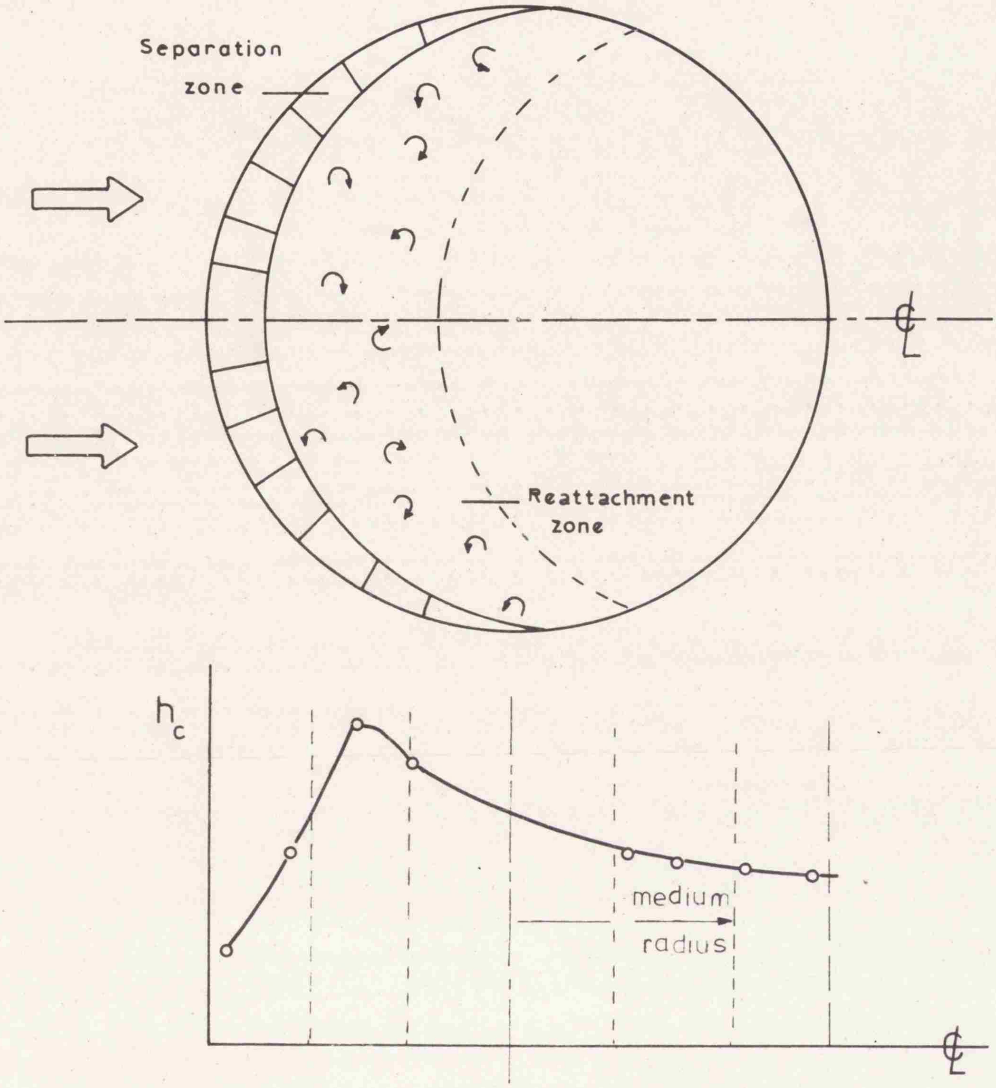

Fig 3.8 Variation of heat transfer across stationary disc

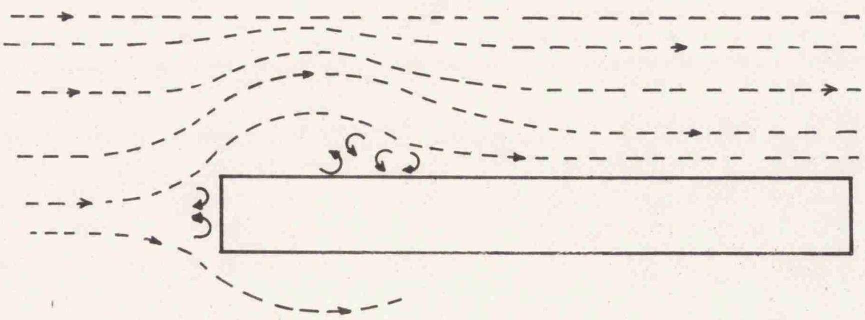

Fig 3·9

pattern dominates the heat transfer process rather than the rotation of the disc, simple flow visualisation tests were carried out.

A single smoke source was positioned slightly upstream of the disc and photographs taken of the resulting traces obtained for both disc stationary and rotating.

Figure (3.10) shows the smoke trace over the stationary disc with an air velocity of 11.5 m/s. Separation at the leading edge and reattachment further downstream can be seen. Figure (3.11) is a similar photograph but with the disc revolving at a matched speed of 436 r.p.m. There is no apparent change in flow.

Figures (3.12) and (3.13) are similar photographs but with the air velocity and disc peripheral velocity no longer matched. In this case the air velocity is low, 1.4 m/s, and the disc rotation higher, 630 r.p.m. Again no serious change in the flow pattern occurs, although the reattachment point does seem to be nearer the leading edge when the disc is revolving.

3.5. Disc Misalignment

To further assess the effect of separation and reattachment tests were done with the disc stationary about an axis which was not perpendicular to the main air flow direction. The shaft was aligned with its axis 2½ degrees from the normal direction. Figures (3.14(a)) and (3.14(b)) show the distribution of the heat transfer coefficient for the two misaligned positions (a) and (b). Figure (3.15) shows the distribution across the centre line of the wind tunnel. Position (c) refers to the case where the disc is properly aligned to the air stream. Tilting the instrumented disc surface away from the air flow, position (a), causes greater separation and consequently lower heat transfer at the leading edge region. Reattachment occurs further downstream than previously encountered, position (c), with slightly higher heat transfer coefficient at the trailing edge.

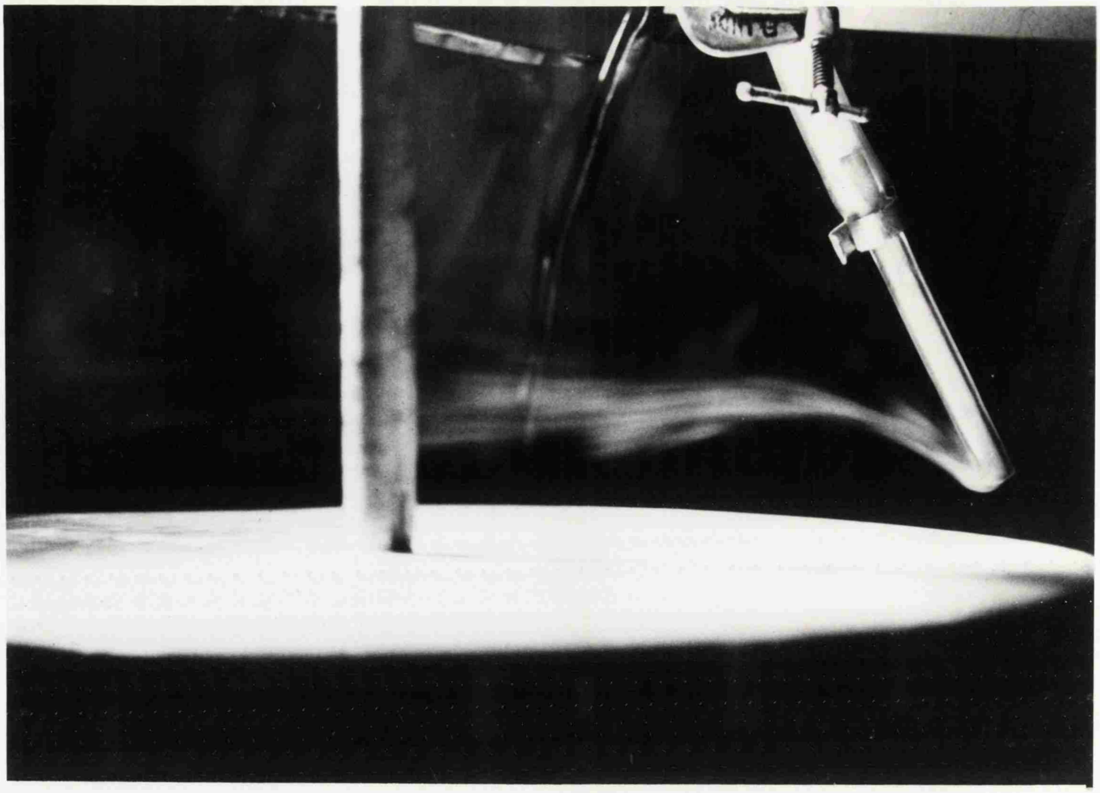

Fig 3·10 N=0 U=11·5 m/s

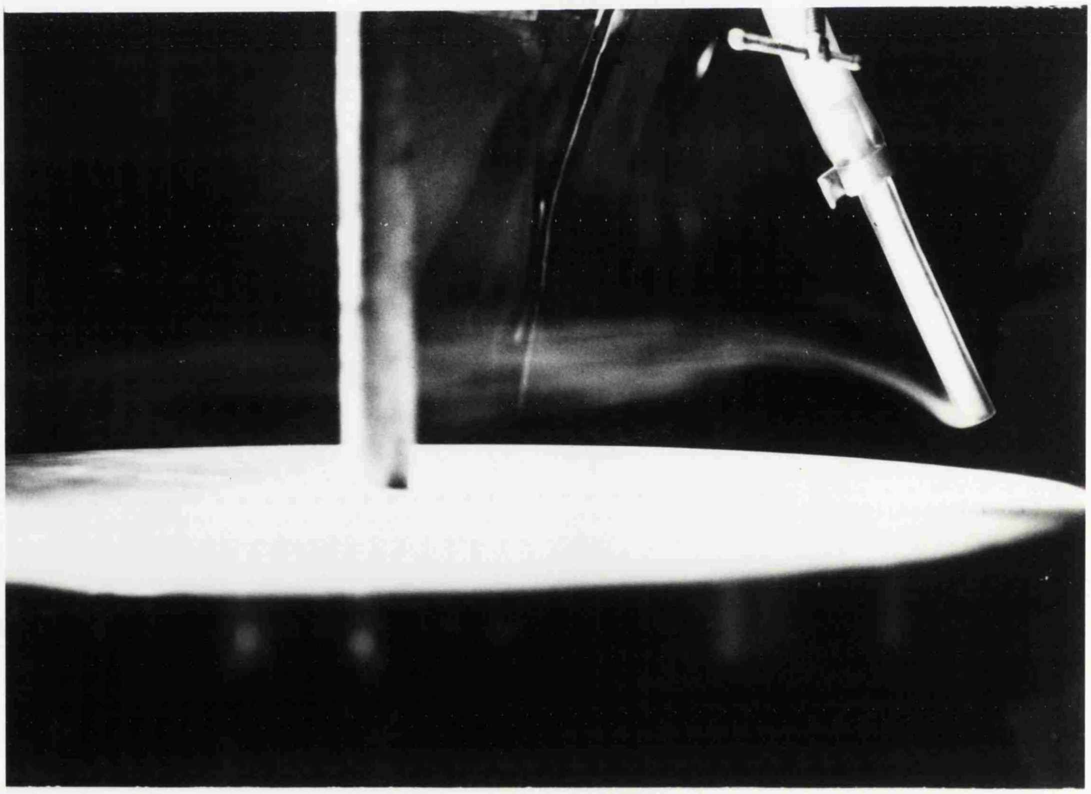

Fig 3·11 N=436rpm U=11·5 m/s

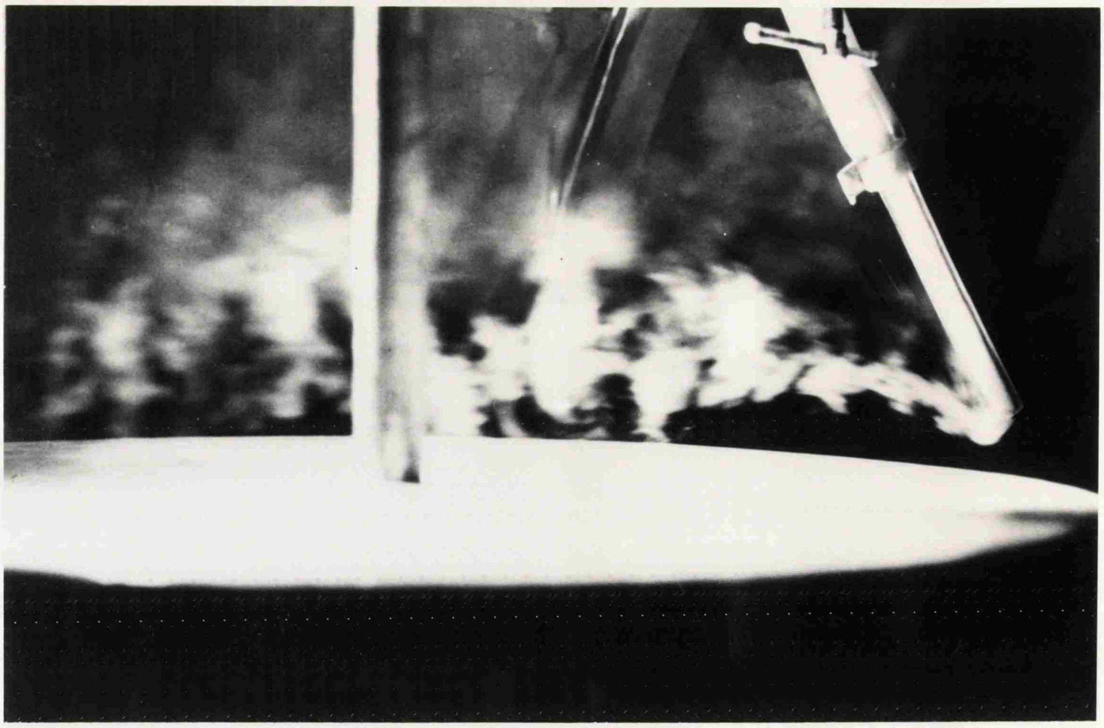

Fig 3·12 N=0 U=1·4 m/s

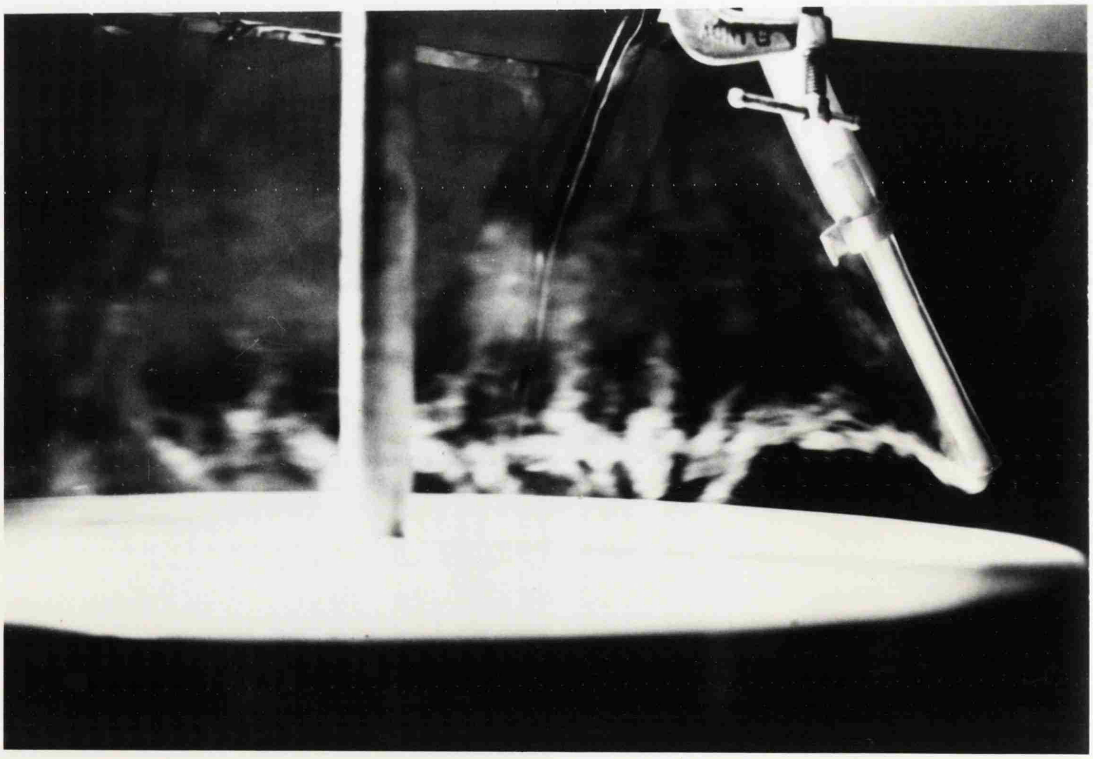

Fig 3·13 N=630rpm U=1·4 m/s

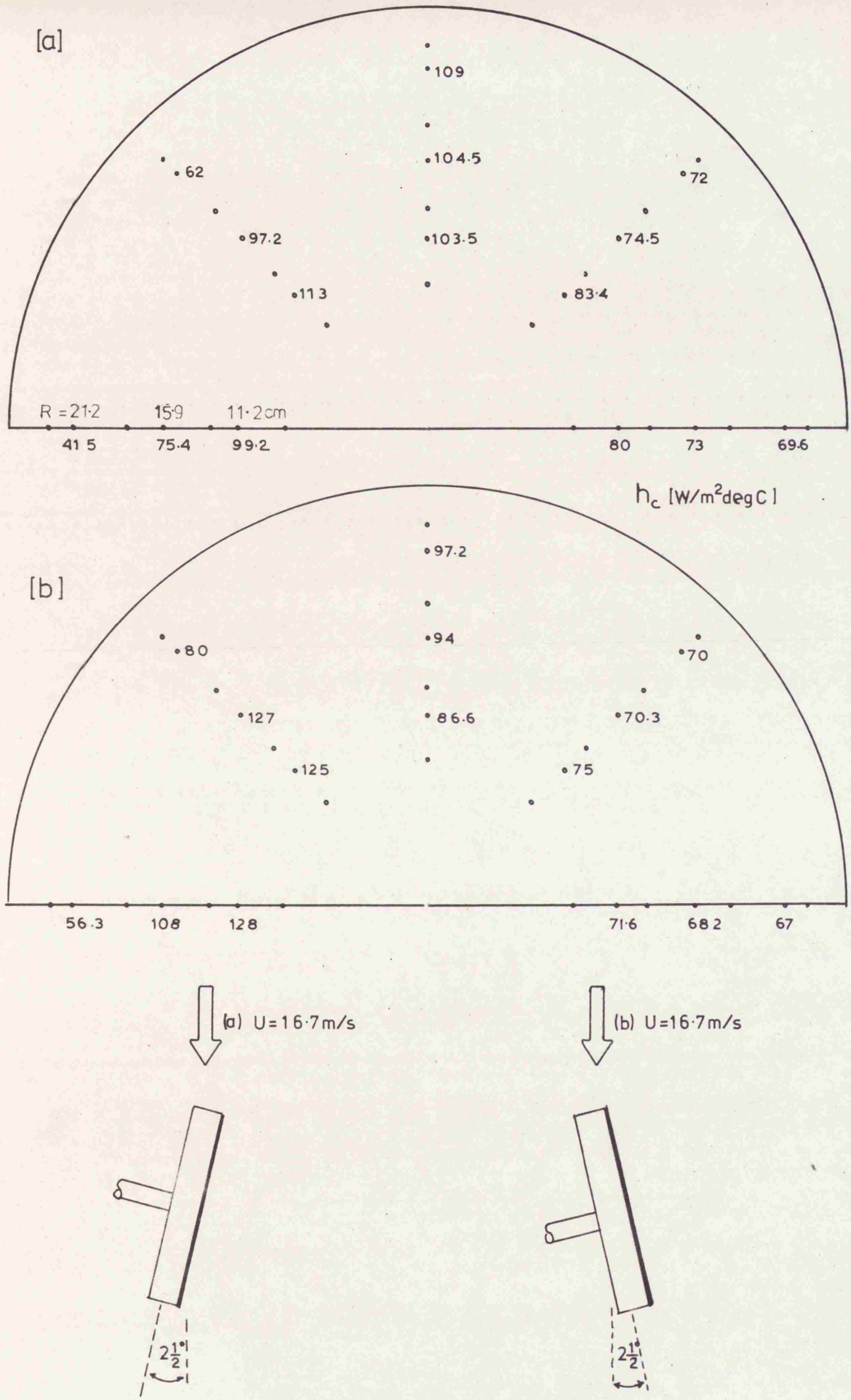

Fig 3.14 Effect of Misalignment on Heat transfer.

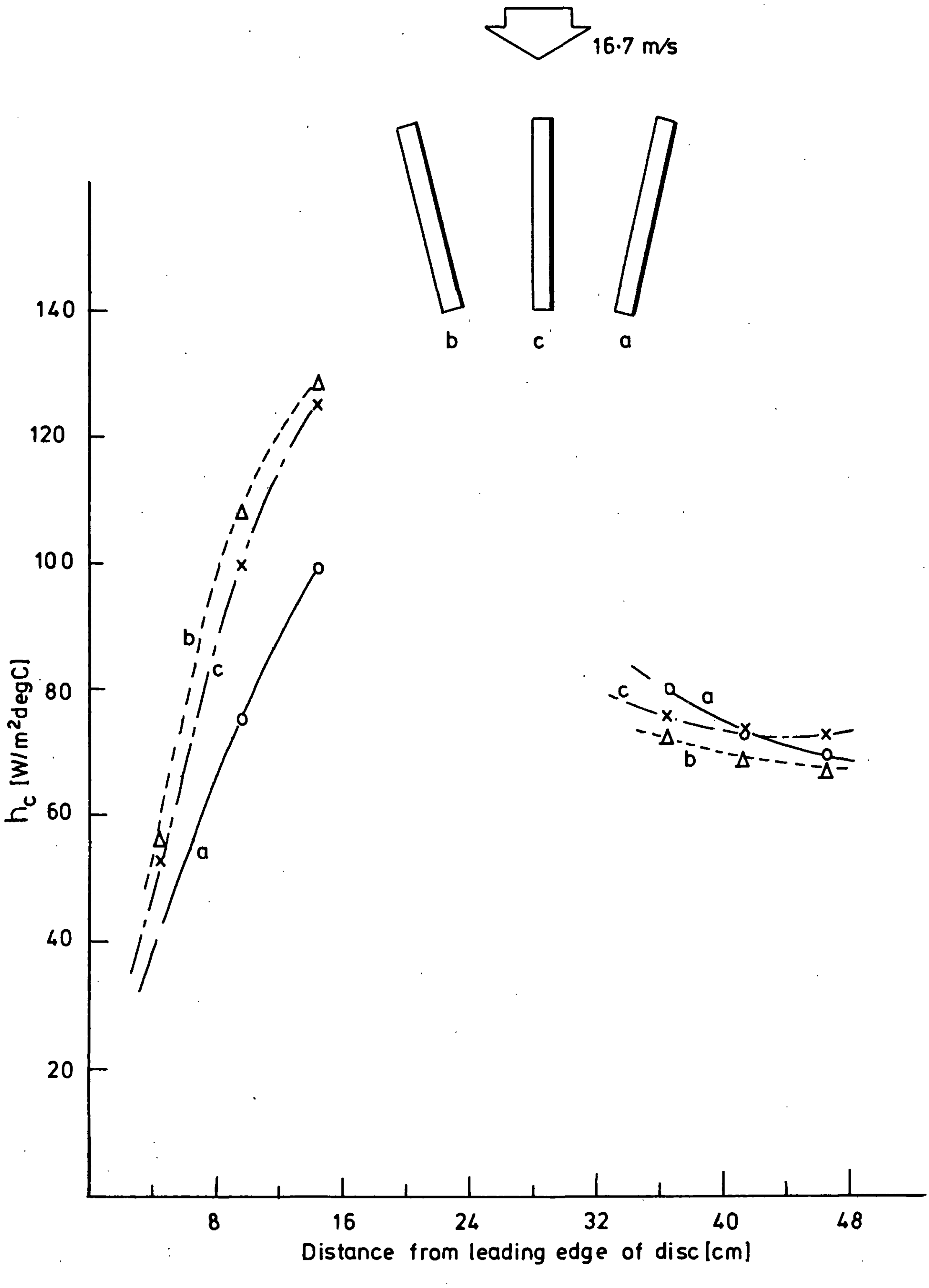

Fig 3·15 Effect of disc misalignment

Tilting the disc in the opposite direction, position (b), has the reverse effect. The separation and reattachment effects are clearly reduced.

3.6. Effect of Aspect Ratio

In Section 3.3 the radial variation of heat transfer is explained in terms of flow separation and reattachment. The experimental disc is a bluff body and the degree of separation is dependent on its aspect ratio (disc radius/disc thickness). To use the existing rig to simulate large aspect ratios an annular shroud of triangular cross section was held just upstream of the first half of the disc. This shroud could be positioned at any point across the width of the disc. The configuration is shown in Figure (3.16).

For three matched conditions, tests were repeated for a number of positions of the shroud. Figure (3.17) shows the radial heat transfer variations and Figure (3.18) an enlarged form of the variation for one matched condition.

At very large aspect ratios, (t small) the picture is consistent with the starting length for flow over a flat plate. Remembering the heat transfer coefficient h_R, is an average value over the path traversed, at larger radii. A large proportion of the path lies in the region of very high heat transfer coefficients. Coming into the centre more and more of the path lies in the region of lower, more slowly varying heat transfer coefficients. Thus the steady increase with radius. As the effective aspect ratio is decreased the radial pattern gradually changes (as the separation region grows,) to the peaked distribution discussed in Section 3.3.

Tests were also repeated with the disc held stationary in the transverse air flow and the shroud flush with disc. Figures (3.19(a),(b),(c)) show the resulting variations in heat transfer coefficient h_c for three wind speeds. The main stream domination and small secondary rotational

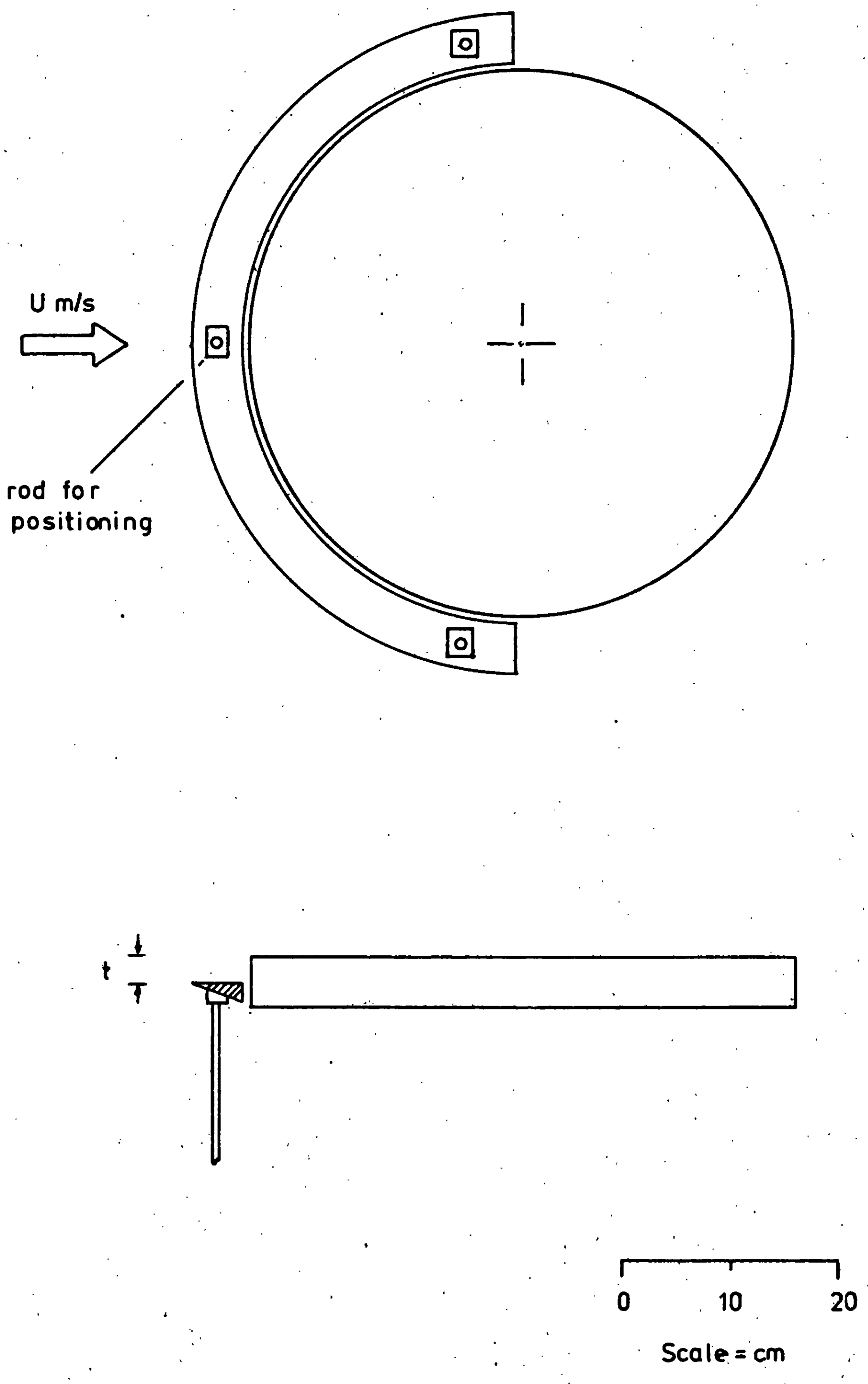

Fig 3·16 Shroud in position around disc

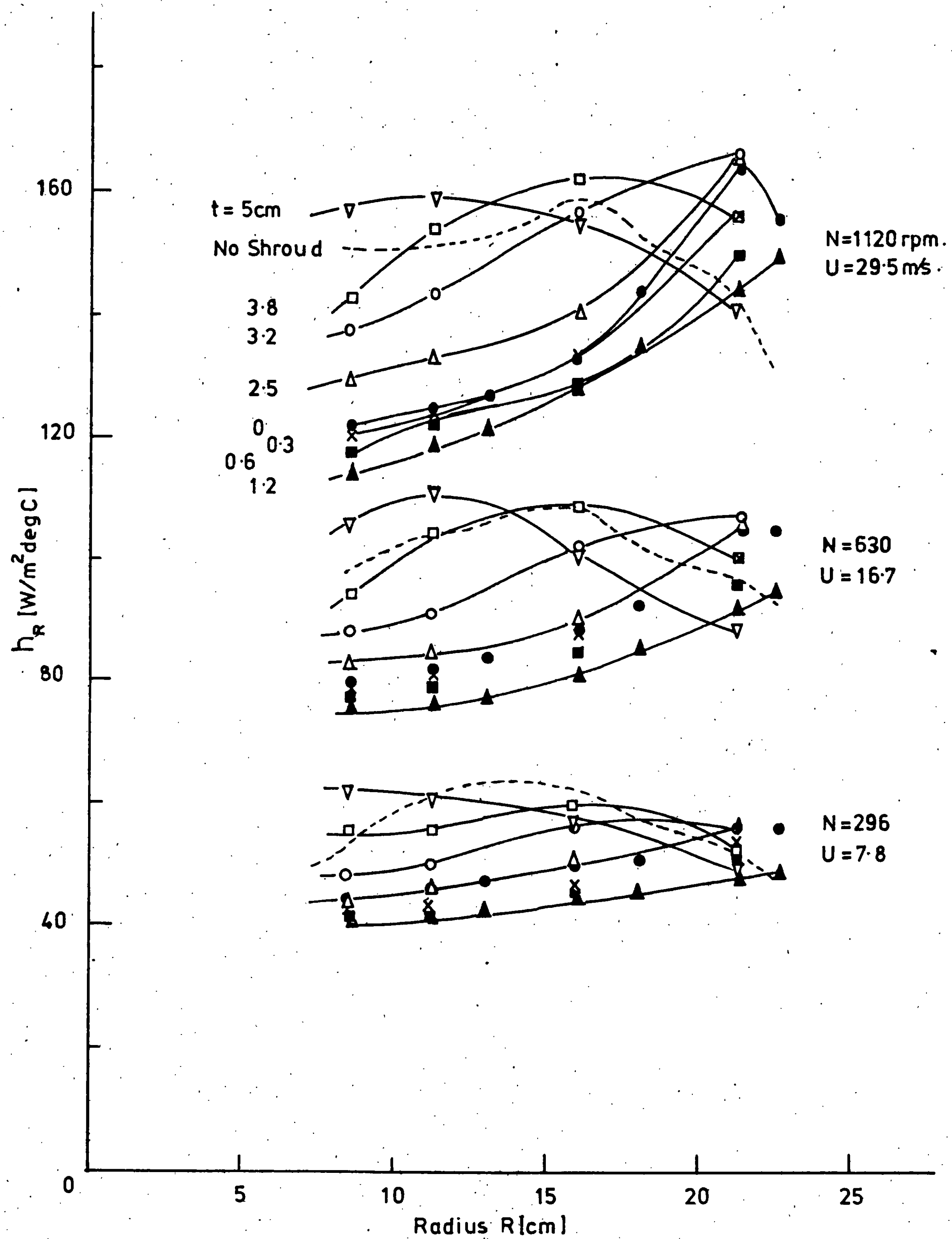

Fig 3·17 Effect of varying Aspect Ratio

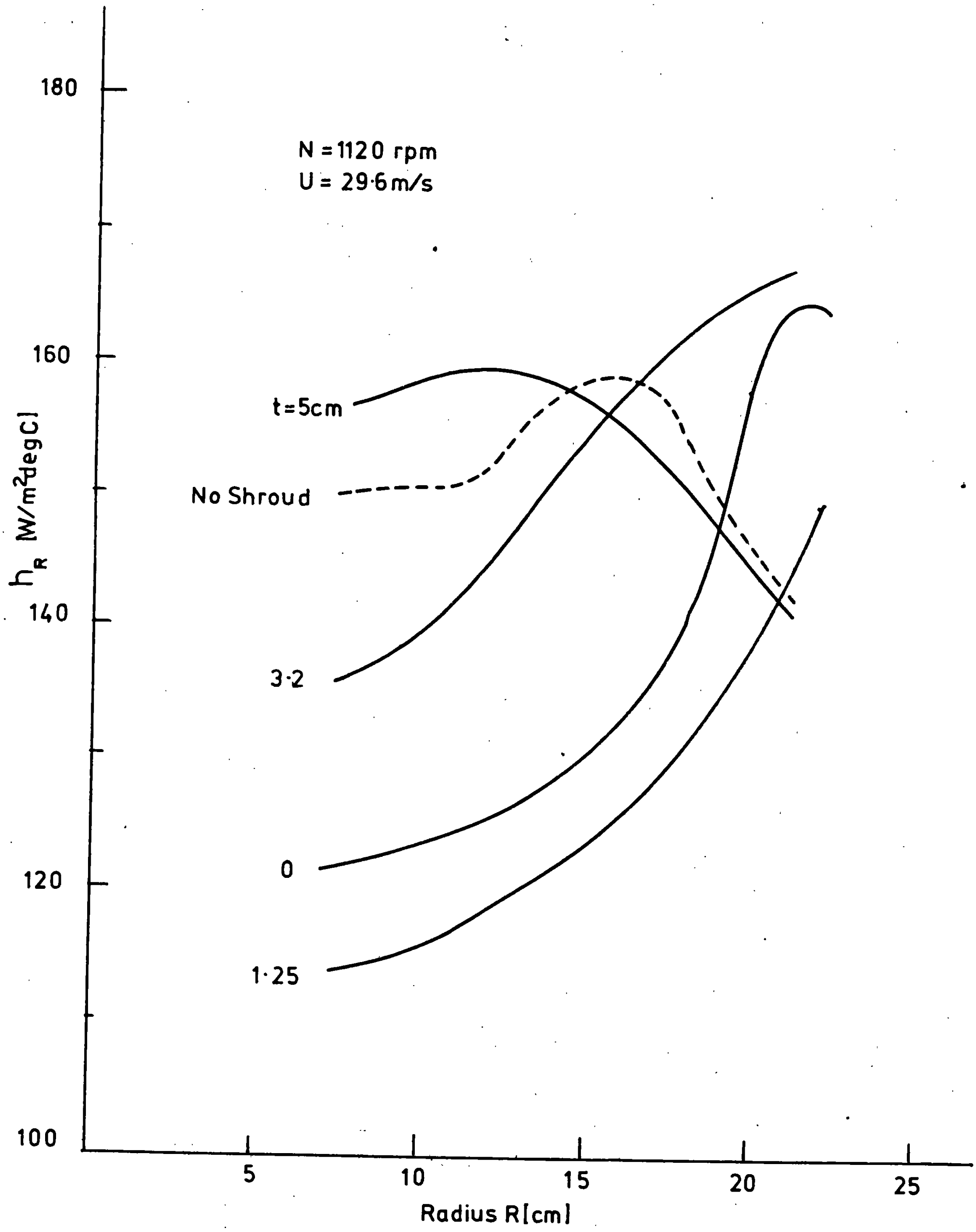
180
160
140
120
100
N = 1120 rpm
U = 29·6 m/s
t=5cm
No Shroud
3·2
0
1·25
h_R [W/m^{2}degC]
5
10
15
20
25
Radius R[cm]

Fig 3·18

Fig 3·19 Heat Transfer Coefficients for Stationary Disc in Air Stream.

Shroud set at $t=0$

Average values over 360 deg.

R[cm]	U=7·8 m/s	16·7	29·5
22·5	55·5	100·5	145·3
21·2	54·3	98·1	142·3
18·0	49·4	88·3	132·3
15·9	46·7	82·2	123·1
13·0	43·1	78·0	114·5
11·2	42·6	77·1	115·1
8·5	41·6	76·0	113·3

[W/m^{2}degC]

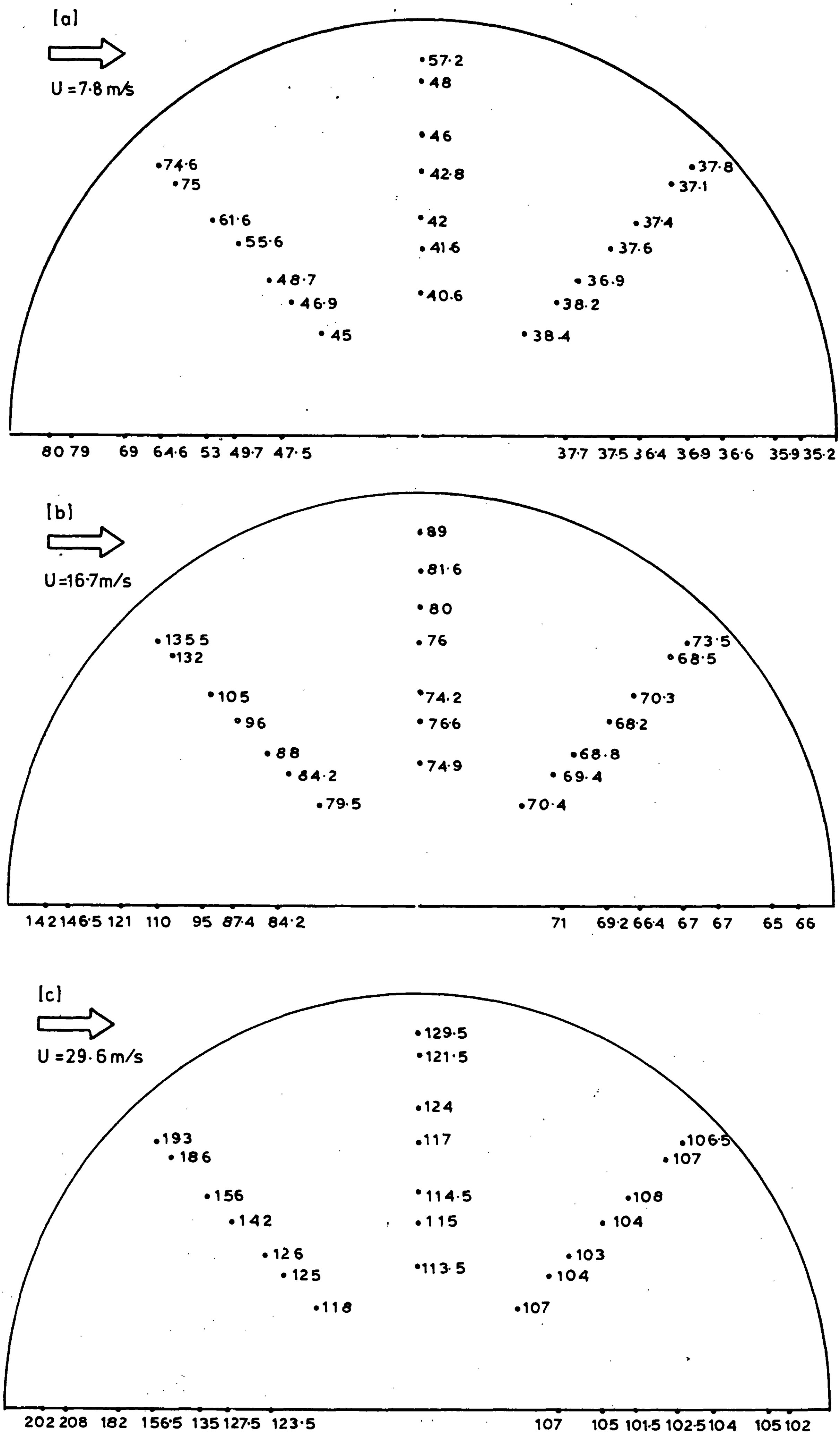

(a)
U = 7·8 m/s
57·2
48
46
42·8
42
41·6
40·6
74·6
75
61·6
55·6
48·7
46·9
45
37·8
37·1
37·4
37·6
36·9
38·2
38·4
80 79 69 64·6 53 49·7 47·5
37·7 37·5 36·4 36·9 36·6 35·9 35·2
(b)
U = 16·7 m/s
89
81·6
80
76
74·2
76·6
74·9
135·5
132
105
96
88
84·2
79·5
73·5
68·5
70·3
68·2
68·8
69·4
70·4
142 146·5 121 110 95 87·4 84·2
71 69·2 66·4 67 67 65 66
(c)
U = 29·6 m/s
129·5
121·5
124
117
114·5
115
113·5
193
186
156
142
126
125
118
106·5
107
108
104
103
104
107
202 208 182 156·5 135 127·5 123·5
107 105 101·5 102·5 104 105 102

effect can be seen from Figure (3.20) where, in a similar fashion to Section 3.3., a straight average of the eight individual positions is taken and compared with the rotational average values of Figure (3.17).

Figure (3.21) shows the variation in heat transfer coefficient across the 0 - 180 degree diameter of the disc when it is held stationary in the air flow. With the shroud flush to the disc face the variation of heat transfer coefficients resembles that from a flat plate. High heat transfer coefficients are present at the leading edge which rapidly fall down to the normal variation. Without the shroud the regions of separation and reattachment are evident. Further downstream the flow settles down to the normal flat plate variation.

3.7. Flow Visualisation Tests 2.

Smoke flow visualisation tests were carried out with the shrouded disc in a similar manner to those of Section 3.4. The disc was kept stationary and the wind speed set at 5 m/s. Figures (3.22(a),(b),(c),(d)) indicate the shroud is a fair simulation of discs of different aspect ratios. However in Figure (3.22(a)), with the face of the shroud set flush with the front face of the disc there is a small separation zone caused by the shroud itself. Complete attachment of the flow over the whole of the disc face occurs when the shroud is set back 1.25 cm as in Figure (3.22(b)). This accounts for the initial drop in heat transfer coefficients as the set back t increases from zero, Figure (3.18).

The approach flow is laminar and all the flow conditions around the disc are a result of the presence of the disc. These flow conditions were studied using an acoustic stethoscope. Typical noise patterns are shown in Figures (3.23(a),(b)). The laminar nature of the approach flow was confirmed by the relative silence in the main air stream. With the shroud set back, as in Figure (3.23(a)), a low level of noise was heard at A in contrast to a high pitch 'scream' in region B where the flow rapidly accelerates

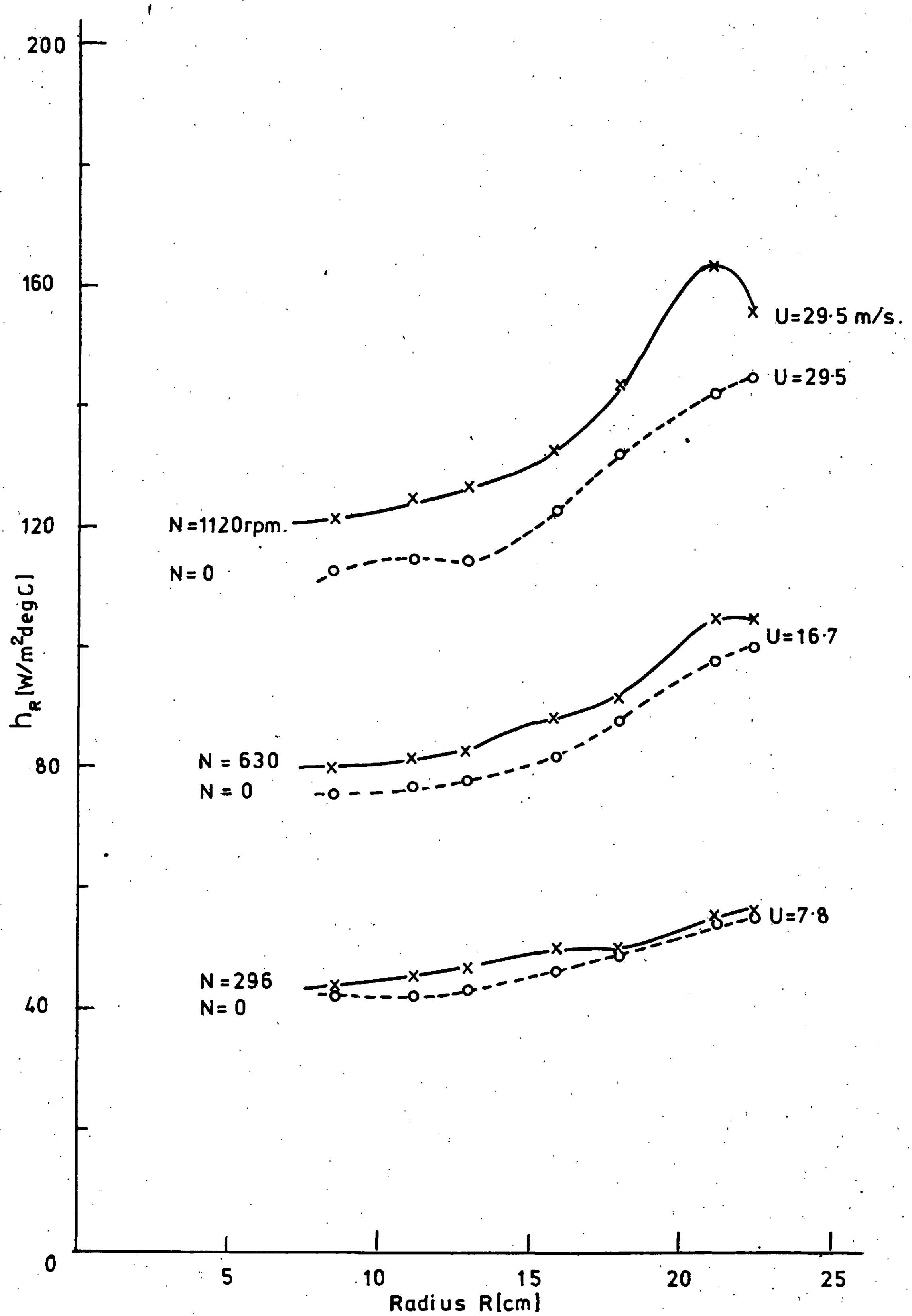

Fig 3·20 Effect of Disc Rotation. Shroud positioned at $\dot{t}$=0

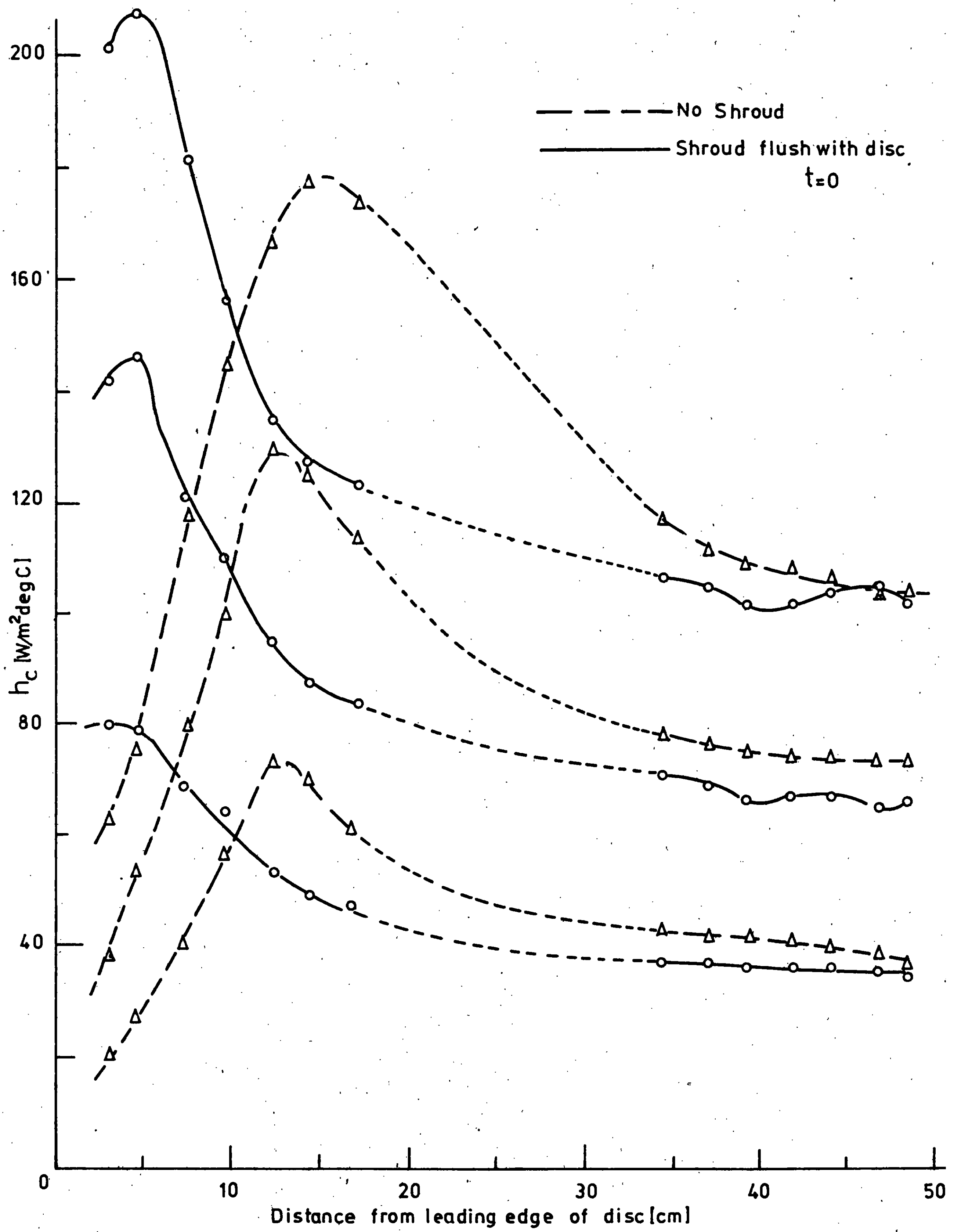

Fig 3·21 Heat transfer across face of stationary disc

Fig 3·22(a) t=0

Fig 3·22(b) t=1·25cm

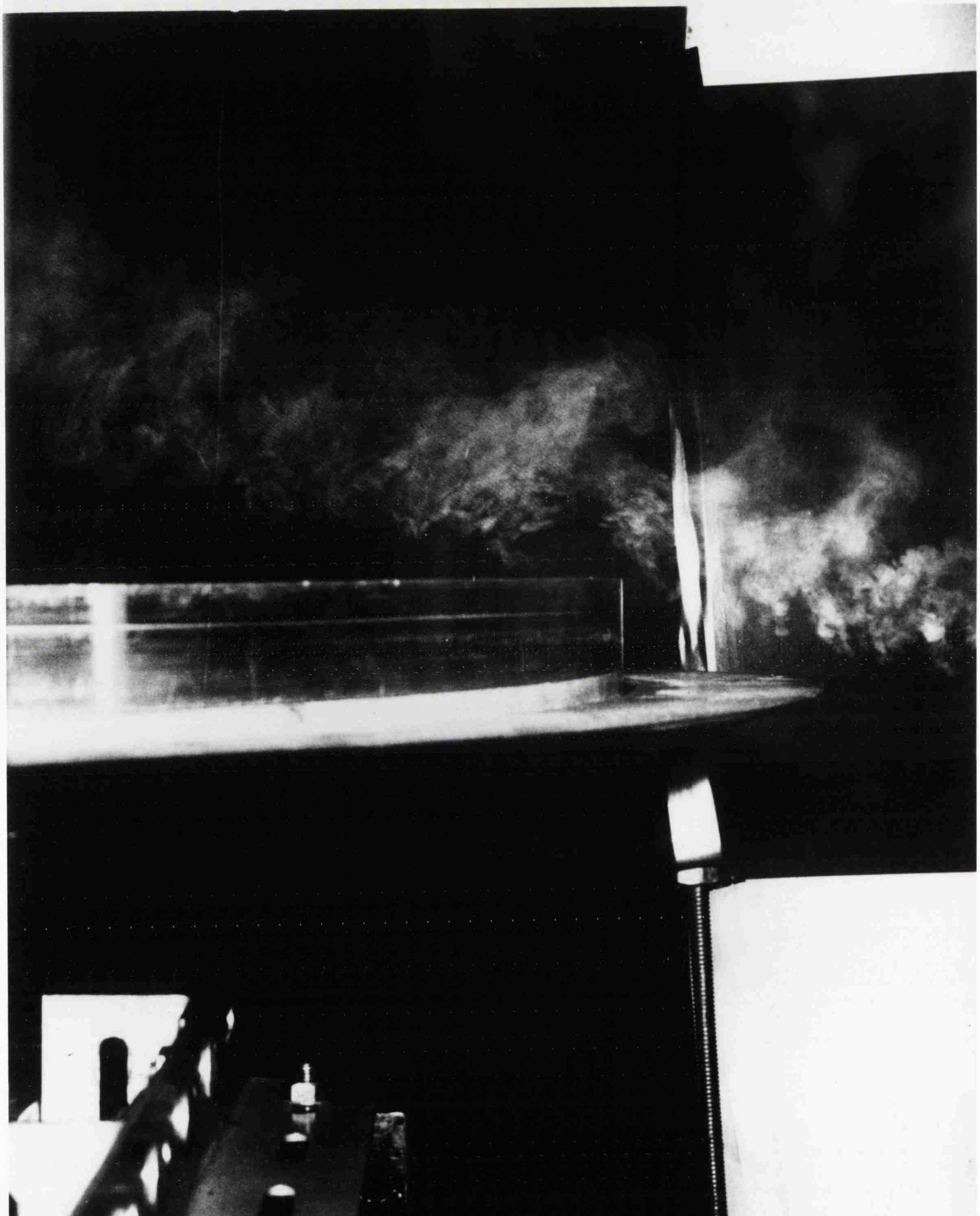

Fig 3·22c t=3cm

Fig 3·22 d t= 5 cm

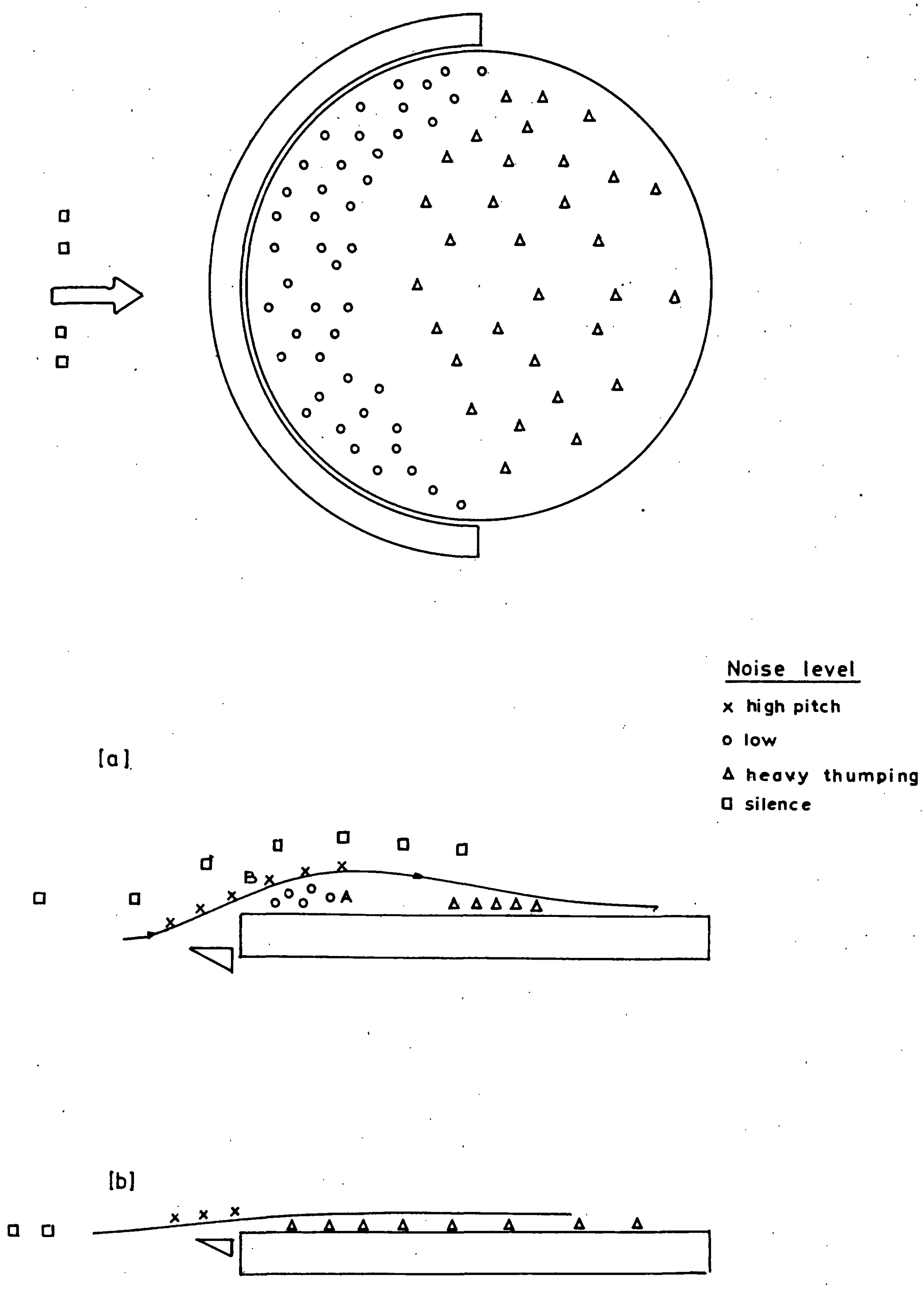

Fig 3·23 Acoustic measurements

over the disc. A heavy thumping noise could be heard over the remaining parts of the disc surface. This turbulent noise was observed over the disc throughout the wind speed range 7.8 - 33 m/s despite the continual silence in the main air stream. With the shroud set at 1.25 cm. the heavy thumping noise was recorded over the entire surface of the disc, Figure (3.23(b)). Over the shroud itself a narrow region of high pitch noise was also recorded.

In addition to confirming the general nature of the flow pattern the acoustic soundings provide an explanation of the dominance of the main air stream. They show the flow to be turbulent over the whole surface of the disc. This is due to both shroud and disc leading edge which act as turbulent promoters in the laminar flow field. The resulting heat transfer by the turbulent motion dominates the cooling process and the disc rotation modifies this turbulence very little.

3.8. Correlation of Data

The heat transfer coefficient h_R, from a rotating disc in a transverse air stream is a function of eight parameters, i.e.

$$h_R = f(\rho, C_p, k, \mu, U, N, R, t).$$

NB. t = shroud setting

In non dimensional terms it can be shown that

$$Nu = f_1(Re, Re_o, t/R_o, Pr)$$

where Re_o is the main stream Reynolds number based on the radius of the disc $= \frac{UR_o}{\nu}$. Since tests are with a single fluid Pr will remain constant.

A requirement for the application of dimensional analysis is that geometrical similarity holds. Changes in the parameter, t, cause changes in the geometry and certainly it has been seen from smoke tests that it causes changes in the flow distribution. Radical changes in the form of the radial heat transfer coefficient variation with change in 't', as opposed to the changes from one speed to another can be seen in Figure (3.17). This suggests that attempts to obtain correlations including this parameter are likely to be extremely difficult if not fruitless.

The variation in the heat transfer coefficient, h_R, has been shown to be dependent on the main stream velocity U; the rotation N, in the main causing a small upward perturbation. However at low wind speeds and higher rotational speeds the pattern is clearly affected by the transition to turbulent flow. Including the unmatched conditions in the correlation would also be extremely difficult. So the following examination is restricted to the matched conditions only.

The shroud was set back at t = 1.25 cm, the position for minimum separation, and the heat transfer coefficient h_R, measured for five matched conditions at seven radial positions. The results are plotted in Figure (3.24). The results are also presented in non-dimensional form in Figure (3.25), where the Nusselt number $Nu = \frac{h_R R}{k}$ is plotted against the rotational Reynolds number $Re = \frac{NR^2}{\nu}$. In this instance $U = NR_o$. A series of curves are obtained which are as ymptotic to one line. The main stream dominance may be gauged by comparison with equations (3.2)and(3.3), corresponding to the laminar and turbulent heat transfer from a rotating disc in still air.

The results can be further described by condensing each curve on to one common line. Experience suggests this line has the form

$$Nu = CRe^m \left(\frac{R}{R_o}\right)^P \tag{3.5}$$

To evaluate the constant P, the Nusselt number is plotted against R/R_o for the five matched speeds at values of constant Re as in Figure (3.26). P is determined from the slope of the lines as - 0.43.

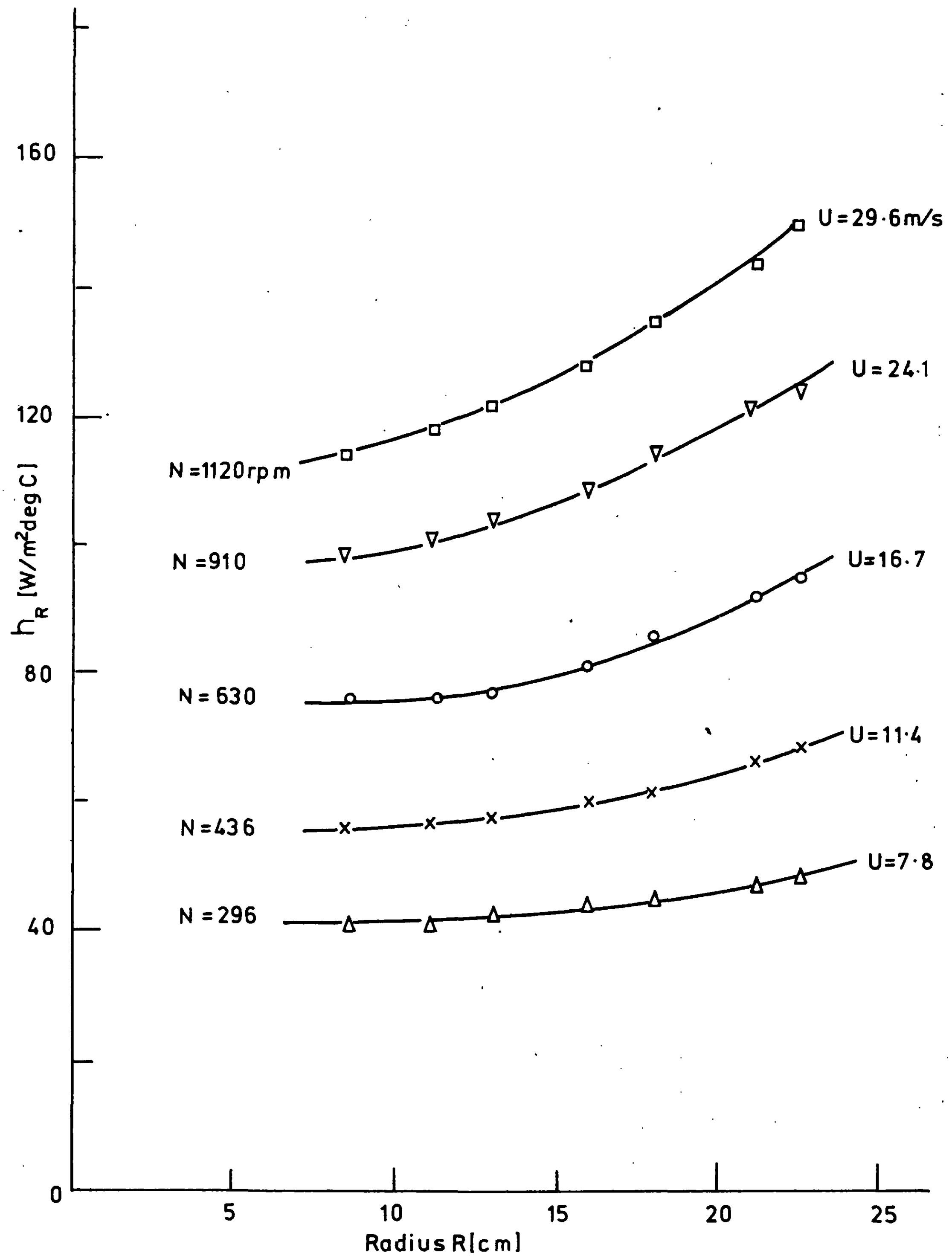

Fig 3·24 Rotating Disc in Matched Air Stream [Shroud at t=1·25cm]

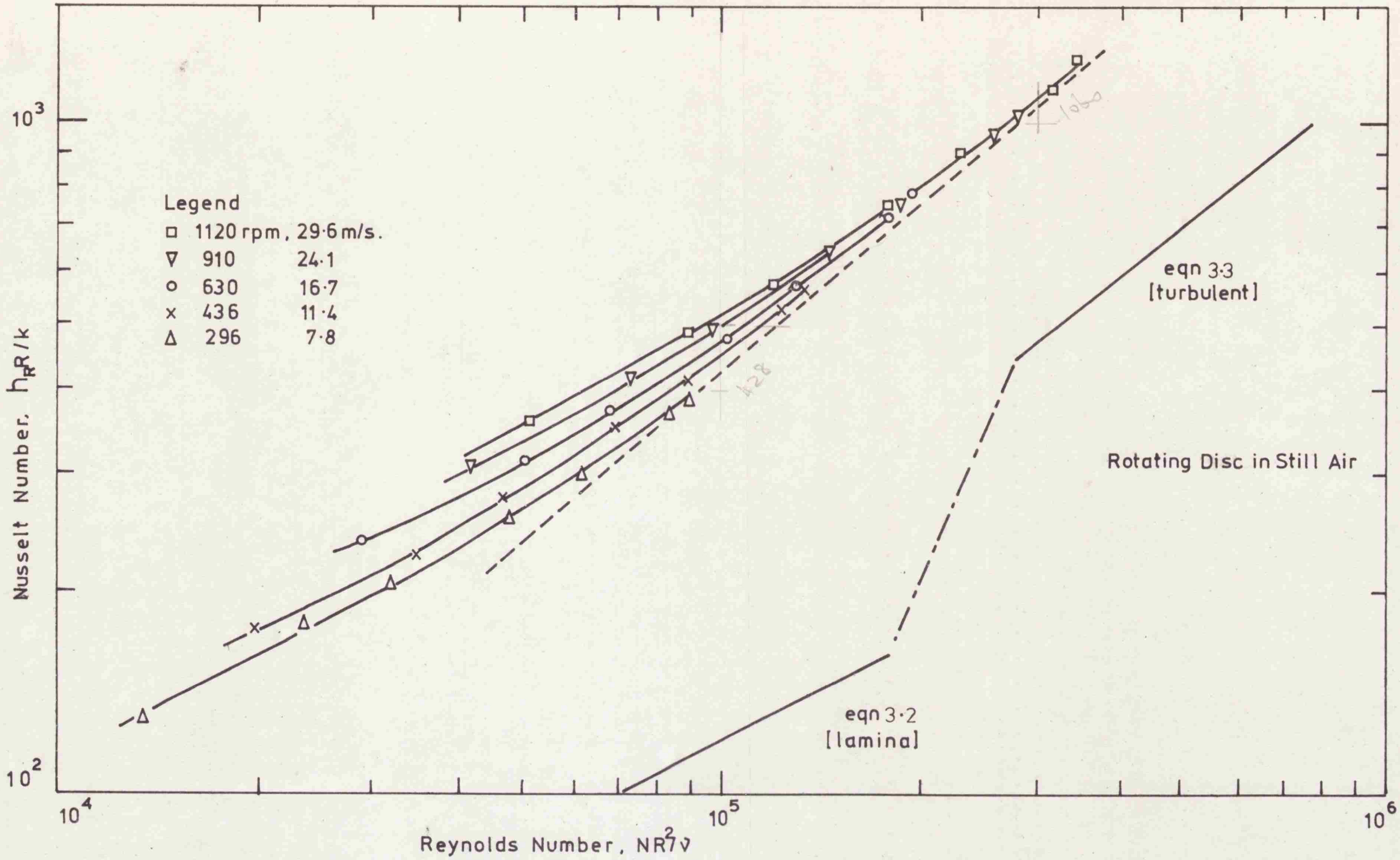

Fig 3.25 Rotating Disc in Matched Air Stream [shroud at t=1·25cm] —Dimensionless Plot

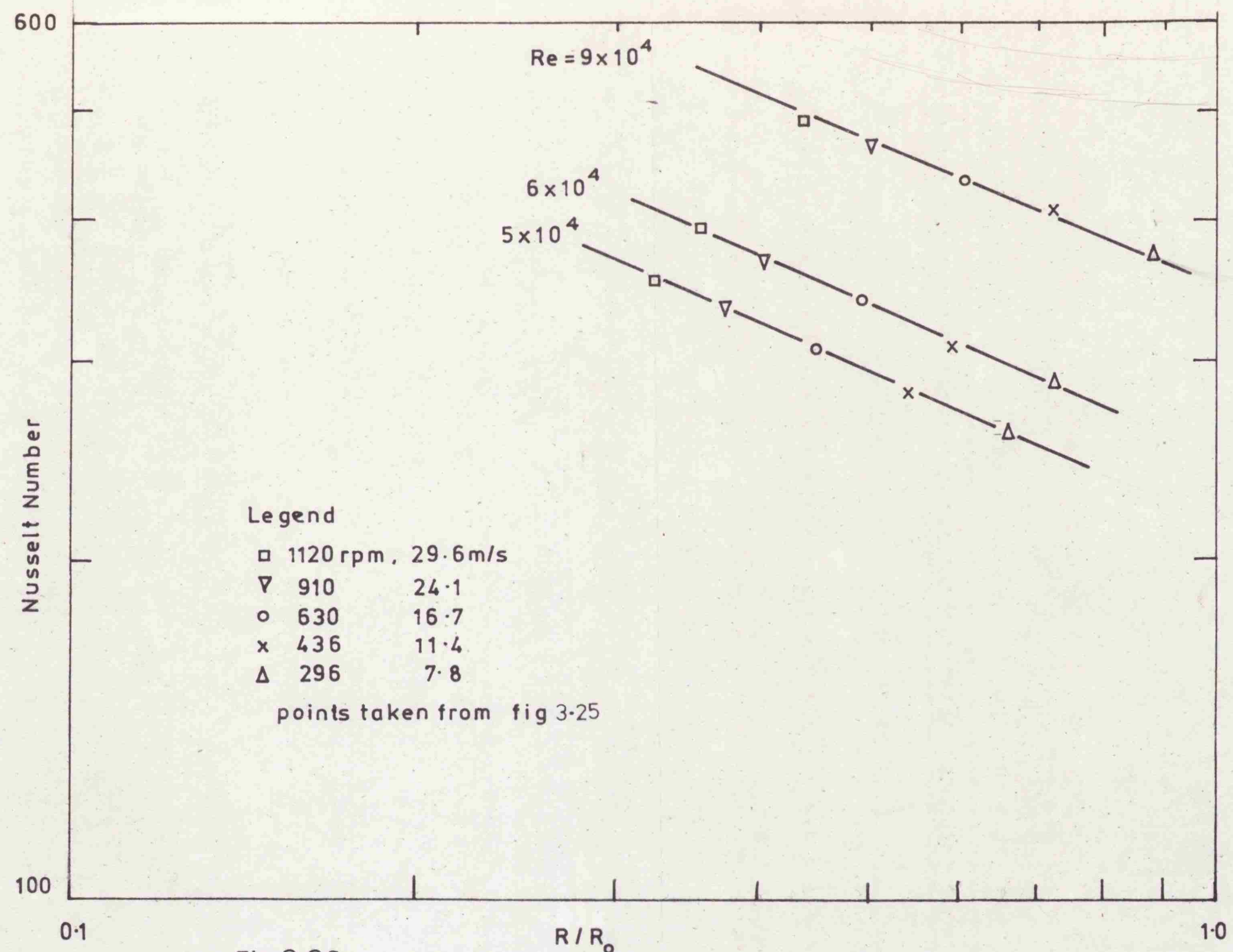

Fig 3·26

Larger need look like this

Figure (3.27) is a non dimensional plot of $Nu\left(\frac{R}{R_o}\right)^{0.43}$ versus Re. The points lie close to a straight line, the equation of which is determined as

$$Nu = 0.0287\ Re^{0.83}\left(\frac{R}{R_o}\right)^{-0.43} \tag{3.6}$$

This equation can be compared with the turbulent heat transfer equation for a flat stationary disc. Firstly it is necessary to reduce the radial heat transfer coefficients to an average value, $\bar{h}_c$, for the whole disc. From equation (1.6)

$$\bar{h}_c = \frac{1}{\pi R_o^{\,2}}\int_o^{R_o} h_R\ 2\pi R\ dR.$$

so that the average Nusselt number, $\overline{Nu}$, obtained from equation (3.5) is

$$\overline{Nu} = \frac{\bar{h}_c R_o}{k} = 0.0258\ Re_o^{0.83} \tag{3.7}$$

It is assumed that the flow is turbulent over the whole of the disc, This is confirmed by the acoustic soundings mentioned in Section 3.5.

For a plate under turbulent conditions the average heat transfer over a length L is given by[11]

$$\overline{Nu}_L = \frac{\bar{h}_c L}{k} = 0.036\ Pr^{1/3}\ Re_L^{0.8} \tag{3.8}$$

so that $\bar{h}_c = DL^{-0.2}$, where $D = 0.0326\ k\left(\frac{u}{\nu}\right)^{0.8}$ for $Pr = 0.72$.

Considering a thin element dx of the disc, a distance x from the origin, as in Figure (3.28). The heat transfer per unit temperature drop from the disc is equal to $DL^{0.8}$ dx. But from Figure (3.28) $L = 2(R_o^2-x^2)^{\frac{1}{2}}$, so that the equation becomes

$$\frac{Q_c}{\Delta T} = D \times 2^{0.8}\ (R_o^2 - x^2)^{0.4}\ dx.$$

Thus
$$\bar{h}_c = \frac{D \times 2 \times 2^{0.8}\ R_o^{0.8}}{\pi R_o^2}\int_o^{R_o}\left(1 - \frac{x^2}{R_o^2}\right)^{0.4} dx.$$

which converges slowly to $\frac{0.8191 \times D \times 2 \times 2^{0.8}}{\pi R_o}$

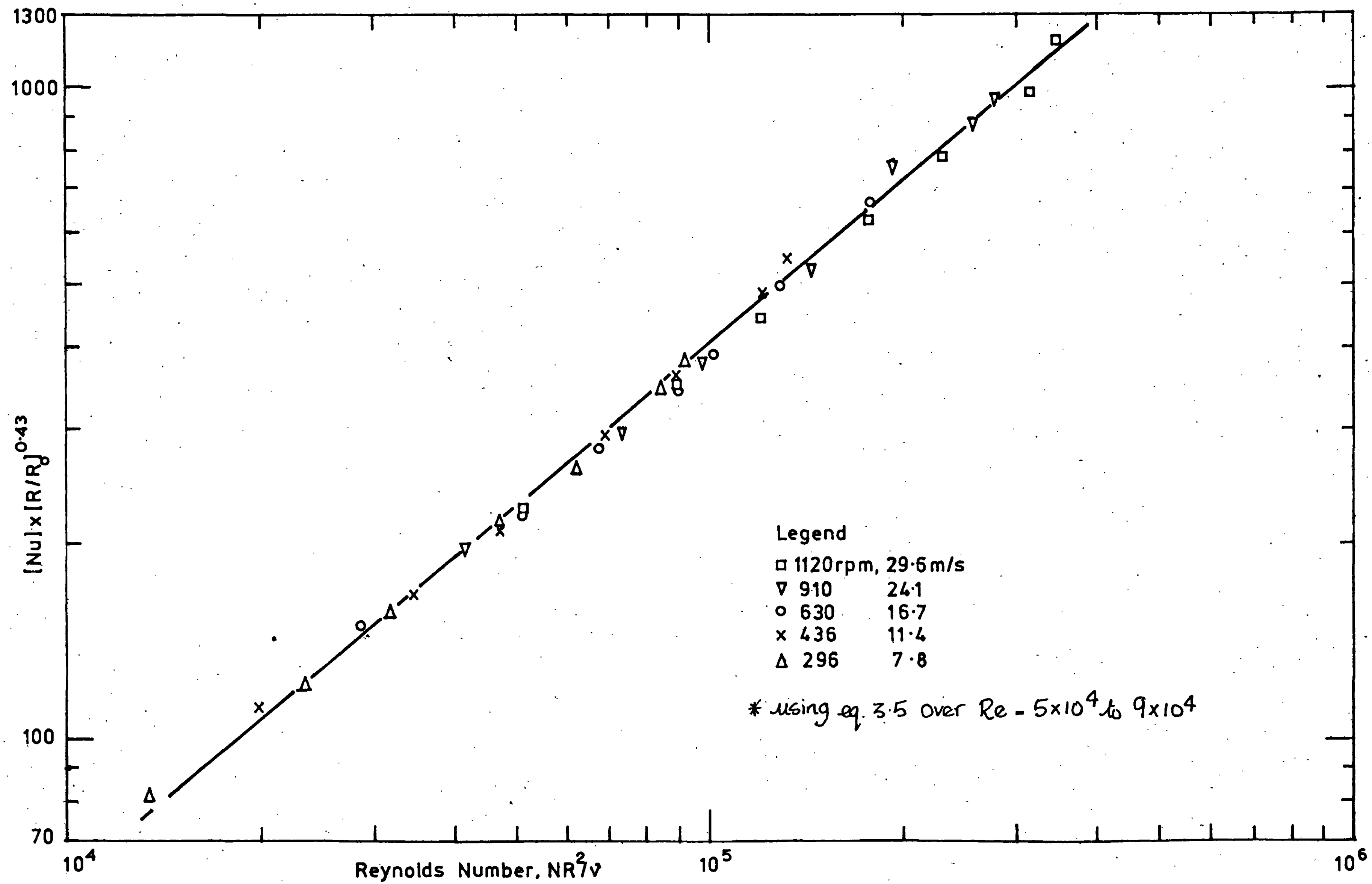

Fig 3·27 Rotating Disc in Matched Air Stream [shroud at t=1·25cm] - Dimensionless Plot

Figure (3.27) is a non dimensional plot of $Nu\left(\frac{R}{R_o}\right)^{0.43}$ versus Re. The points lie close to a straight line, the equation of which is determined as

$$Nu = 0.0287\ Re^{0.83}\left(\frac{R}{R_o}\right)^{-0.43} \qquad (3.6)$$

This equation can be compared with the turbulent heat transfer equation for a flat stationary disc. Firstly it is necessary to reduce the radial heat transfer coefficients to an average value, $\bar{h}_c$, for the whole disc. From equation (1.6)

$$\bar{h}_c = \frac{1}{\pi R_o^{\,2}} \int_o^{R_o} h_R\ 2\pi R\ dR.$$

so that the average Nusselt number, $\overline{Nu}$, obtained from equation (3.5) is

$$\overline{Nu} = \frac{\bar{h}_c R_o}{k} = 0.0258\ Re_o^{0.83} \qquad (3.7)$$

It is assumed that the flow is turbulent over the whole of the disc, This is confirmed by the acoustic soundings mentioned in Section 3.5.

For a plate under turbulent conditions the average heat transfer over a length L is given by[11]

$$\overline{Nu}_L = \frac{\bar{h}_c L}{k} = 0.036\ Pr^{1/3}\ Re_L^{0.8} \qquad (3.8)$$

so that $\bar{h}_c = DL^{-0.2}$, where $D = 0.0326\ k\left(\frac{u}{\nu}\right)^{0.8}$ for $Pr = 0.72$.

Considering a thin element dx of the disc, a distance x from the origin, as in Figure (3.28). The heat transfer per unit temperature drop from the disc is equal to $DL^{0.8}$ dx. But from Figure (3.28) $L = 2(R_o^2 - x^2)^{\frac{1}{2}}$, so that the equation becomes

$$\frac{Q_c}{\Delta T} = D \times 2^{0.8}\ (R_o^2 - x^2)^{0.4}\ dx.$$

Thus

$$\bar{h}_c = \frac{D \times 2 \times 2^{0.8}\ R_o^{0.8}}{\pi R_o^2} \int_o^{R_o} \left(1 - \frac{x^2}{R_o^2}\right)^{0.4} dx.$$

which converges slowly to $\dfrac{0.8191 \times D \times 2 \times 2^{0.8}}{\pi R_o}$

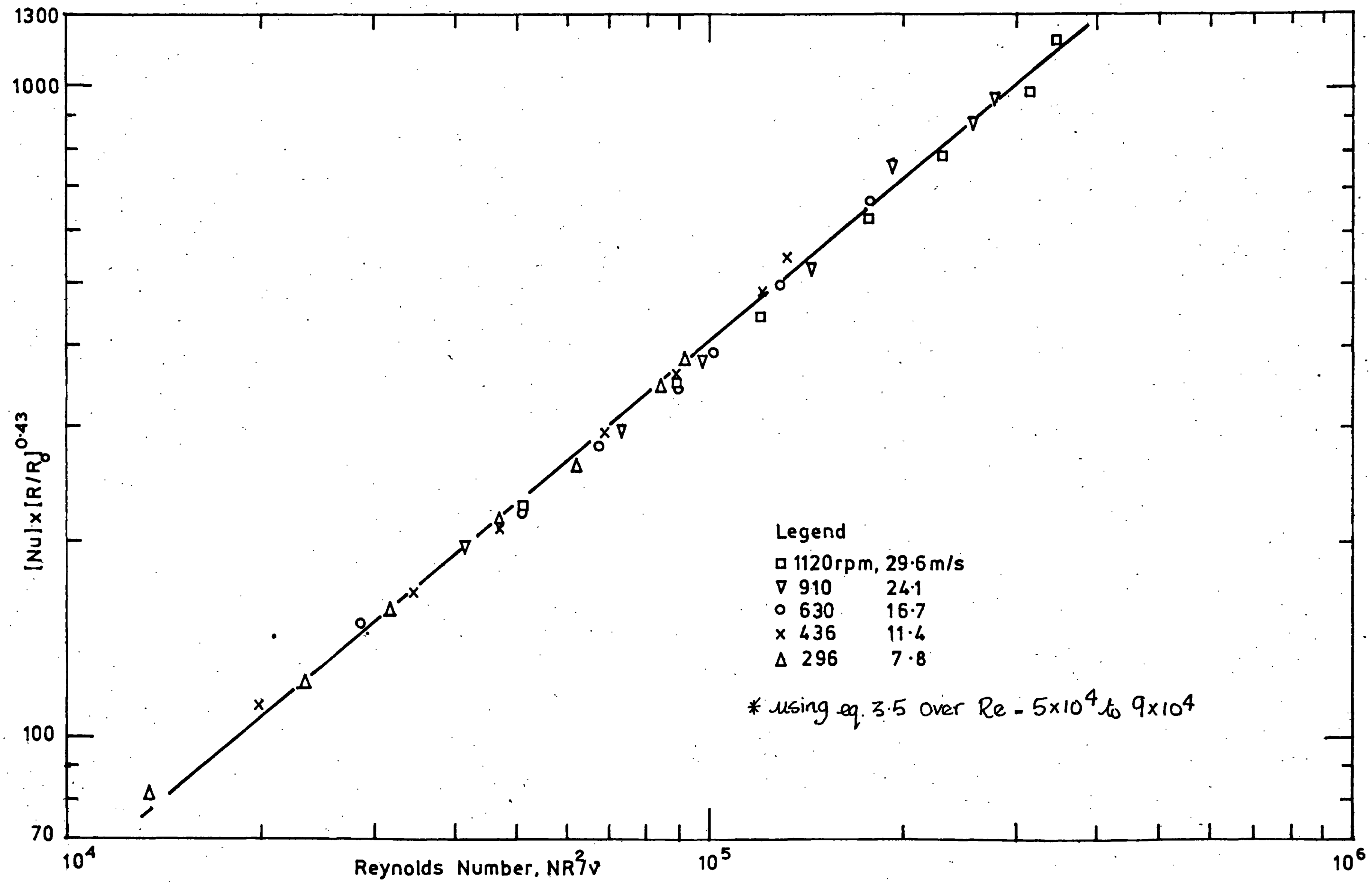

Fig 3·27 Rotating Disc in Matched Air Stream [shroud at t=1·25cm] - Dimensionless Plot

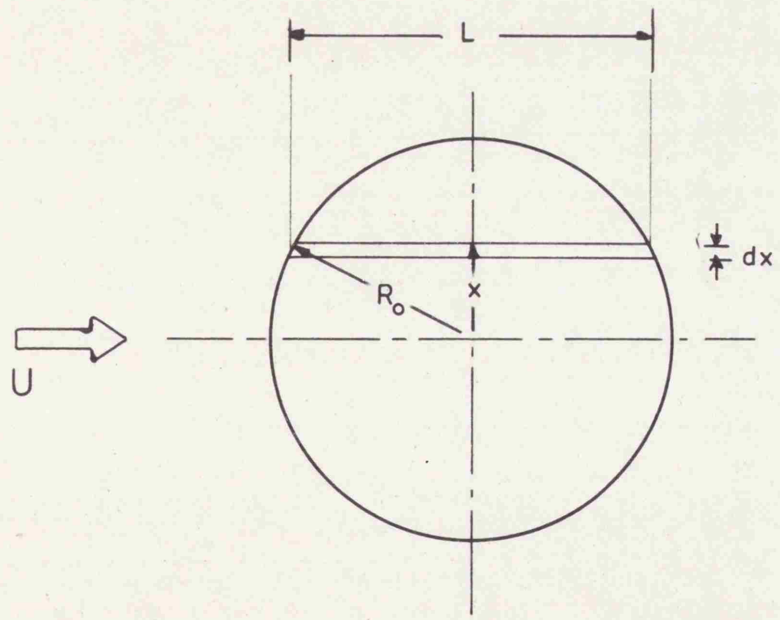

Fig 3·28

yielding $$\overline{Nu} = \frac{\bar{h}_c R_o}{\kappa} = 0.0296\ Re_o^{0.8} \qquad (3.9)$$

Comparison is made in Figure (3.29) between this equation and the correlation equation (3.7). For the range considered the rotation causes between 25 and 17 per cent increase in the heat transfer coefficients from the theoretical predictions for turbulent flow over a flat stationary disc. This confirms the view that the level of heat transfer coefficients is determined by the main transverse air stream, the rotation giving this small percentage upward perturbation.

The recent work of Dennis, Newstead and Ede[21] allows a comparison with their experimental work to be made. A direct comparison is not possible as their results are only average values over the whole disc. Equation (3.7) is compared in the table below with the mean Nusselt number for three matched conditions $Re_o = 1.25$, 2.56 and 5.05×10^5. These are the only results suitable for comparison.

Re_o	Mean Nusselt No. from [21]	From eq.(3.7) $Nu = 0.0258\ Re_o^{0.83}$
125,000	4.7×10^2	4.386×10^2
256,000	8.5×10^2	7.95×10^2
505,000	14.1×10^2	13.97×10^2

Dennis et al used two aluminium plates, 11 mm thick with a heater sandwiched in between. The effective thickness may be considered very similar to that used in the present correlation with t = 12.5 mm. The separation conditions at the leading edge appear similar. In view of the sensitivity of the radial variation to the aspect ratio the agreement between the correlated results and those of Dennis et al is remarkably good. This comparison gives added strength to the quantitative nature of the heat transfer coefficients.

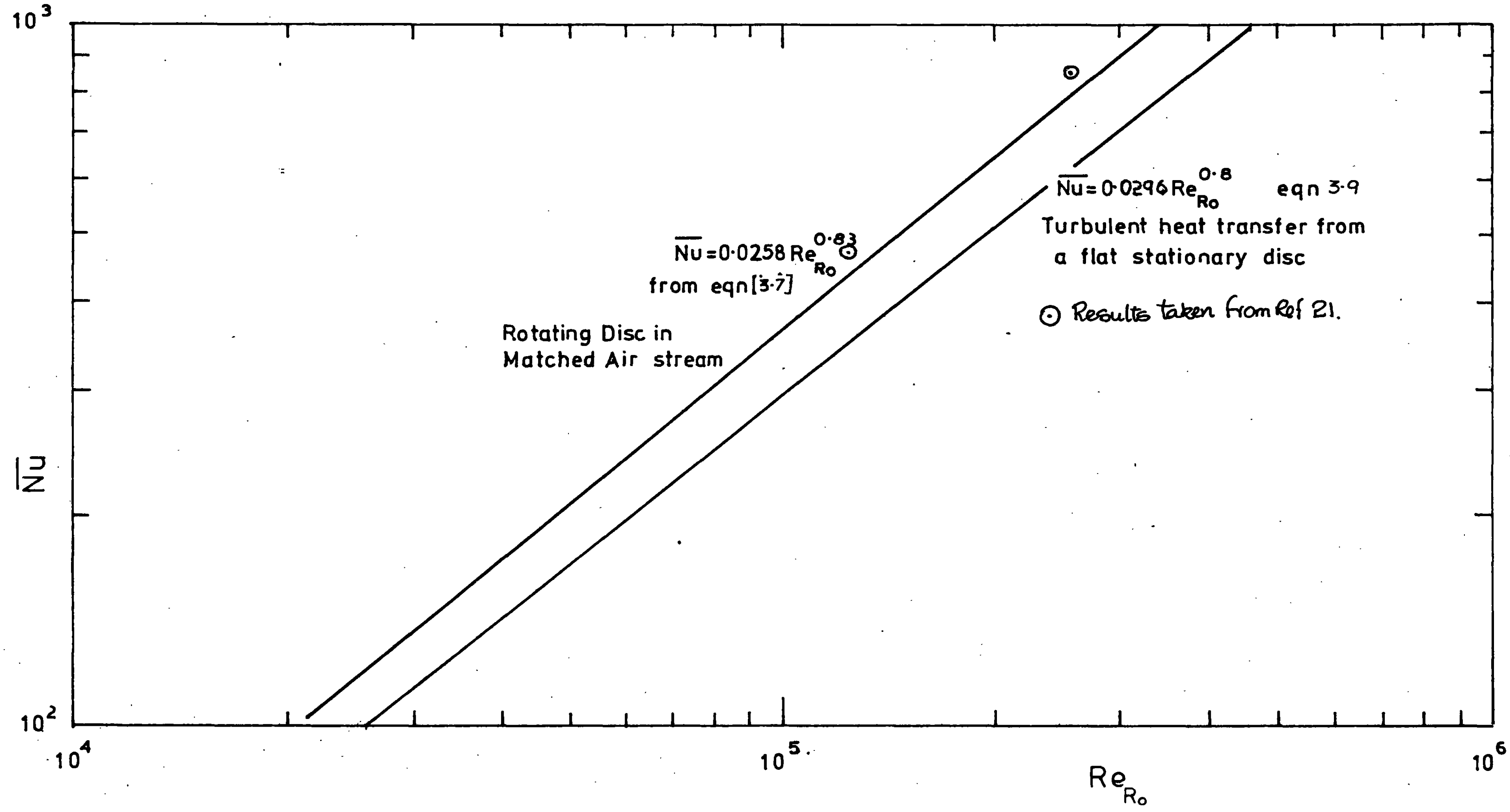

10^3
10^2
$\overline{Nu}$
10^4
10^5
10^6
Re_{R_o}
$\overline{Nu} = 0{\cdot}0258\, Re_{R_o}^{0{\cdot}83}$
from eqn [3·7]
Rotating Disc in
Matched Air stream
$\overline{Nu} = 0{\cdot}0296\, Re_{R_o}^{0{\cdot}8}$ eqn 3·9
Turbulent heat transfer from
a flat stationary disc
⊙ Results taken from Ref 21.

Fig 3·29

Chapter 4

Instantaneous Heat Transfer Measurements

4.1. Introduction

In the context of a train wheel only average radial heat transfer coefficients are of interest. However for an understanding of the processes which go to make up these average values, local measurements over the whole face are important.

The limitations of the previous heat flux sensor have been discussed in Chapters 2 and 3. Although suitable for determining the average radial heat transfer coefficient h_R, the thermal mass of the copper disc only permits slow changes, $>$ 20 secs. to be monitored. Much more sensitive measuring equipment is needed. The Gardon Hot Foil Radiometer(12) was initially considered but due to difficulties in construction which became apparent in preliminary investigations, attention was concentrated on the Thin Film Gauge.

4.2. The Thin Film Gauge

The thin film gauge consists of a cylindrical Pyrex substrate with a very thin ($\approx 0.1\mu m$) platinum resistance film mounted on the front surface. The purpose of the film is to monitor the surface temperature of the substrate and it is of such a thickness that it does not affect the temperature history of the substrate. Figure (4.1) illustrates the gauge and Figure (4.2) indicates the seating arrangements of the substrate in the cylindrical plug C. The Tufnol, B, and aluminium plug, C, allow the gauge to be positioned flush inside any one of the seven holes in the main rotating disc. The Tufnol washer reduces heat leakage into the substrate and provides an isothermal boundary around the external surface of the Pyrex substrate.

The usual application of this type of sensor is in Hypersonic facilities

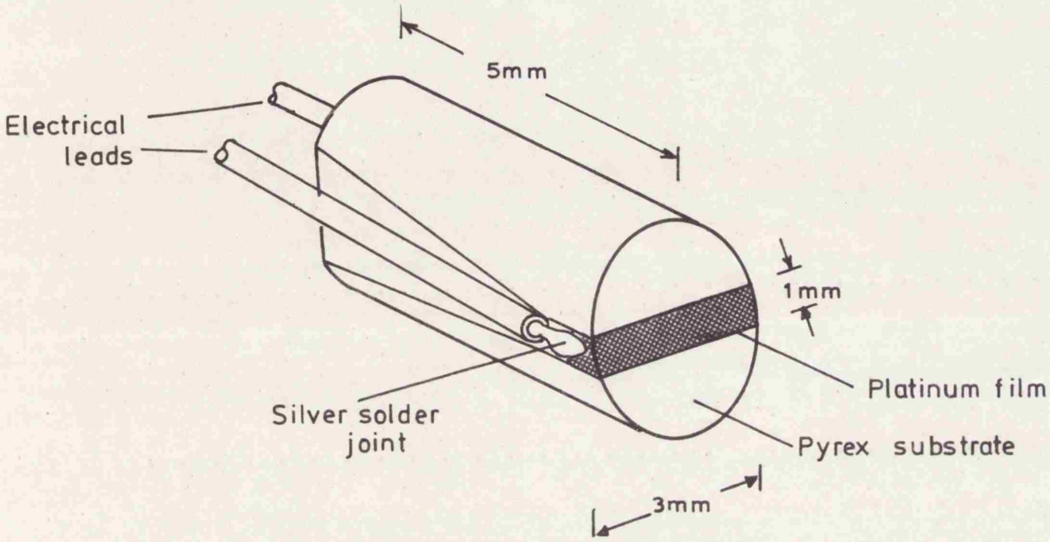

Fig 4·1 The Thin Film Sensor

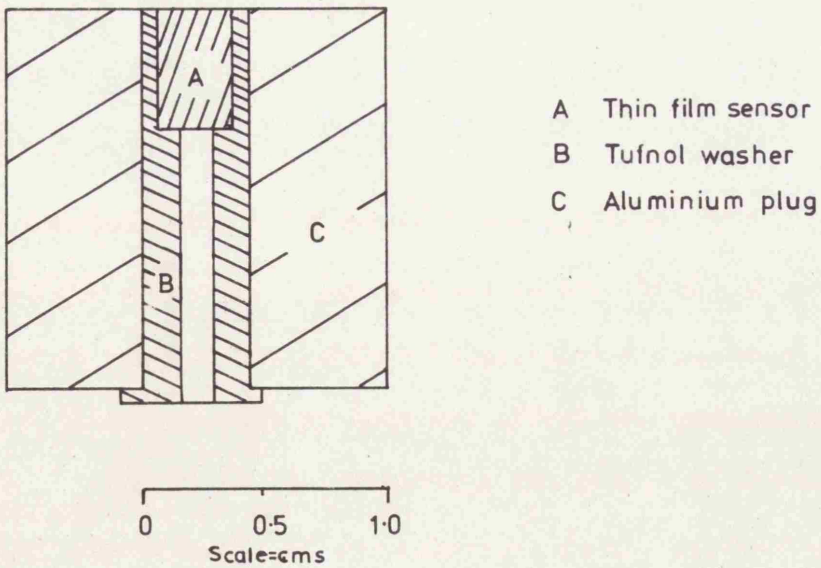

Fig 4·2 Sensor seating arrangement

where short duration heat transfer coefficients are measured. A sudden cooling over the front surface of the substrate causes its temperature to fall in a determined manner. The analysis pertinent to the operation is discussed below. A film heating term $\dot{E}$, (W/m^2) is included in the analysis for two reasons. Firstly the sensitivity of the platinum film is greatly improved by increasing the current through the Wheatstone bridge circuit used to monitor film resistance changes. Secondly by the time both wind speed and rotational speed have reached their desired levels ($t > 60$ secs.) the substrate surface temperature would otherwise have fallen far below the surrounding disc temperature with the result that incorrect heat transfer coefficients are measured, due to the step in surface temperature variation.

4.3. Analysis

This one-dimensional model is an approximation due to Schultz & Jones [13]. Let us assume that the probe can be represented as a semi-infinite slab as shown in Fig.(4.3). The temperature T, at a distance z is measured relative to the boundary temperature at $z = \infty$. In normal practice this temperature is maintained at the disc surface temperature T_w.

The differential equation governing the temperature distribution in the medium is

$$\frac{\partial^2 T}{\partial z^2} = \frac{1}{\alpha}\frac{\partial T}{\partial t} \qquad 4.1.$$

where α is the thermal diffusivity of the medium, $\alpha = k_s/\rho C_p$, with the boundary conditions that at

$$z = \infty\ ,\ T = 0 \text{ for all } t$$

$$t = 0\ ,\ T = 0 \text{ for all } z$$

and at $$t > 0 \quad \dot{E} - q_c(t) = -k_s \left.\frac{\partial T}{\partial z}\right|_{z=0}.$$

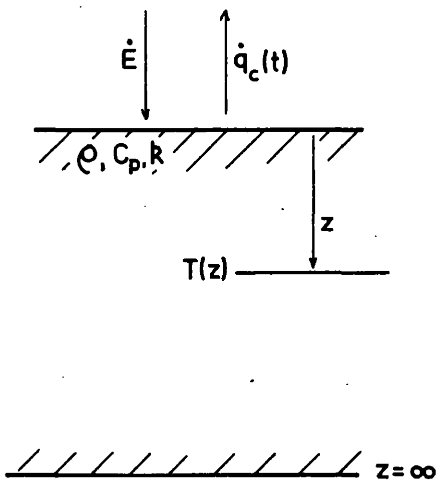

Fig 4·3 Coordinate system for Semi Infinite substrate

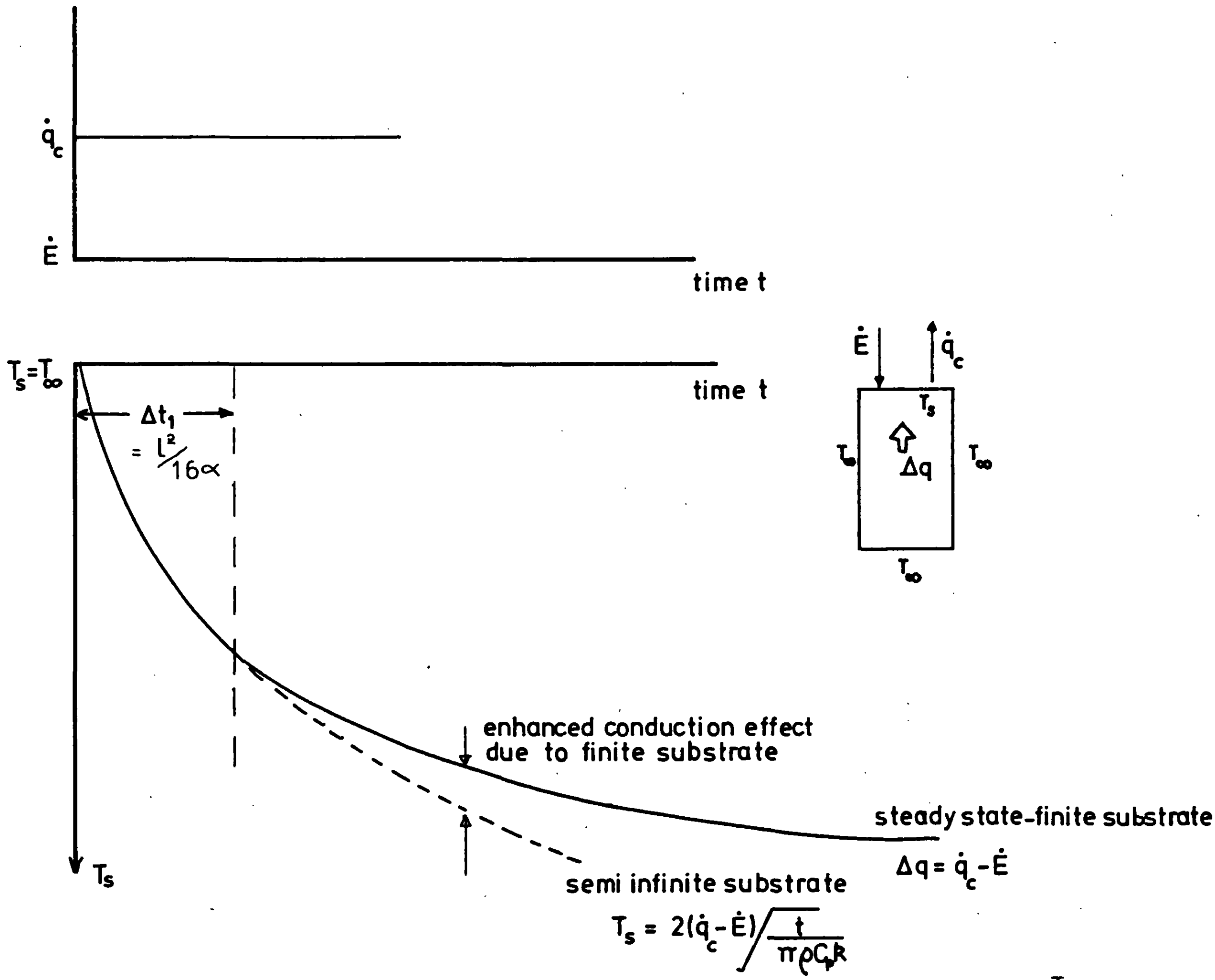

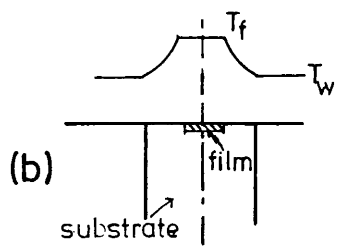

Fig 4·4 Film Temperature response to step input

Taking the Laplace transforms, denoted by $\bar{}$

$$\frac{d^2\bar{T}}{dz^2} = \frac{P}{\alpha}\bar{T}$$

which has the general solution

$$\bar{T} = Ae^{z\left(\frac{P}{\alpha}\right)^{\frac{1}{2}}} + Be^{-z\left(\frac{P}{\alpha}\right)^{\frac{1}{2}}} \qquad 4.2$$

subject to the conditions $\bar{T} = 0$ at $z = \infty$ and $\frac{\dot{E}}{P} - \bar{\dot{q}}_c = -k_s \left.\frac{d\bar{T}}{dz}\right|_{z=0}$

giving
$$\bar{\dot{q}}_c(t) = \frac{\dot{E}}{P} - \sqrt{k_s\rho C_p}\,\sqrt{P}\,\bar{T}_s \qquad 4.3$$

and inverting yields

$$\dot{q}_c(t) = \dot{E} - \frac{\sqrt{\rho C_p k_s}}{\sqrt{\pi}}\int_0^t \frac{\frac{dT}{d\tau}(\tau)}{(t-\tau)^{\frac{1}{2}}}\,d\tau \qquad 4.4$$

where τ is the variable of integration.

Integrating equation 4.4 by parts yields

$$\dot{q}_c(t) = \dot{E} - \frac{\sqrt{\rho C_p k_s}}{\sqrt{\pi}}\left[\frac{T(t)}{\sqrt{t}} + \frac{1}{2}\int_0^t \frac{T(t) - T(\tau)}{(t-\tau)^{3/2}}\,d\tau\right] \qquad 4.5$$

These temperatures are the film substrate surface temperatures.

Numerical integration of the second part of the expression enables $\dot{q}_c(t)$ to be evaluated. Cook and Felderman(14) have assumed that $T(\tau)$ may be approximated by a piecewise linear function of the form

$$T(\tau) = T(t_{i-1}) + \frac{T(t_i) - T(t_{i-1})}{(t_i - t_{i-1})}(\tau - t_{i-1}) \qquad 4.6$$

and writing the integral as

$$\frac{1}{2}\int_0^t \frac{T(t) - T(\tau)}{(t-\tau)^{3/2}}\,d\tau = \frac{1}{2}\sum_{i=1}^{N}\int_{t_{i-1}}^{t_i} \frac{T(t_N) - T(\tau)}{(t_N - \tau)^{3/2}}\,d\tau \qquad 4.7$$

yields

$$\frac{1}{2}\int_0^t \frac{T(t) - T(\tau)}{(t-\tau)^{3/2}}\,d\tau = \frac{1}{2}\sum_{i=1}^{N}\left[(T_N - T_{i-1}).2.\left\{\frac{1}{(t_N - t_i)^{\frac{1}{2}}} - \frac{1}{(t_N - t_{i-1})^{\frac{1}{2}}}\right\}\right.$$

$$\left. - \frac{(T_i - T_{i-1})}{\Delta t}\left\{\frac{2\Delta t}{(t_N - t_i)^{\frac{1}{2}}} + 4\,[t_N - t_i]^{\frac{1}{2}} - (t_N - t_{i-1})^{\frac{1}{2}}\right]\right]$$

$$= \sum_{i=1}^{N}\left[\frac{(T_N - T_{i-1})}{(t_N - t_i)^{\frac{1}{2}}} - \frac{(T_N - T_{i-1})}{(t_N - t_{i-1})^{\frac{1}{2}}} - \frac{(T_i - T_{i-1})}{(t_N - t_i)^{\frac{1}{2}}} + \frac{2(T_i - T_{i-1})}{(t_N - t_i)^{\frac{1}{2}} + (t_N - t_{i-1})^{\frac{1}{2}}}\right]$$

$$\therefore\ \dot{q}_c(t_N) = \dot{E} - \frac{\sqrt{\rho C_p k_s}}{\sqrt{\pi}}\left[2\sum_{i=1}^{N-1}\left[\frac{T_i - T_{i-1}}{(t_N - t_i)^{\frac{1}{2}} + (t_N - t_{i-1})^{\frac{1}{2}}}\right] + 2\,\frac{(T_N - T_{N-1})}{(t_N - t_{N-1})}\right]$$

$$= \dot{E} - \frac{\sqrt{\rho C_p k_s}}{\sqrt{\pi}}\left[2\sum_{i=1}^{N}\frac{(T_i - T_{i-1})}{(t_N - t_i)^{\frac{1}{2}} + (t_N - t_{i-1})^{\frac{1}{2}}}\right] \qquad 4.8$$

---

with the initial conditions that $t_o = 0$ $T = 0$.

4.3.1. Effect of Finite Substrate

If the heat transfer rate is, however, constant, equation 4.3 reduces to

$$\bar{T}_s = \frac{\dot{E} - \dot{q}_c}{\sqrt{\rho C_p k_s}\,P^{3/2}}$$

$$\therefore \qquad T_s = \frac{2(\dot{E} - \dot{q}_c)}{\sqrt{\pi}}\sqrt{\frac{t}{\rho C_p k_s}} \qquad 4.9$$

and it is seen under these conditions the surface temperature, T_s, is parabolic in form. In the case of a finite substrate of length ℓ, the conduction towards the surface is greater, since the boundary, maintained at T_w, is very much closer. The rate of change of surface temperature will be consequently slower. Fig.(4.4) shows the two responses to a step input in heat transfer, $\dot{q}_c$. For a finite substrate Schultz and Jones[13] show that over the time intervals less than $\Delta t_{\ell} = \frac{\ell^2}{16\alpha}$, equation 4.9 gives the surface temperature within one per cent.

For this particular substrate, see Figure (4.1), Δt is evaluated at 2 secs. Provided the period of the transient fluctuations, equivalent to $\frac{1}{N}$ for the rotating disc in transverse air streams, lies well within this interval, then it can be assumed that the semi-infinite equation will apply to the finite substrate.

4.3.2. Effect of Platinum Film

For the analysis and a constant heat transfer rate $\dot{q}_c$ a certain level of film heating $\dot{E}$, is required to maintain the temperature level at T_w, the wall boundary and surrounding disc temperature. Because the film only occupies 30 per cent of the substrate surface area, see Figure(4.1), losses at the sides (through the substrate) occur and $\dot{E}$ is greater in order to maintain the film temperature at T_w. The amount by which $\dot{E}$ exceeds the heat transfer rate is discussed in Section 4.5. The cooling over the substrate face produces a surface temperature profile as shown in Figure (4.4(b)).

It might be expected that the presence of the film could affect the value of the cyclic variation as well as the mean level. If $\dot{q}_c(t)$ varies this has the effect of causing a similar surface temperature variation over the whole surface, so the level of heat loss at the film sides will not change significantly; the source and sink temperatures change by the same amount. One might therefore expect the surface temperature variation about the mean not to be different from that predicted by analysis.

A more detailed analysis could predict both mean and cyclic levels more accurately. However, for the present study the mean level is assumed the same as that given by the long time constant sensor, as discussed in Chapters 2 and 3. The cyclic fluctuations are determined from the analysis (equation 4.8). These results are discussed essentially in a qualitative manner.

4.4. Experimental Arrangement

The film temperature, T_f, and consequently the substrate surface temperature, is measured by the film resistance. The film is connected in the Wheatstone bridge as shown in Figure (4.5). If the bridge is initially balanced then $R_1 R_f = R_2 R_3$, where R_f represents the film resistance.

The change in film resistance ΔR_f is monitored by an out of balance bridge voltage ΔV, and given by the relation

$$\frac{\Delta V}{I_o} = \frac{\Delta R_f \; R_1}{R_1 + R_2} \tag{4.10}$$

where I_o represents the film current. ΔR_f may be expressed in terms of a change in film temperature ΔT_f by the equation

$$\Delta R_f = \alpha_R R_f \; \Delta T_f \tag{4.11}$$

The out of balance bridge voltage is fed through a D.C. amplifier (Fenlow ZA2) to a storage oscilloscope.

The temperature coefficient α_R was determined from measurements of the film resistance over the whole range of surface temperatures encountered. The sensor was mounted in the main disc with the front face blanked off to reduce errors due to natural convection from the front surface. The disc was then heated up slowly and the film resistance measured at a number of temperatures given by a thermocouple mounted in the main disc. Figure (4.6) gives the calibration. The film temperature coefficient, α_R, is determined as

$$\alpha_R = 1.5 \times 10^{-3} \; K^{-1}.$$

Spot checks of this value made throughout the testing showed it did not alter with time.

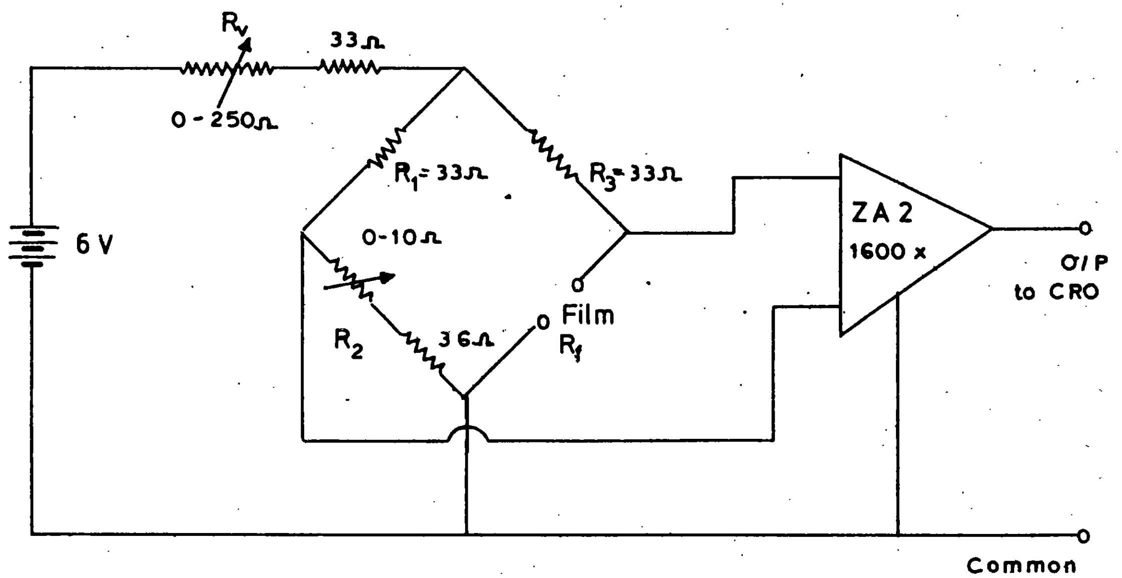

Fig 4·5 Bridge Circuit

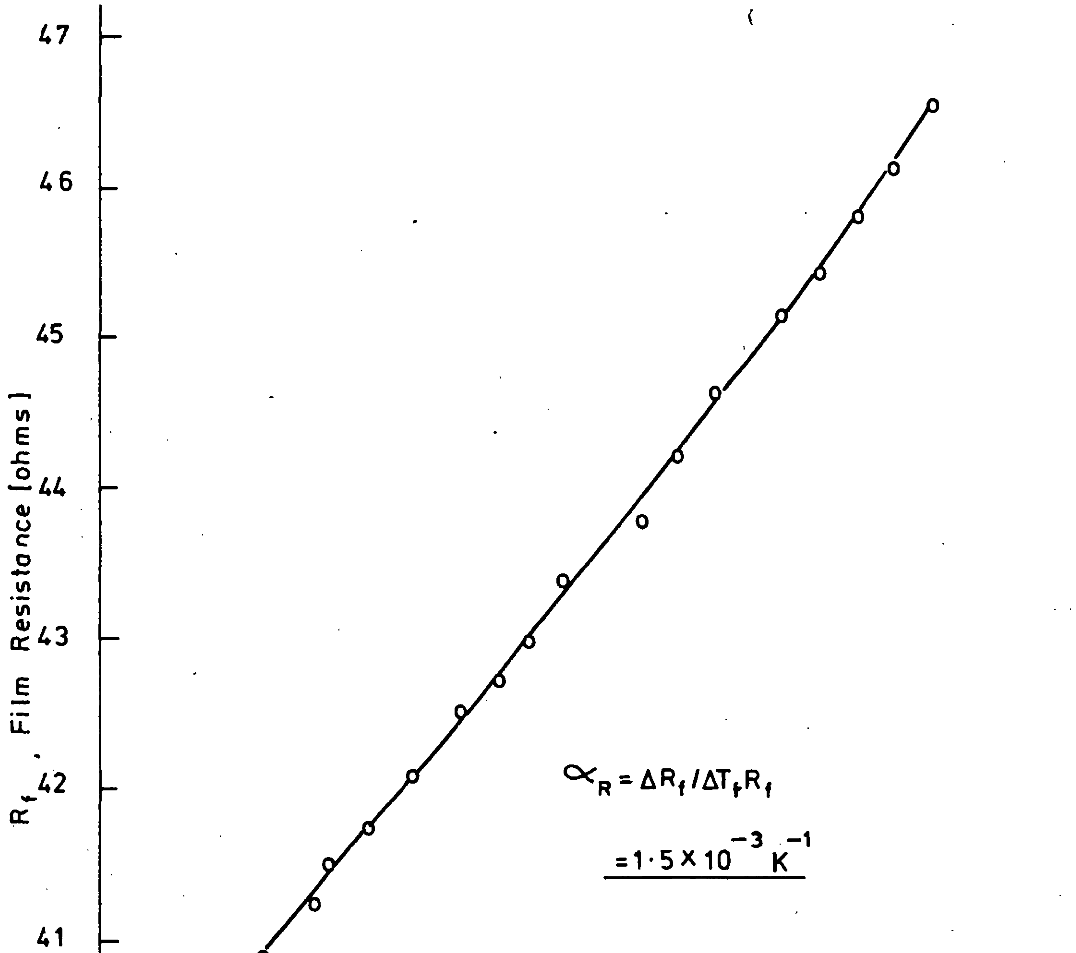

Fig 4·6 Film Resistance - Temperature Calibration

The angular position of the sensor relative to the oscilloscope output was determined by a simple make/break contact mechanism. One arm was attached to the disc at the periphery and the other to the supporting structure beneath the disc. The electrical pulses so generated were fed to the second channel on the storage oscilloscope.

4.4.1. Procedure

The experimental testing procedure used was as follows. The whole disc, with the thin film sensor in position, was heated up to temperature well above ambient conditions, i.e. $T_w - T_\infty > 40$ deg.C. When steady state conditions were achieved the bridge circuit was balanced on the oscilloscope with a very small bridge current. The bridge resistance, R_2, was then noted and fixed at this position. Further heat was then applied to the disc to raise the bulk temperature approximately five degrees above the fixed temperature level, T_w, corresponding to the resistance R_2 setting.

The air stream and disc were then set in motion and the heat input adjusted to maintain the disc surface temperature, monitored by the thermocouple nearest the sensor, at T_w. The film current I_o, was then raised until the mean voltage signal on the oscilloscope was balanced at the previous level, T_w. The output signal was then stored on the oscilloscope and photographed. The bridge and circuit resistances, R_2 and R_v, and temperatures, T_w and T_∞, were then noted in addition to the oscilloscope and amplifier conditions. N.B. T_f at this condition is equivalent to T_w, the surrounding disc surface temperature.

4.5. Experimental Testing

Initially tests were carried out to ascertain the degree of slip ring and spurious electrical noise. Figure (4.7(a)) shows the oscilloscope trace giving the cyclic variation in temperature, with the positional

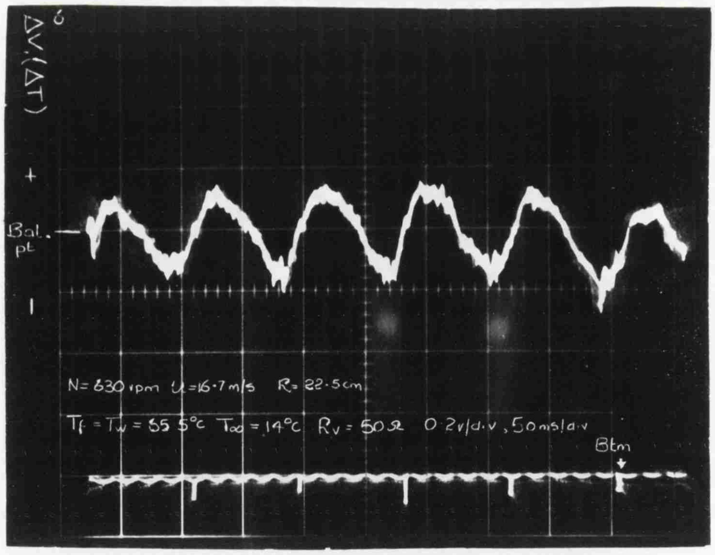

a) N=630 rpm. U=16·7 m/s

$$\frac{\dot{E}}{T_f - T_\infty} = 178\ \mathrm{W/m^2 degC}$$

$$h_R = 95\ \mathrm{W/m^2 degC}$$

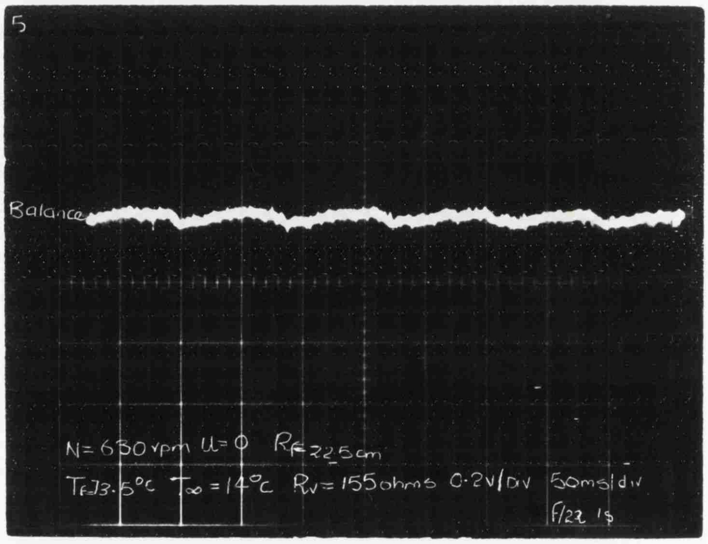

b) N=630 rpm. U=0

$$\frac{\dot{E}}{T_f - T_\infty} = 39{\cdot}0$$

$$h_R = 24{\cdot}0$$

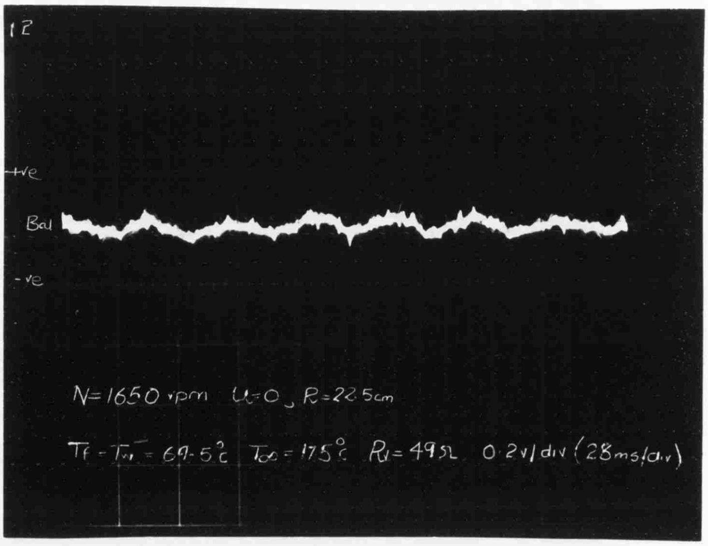

c) N=1650 rpm U=0

$$\frac{\dot{E}}{T_f - T_\infty} = 181{\cdot}0$$

$$h_R = 99{\cdot}5$$

Fig. 4·7 Oscilloscope traces (shroud set at 1·25cm, R = 22·5cm)

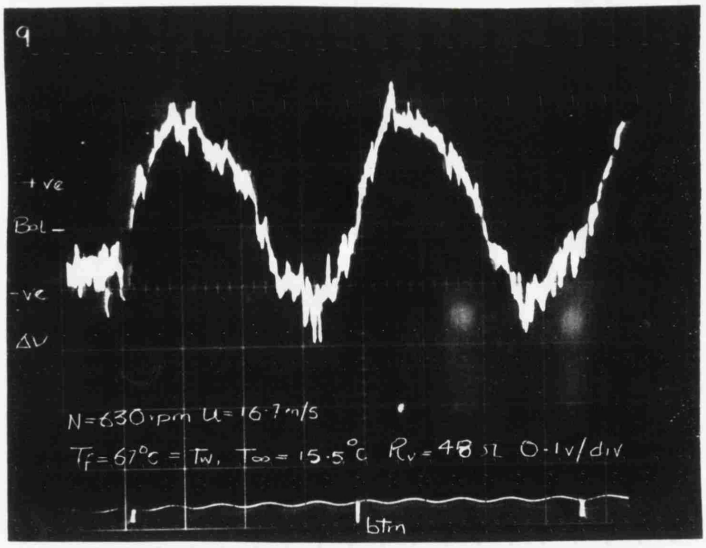

a) R = 22·5cm

$$\frac{\dot{E}}{T_f - T_\infty} = 183\ \text{W/m}^2\text{degC}$$

$$h_R = 95\ \text{W/m}^2\text{degC}$$

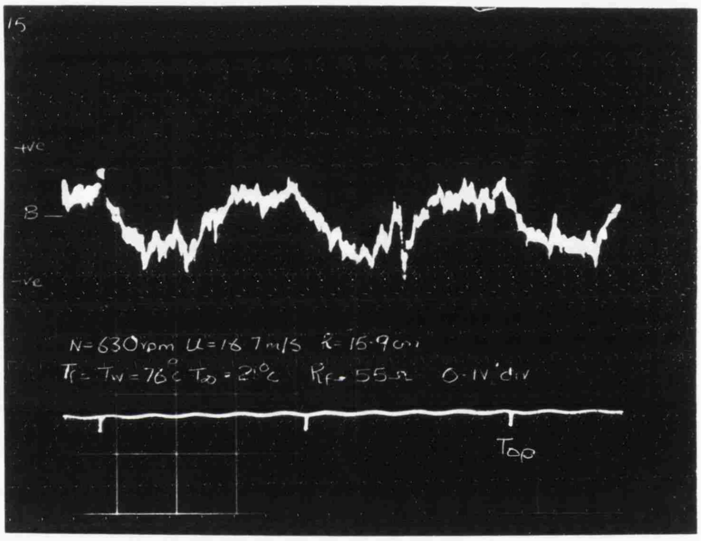

b) R=15·9cm

$$\frac{\dot{E}}{T_f - T_\infty} = 160{\cdot}0$$

$$h_R = 81{\cdot}0$$

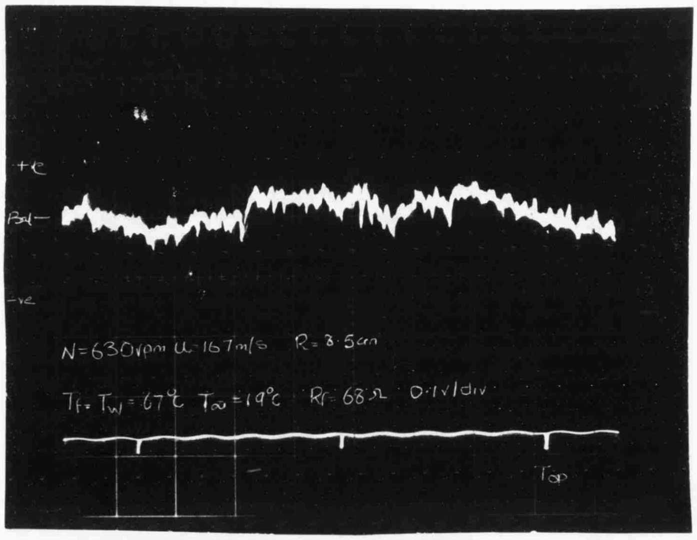

c) R=8·5cm

$$\frac{\dot{E}}{T_f - T_\infty} = 146{\cdot}0$$

$$h_R = 75{\cdot}0$$

Fig 4·8 Oscilloscope traces [N= 630rpm / U=16·7m/s, t= 1·25cm.]

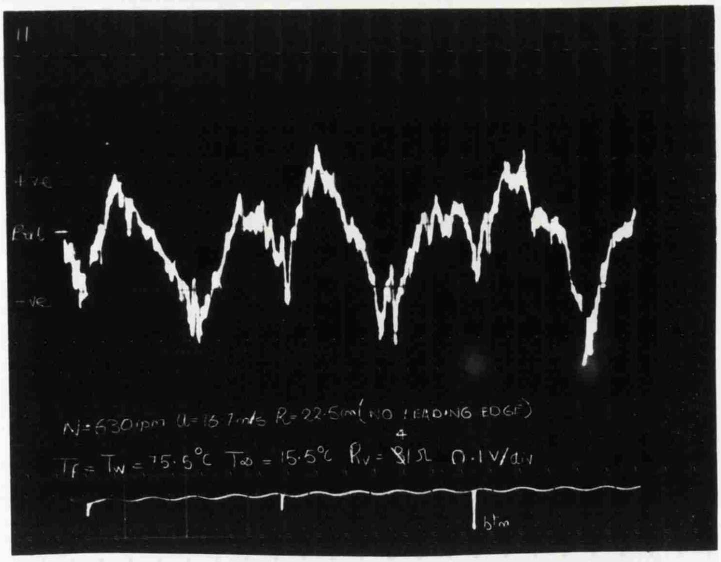

a) R=22·5cm

$$\frac{\dot{E}}{T_f - T_\infty} = 178\ \mathrm{W/m^2 deg\,C}$$

$$h_R = 93\ \mathrm{W/m^2 deg\,C}$$

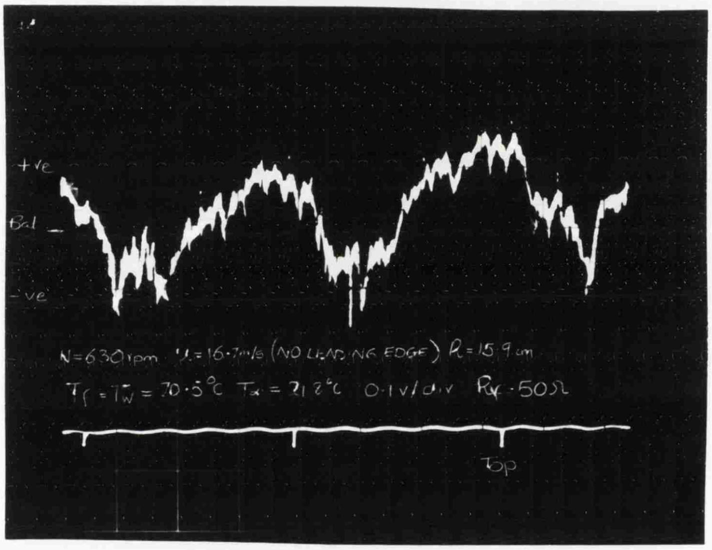

b) R = 15·9cm

$$\frac{\dot{E}}{T_f - T_\infty} = 190$$

$$h_R = 108{\cdot}0$$

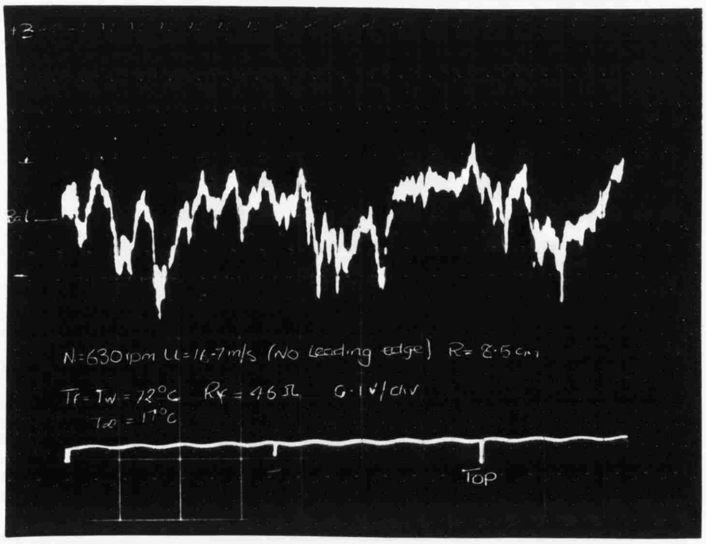

c) R= 8·5cm

$$\frac{\dot{E}}{T_f - T_\infty} = 181$$

$$h_R = 98{\cdot}0$$

Fig 4·9 Oscilloscope traces [N=630rpm, U=16.7 No Shroud] reference underneath, when the rotation and wind tunnel air speed are in the matched condition, N = 630 r.p.m., U = 16.7m/s. The leading edge shroud was fixed at 1.25cm. in the position for minimum separation. Tests were then carried out in still air where the heat transfer coefficient and hence film temperature is expected to remain constant with angular position. Figures(4.7(b)(c)) show the traces obtained for disc speeds of 630 r.p.m. and 1650 r.p.m. respectively. These traces show that the noise is small compared to the size of the temperature signal.

Information giving the conditions under which these tests were carried out is added to the pictures in Figure (4.7). The ohmic heating term $\dot{E}$, based on the film area, A_f, is also given for comparison with the heat transfer coefficient h_R, as measured by the previous heat flux sensor.

The matched condition was then repeated with a larger oscilloscope amplification and smaller periodic scan to provide suitable traces for analysis. The sensor was positioned at three different radii, R = 22.5, 15.9 and 8.5cm. The resulting traces are shown in Figures (4.8(a),(b),(c)) respectively.

In addition to these tests, measurements were also made with the previous heat flux sensor with the disc held stationary in the air stream. The results are presented pictorially in Figure (4.10). These tests were done with the previous sensor due to the uncertainty in the mean heat transfer level given by the film sensor.

The leading edge shroud was then removed and the three tests repeated for the same matched condition. The results are shown in Figure (4.9(a),(b),(c)).

4.6. Analysis of Results

From equations (4.8, 4.10 and 4.11), the cyclic fluctuation in heat transfer coefficient h_c', about the mean level, h_R, may be determined from the equation

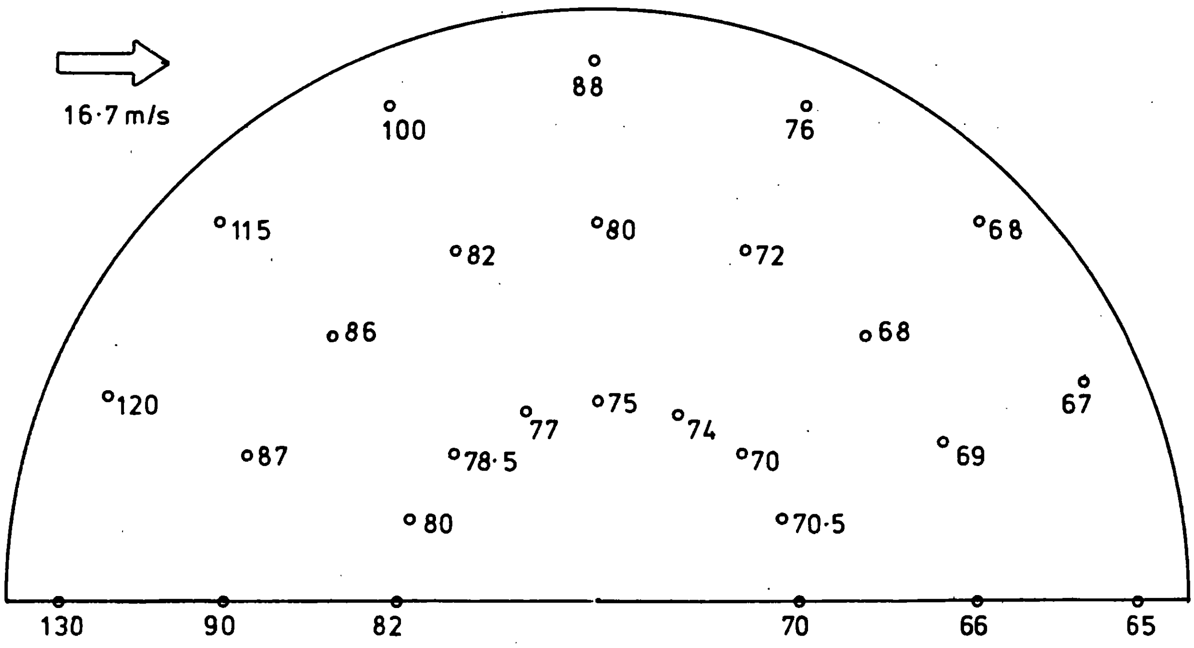

Fig 4·10 Heat transfer coefficients of stationary disc in air stream at R = 22·5 , 15·9 & 8·5 cm. Shroud at 1·25cm

$$h_c'(t_N) = C \times \left[\sum_{i=1}^{N} \frac{E(t_i) - E(t_{i-1})}{(N - i)^{\frac{1}{2}} + (N + 1 - i)^{\frac{1}{2}}} \right] \qquad 4.12$$

where $E(t_i)$ refers to the out of balance bridge voltage at $t = i$ on the oscilloscope, the balance point referring to the condition where $T_f = T_w$ = disc surface temperature, and where the constant C is determined by

$$C = 2\sqrt{\frac{\rho c_p k_s}{\pi}} \, \frac{(R_1 + R_2)}{I_o R_1 \times 1600 \times \alpha_R R_f (T_f - T_\infty)} \left(\frac{P_T}{T}\right)^{\frac{1}{2}} \qquad 4.13$$

where P_T is the number of steps chosen in each cycle of periodic time T.

and $$I_o = \frac{6.0(\text{volts})}{2(R_v + 33 + 0.5(R_f + R_3)}$$

NB. The actual variation in film temperature ΔT_f($\doteq$ $\frac{1}{4}$ deg.C) is small compared with the mean level $T_f - T_\infty$, ($\approx$ 40 deg.C), so I_o may be assumed constant.

The value of the thermal product, ρck, is taken from experimental tests on Pyrex done by Hartunian and Varwig[15]. Typical values are listed in the table below.

Temp ^oC	$(\rho c_p k_s)^{\frac{1}{2}}$ $\frac{J}{cm^2 {}^0k_s^{\frac{1}{2}}}$
24	0.152
50	0.164
82	0.185
100	0.188

Equation (4.12) is solved numerically by computer. The program is listed in Figure (4.11.). It was found that P = 16 was a sufficient number of steps to accurately evaluate the integral in equation 4.5. The numerical values of $E(t_N)$ were taken from pencil traces of the photographs, Figures (4.8 and 4.9), and measured from the balance point. A positive voltage change corresponds to a decrease in the heat transfer coefficient h_c'.

The summation of equation 4.12 is done over all time from time zero, and assumes that the whole heat transfer process starts at t = 0, i.e. the

```
&JOB;EN021501;RAW74;

&FORTRAN;

&LIST;
      DIMENSION E(33)
      E(0)=0.0
      N=1
    2 CONTINUE
      READ(7,9) EE
    9 FORMAT (1F0.0)
      SUM=0.0
      E(N)= EE
      DO 33 I= 1,N
      Y=(E(I)-E(I-1))/(SQRT(N-I)+SQRT(N-(I-1)))
      SUM=SUM+Y
   33 CONTINUE
      CON=42.75
      Q=CON*(-SUM)
      WRITE(2,50) N,E(N),Q
   50 FORMAT(1H ,I2,2F12.3)
      IF(N-33)71,72,72

   71 N=N+1
      GO TO 2
   72 CONTINUE
      STOP
      END
```

FIGURE 4.11

N	E x 10 volts	leading edge R = 22.5 h'_c $w/m^2 deg.C.$
1	0.730	-31.207
2	1.160	-31.309
3	1.630	-37.626
4	2.060	-40.910
5	1.630	-7.911
6	1.340	-2.215
7	1.100	1.521
8	0.770	9.287
9	0.220	23.699
10	-0.330	31.838
11	-0.850	37.293
12	-1.250	37.538
13	-1.610	38.623
14	-1.100	3.637
15	-0.590	-9.446
16	0.000	-22.371
17	0.730	-37.468
18	1.160	-34.777
19	1.630	-39.782
20	2.060	-42.328
21	1.630	-8.872
22	1.340	-2.875
23	1.100	1.066
24	0.770	8.977
25	0.220	23.495
26	-0.330	31.711
27	-0.850	37.224
28	-1.250	37.513
29	-1.610	38.631
30	-1.100	3.671
31	-0.590	-9.393
32	0.000	-22.303

```
&END;
RESULT =     B
CPU  TIME  =0000  05.854
REAL TIME  =0000  13
SLAVE SIZE =   51712
CARDS READ =     0059
PRINT LINES=     0086
DISC TRANS =     0097
```

initial condition is $t < 0$ $E(t) = 0$. This condition is not satisfied by the voltage (temperature) variation recorded on the oscilloscope traces of Figures(4.8 and 4.9.). The process is continuous and periodic. Fortunately applying this condition to the traces only affects the computed heat transfer coefficient h_c' for a limited number of steps. The numerical value $h_c'(t_N)$ at $N = k$ is only significantly affected by the summation over the preceding five or six voltage readings i.e. $E(t_N)$ at $N = k, k - 1, k - 2 \ldots\ldots\ldots k - 6$. Any voltage (temperature) fluctuation before these times i.e. $E(t_N)$ at $N = k - 7, k - 8 \ldots\ldots\ldots$ etc. are relatively insignificant.

Referring to Figure(4.11),the program and sample results, after $N = 6$ the heat transfer coefficient h_c' settles down and appears to follow the continuous periodic voltage temperature variation. This is confirmed by repeating the cycle at $N = 16$ to $N = 32$. After $N = 6$ the value of h_c' corresponds closely with its next periodic value at $N = 22$.

The variation in the local heat transfer coefficient, h_c', from its mean, is determined from Figure (4.8(a),(b)), with the leading edge shroud present, and Figures (4.9(a),(b),(c)) without the shroud. Figure 4.8(c) is omitted as the output, $E(t_N)$ remains fairly linear over each cycle. The computed results are given in Figures (4.12(a),(b)) and(4.13(a),(b),(c)). A subsidiary diagram relates the heat transfer coefficient values to an angular position around the disc. (NB. The positions 1 to 16 do not necessarily refer to the values of N used in the computer program.

It was stated in Section 4.3.2 that the platinum film only occupies 30 per cent of the substrate surface area, and as a result losses from the sides through the substrate cause $\dot{E}$ to be greater than the mean convective heat transfer.

The value of $\dot{E}$ is determined from the ohmic heating of the film $I_o^2R_f$ and the film area A_f by the equation,

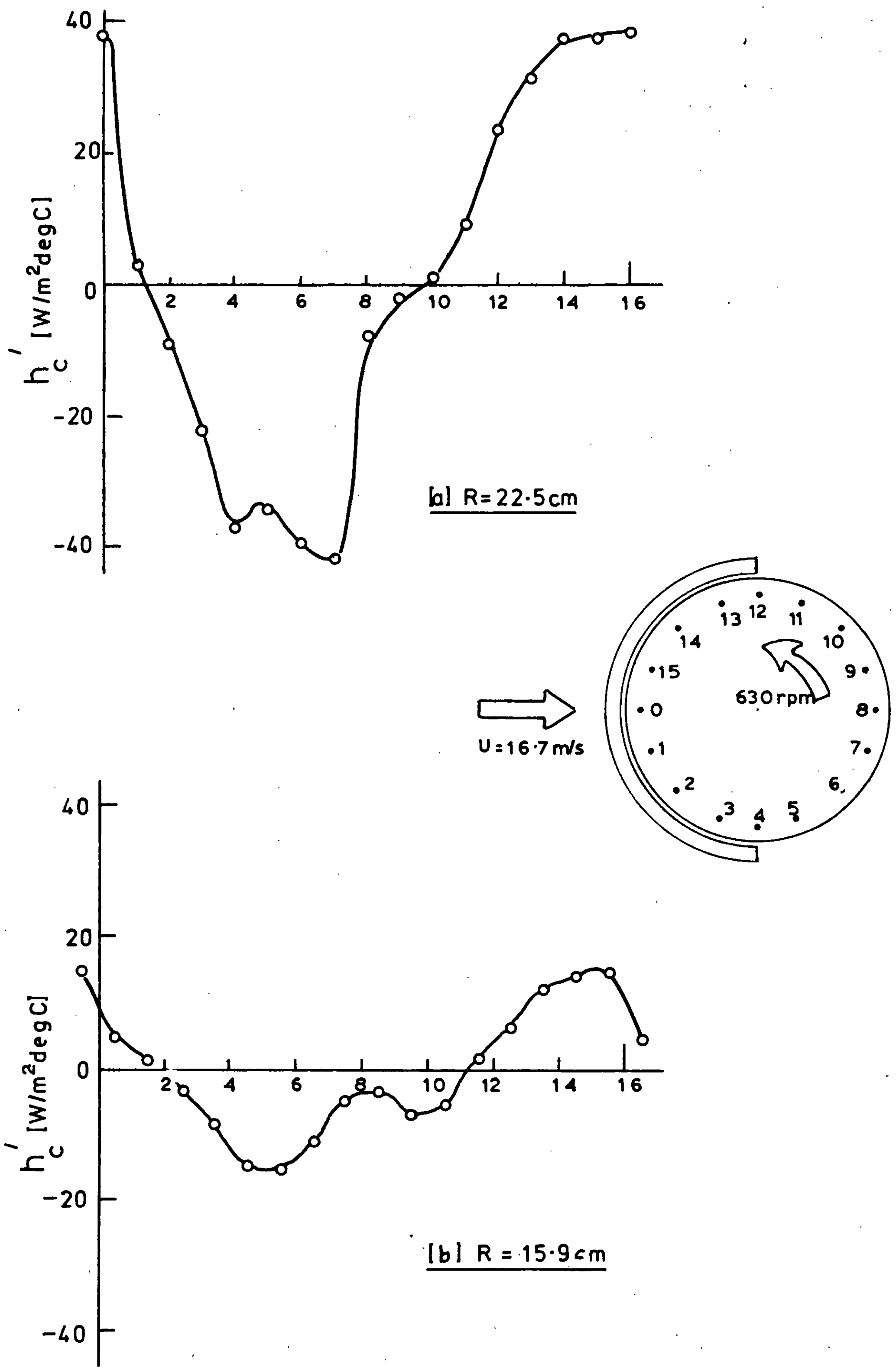

Fig 4·12 Cyclic variation in heat transfer[shroud at 1·25cm]

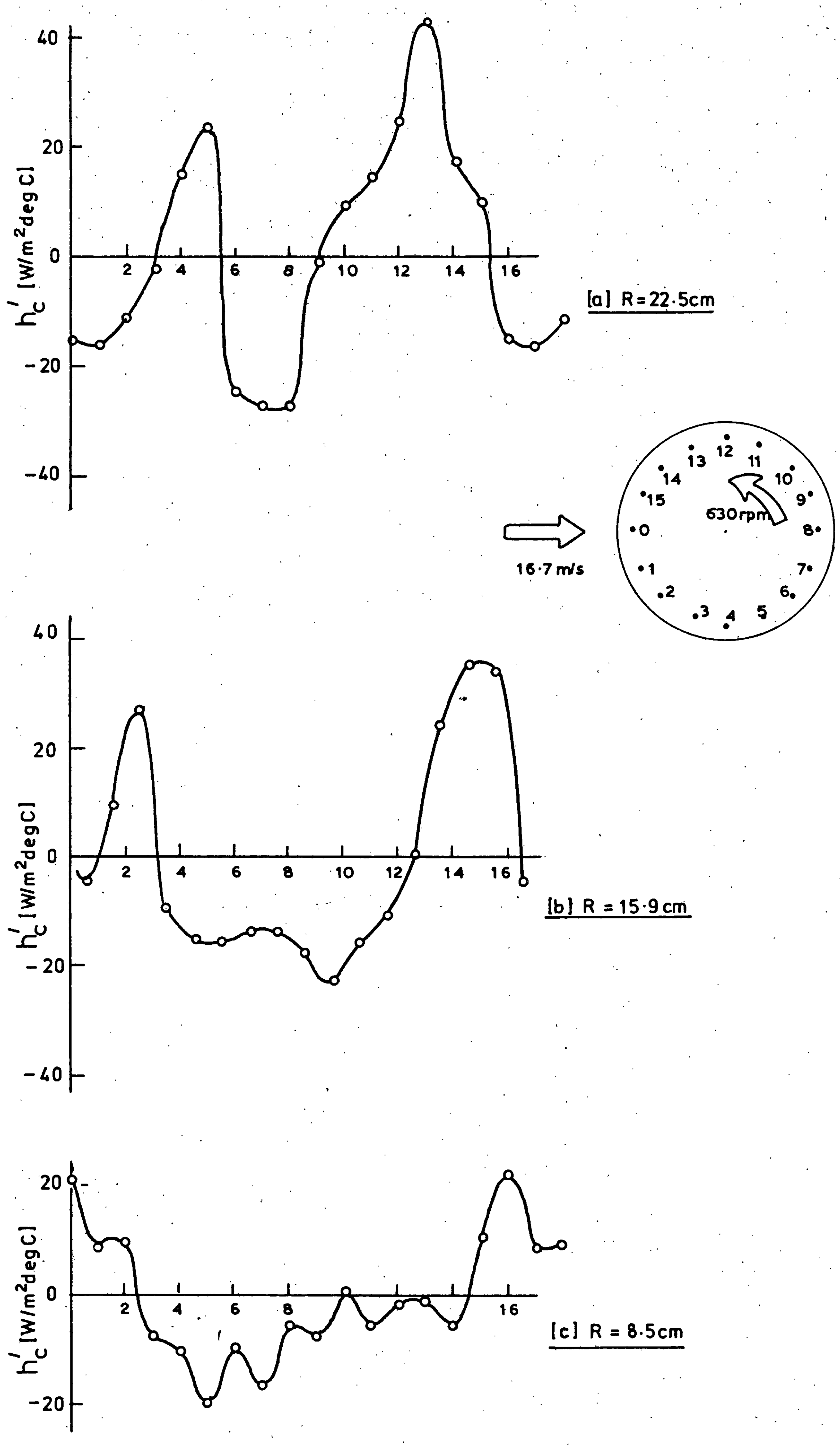

Fig 4·13 Cyclic Variation in heat transfer [no shroud]

$$\dot{E} = I_o^2 R_f / A_f ,$$

where $A_f = 2.9 \times 10^{-6} m^2$.

It cannot be used to predict the mean heat transfer coefficient, h_R. Comparison is made between $\dot{E}/(T_f - T_\infty)$ and h_R, determined by the slow response sensor, in Figures (4.7, 4.8 and 4.9). The difference indicates the level of heat loss from the film to the substrate. If an effective area, twice that of the film area A_f, is used in determining $\dot{E}$ then the two coefficients correspond more closely.

For the reasons above the cyclic variations are used in conjunction with the mean heat transfer measurements of the slow sensor. The total heat transfer variation is given in Figures (4.14 and 4.16).

4.7. Discussion

4.7.1. Shroud Present (t = 1.25cm.) Figure 4.14.

Previous tests with the slow response sensor (see Chapter 3) have indicated that the level of the heat transfer coefficient is determined in the main by the free stream flow with the disc rotation causing a small upward perturbation. A qualitative picture of the expected variation of heat transfer coefficient around the circumference can be built up by modifying the pattern obtained for the disc treated as a stationary flat plate in terms of the local relative velocity between a point on the rotating disc and the free stream. A relative velocity higher than the free stream augments the stationary heat transfer coefficient whilst a lower relative velocity reduces it.

Experimental work discussed in Chapter 3 shows that when the shroud is positioned at t = 1.25cm. there is no separation of the flow from the disc surface. Flat plate behaviour with attached flow is high heat transfer falling off rapidly at first and then more slowly as the distance along the plate increases. Applying this to the circular disc leads to

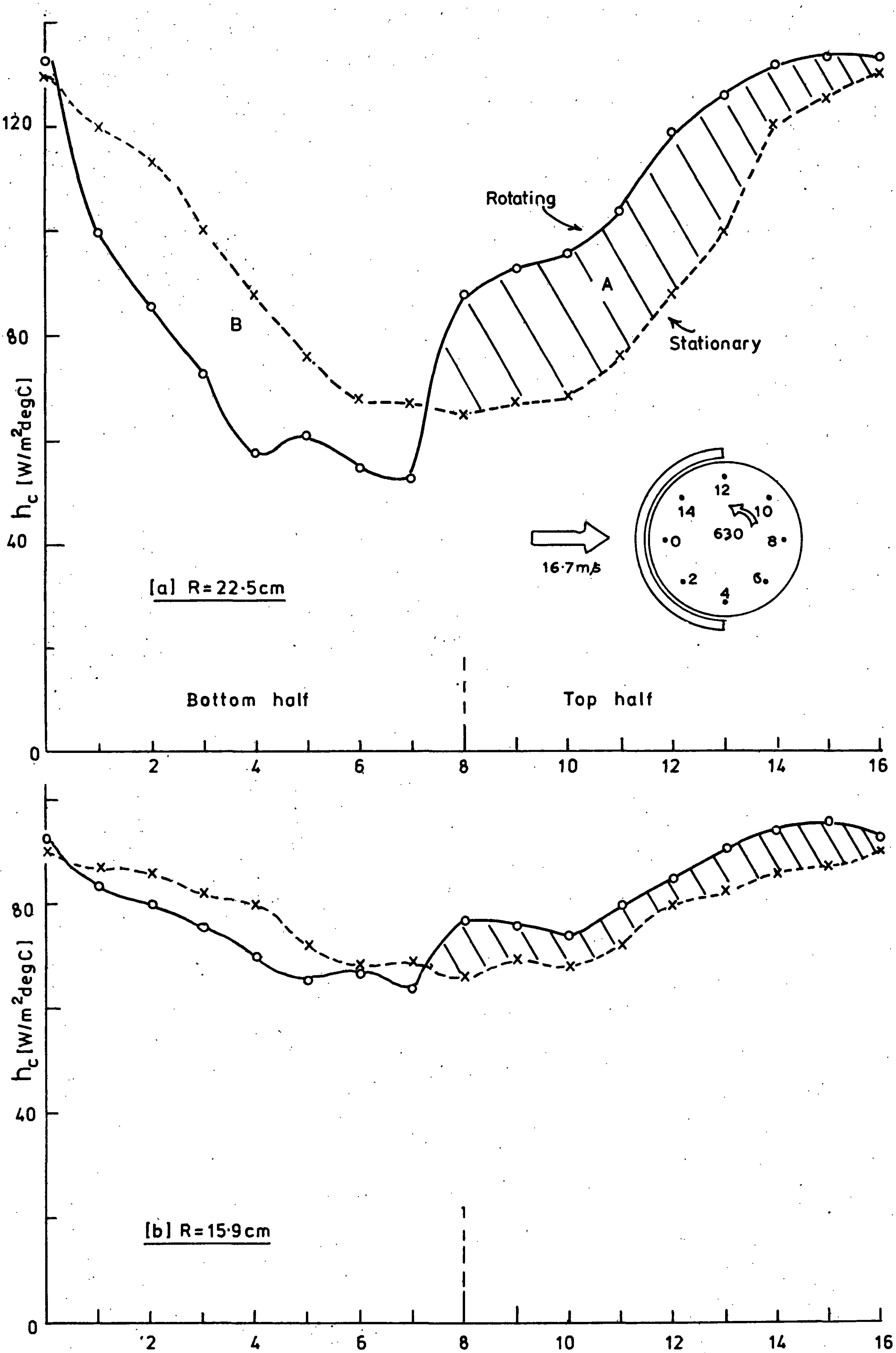

Fig 4·14 Cyclic variation in heat transfer [t=1·25cm]

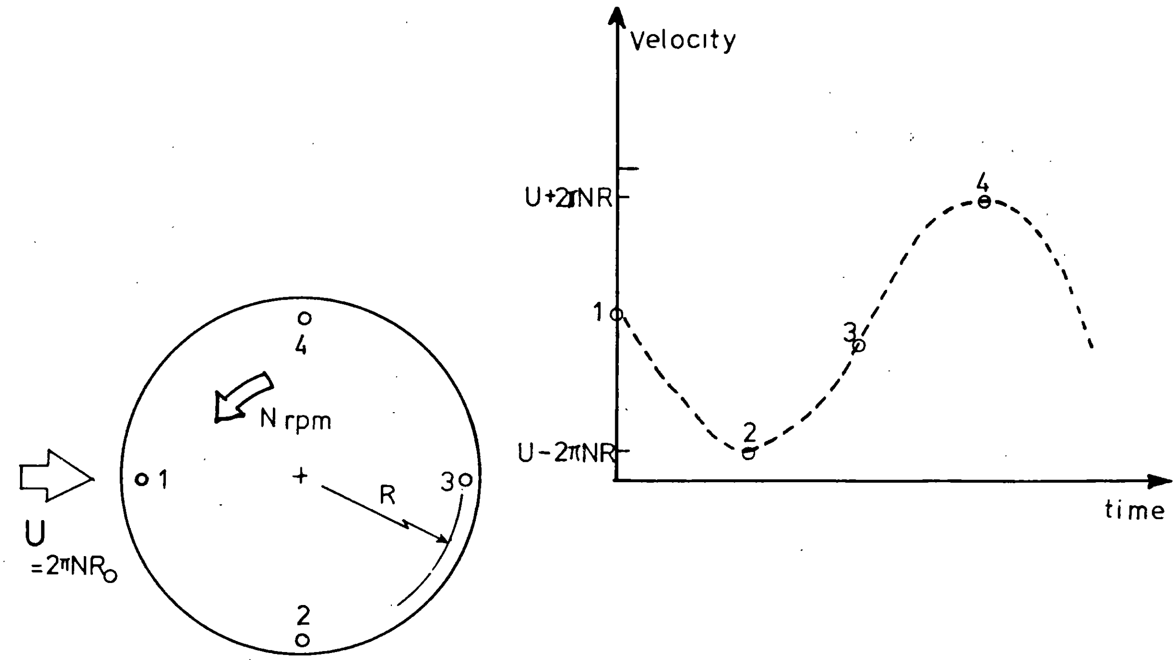

Fig 4·15 Variation in local relative velocity with rotation

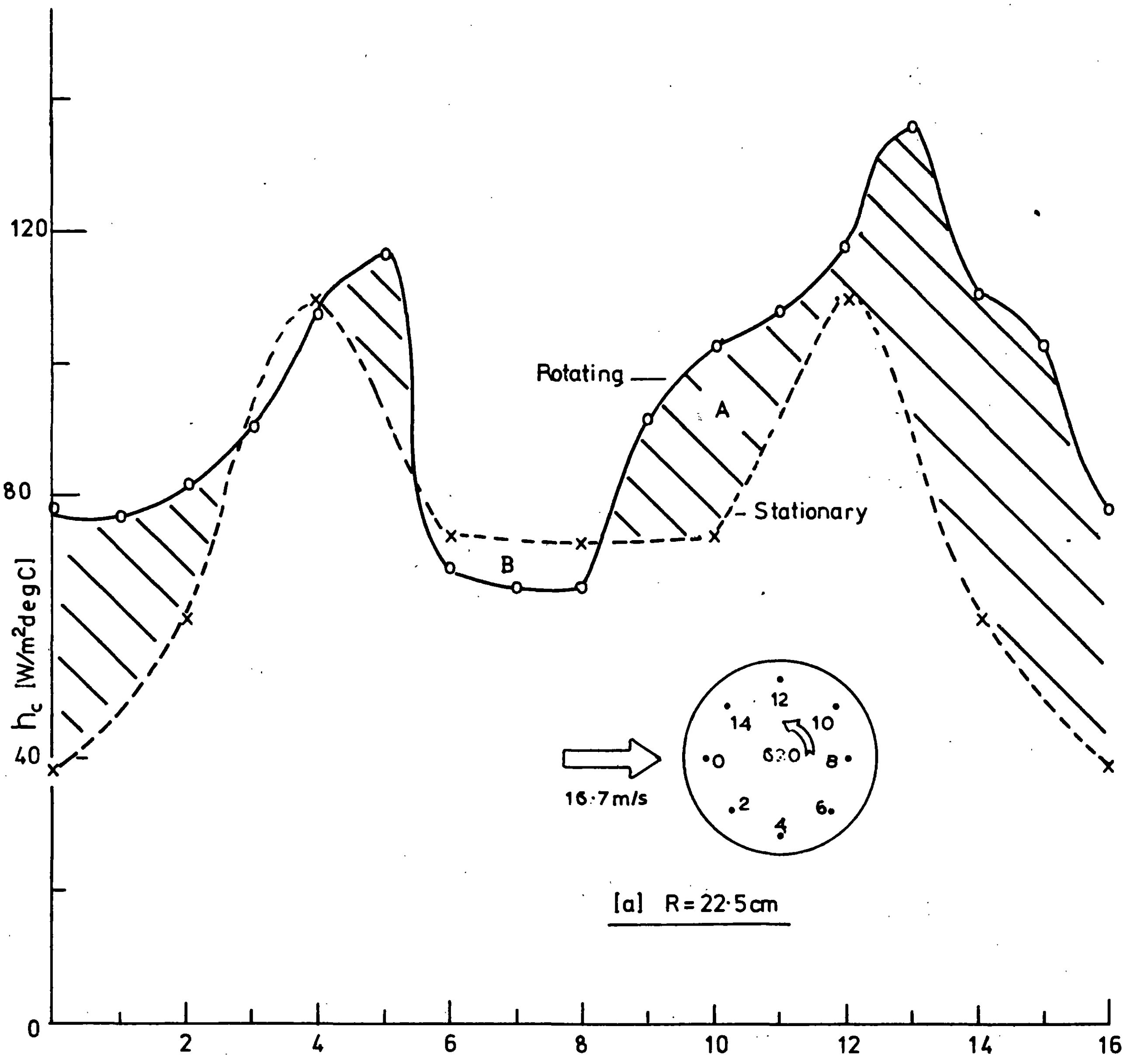

Fig 4·16 Cyclic variation in heat transfer [no shroud]

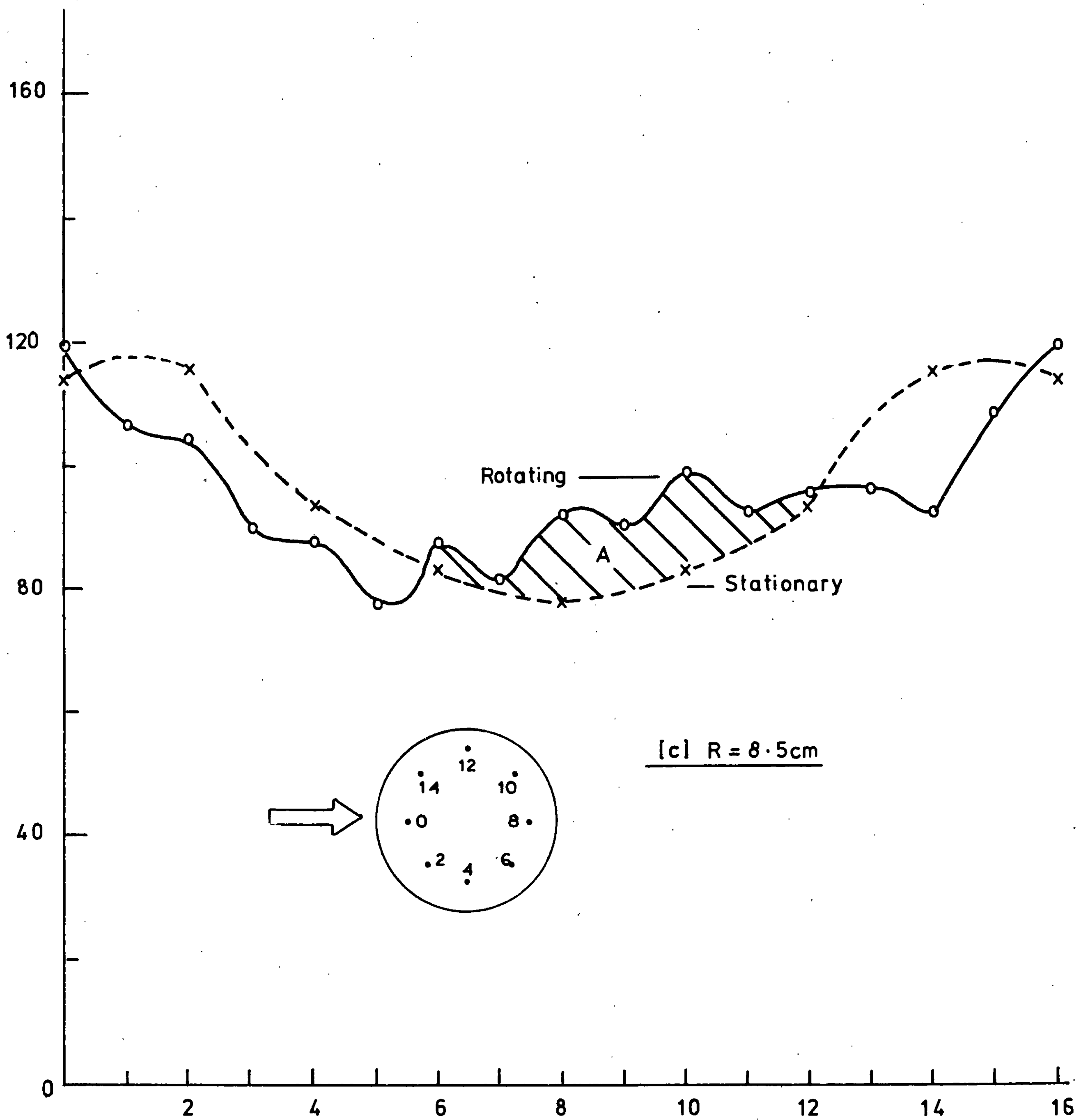

Fig 4·16 Cyclic variation of heat transfer [no shroud]

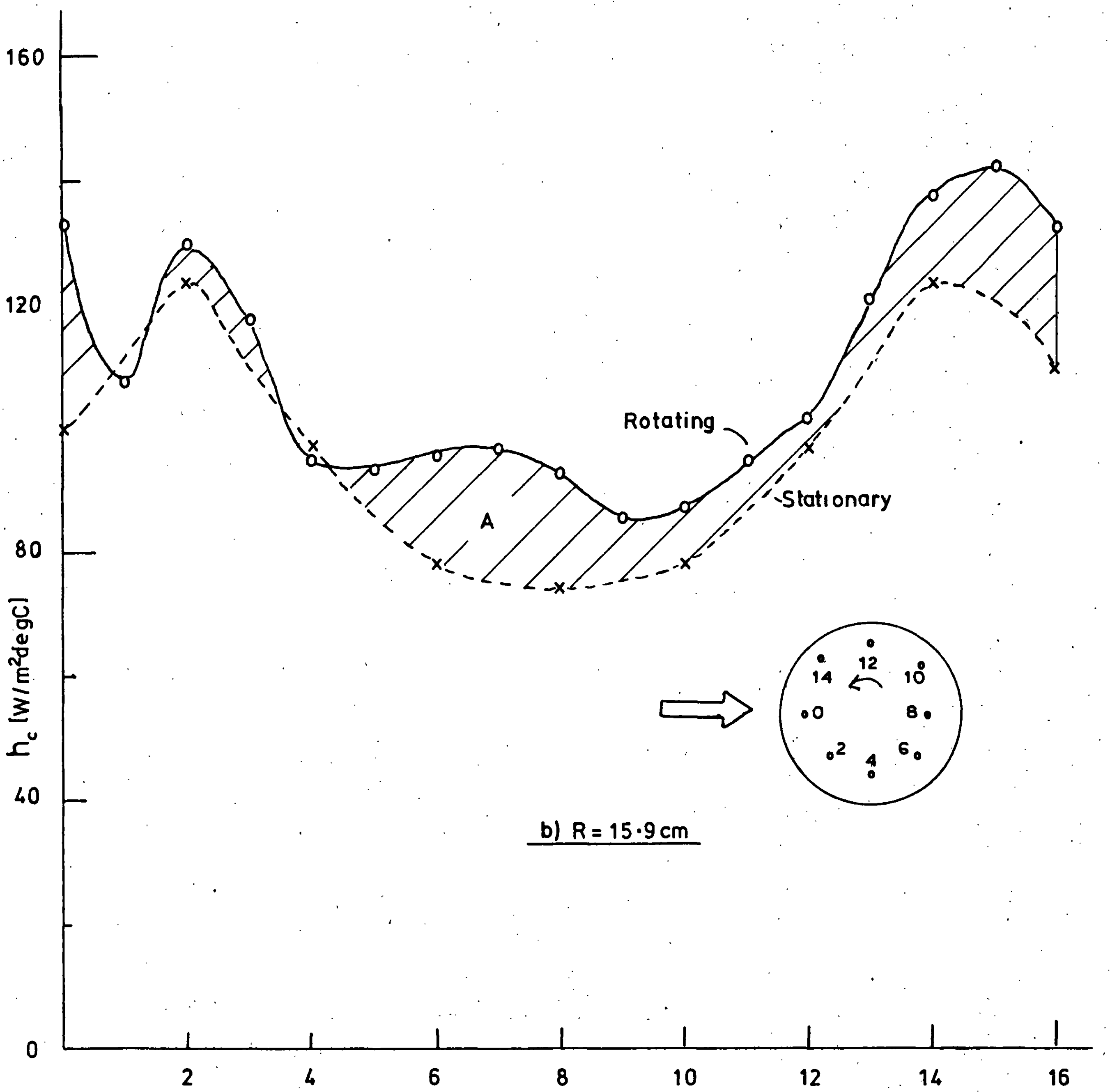

Fig 4·16 Cyclic variation of heat transfer a high heat transfer variation around a circumference which is roughly sinusoidal in shape. The variation is symmetrical about the 0-8 angular position line. At the large radii the amplitude of this variation is substantial. This is shown in Figure (4.14(a)) where the values of the heat transfer coefficient at R = 22.5cm. for the disc stationary, taken from Figure (4.10), are plotted showing the sinusoidal type variations.

The variation in local relative velocity around the circumference for R = 22.5cm. is shown in Figure (4.15). Modifying the stationary disc pattern in the light of the local relative velocity, as suggested earlier leads to the following pattern for the rotating disc. Over much of the lower half of the disc heat transfer coefficients lower than the stationary values are expected, whereas over the top half higher values are expected. In Figure (4.14(a)) the experimental variation for the rotating disc case is superimposed on the stationary values and it is seen the suggested pattern is found in practice.

In Chapter 3 it was shown that the slow response sensor gives a straight average over the path traversed. In Figure (4.14(a)) the area A is larger than area B , so the area under the rotating curve is larger than that under the stationary curve. This is in accord with the average values for the stationary and rotating disc shown in Figure (3.20).

At a smaller radius a similar performance is expected but with a reduced amplitude, since the whole of the traverse of the sensor lies in a more slowly varying part of the flat plate variation. The experimental values given in Figure (4.14(b)), R = 15.9cm. show this to be the case. Finally at R = 8.5cm. the flat plate variation suggests little change in heat transfer values over the circumference. This is confirmed by the lack of change in the thin film temperature at R = 8.5cm. shown in Figure (4.8(c)).

4.7.2. Shroud Absent

Reference is here made to the stationary tests done in Chapter 3, Figure(3.6(b)). The flow is again symmetrical about the centre line 0-8. The variation around the disc is modified from the previous case by the separation and reattachment zones caused by the bluff edge of the disc. Low heat transfer coefficients occur in the separation zone at the leading edge with the high heat transfer coefficients at the start of the reattachment zone occurring further across the face of the disc. Thus the stationary disc exhibits a double peak behaviour and this is shown in Figure (4.16(a)).

Rotation again enhances the heat transfer process in the top half and reduces it in the bottom half of the disc. There is also a tendency for the separation and reattachment zones to be dragged round in the direction of rotation. Where the rotation is against the flow these regions are closer to the leading edge of the disc; conversely they are further away in the bottom half of the disc. Figure (4.17) has been exaggerated to illustrate this effect which was observed with smoke flow visualisation tests. As the separation and reattachment are dragged round the disc areas which were previously in low heat transfer coefficient zones with the disc stationary are now in the reattachment zone with the resulting higher heat transfer coefficients. This gives some explanation as to why, at some positions over the bottom half of the disc, the heat transfer coefficients actually increase with rotation, despite the reduction in relative velocity, see Figure (4.16(a)).

At smaller radii, Figures (4.16(b) and (c)), the cyclic variation follows the stationary variation. The effects of the rotation on the separation and reattachment are still evident over the bottom half of the disc.

The effect of rotation with the shroud removed is more obvious than

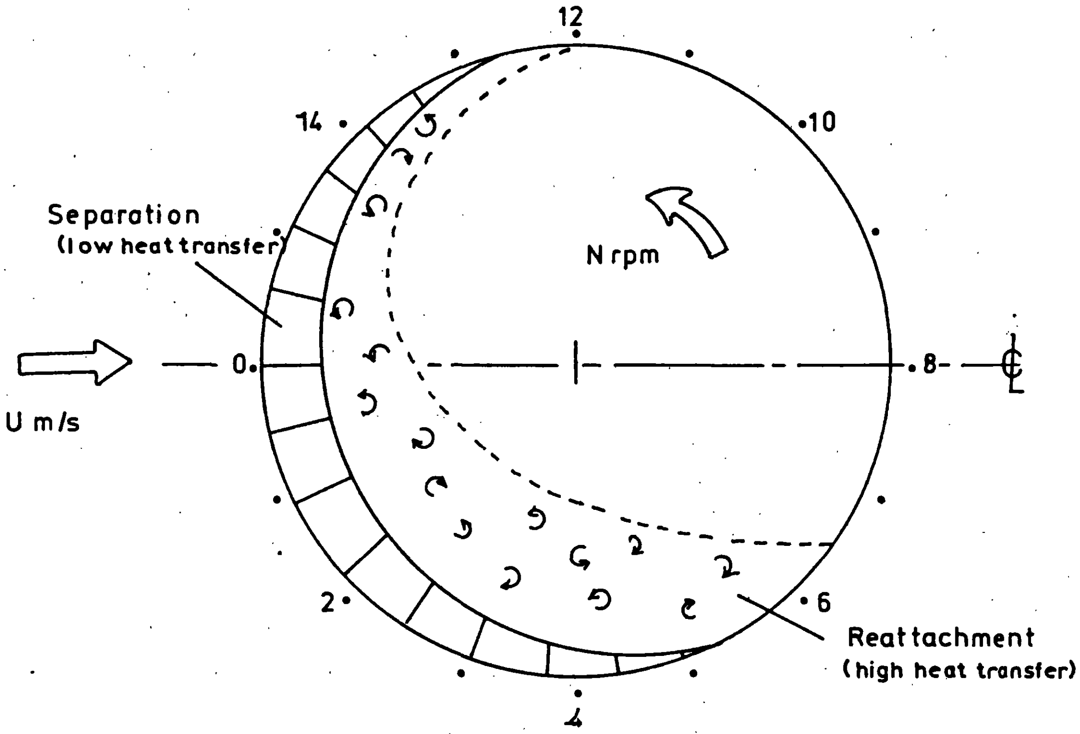

Fig 4·17 Effect of Rotation on Separation and Reattachment with it present, as indicated by the difference between areas A and B in Figures (4.14) and (4.16). This confirms the results from the slow response sensor given in Chapter 3.

4.8. Recommendations

Whilst any conclusions drawn are considered to be qualitatively correct because of the discussion on the sensor in Section 4.3., the quantitative level is in some doubt. It is therefore recommended that the results should be repeated with modifications to the sensor design. In particular the platinum film should be so arranged as to cover the whole of the substrate surface. Calibration of the sensor would remove the errors and inaccuracies present in the theoretical revaluation of the heat transfer coefficient.

Chapter 5

Velocity Measurements

5.1. Introduction

The smoke visualisation tests described in Chapter 3 provided a crude evaluation of the flow pattern over the disc. Although these tests illustrate the general nature of the flow, they do not show what occurs close to the surface of the disc, where, to a large extent the velocity gradients determine the level of heat transfer. A more quantitative assessment of the velocity distribution is obtained from hot wire anemometer traverses out from the disc surface.

The experimental technique was first proved by taking velocity measurements with the disc rotating in still air. Published theoretical and experimental data is available with which comparison of the present measurements was made. Smoke visualisation tests have shown that the flow pattern over the disc is complicated by separation at the leading edge followed by reattachment on the disc face. Furthermore this effect could be reduced by positioning a shroud just below the surface of the disc. Velocity measurements with the disc held stationary in a transverse air stream were used to confirm this. Finally with the shroud set at the position for minimum separation the velocity profile patterns over the disc surface were obtained for the disc rotating in a transverse air stream. The main air stream dominance over the heat transfer performance is discussed in the light of these patterns.

5.2. Rotating Disc in Still Air

Velocity measurements on this configuration are to be used to confirm the experimental technique by making comparisons with published experimental and theoretical works.

Fig.(5.1)[19] shows pictorially the laminar motion produced by an infinite plane disc rotating in a viscous medium around the axis $r = 0$, with constant angular velocity ω. The Navier Stokes equations for the axially symmetric fluid motion expressed in cylindrical co-ordinates r, ϕ and z for an incompressible viscous fluid are given as:

$$\left.\begin{aligned}
&\frac{\partial v_r}{\partial t} + v_r \frac{\partial v_r}{\partial r} + v_z \frac{\partial v_r}{\partial z} - \frac{v_\phi^2}{r} = -\frac{1}{\rho}\frac{\partial p}{\partial r} + \nu\left[\frac{\partial^2 v_r}{\partial r^2} + \frac{1}{r}\frac{\partial v_r}{\partial r} - \frac{v_r}{r^2} + \frac{\partial^2 v_r}{\partial z^2}\right] \\
&\frac{\partial v_\phi}{\partial t} + v_r \frac{\partial v_\phi}{\partial r} + v_z \frac{\partial v_\phi}{\partial z} + \frac{v_\phi v_r}{r} = \nu\left[\frac{\partial^2 v_\phi}{\partial r^2} + \frac{1}{r}\frac{\partial v_\phi}{\partial r} - \frac{v_\phi}{r^2} + \frac{\partial^2 v_\phi}{\partial z^2}\right] \\
&\frac{\partial v_z}{\partial t} + v_r \frac{\partial v_z}{\partial r} + v_z \frac{\partial v_z}{\partial z} = -\frac{1}{\rho}\frac{\partial p}{\partial z} + \nu\left[\frac{\partial^2 v_z}{\partial r^2} + \frac{1}{r}\frac{\partial v_z}{\partial r} + \frac{\partial^2 v_z}{\partial z^2}\right]
\end{aligned}\right\} \tag{5.1}$$

Here v_r, v_ϕ, and v_z respectively are the radial, tangential and axial components of the velocity vector, p is the pressure and ν the kinematic viscosity.

The equation of continuity for an incompressible fluid is

$$\frac{\partial v_r}{\partial r} + \frac{v_r}{r} + \frac{\partial v_z}{\partial z} = 0 \tag{5.2}$$

The boundary conditions of this problem are

$$\left.\begin{aligned}
&v_r = 0,\ v_\phi = r_\omega,\ v_z = 0 \quad \text{for } z = 0 \\
&v_r = 0,\ v_\phi = 0 \qquad\qquad\quad \text{for } z = \infty
\end{aligned}\right\} \tag{5.3}$$

By a suitable change of variables equations (5.1) and (5.2) may be reduced to form simultaneous ordinary differential equations for the functions F, G, H and P, given by

$$\left.\begin{aligned}
&F^2 - G^2 + F'H = F'' \\
&2FG + G'H = G'' \\
&HH' = P' + H'' \\
&2F + H' = 0
\end{aligned}\right\} \tag{5.4}$$

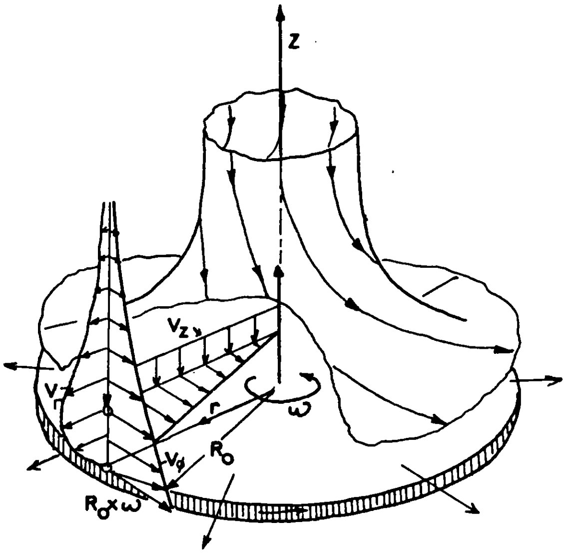

[19]

Fig 5·1 Flow in the neighbourhood of a rotating disc in still air

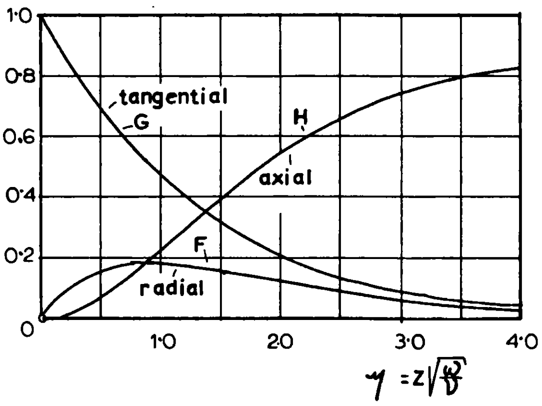

Fig 5·2 Velocity distribution [16]

where $v_r = r\omega F(\eta)$, $v_\phi = r\omega G(\eta)$, $v_z = \sqrt{\nu\omega}H(\eta)$, $p = -\rho\nu\omega P(\eta)$

and $$\eta = z\sqrt{\frac{\omega}{\nu}}$$

The three velocity functions F, G and H have been determined by Cochran[16] and are represented graphically in Figure (5.2). The two velocity components of particular interest are v_r and v_ϕ. The axial component v_z is of the order $\sqrt{\nu\omega}$; except in cases of larger η and small radii it can normally be neglected in comparison to the other two.

Figure (5.3) gives the results of Gregory, Stuart and Walker[8] of the velocity field near a rotating disc in conditions of laminar flow. The figure gives values for the total tangential velocity $v_T = \sqrt{(v_r^2 + v_\phi^2)}$. The agreement between the experimental and theoretical values is good. Measurements done by Cobb and Saunders[3] have also shown similar agreement. In both these cases the total tangential velocity was measured by a small pitot tube.

The experiments[8] were continued into the transition and turbulent regions of flow. Here no exact solution exists with which to make suitable comparisons. Assessments of F and G based on assumed types of velocity profiles have been made[18,10]. However Figure (5.4) illustrates the wide disagreement between experiment and the predictions of these theories.

5.3. Experimental Testing

The velocity profiles were measured with a 5 micron tungsten hot wire probe mounted on a traversing mechanism. The electric power required to maintain the wire at a constant temperature was monitored by a Disa 55D01 Anemometer unit, in the form of a bridge voltage V_B. Each wire was calibrated in the free stream of the wind tunnel.

The two velocity components v_r and v_ϕ were initially measured individually by positioning the wire normal to each direction. Figure (5.6) shows the velocities measured in the laminar region for three disc speeds,

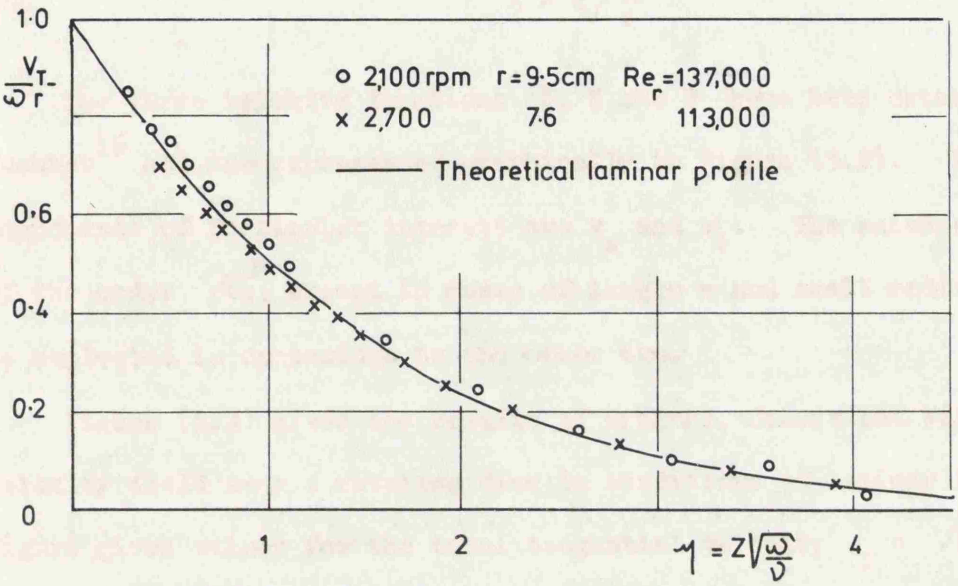

Fig 5·3 Variation of resultant velocity through the laminar boundary layer [8]

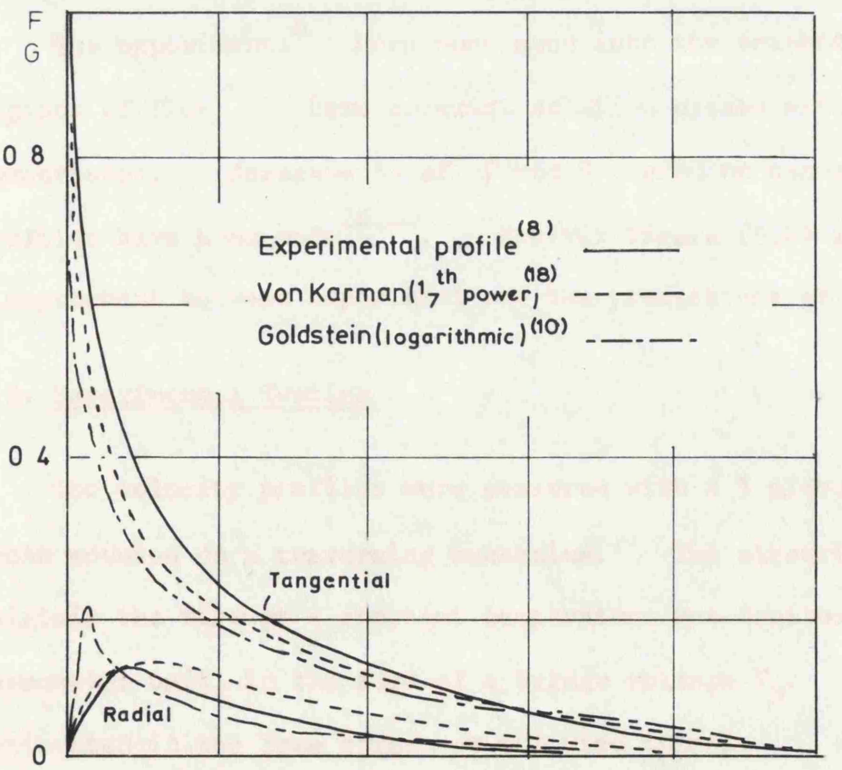

Fig 5·4 Radial and Tangential components of experimental and theoretical turbulent velocity profiles (8)

N = 296, 530 and 630 r.p.m. together with the theoretical prediction of Cochran[16]. The main problem associated with this method is the influence of one component on the other being measured. The formation of eddies from the wire supports enhances the cooling of the hot wire with the result that higher velocities are inferred from the anemometer unit than those actually present. The influence of v_ϕ on the radial component can be seen from Figure (5.6); the readings are between 20 and 40 per cent higher than the theoretical predictions of Cochran. The tangential velocity measurements show better agreement, which is to be expected as the radial component is relatively small and its influence is swamped by the tangential velocity.

A more accurate method of measuring these two components was achieved by positioning the wire at the two 45 degrees orientations, to each component. v_r and v_ϕ were then determined in the following manner.

Referring to Figure (5.7) which gives the geometrical situation, Heinz[18] has suggested that the velocity u_2, as measured by the hot wire anemometer, is given as

$$u_2^2 = V_T^2(\sin^2\theta + A^2\cos^2\theta) \tag{5.5}$$

where the factor 'A' has a value between 0.1 and 0.3 depending on the magnitude of the velocity (the value of A increases with decreasing velocity). Also from Figure (5.7)

$$u_1^2 = V_T^2(\cos^2\theta + A^2\sin^2\theta) \tag{5.6}$$

u_2 and u_1 are not velocities in the true sense as they do not actually exist anywhere. They are the computed velocity values from the anemometer bridge voltages taken from the calibration curve when the wire is set normal to the wind tunnel free air stream.

From equation (5.5) and (5.6) it can be seen that

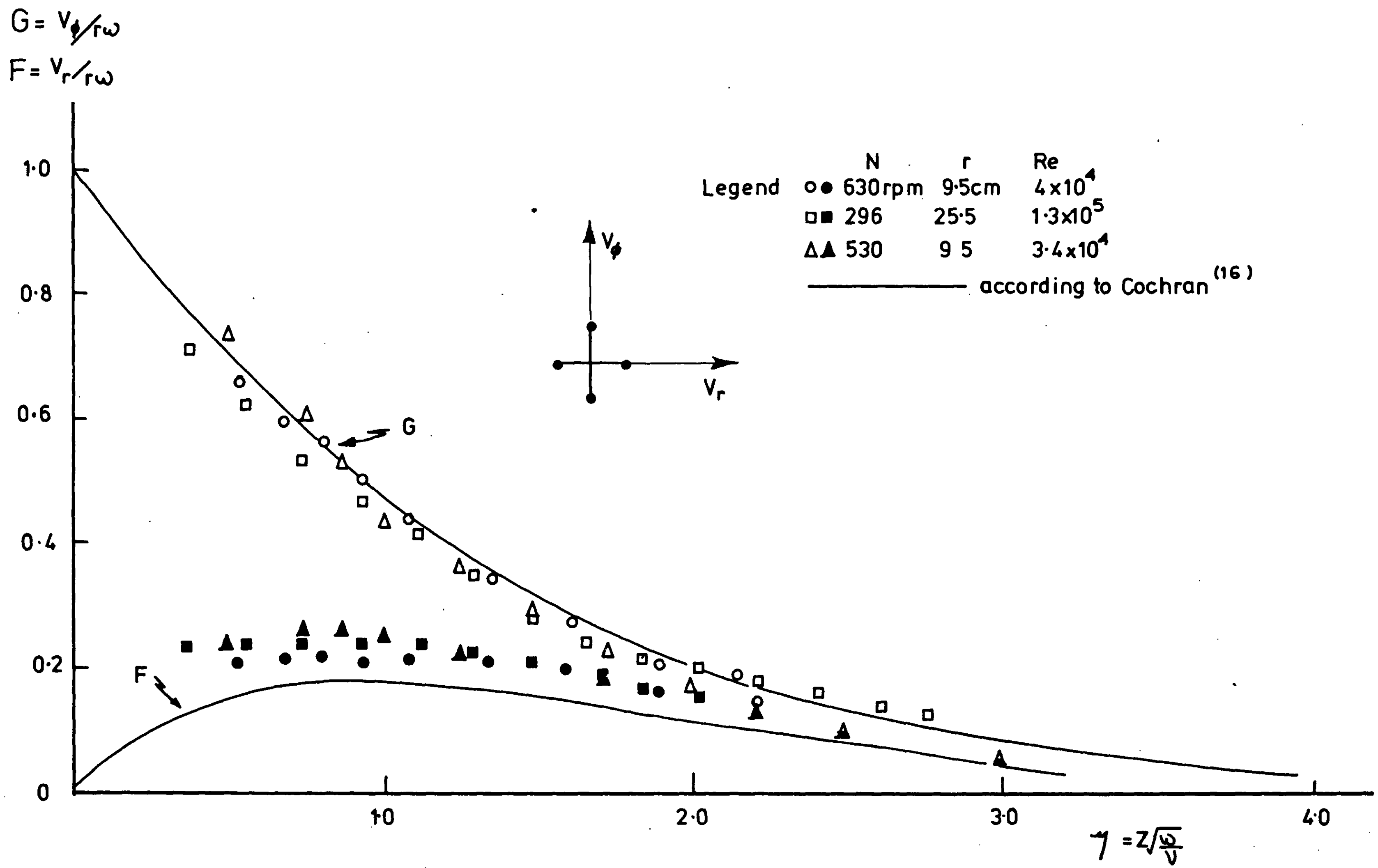

Fig 5·6 Rotating Disc in still air (probe set normal to components)

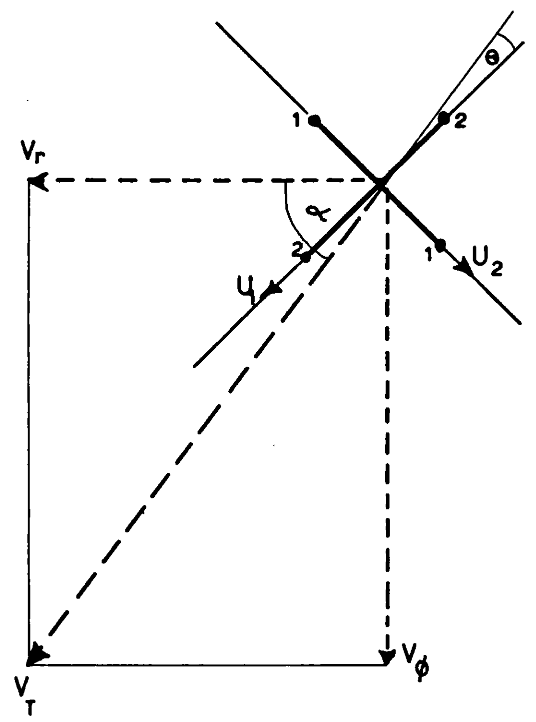

Fig 5·7 Velocity notation

$$\left(\frac{u_2}{u_1}\right)^2 = \frac{\sin^2\theta + A^2\cos^2\theta}{\cos^2\theta + A^2\sin^2\theta} = \beta^2$$

so that
$$\sin^2\theta = \frac{\beta^2 - A^2}{(1 - A^2)(1 + \beta^2)} \tag{5.7}$$

From Figure (5.7) the radial and tangential velocities are given as

$$v_r = V_T \cos\alpha \ , \ v_\phi = V_T \sin\alpha \ ,$$

where $\alpha = 45 + \theta$.

The velocities can be evaluated provided u_2, u_1 and the factor 'A' are known. 'A' unfortunately is dependent on the velocity V_T, so that it is necessary to guess an initial value, determine V_T, and then update accordingly. The dependence on the velocity was determined experimentally by placing the hot wire parallel to the free air stream. θ in this instance is zero, so that equation (5.5) and (5.6) give

$$u_1 = V_T \ , \text{ and } u_2 = AV_T$$

so that $A = \dfrac{u_2}{u_1}$.

A typical calibration for 'A' is given below.

U m/s	V_{B1} volts	V_{B2}	u_1 m/s	u_2	A
16.7	8.75	6.88	16.7	2.7	0.16
14.0	8.49	6.76	14.0	2.35	0.17
11.1	8.22	6.65	11.1	2.0	0.18
7.9	7.85	6.49	7.9	1.6	0.20
5.55	7.52	6.3	5.55	1.2	0.216
3.53	7.11	6.13	3.53	0.95	0.27
2.5	6.8	5.99	2.5	0.70	0.28
2.0	6.65	5.92	2.0	0.60	0.30

The tests on the rotating disc in the still air were repeated with the hot wire probe set at the two-45 degree orientations to the velocity components. The accurate positioning of the probe was achieved with the traversing gear so that the readings from the two positions corresponded with each other. The minimum distance from the disc surface was 0.25 mm. Below this value the conduction and radiation effects from the wire to the disc become predominant. v_r and v_ϕ were determined in the manner described above. The results are given in Figure 5.8. A marked improvement in agreement is found between the measured radial component F and the theoretical predictions. The tangential component G , shows excellent agreement.

This correlation between theory and measurements was taken as proving the experimental technique and the hot wire anemometer unit was used to measure the velocity profiles over the stationary and rotating disc in the transverse air stream. However, it is appreciated that, in both these cases, the flow may not be laminar and that any hot wire signals analysed may be affected by the fluctuating velocity component as well as by the factor 'A'. For the case of the rotating disc in the transverse air stream these effects have been ignored and the flow assumed to be 'laminar'. The complex analysis of the turbulent motion was beyond the capabilities of the anemometer unit. The results are therefore discussed in a qualitative manner.

5.4. Stationary Disc in a Transverse Air Stream

In Chapter 3 an explanation of the radial variation of the heat transfer coefficient in terms of flow separation at the disc leading edge followed by reattachment to the disc face is given. Smoke tests confirm this pattern. Further tests with a shrouded disc, to simulate discs of differing aspect ratios, add weight to the explanation. In particular complete flow attachment over the whole disc face is obtained when the shroud is set back a small distance from the face of the disc.

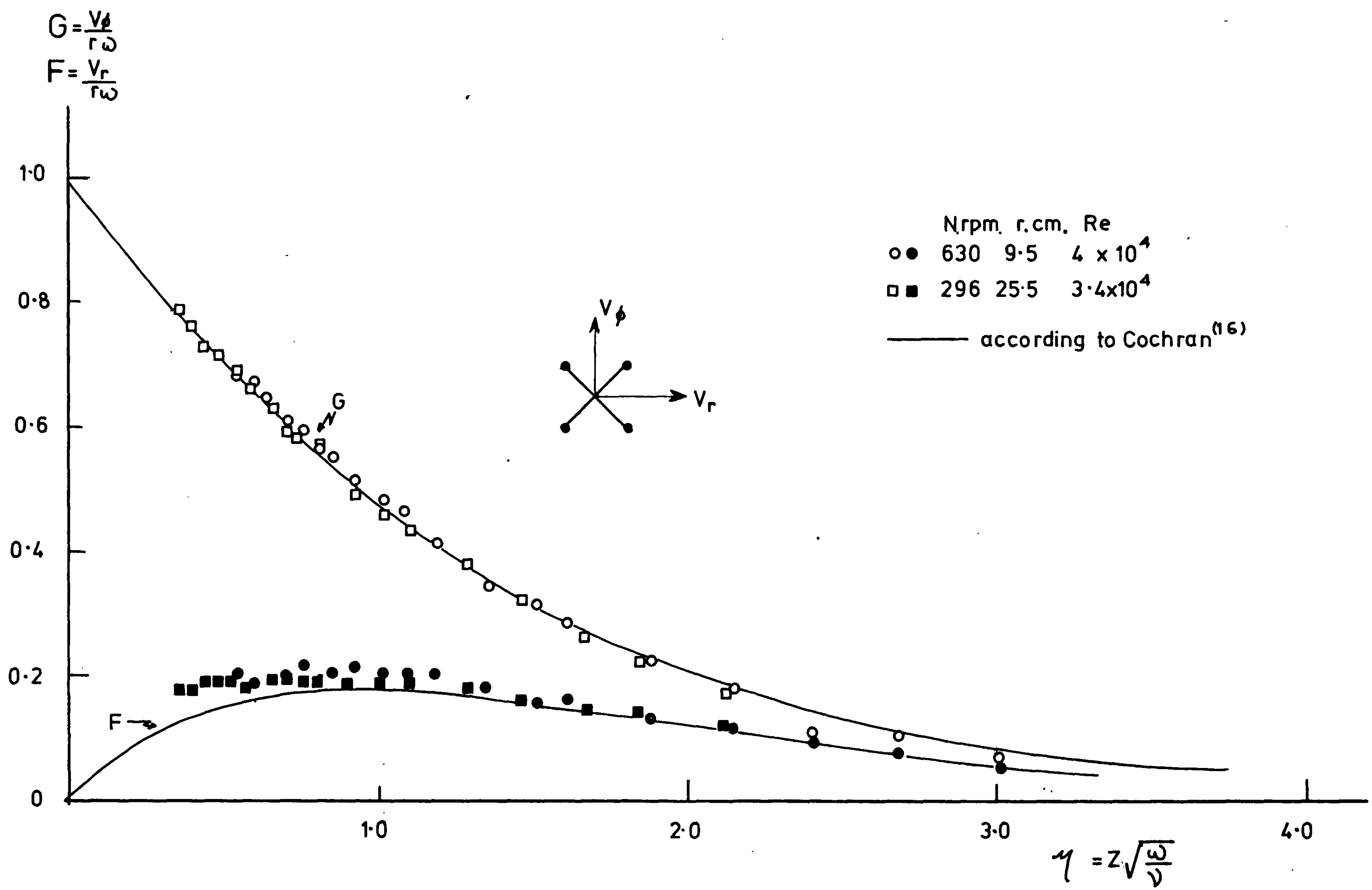

Fig 5·8 Rotating Disc in still air (probe at 45 deg to components)

To confirm this flow separation pattern in more detail, velocity profiles were measured at four positions on the leading half of the disc on the centre line of the tunnel with the disc stationary. These positions are indicated in Figure (5.9). For this particular configuration the hot wire was placed normal to the air stream direction; there being only one velocity component present. Three shroud positions, t = 5 cm, 1.25 cm and 0 cm were investigated. Figures (5.9(a),(b),(c)) show the velocity profiles obtained.

With the shroud set at t = 5 cm, Figure (5.9(a)), the separation at the leading position A, is shown by a low velocity stagnant region close to the surface and a thin region of high shear stress where the velocity increases rapidly to the free stream level. Downstream at positions B,C the stagnant region has grown considerably. The region of high shear has been dispersed by diffusion and mixing processes. At position D the velocity profile is consistent with fully attached flow.

With the shroud set at t = 1.25 cm, Figure (5.9(b)) shows the velocity profiles are considerably altered from the previous case. Very little separation at the leading edge is found. The velocities approximate to those found in developing turbulent flow over a flat plate. For comparison turbulent velocity profiles and laminar velocity profiles on a flat plate are shown. The turbulent profiles are calculated using[20]

$$\frac{u}{U} = \left(\frac{z}{\delta}\right)^{1/7} \tag{5.8}$$

where $\frac{\delta}{x} = 0.379\left(\frac{\nu}{Ux}\right)^{1/5}$, and x is the distance from the leading edge, in this instance the distance from the tip of the shroud.

The laminar profiles are calculated from the numerical solution of the Blasius equation[19]. The boundary layer thickness in this case is given as

$$\delta = 5.0\sqrt{\frac{\nu x}{U}} \tag{5.9}$$

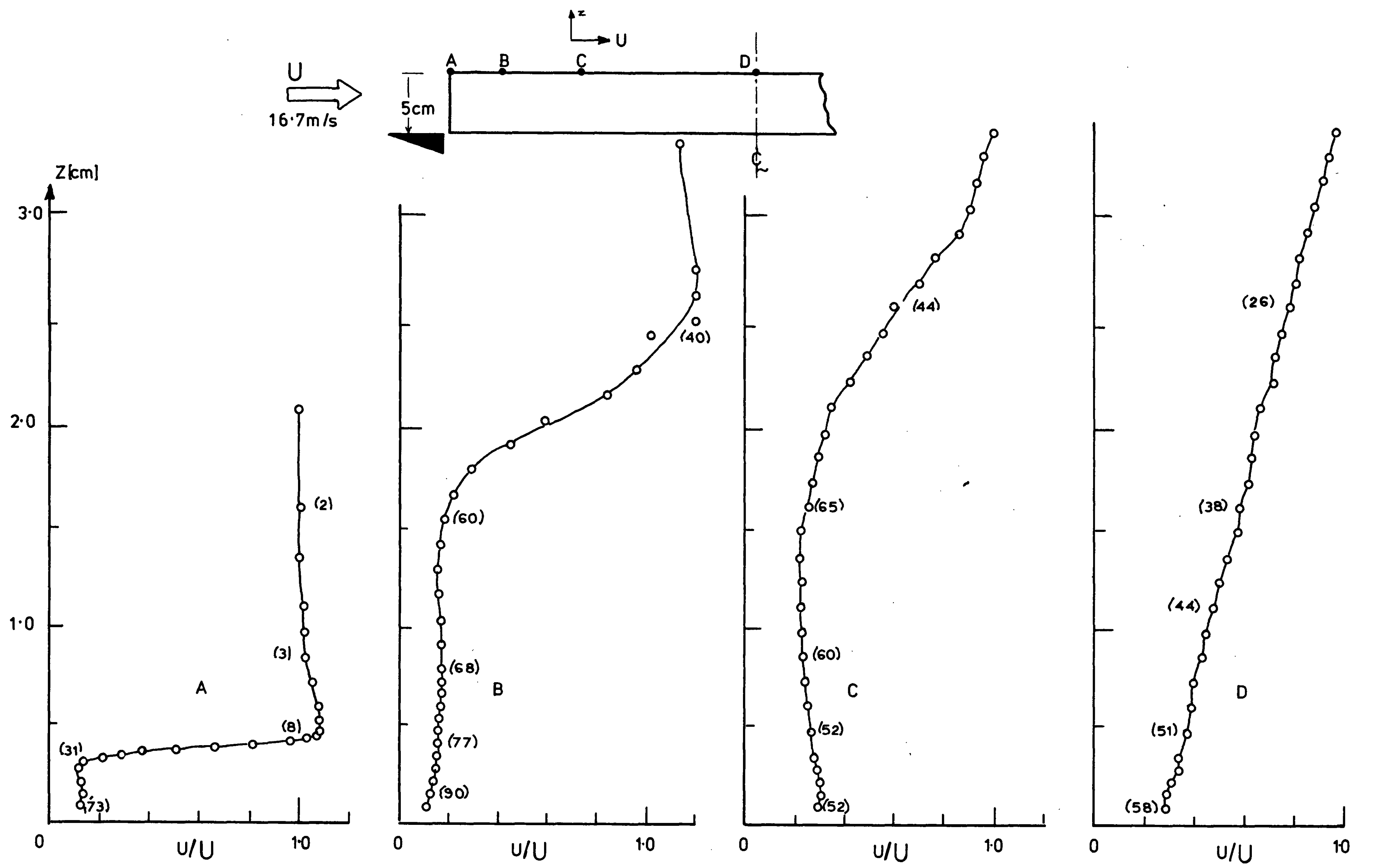

Fig 5·9a Velocity profiles over stationary disc [shroud at 5cm]

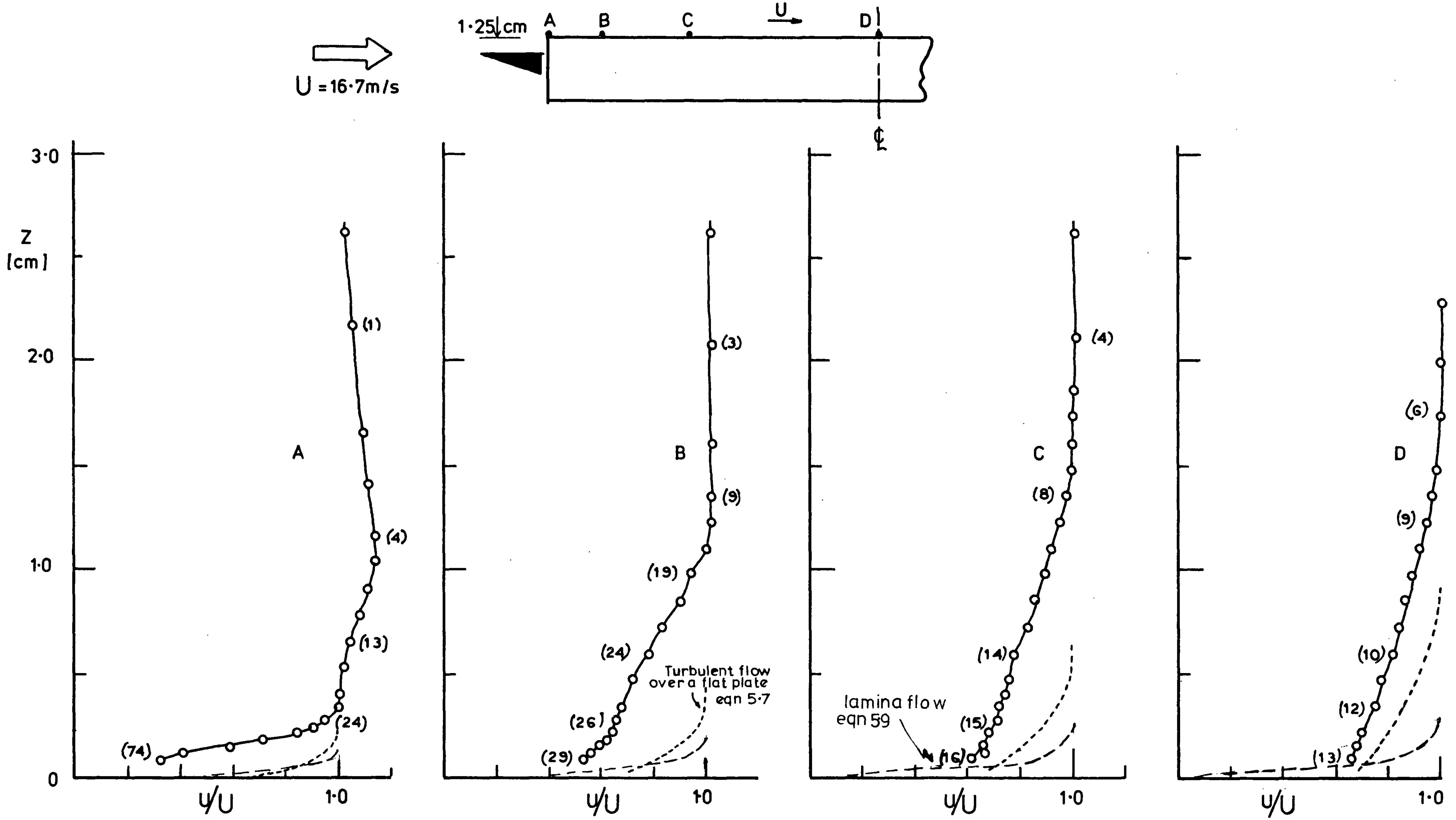

Fig 5·9 b Velocity profiles over stationary disc [shroud at 1·25cm]

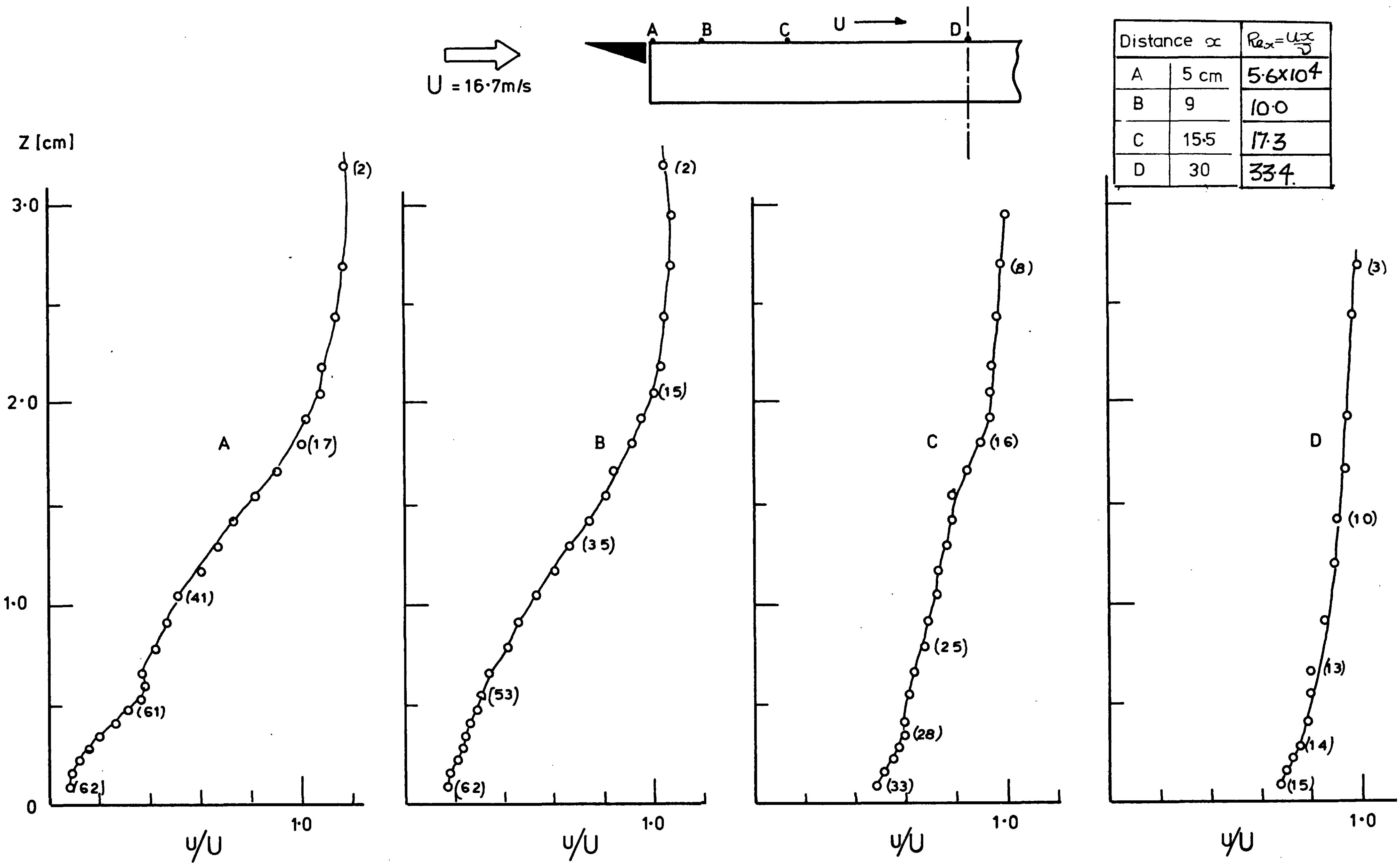

Distance x		$Re_x = \frac{Ux}{\nu}$
A	5 cm	5.6×10^4
B	9	10·0
C	15·5	17·3
D	30	33·4

Fig 5·9c Velocity profiles over stationary disc[shroud flush]

With the shroud set flush with disc face, Fig.(5.9(c)) shows a thick boundary layer at positions A and B . These profiles are similar to position C of Figure (5.9(a)), characterising the rear part of the separation bubble. This is consistent with separation occurring at the tip of the shroud. The profiles at position C and D , Figure (5.9(c)), indicate that the flow is reattached.

In addition to measuring velocities the hot wire gives a measure of turbulence intensity. The percentage turbulent intensity is given by

$$Tu = 100\, V_{RMS} \frac{4V_B}{V_B^2 - V_o^2}$$

where V_{RMS} is the root mean square voltage recorded by the anemometer unit. The bracketed numbers against each profile in Figures (5.9) give the local value of Tu. In every case it is seen that considerable turbulence exist throughout the boundary layer. The shroud and leading edge of the disc both act as turbulence promoters. This explains why the measured profiles are closer to the turbulent prediction despite the Reynolds numbers suggesting that the flow should remain laminar over the first leading half of the disc.

5.5. Rotating Disc in a Transverse Air Stream

All the heat transfer coefficient measurements suggest that the heat transfer process is dominated by the main air stream. For a fixed disc speed of 630 r.p.m. changes in main stream velocity from 0 - 33 m/s cause an eight fold change in the heat transfer coefficient, see Fig.(3.5(b)); whereas at a fixed wind speed of 33 m/s a change in the disc speed from 296 - 1120 r.p.m. only causes a 10 per cent change in heat transfer coefficient. If the shape of velocity profile and in particular the steepness close to the disc surface is a measure of the heat transfer coefficient level, then this heat transfer pattern suggests a velocity profile which is a function of both main air stream speed and disc speed but much more heavily dependent on the main air stream speed.

The heat transfer results of Chapter 3 are average values over the circular path traversed by the sensor. Since it is not possible to present velocity profiles in this way a picture over the whole disc face has been built up. Velocity measurements were taken with the disc rotating at 630 r.p.m. for a range of transverse air speeds from 2.5 m/s to the matched speed of 16.7 m/s. To remove complications due to flow separation and reattachment, the shroud was set at t = 1.25 cm in all the tests. For each condition measurements were taken at two radial positions, R = 23.7 cm and 9.5 cm at each of the four angular positions as illustrated in Figure (5.9). The two velocity components v_r and v_ϕ were determined using the 45^o technique discussed in Section 5.2.

The results are presented graphically in Figures (5.10(a - h)) and Figures (5.11(a - h)). Figures (5.12(a)) and (5.12(b)) show the resultant velocity v_T, plotted for seven locations out from the surface of the disc for u = 2.5 m/s and 16.7 m/s respectively. They illustrate how the velocity swirls round from the peripheral direction at z = 0 to the main stream direction at position 7. The centrifugal action on the velocity can be seen quite clearly at the low velocity u = 2.5 m/s, and at u = 16.7 m/s, where the velocity profiles at top and bottom angular positions are forced outwards from the centre.

It is obvious from all the velocity profiles presented that changes in the main air stream velocity have a marked effect on the steepness of the profile close to the disc surface, (this can be inferred from an extrapolation of the surface value, zero or local disc surface velocity and the closest hot wire measurement made. In particular the comparative effect on the velocity profiles of the main stream and disc rotational speed is clearly shown in Figure (5.13(a) and (b)).

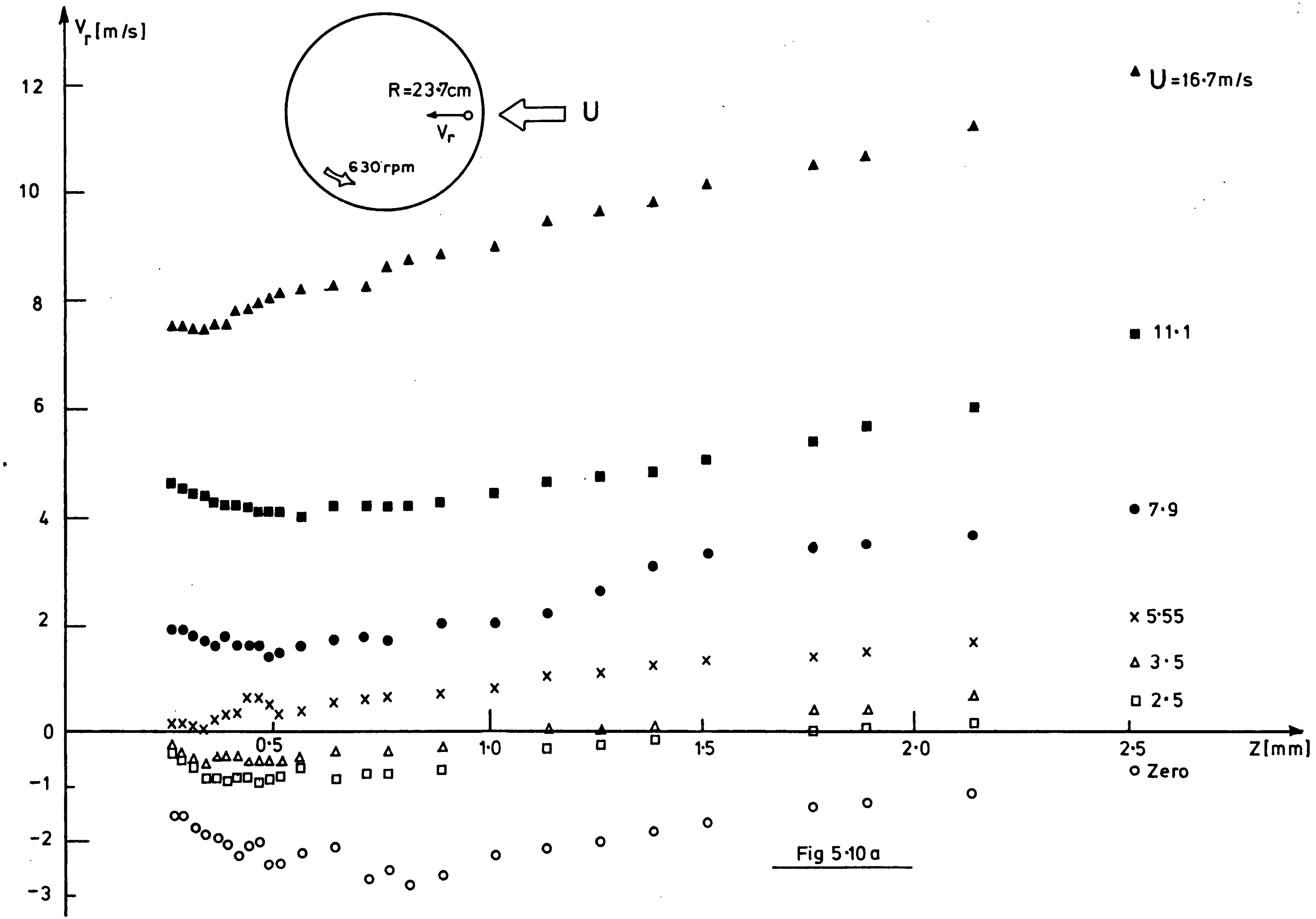

V_r [m/s]
12
10
8
6
4
2
0
-1
-2
-3
R=23·7cm
V_r
U
630 rpm
0·5
1·0
1·5
2·0
2·5
Z [mm]
U=16·7m/s
11·1
7·9
5·55
3·5
2·5
Zero

Fig 5·10 a

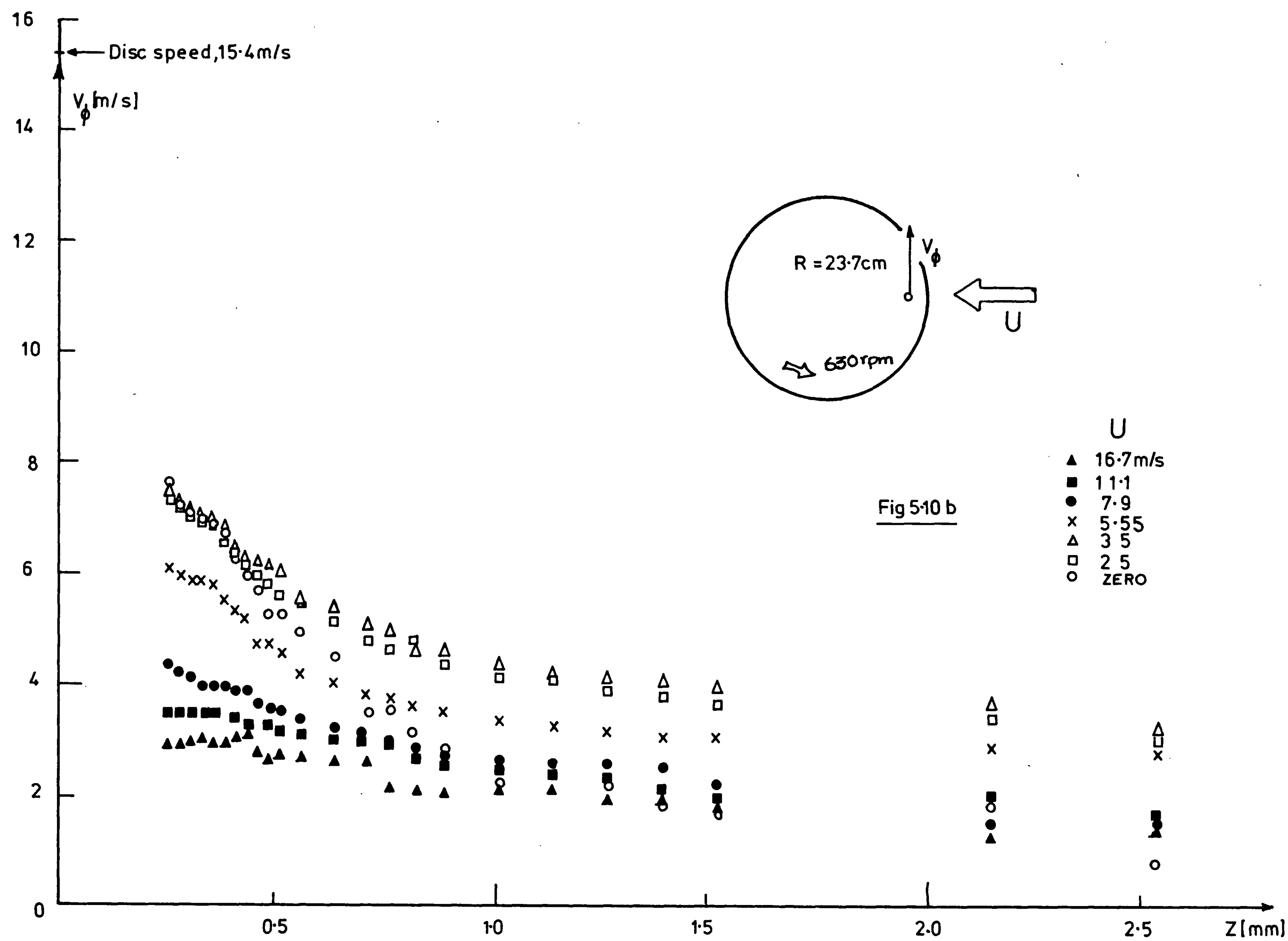

Disc speed, 15·4 m/s
V_ϕ [m/s]
R = 23·7cm
V_ϕ
U
630 rpm
U
16·7 m/s
11·1
7·9
5·55
3 5
2 5
ZERO
Z [mm]

Fig 5·10 b

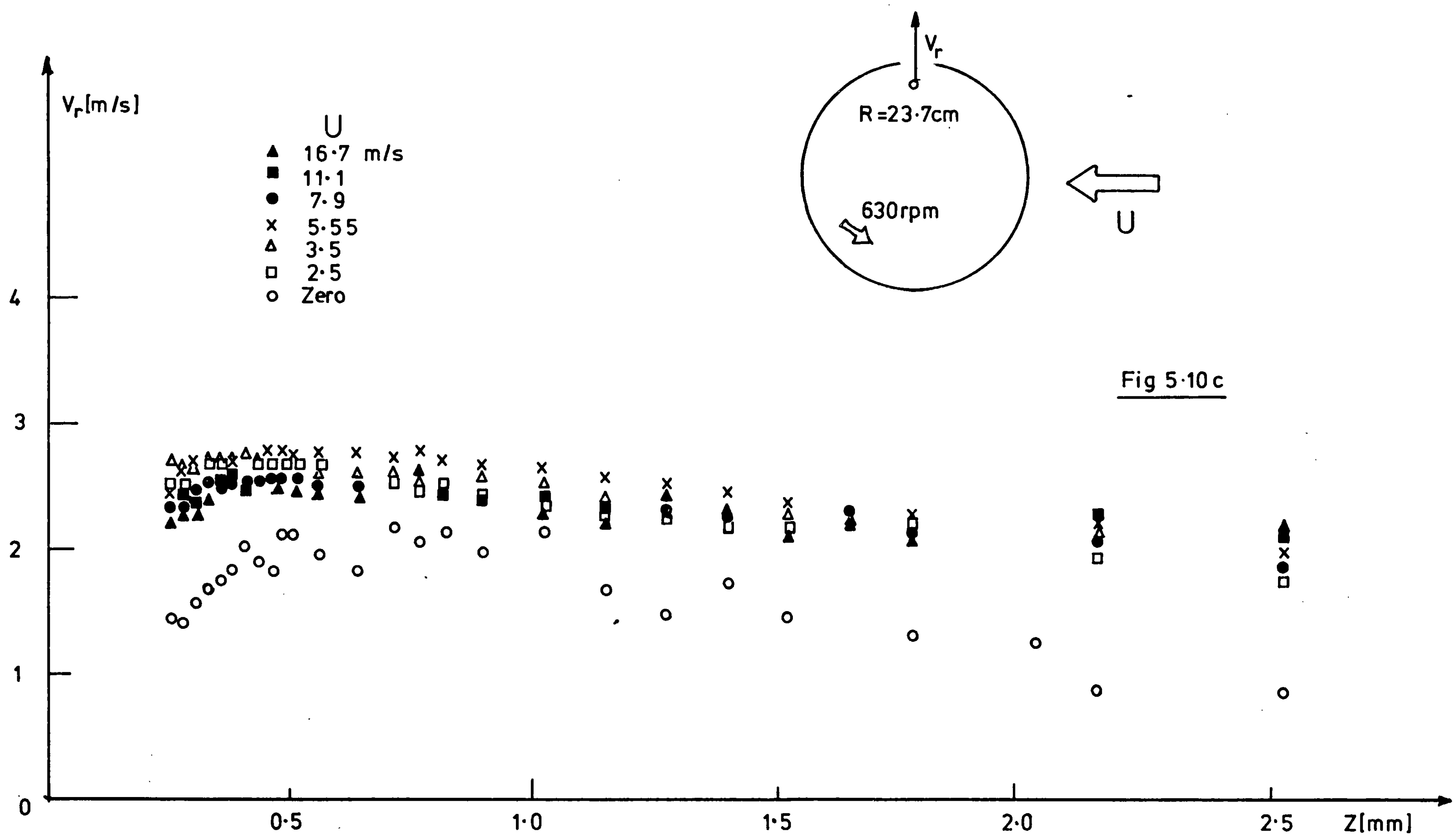

V_r [m/s]
U
16·7 m/s
11·1
7·9
5·55
3·5
2·5
Zero
V_r
R = 23·7cm
630rpm
U
0
1
2
3
4
0·5
1·0
1·5
2·0
2·5
Z[mm]

Fig 5·10c

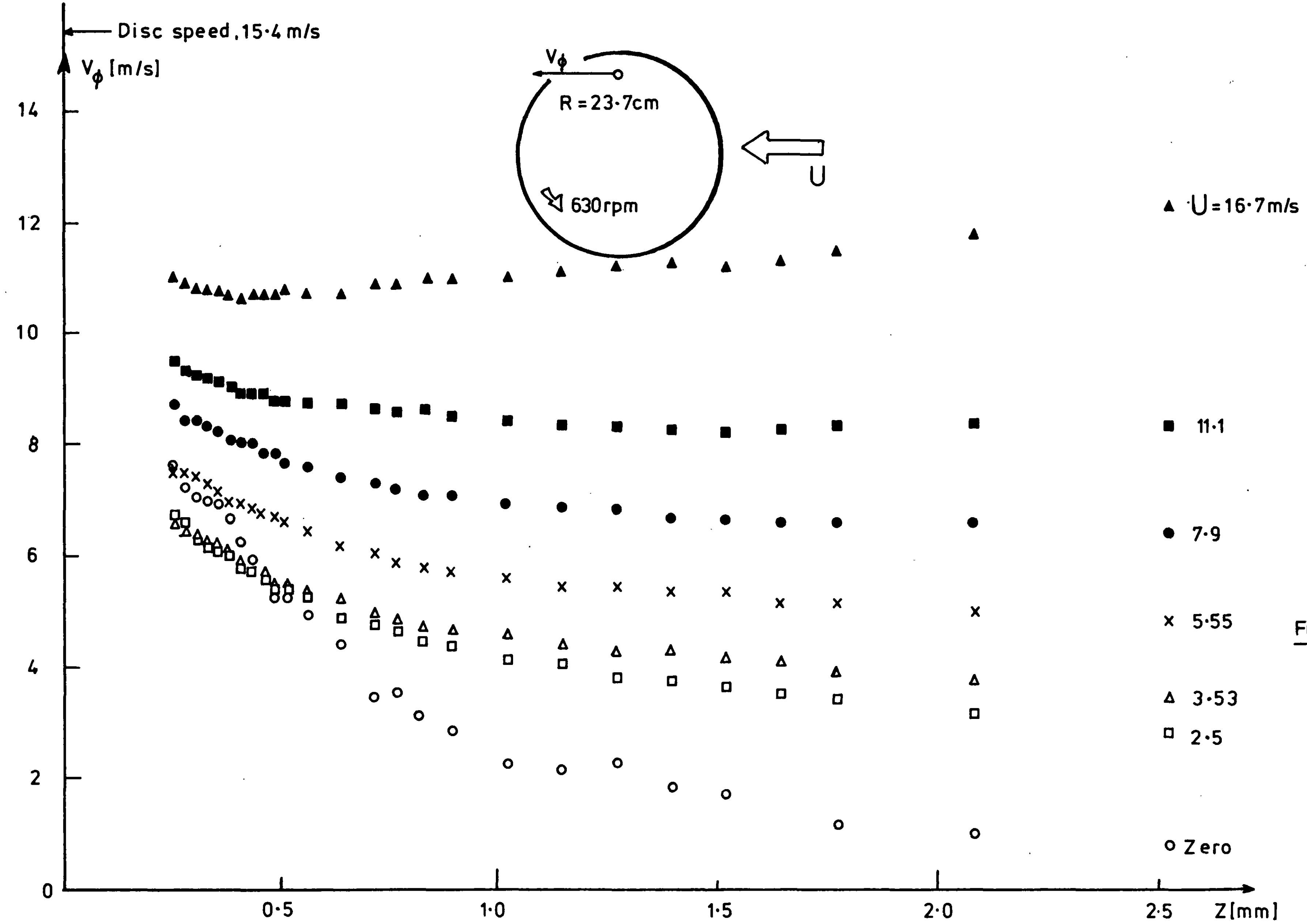
Disc speed, 15·4 m/s
V_ϕ [m/s]
V_ϕ
R = 23·7cm
630rpm
U
U = 16·7m/s
11·1
7·9
5·55
3·53
2·5
Zero
0
2
4
6
8
10
12
14
0·5
1·0
1·5
2·0
2·5
Z [mm]

Fig 5·10 d

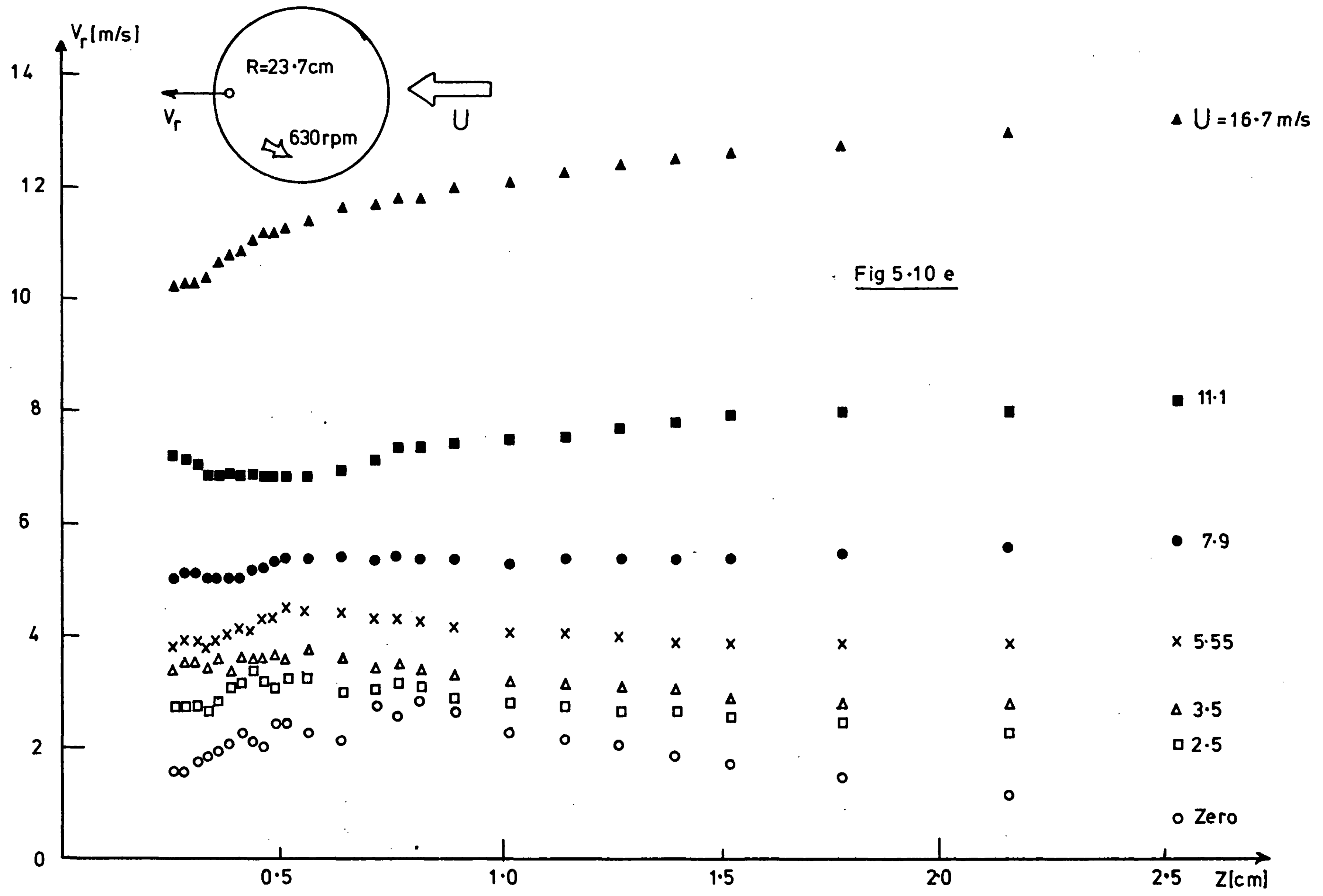

V_r [m/s]
14
12
10
8
6
4
2
0
R=23·7cm
630rpm
V_r
U
U =16·7 m/s
11·1
7·9
5·55
3·5
2·5
Zero
0·5
1·0
1·5
2·0
2·5
Z[cm]

Fig 5·10 e

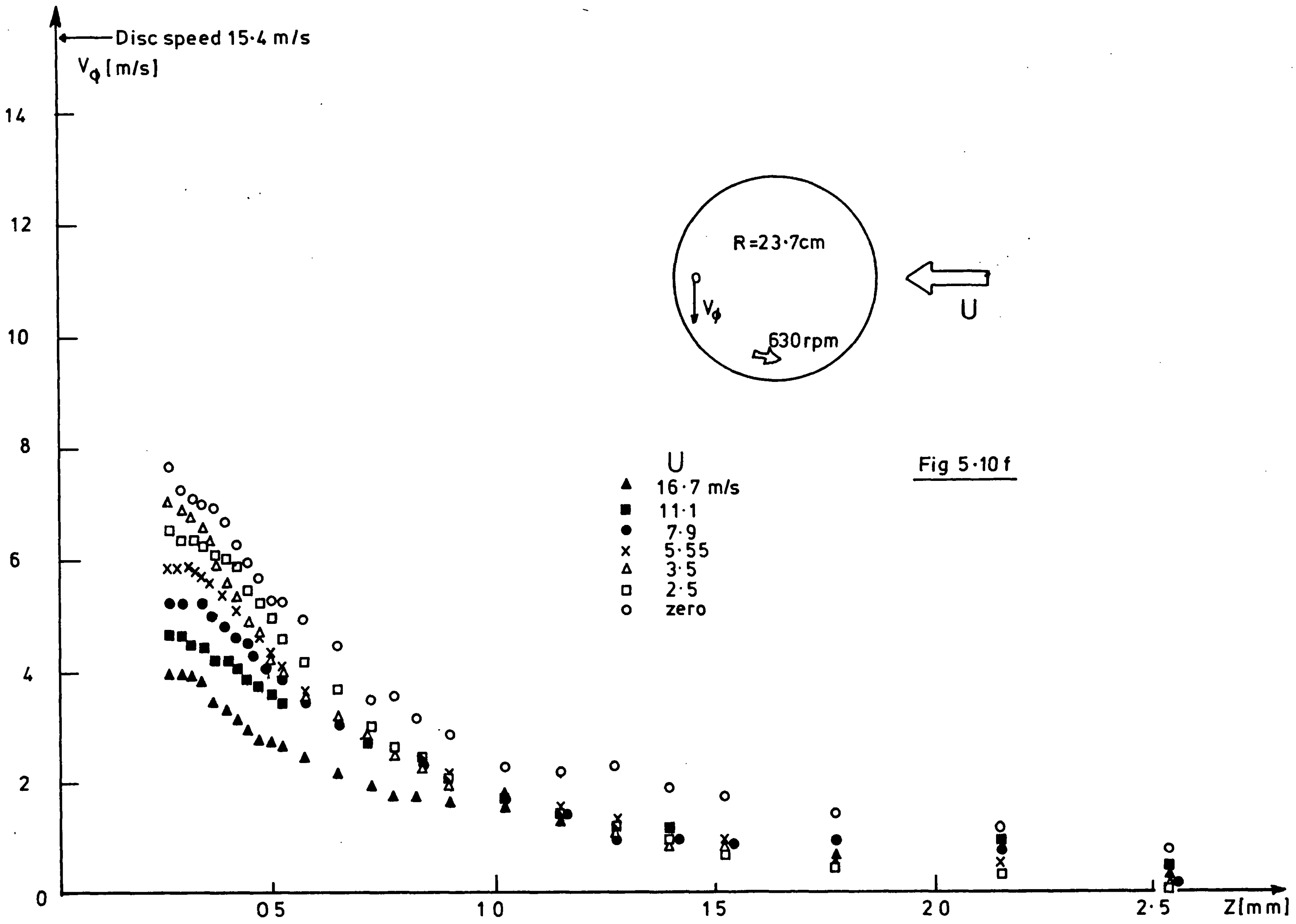
Disc speed 15·4 m/s
V_ϕ [m/s]
14
12
10
8
6
4
2
0
0 5
1 0
1 5
2 0
2·5
Z[mm]
R=23·7cm
V_ϕ
630rpm
U
U
16·7 m/s
11·1
7·9
5·55
3·5
2·5
zero

Fig 5·10 f

Fig 5·10g

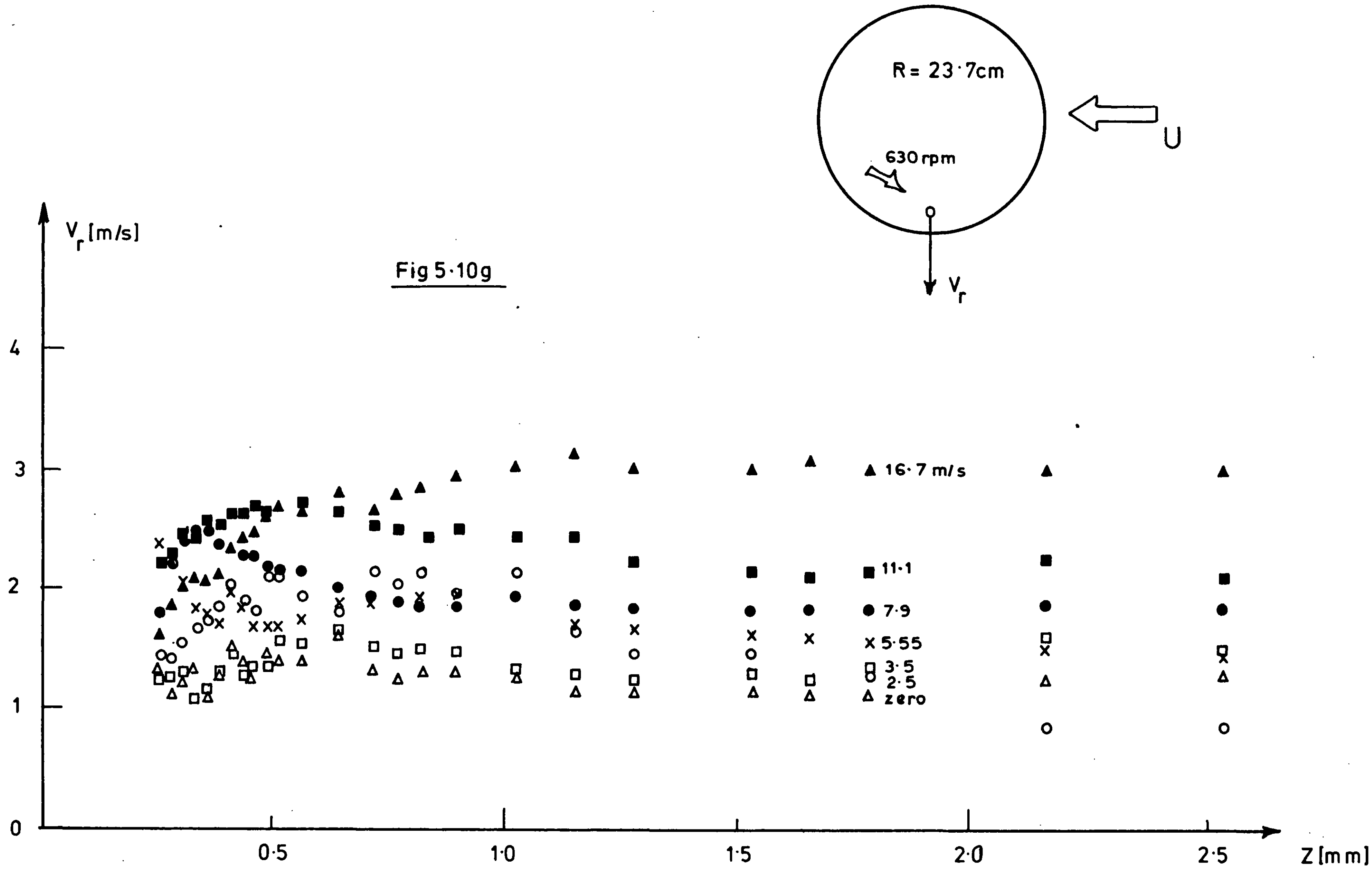

R = 23·7cm
630 rpm
U
V_r
V_r [m/s]
Z [mm]
0
1
2
3
4
0·5
1·0
1·5
2·0
2·5
16·7 m/s
11·1
7·9
5·55
3·5
2·5
zero

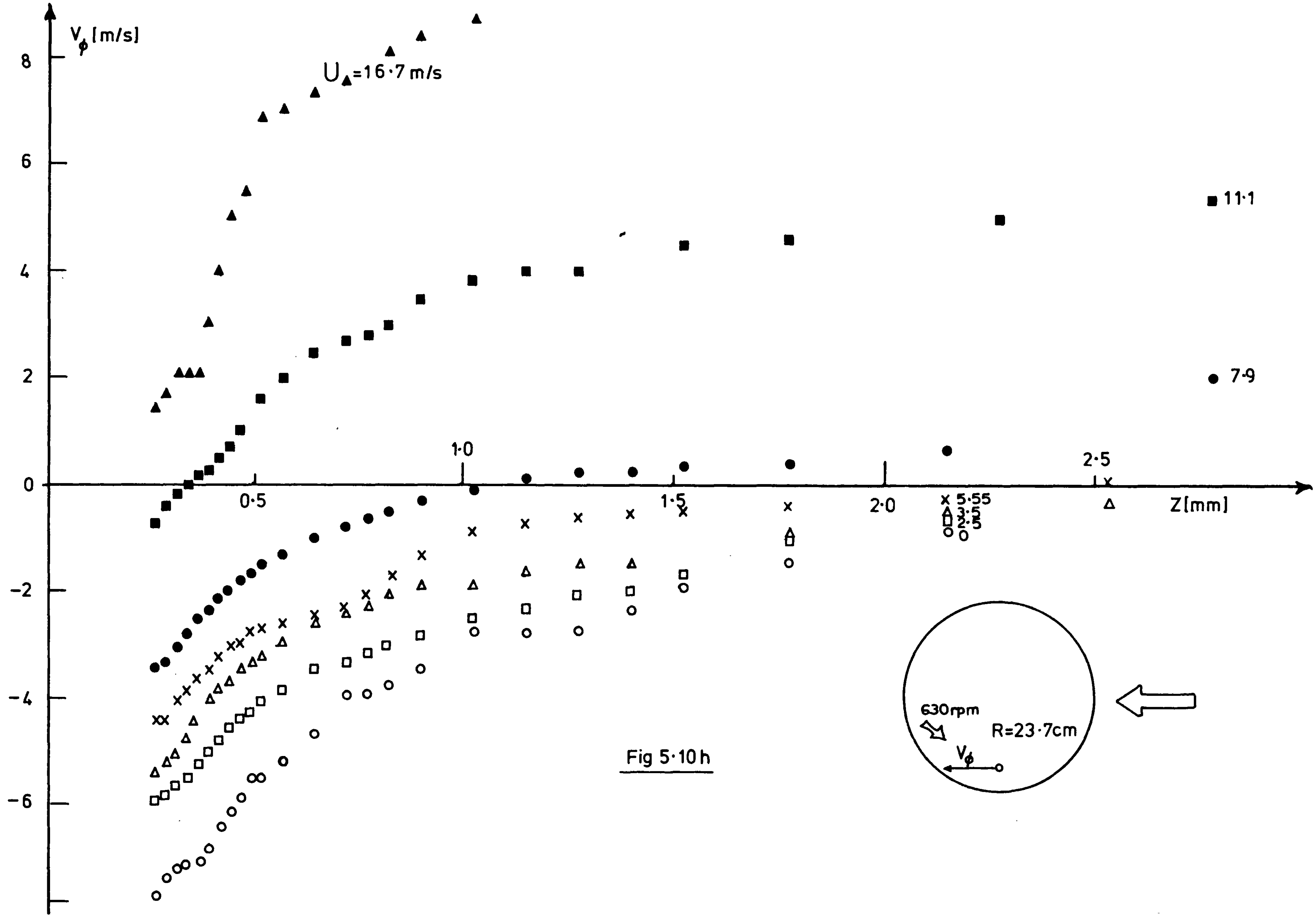

V_ϕ [m/s]
$U_\blacktriangle$=16·7 m/s
11·1
7·9
× 5·55
△ 3·5
□ 2·5
○ 0
Z [mm]
630 rpm
R=23·7cm
V_ϕ

Fig 5·10h

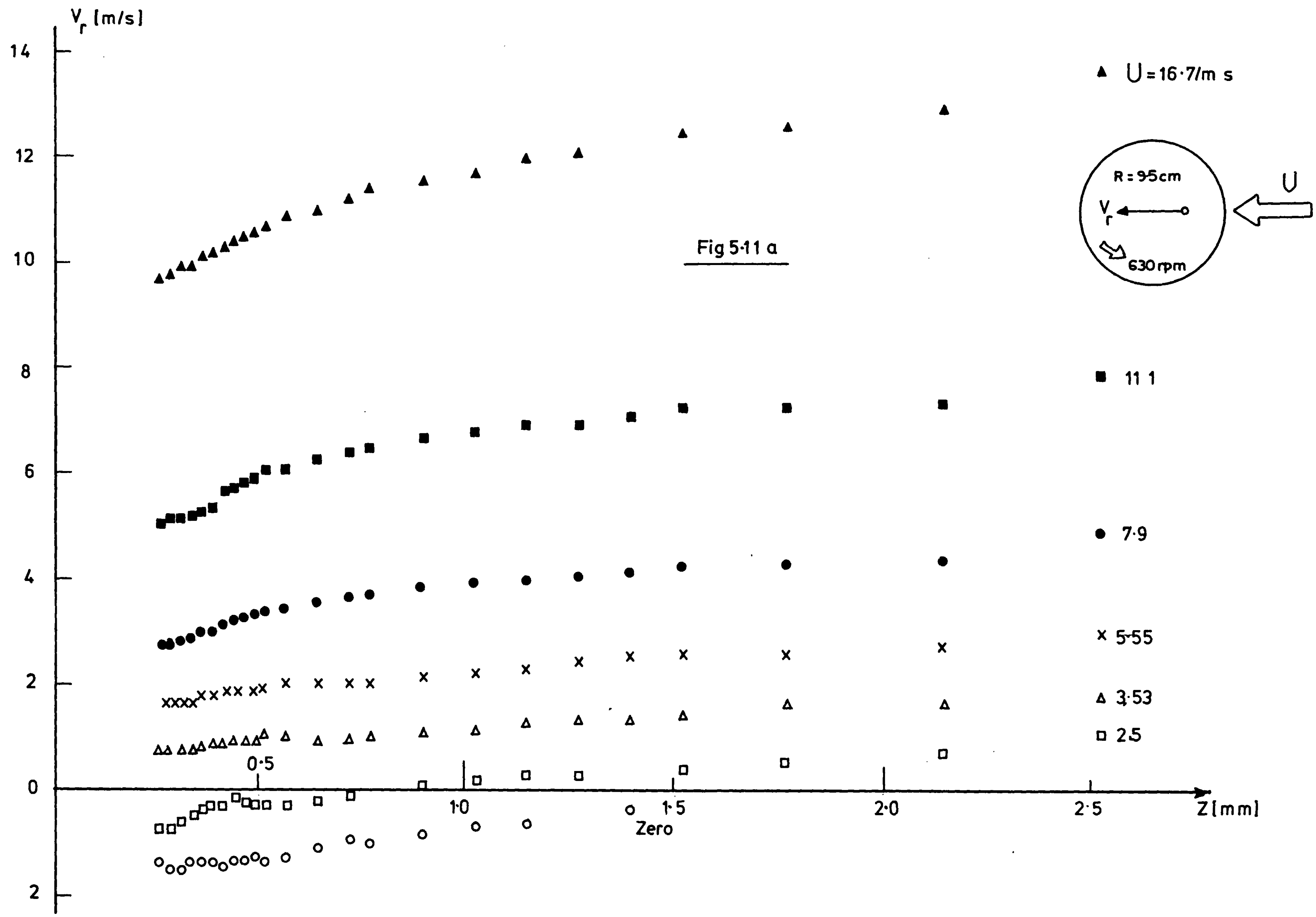

V_r [m/s]
14
12
10
8
6
4
2
0
2
0·5
1·0
1·5
2·0
2·5
Z [mm]
Zero
U = 16·7/m s
11 1
7·9
5·55
3·53
2·5
R = 9·5cm
V_r
630 rpm
U

Fig 5·11 a

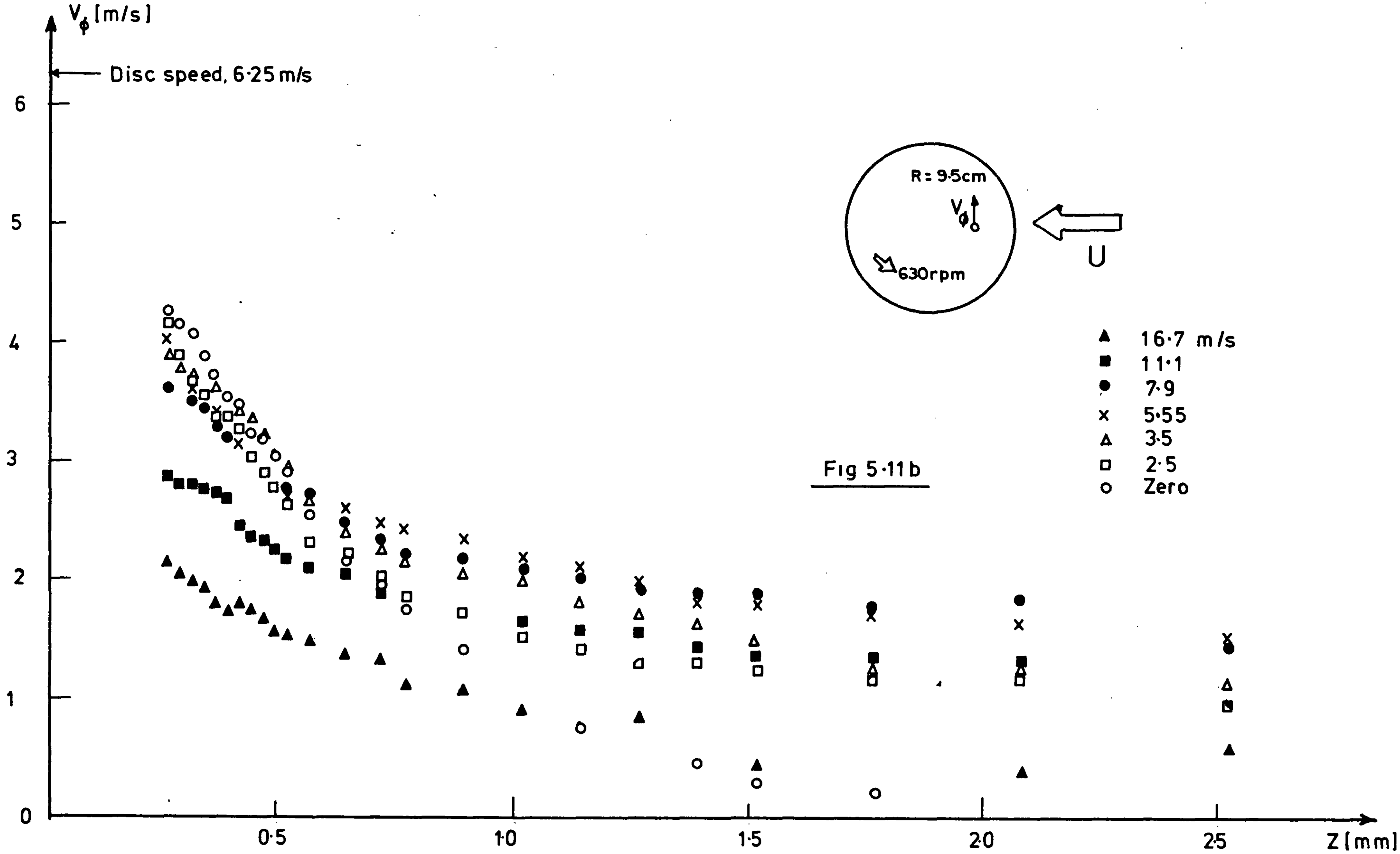

V_ϕ [m/s]
Disc speed, 6·25 m/s
6
5
4
3
2
1
0
0·5
1·0
1·5
2·0
2·5
Z [mm]
R = 9·5cm
V_ϕ
630rpm
U
16·7 m/s
11·1
7·9
5·55
3·5
2·5
Zero

Fig 5·11b

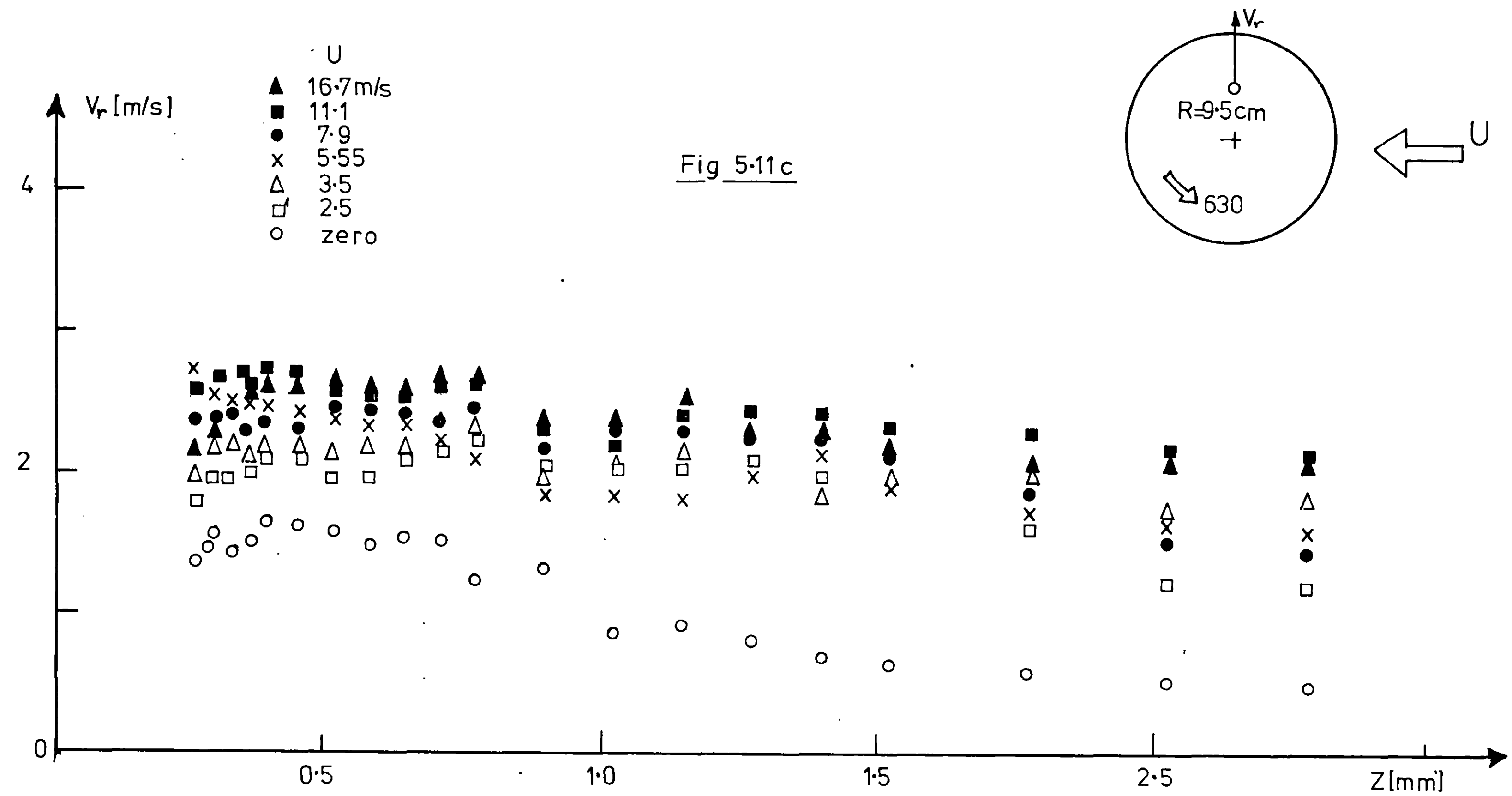

U
16·7m/s
11·1
7·9
5·55
3·5
2·5
zero
V_r [m/s]
4
2
0
0·5
1·0
1·5
2·5
Z [mm]
R=9·5cm
630
V_r
U

Fig 5·11c

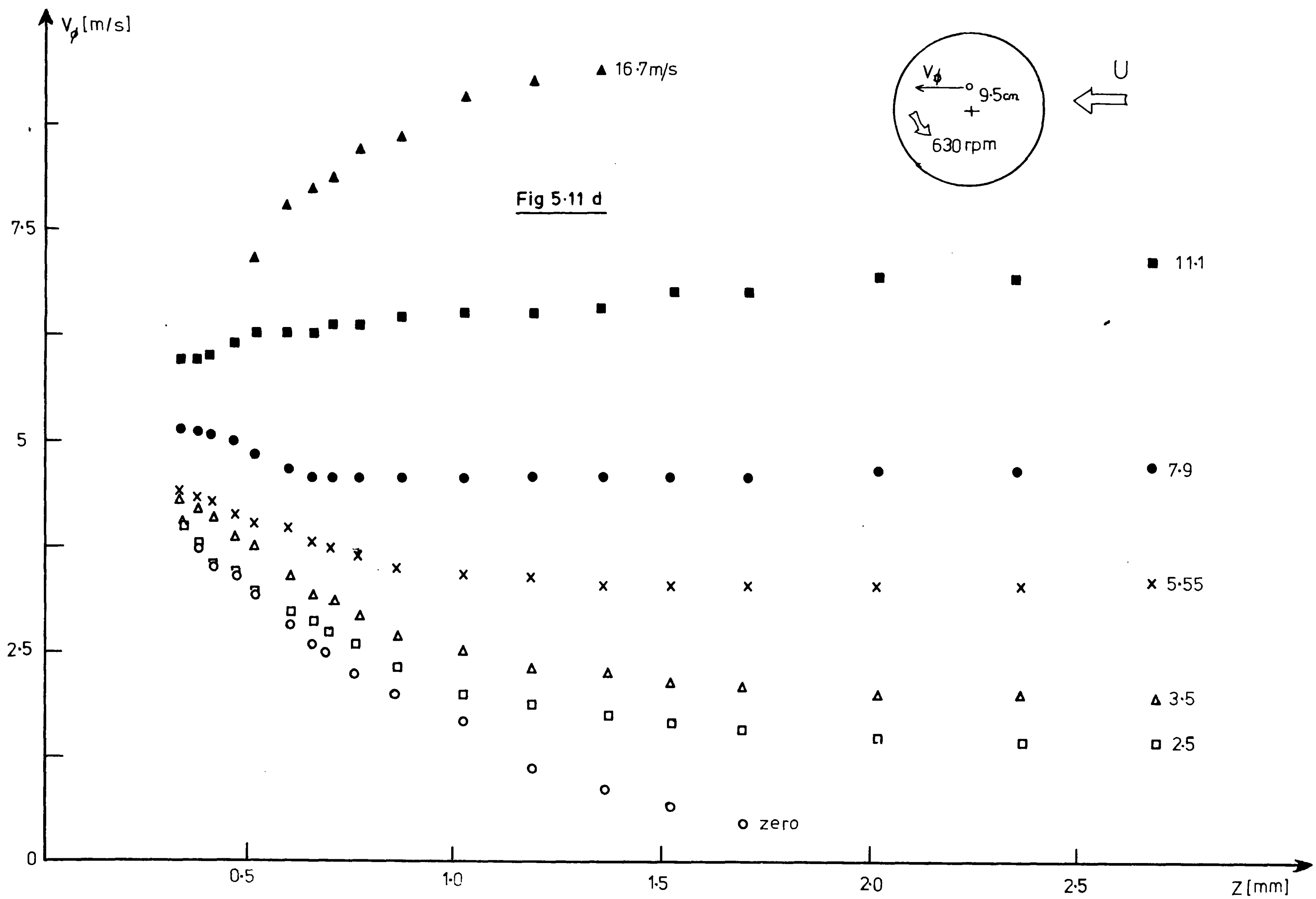

V_ϕ [m/s]
16·7m/s
11·1
7·9
5·55
3·5
2·5
zero
V_ϕ
9·5cm
630 rpm
U
7·5
5
2·5
0
0·5
1·0
1·5
2·0
2·5
Z [mm]

Fig 5·11 d

Fig 5·11e

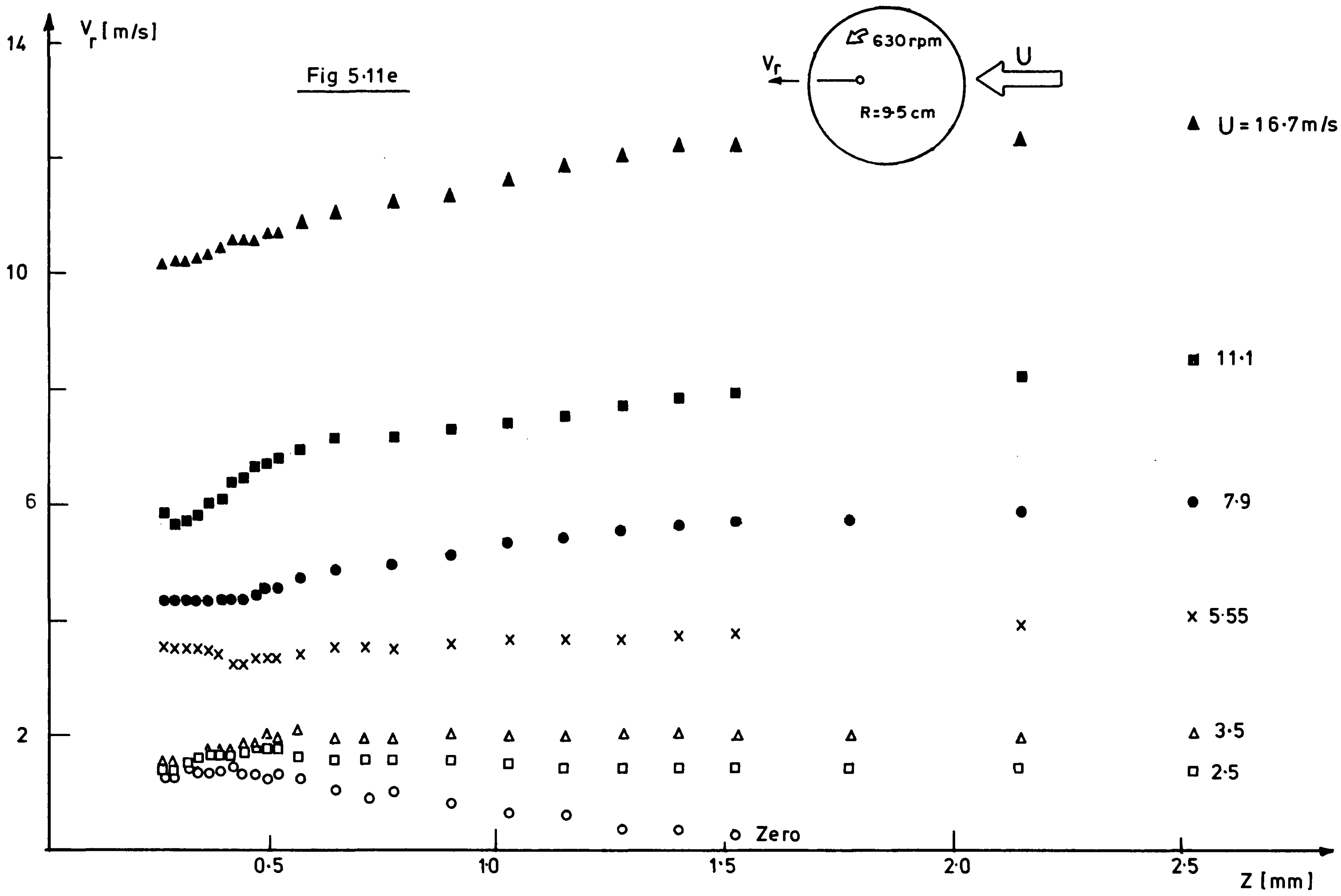

V_r [m/s]
14
10
6
2
630 rpm
V_r
R=9·5 cm
U
U = 16·7 m/s
11·1
7·9
5·55
3·5
2·5
Zero
0·5
1·0
1·5
2·0
2·5
Z [mm]

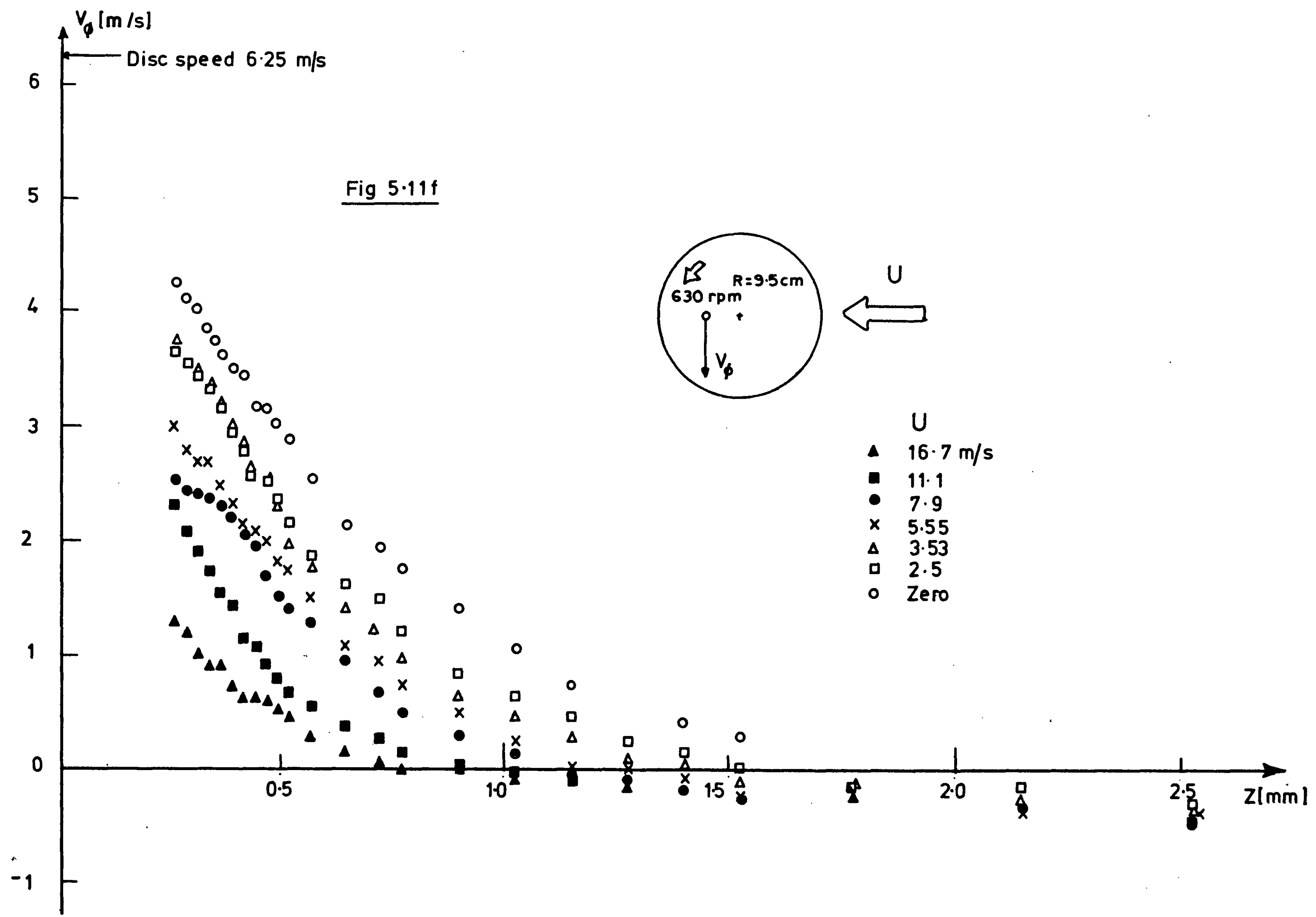
V_ϕ [m/s]
Disc speed 6·25 m/s
6
5
4
3
2
1
0
-1
0·5
1·0
1·5
2·0
2·5
Z[mm]
630 rpm
R=9·5cm
V_ϕ
U
U
16·7 m/s
11·1
7·9
5·55
3·53
2·5
Zero

Fig 5·11f

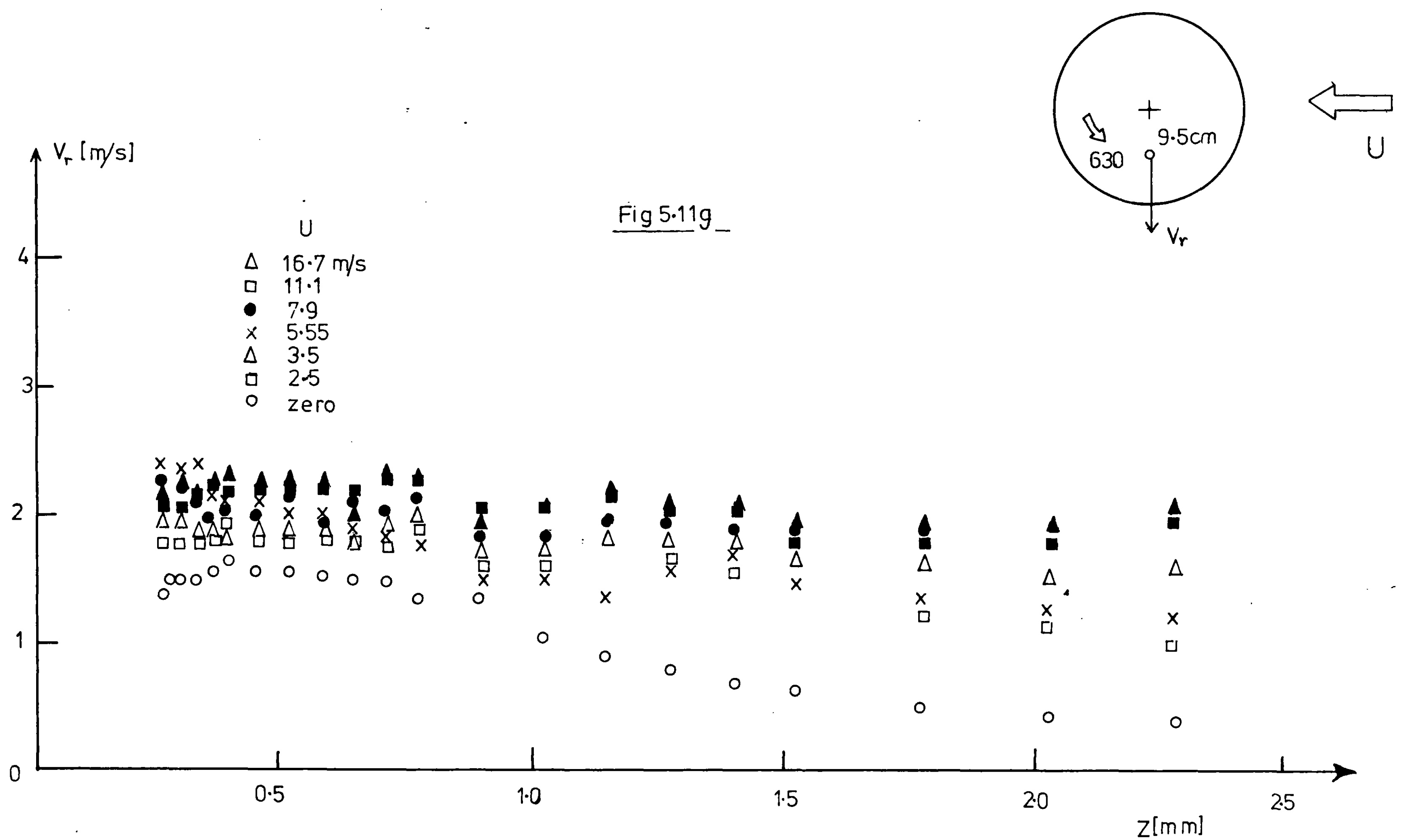

V_r [m/s]
U
16·7 m/s
11·1
7·9
5·55
3·5
2·5
zero
9·5cm
630
V_r
U
0
1
2
3
4
0·5
1·0
1·5
2·0
2·5
Z[mm]

Fig 5·11g

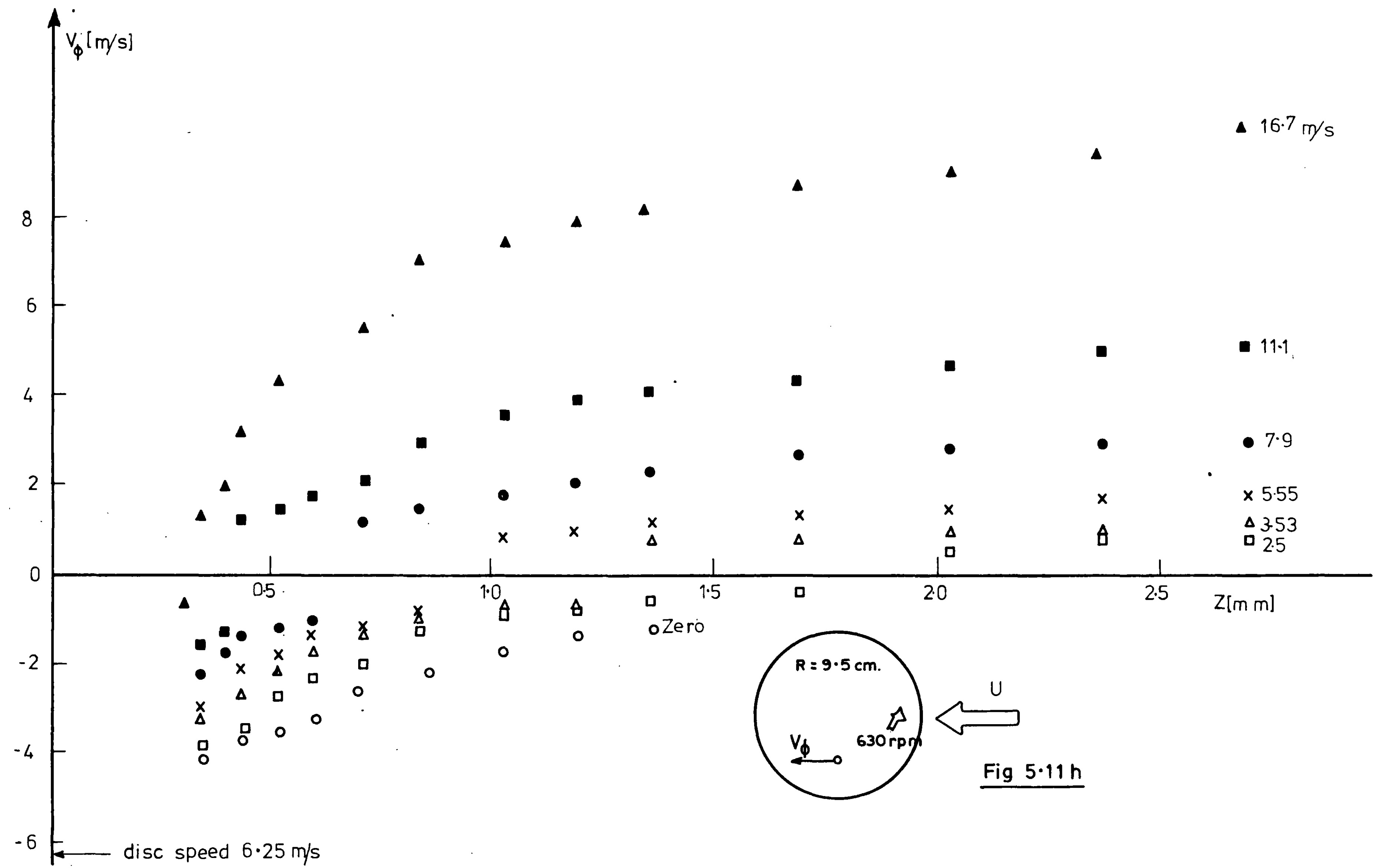

V_ϕ [m/s]
8
6
4
2
0
-2
-4
-6
0.5
1.0
1.5
2.0
2.5
Z[m m]
16.7 m/s
11.1
7.9
5.55
3.53
2.5
Zero
disc speed 6·25 m/s
R = 9·5 cm.
630 rpm
U
V_ϕ

Fig 5·11 h

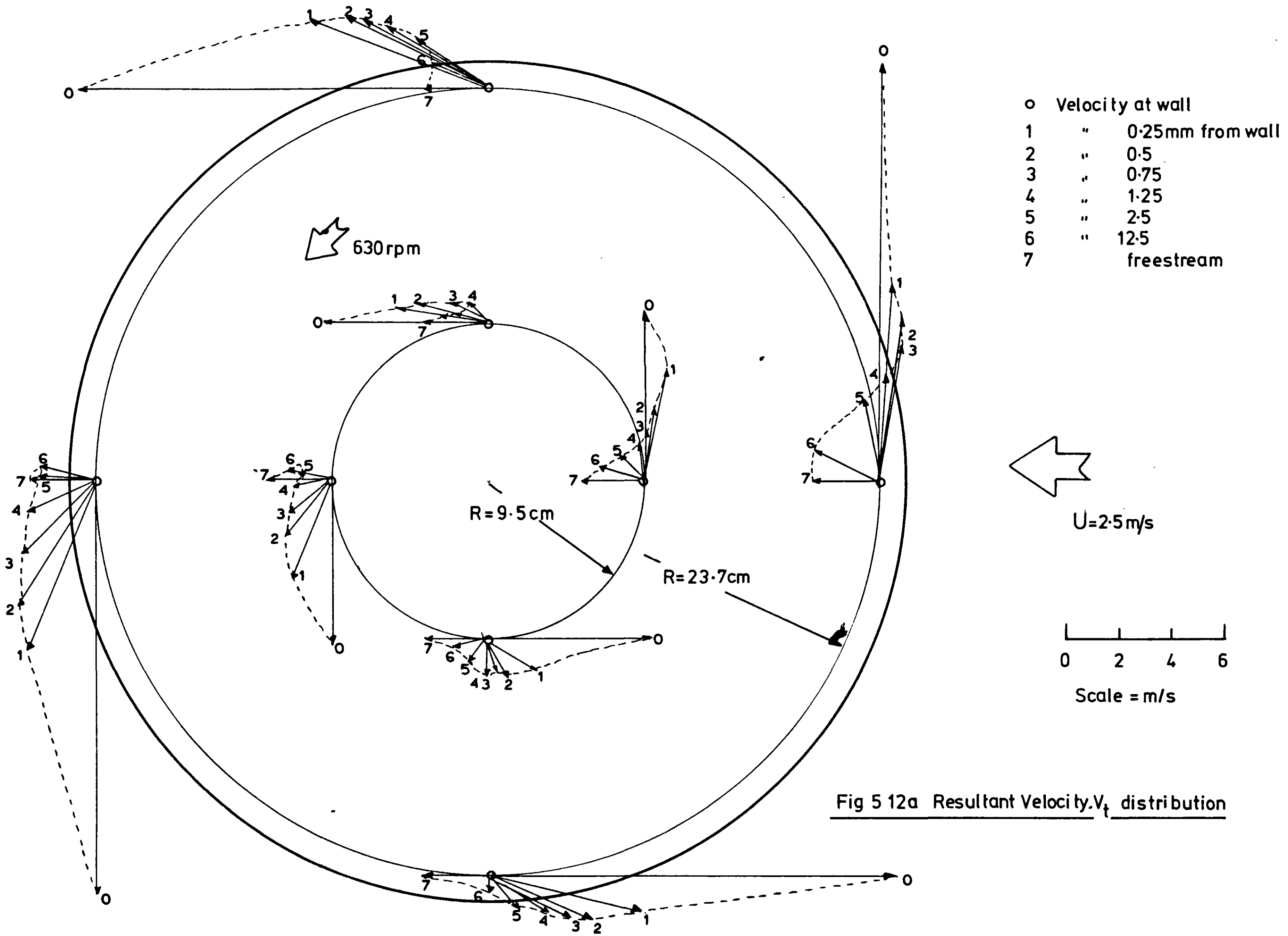

Fig 5 12a Resultant Velocity.V_t distribution

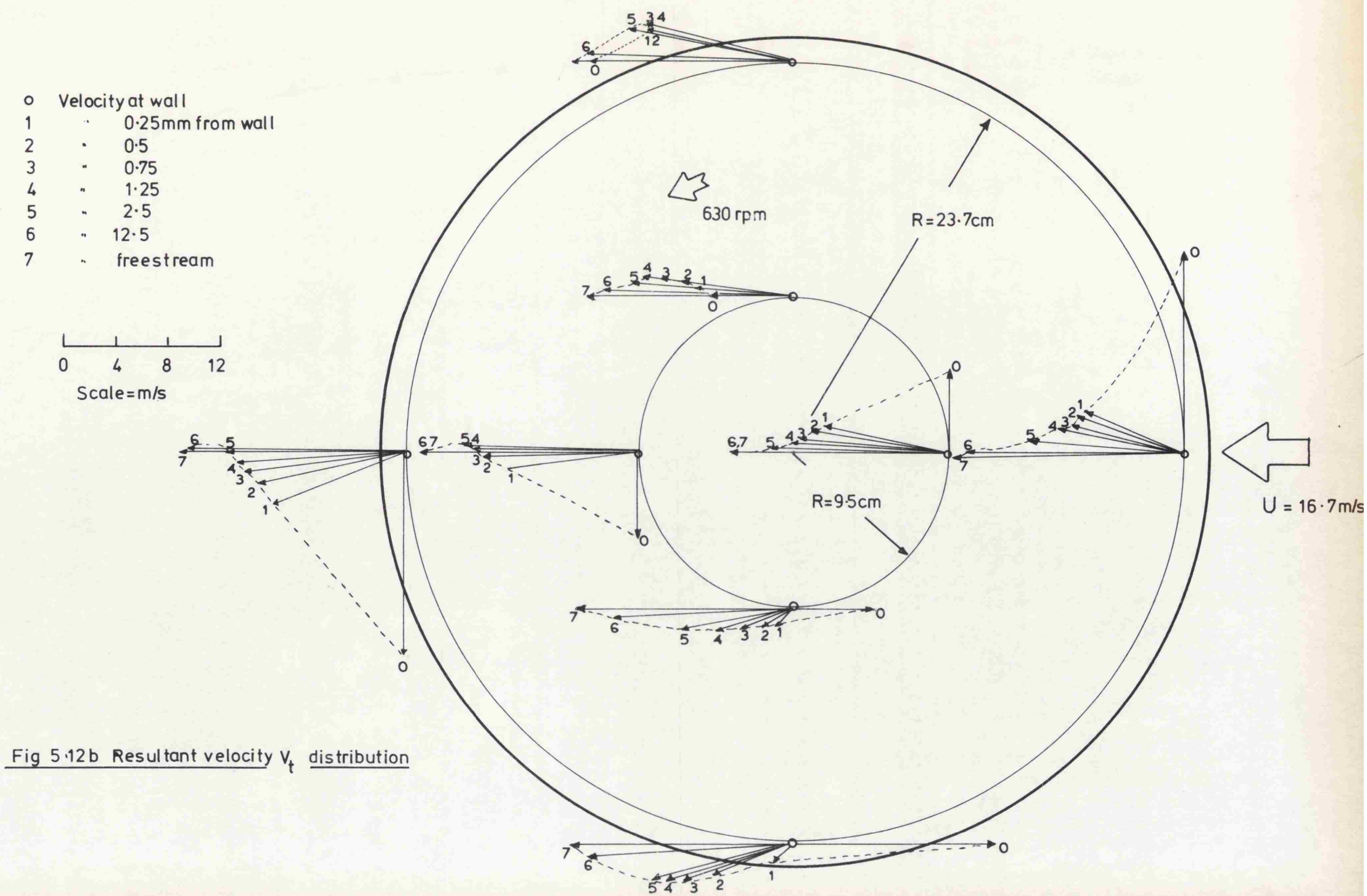

Fig 5·12b Resultant velocity V_t distribution

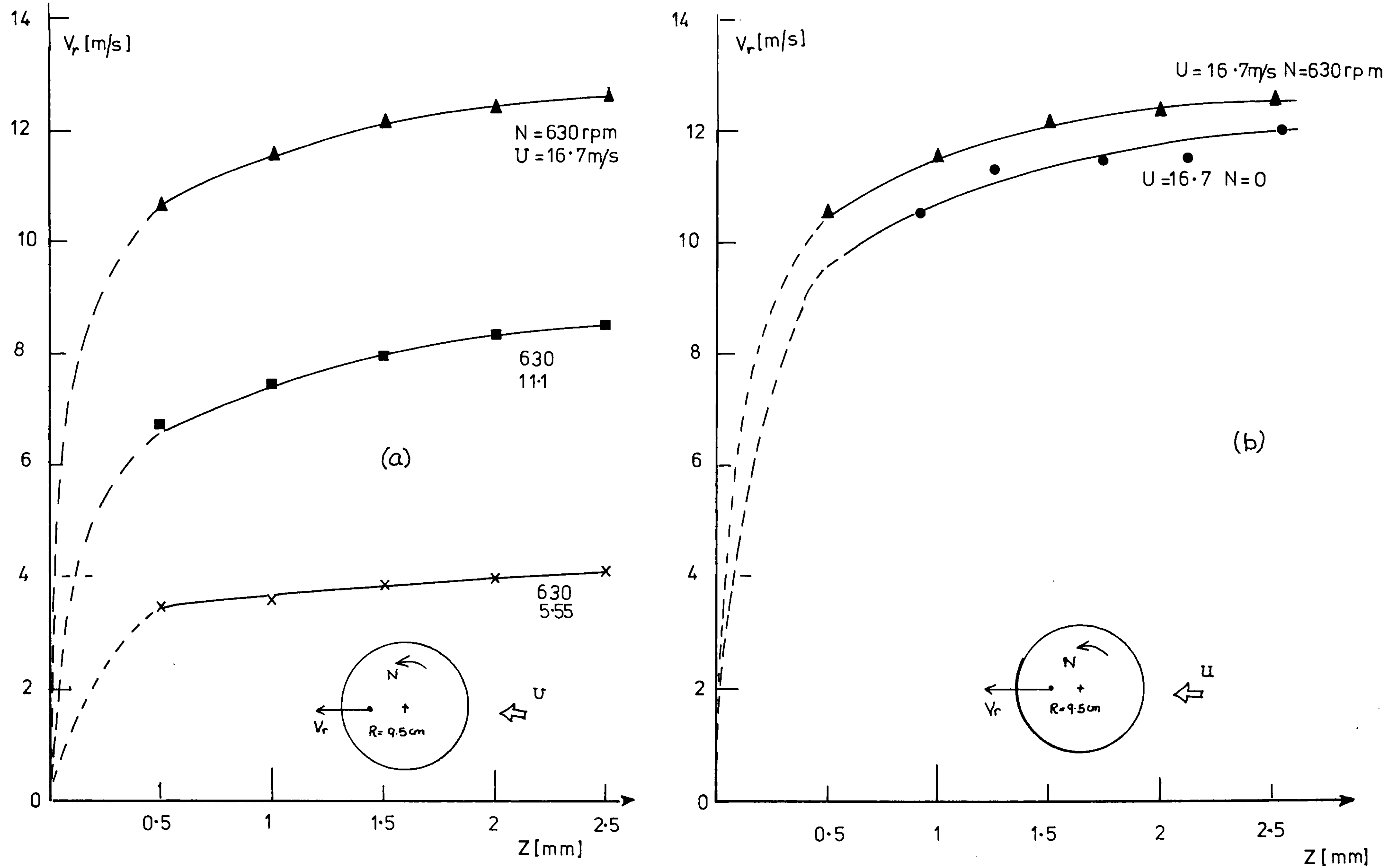

Fig 5.13 Effects of Main Air Stream and Rotation

5.6. Conclusions

In the absence of a developed theory to predict velocity profiles and heat transfer coefficients for the complex three dimensional flow pattern that exists over the disc surface only qualitative conclusions can be drawn from these measurements. Certainly the conclusions drawn earlier from the heat transfer measurements regarding the dominance of the main air stream is reinforced by the velocity patterns emerging from these measurements and in a way that was not possible from the smoke visualization tests.

Chapter 6

Convective Heat Transfer from a Rotating Wheel Shape Rotating in a Transverse Air Stream

6.1. Introduction

This particular piece of work was done for British Rail to provide them with heat transfer coefficients for use in their train wheel stress analysis.

The present plain circular disc is only an idealisation of a train wheel shape. In particular the thickening at the rim and the central axle boss are missing. The simple wheel was formed by screwing suitable aluminium pieces, an annular ring and a central hub, to the original plain disc. The important dimensions were supplied by British Rail, Technical Centre, Derby.

Measurements of surface heat transfer coefficients are reported for a simple wheel shape placed in a transverse air stream. Results are given for tests on the wheel stationary in an air stream up to 30 m/s and at rotational speeds matched to the main air stream. The results of simple flow visualisation smoke tests give a qualitative explanation to the general trend of the results and indicate the nature of the flow over the surface of the wheel.

6.2. Experimental Arrangement

The test wheel, on an overhung shaft, rotates in the neck of the open jet wind tunnel with the face of the wheel aligned to the direction of the main air flow. Local radial heat transfer coefficients are measured with the heat flux sensor as described in Chapter 3. A cross section of the wheel is given in Figure (6.1), which also marks the nine radial positions at which measurements are taken. A typical wheel shape is superimposed upon this diagram to illustrate the degree of simplification that has been

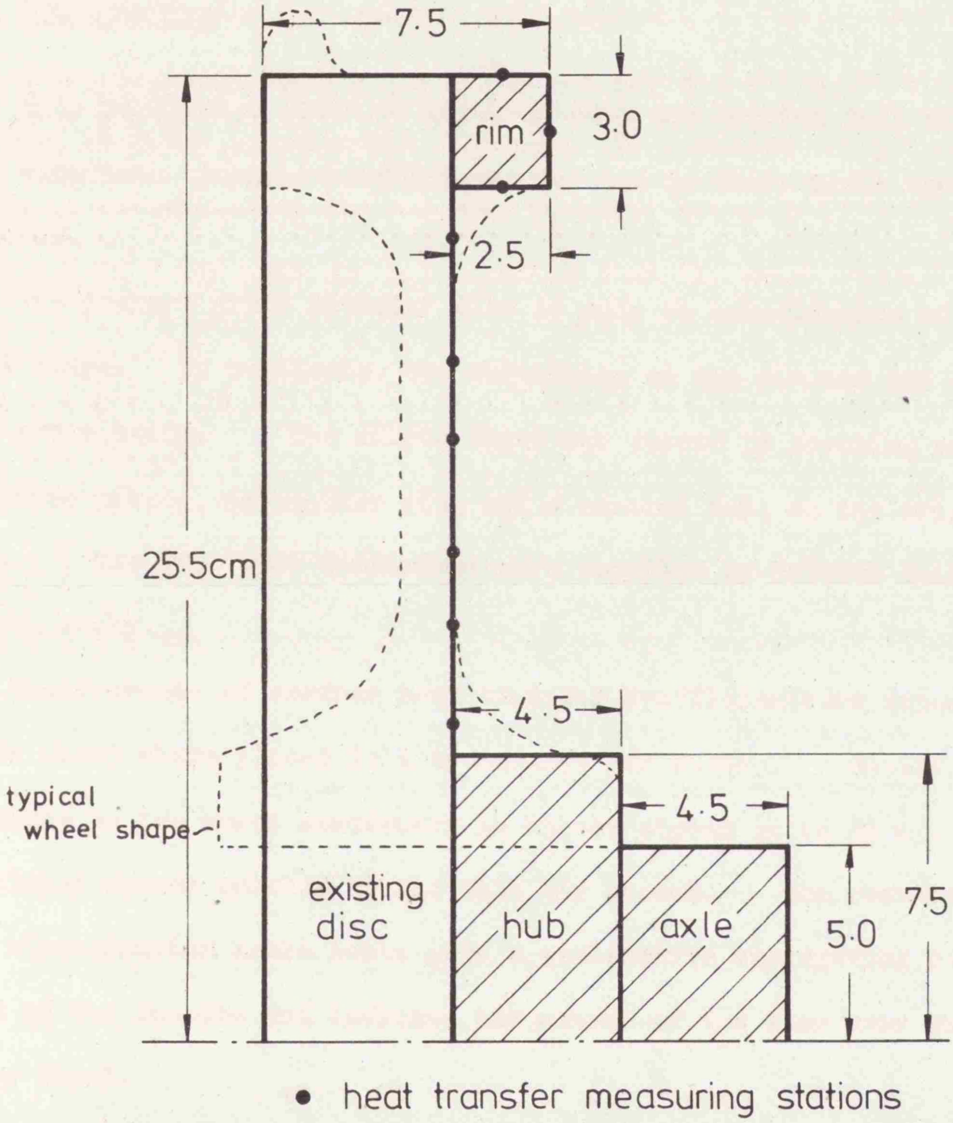

Fig. 6.1 Train wheel shape

made in arriving at the wheel shape under test.

The original disc carries heaters which can raise the whole surface temperature 40 deg.C above ambient. The additional aluminium pieces are heated by conduction from the main disc. Thermocouples are placed just below the main disc surface and a further thermocouple is located near the outside surface of the annular ring. Under test conditions a six degree variation over these thermocouples is found. A photograph of the wheel is shown in Figure (6.2). (The blackening over half the surface was applied after the heat transfer tests to provide contrast for flow visualisation photography.)

6.3. Test Results

6.3.1. Wheel Stationary

With the wheel stationary and the air stream on, heat transfer coefficients were determined at each of the nine radial positions for five angular positions, 0, 45, 90, 135 and 180 degrees. 0 corresponds to the leading edge of the wheel on the centre line of the tunnel. Since the flow is symmetrical it is assumed that similar values hold for the bottom half of the wheel.

The individual results obtained are shown graphically in Figures (6.3) and (6.4) for four wind speeds of 7.8, 14.2, 20.5 and 29.6 m/s. Additionally in Figure (6.3) a table of average radial values is given. The average value is a straight average of the eight individual values for any circumference.

6.3.2. Wheel Rotating

Measurements were taken for four wheel speeds 296, 530, 780 and 1120 rpm. For each wheel speed the air speed was set to match the peripheral wheel velocity, i.e. 7.8, 14.2, 20.5 and 29.6 m/s respectively. The radial values of heat transfer coefficient obtained are shown in Figure (6.5).

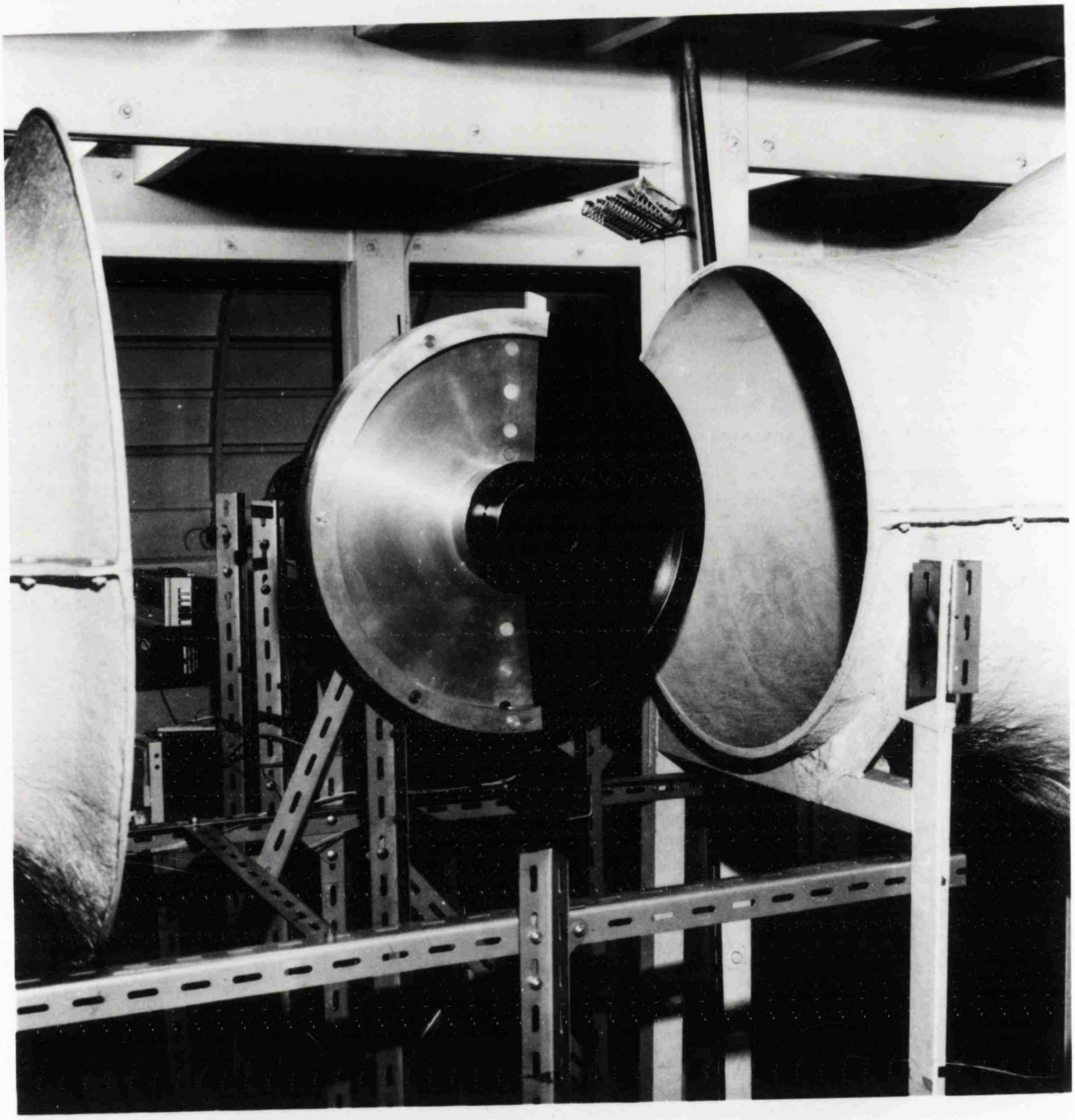

Fig 6.2 Photograph of wheel in mouth of tunnel

U=7·8 m/s

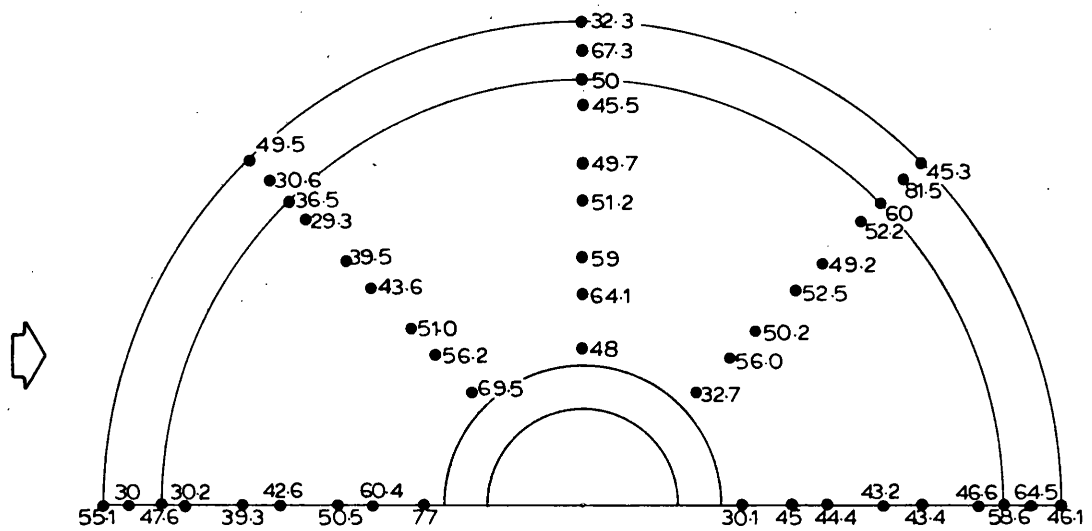

U=14·2 m/s

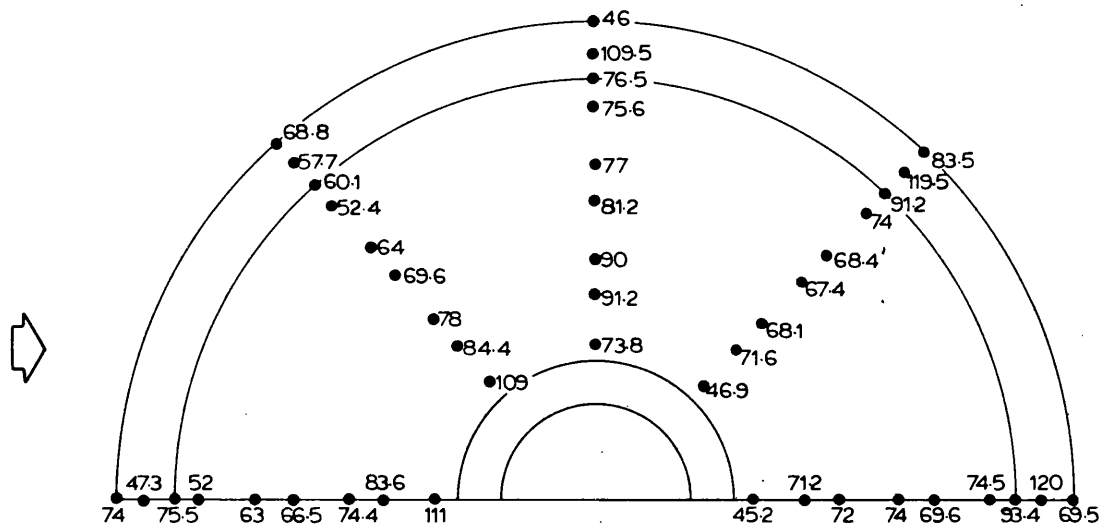

R cms \ U m/s	7·8	14·2	20·5	29·6
25·5	44·4	67·5	80·1	116
24·0	56·7	92·6	108·2	145
22·5	49·9	78·1	100·6	130·7
21·2	41·3	66·3	82·2	111
18·0	44·9	68·9	90·1	120·9
15·9	47·6	72·1	94·4	124·0
13·1	51·9	77·3	99·4	133·0
11·2	57·2	81·1	105·9	139·1
8·5	50·9	76·9	100·3	135·4

Fig. 6·3 Wheel stationary in transverse air flow

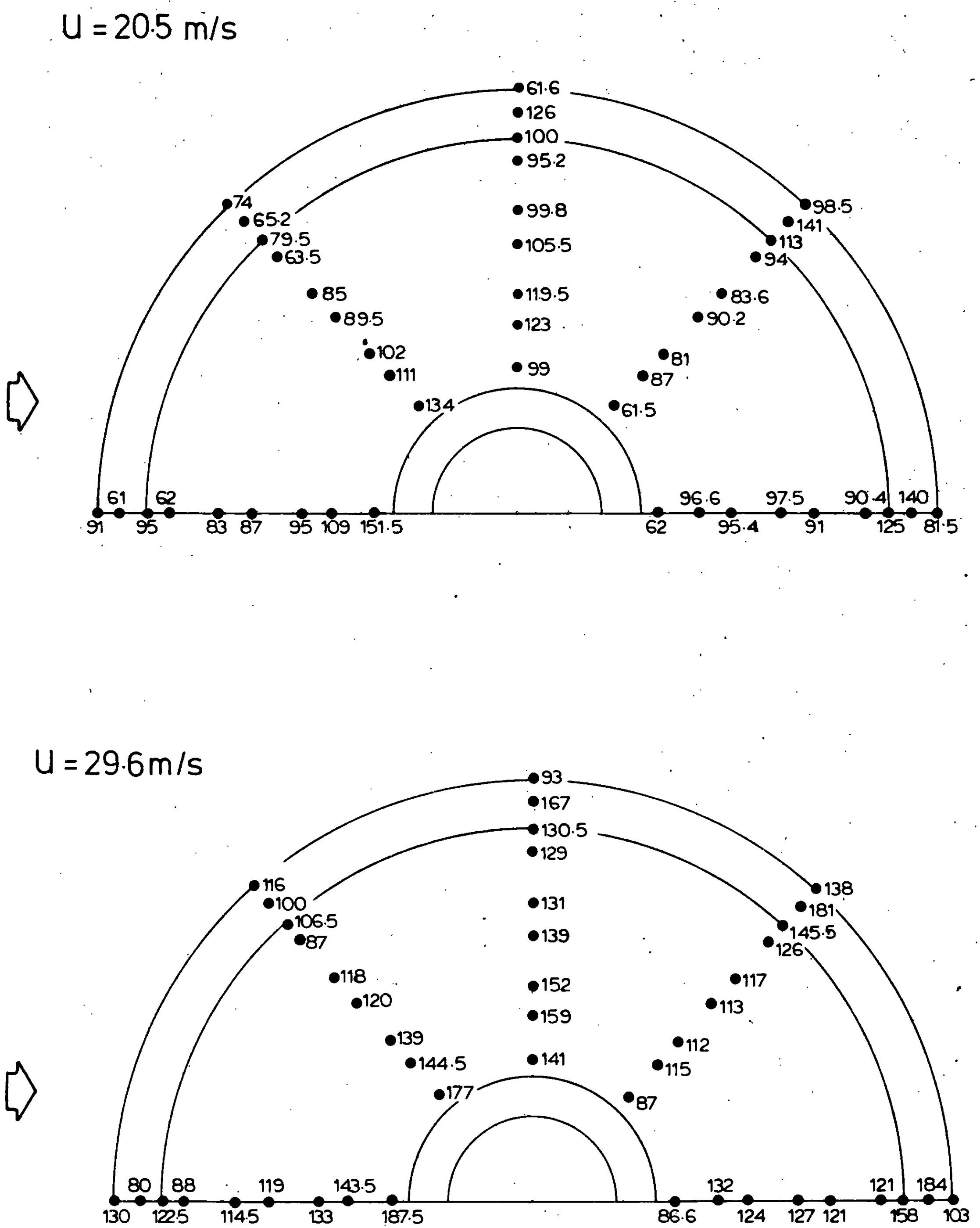

U = 20.5 m/s
61.6
126
100
95.2
99.8
105.5
119.5
123
99
74
65.2
79.5
63.5
85
89.5
102
111
134
98.5
141
113
94
83.6
90.2
81
87
61.5
61
62
91
95
83
87
95
109
151.5
96.6
97.5
90.4
140
62
95.4
91
125
81.5
U = 29.6 m/s
93
167
130.5
129
131
139
152
159
141
116
100
106.5
87
118
120
139
144.5
177
138
181
145.5
126
117
113
112
115
87
80
88
119
143.5
130
122.5
114.5
133
187.5
132
121
184
86.6
124
127
121
158
103

Fig. 6.4

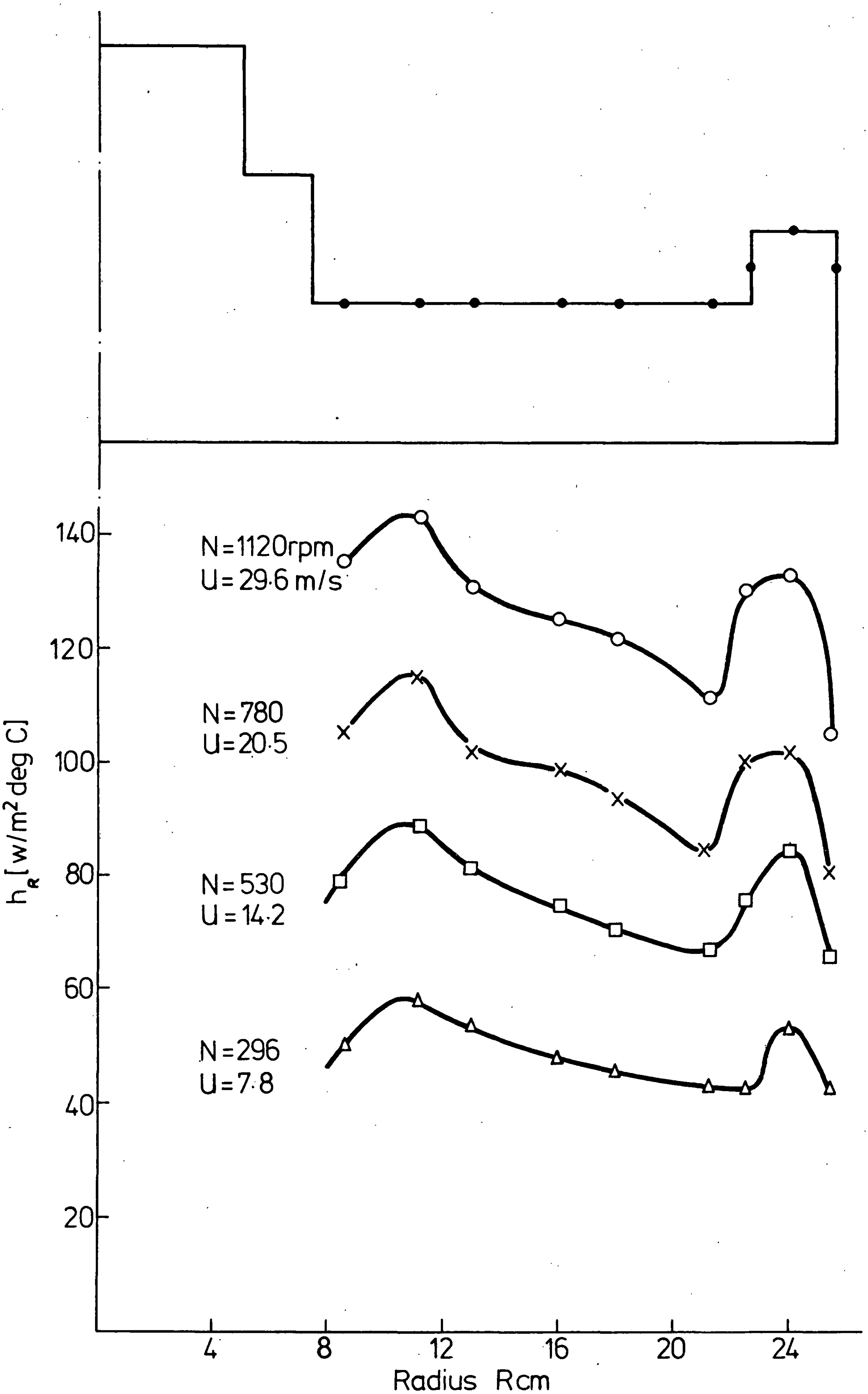

Fig. 6.5 Rotating wheel in a matched stream

6.4. Flow Visualisation

A very limited qualitative picture of the air flow distribution about the wheel was obtained by introducing smoke tracers into the flow. This technique is only successful at low velocities. At high velocities the smoke is dispersed too rapidly to gain an impression of the flow distribution. Consequently all pictures shown were taken at the lowest air velocity 7.8 m/s.

Two sets of pictures are shown. The first set, Figure (6.6), shows how the main stream separates around the wheel both with and without wheel rotation. Here smoke is introduced on the tunnel axis upstream of the wheel. The second set, Figure (6.7), shows secondary flow in the region within the re-entrant section defined by the annular ring. Two cases are shown, one with smoke introduced close to the central hub, the second with smoke introduced near to the rim.

6.5. Discussion

A number of qualitative observations are worth making about the results presented.

In Figure (6.8) the results of the rotating tests andthe average radial values obtained from the stationary tests are plotted on the same graph. Two sets of results are very similar. This confirms previous findings with the plain disc. The level of the heat transfer coefficient and its radial variation is dominated by the main stream flow. The rotation only causes small perturbations about the main stream level.

In Figure (6.9) the results of the rotating tests are compared with results of previous work on the plain disc. Except at the outer annular ring the values for the plain disc are higher than forthe wheel shape.

These observations tie in with the general picture of the flow pattern around the wheel. Firstly the disc rotation produces little change in

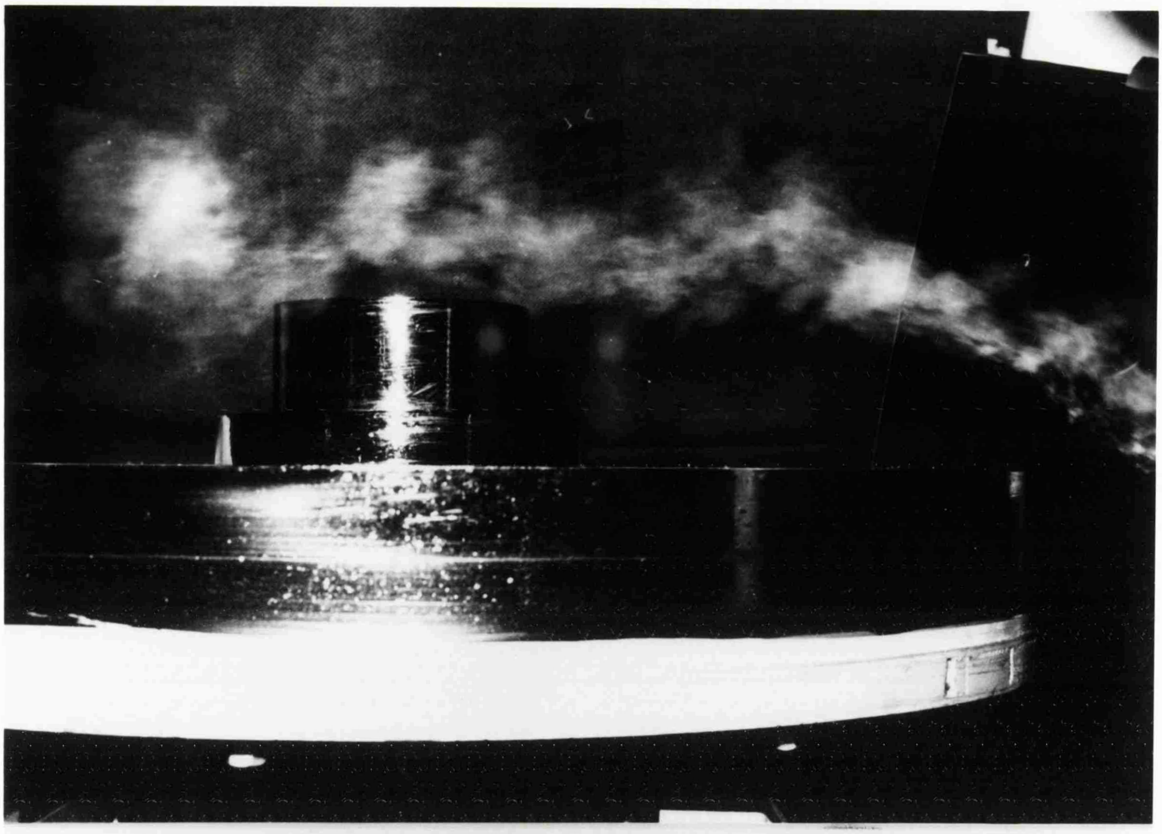

a) Stationary

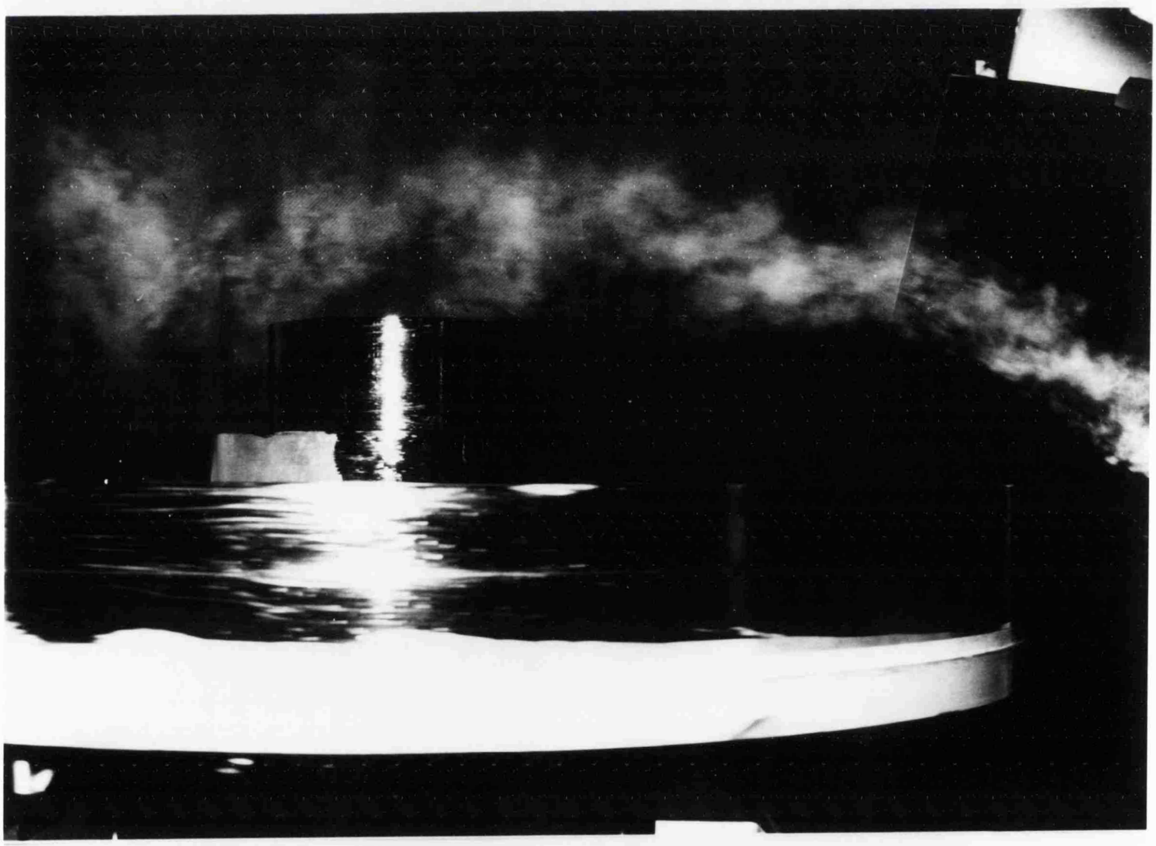

b) Rotating

Fig. 6.6

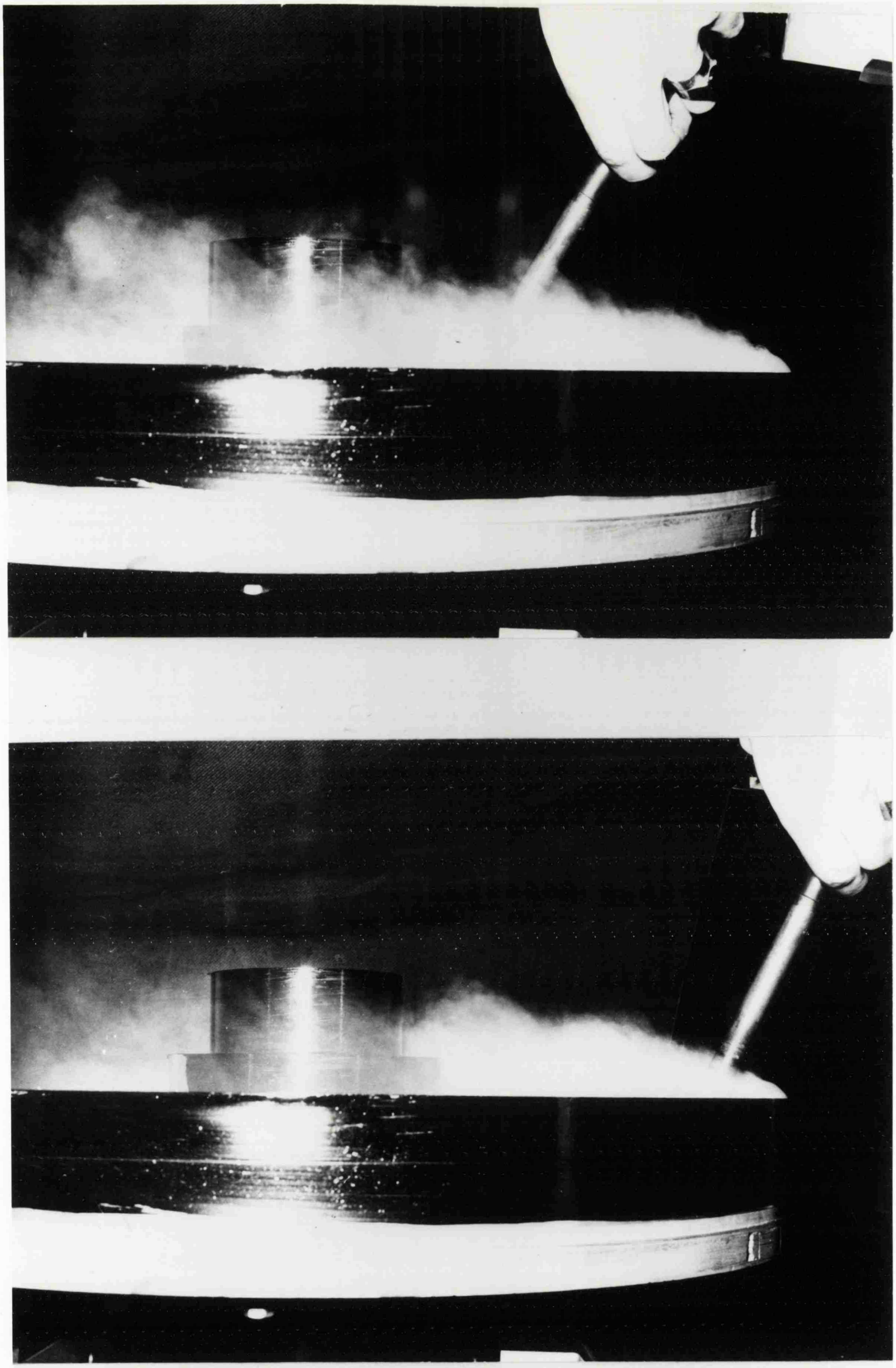

Fig 6.7 Wheel stationary

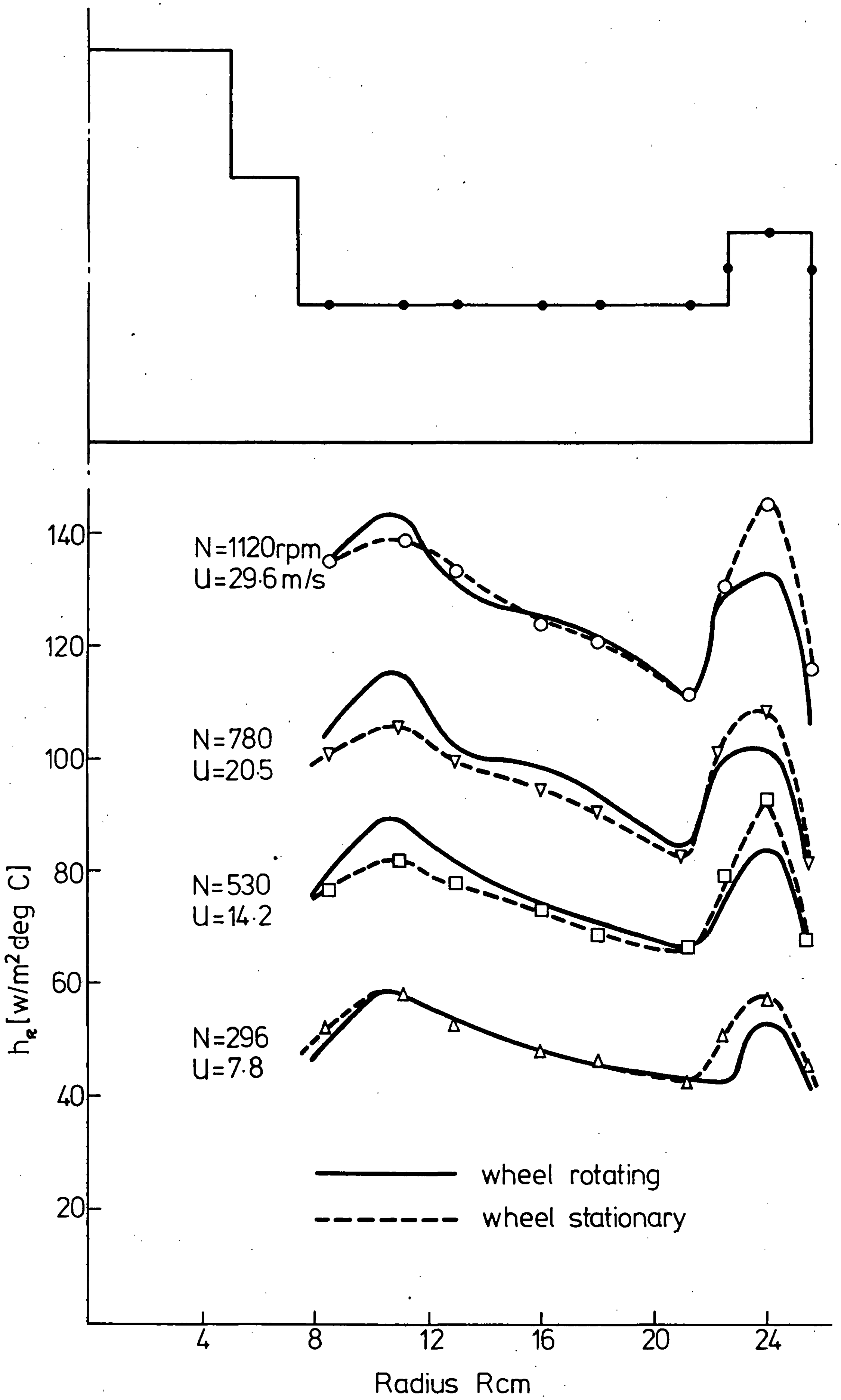

Fig6·8. Effect of wheel rotation

the flow distribution and then only very close to the wheel surface. Secondly the main stream separates around the wheel, Figure (6.6), leaving a re-entrant region of generally lower velocity flow. This picture of separated flow over the majority of the wheel face contrasts with the plain disc where separation occurs at the leading edge region with re-attachment well before the axle.

The flow in the separated region is very complex with fluid feeding in from the main stream to be re-entrained at other positions. In the region forward of the central boss there is considerable flow reversal. This is particularly emphasised immediately in front of the boss as some of the main stream hitting the boss is forced in to the surface and then back towards the rim. As the heat flux sensor rotates through 360 degrees it "sees" all the facets of this complex flow field and gives an averaged heat transfer coefficient. Measurements with a fast response sensor would be necessary to tie in heat transfer coefficients with the detailed flow pattern.

It is interesting to look at variation of heat transfer coefficient across the horizontal diameter, 0^{o} - 180^{o}, taken from the stationary tests. This is shown in Figure (6.10) for a mainstream velocity of 20.5 m/s. The variation is similar for the other velocities tested.

Moving from left to right across the wheel, the first fall in heat transfer coefficient is due to the flow separation at the leading edge, measurement position 2. Over positions 3 to 9 the flow is in the reverse direction and the heat transfer coefficient variation is consistent with flat plate behaviour with a high heat transfer coefficient at the leading edge falling off as the flow moves over the surface. Hence the high value at position 9 falling off towards position 3. The measurement position 10 is in the shadow of the central boss with flow starvation and consequently a low heat transfer coefficient. Over the rest of the diameter flow sweeps in from either side of the boss giving a fairly

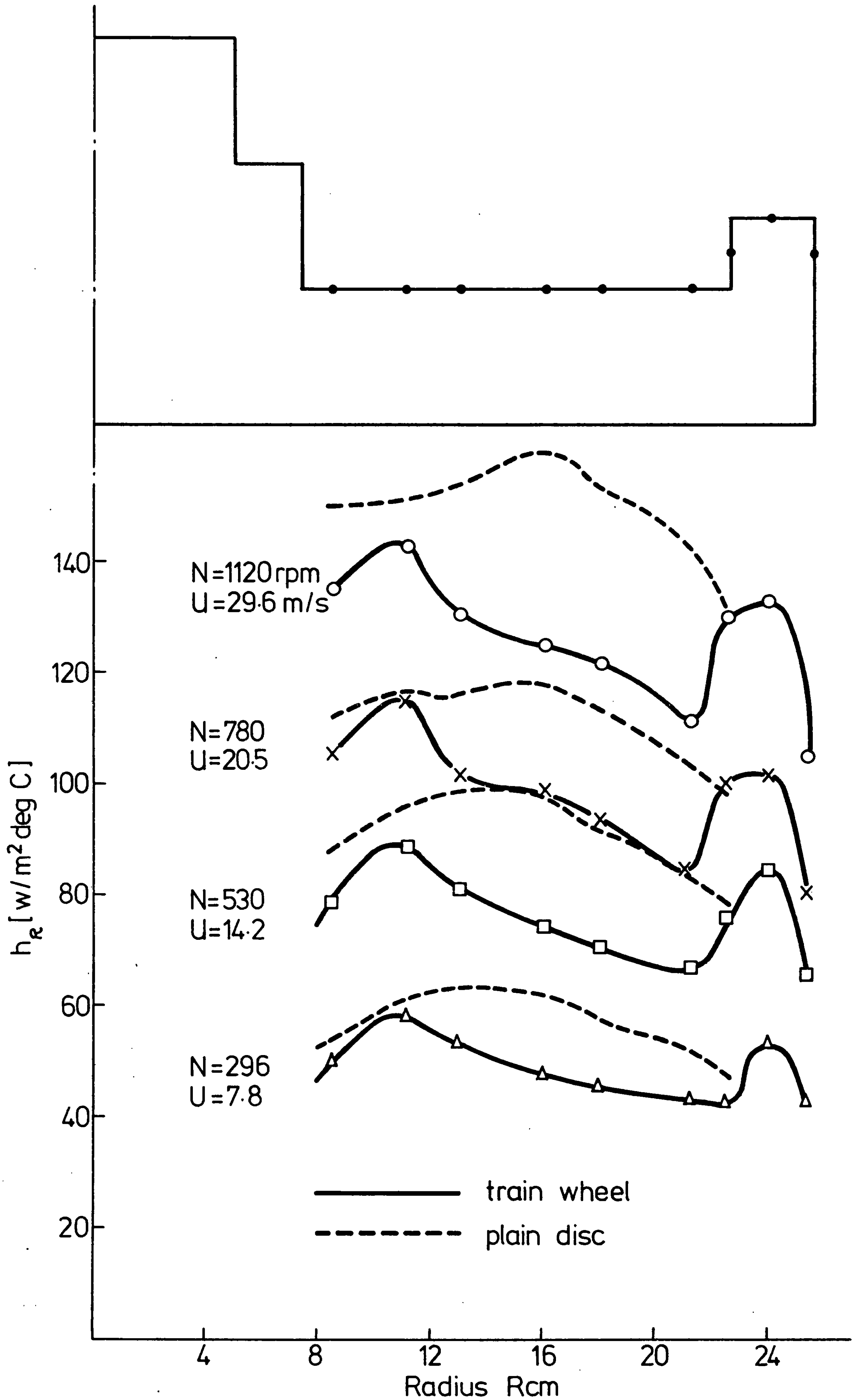

Fig. 6·9 Comparison between a plain disc and the wheel rotating in a transverse air stream

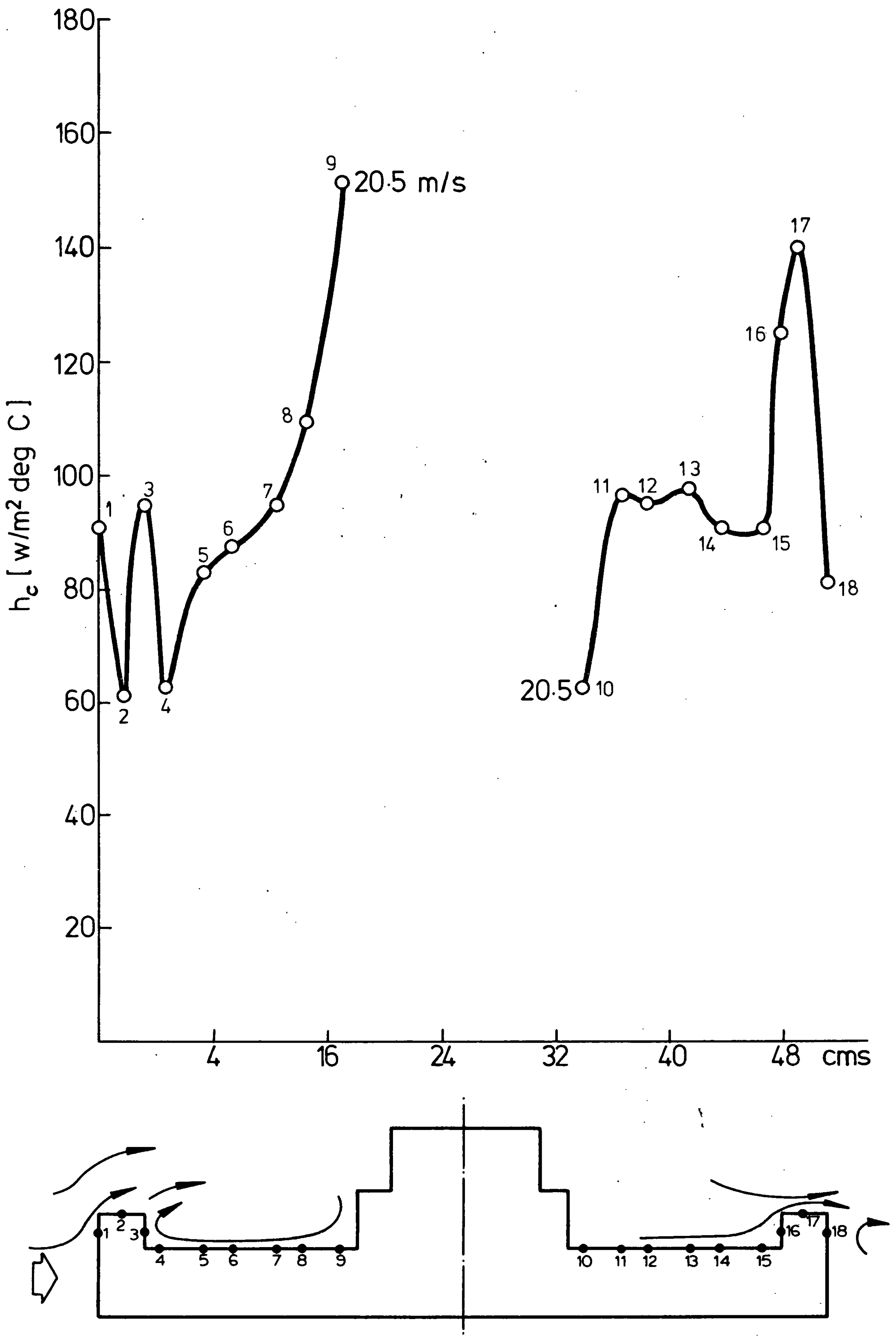

Fig. 6·10 Variation in heat transfer across 0-180° line on wheel constant value of heat transfer coefficient. The high values at measurement parts 16 and 17 are due to re-attachment of the main flow. As the flow again separates to give a wake region behind the wheel, the measurement position 18 is in the shadow with a consequent low heat transfer coefficient. The small variations in heat transfer coefficient that are shown, particularly between stations 11 and 15, are believed to be real and not just a result of random measurement errors. To be absolutely certain measurements at intermediary radial positions would be necessary.

Conclusions

The problem of convective cooling from train wheels subjected to continued braking has been simplified by examining the heat transfer from a plane rotating disc in a transverse air stream. A sensor has been developed to determine local heat transfer coefficients, and from the comprehensive set of measurements made the dominant parameters affecting the cooling process have been isolated. It has been shown that the level of the heat transfer coefficient is determined in the main by the speed of the transverse air flow. The rotation of the disc results in a small upward perturbation on this level. When the disc is held stationary in the transverse air flow this view of main stream dominance is further strengthened by the experimental results.

The radial variations in the heat transfer coefficients are explained in terms of the flow separation and reattachment over the leading half of the disc. The experimental disc is a bluff body and the degree of separation is dependent on the aspect ratio of the disc. This aspect ratio, which has been simulated by the existing disc, greatly modifies the radial distribution of the heat transfer coefficient, but again the main air stream speed is dominant in determining the level of the heat transfer coefficient.

When the aspect ratio is set to the position for minimum separation the variation in heat transfer coefficients for the matched condition have been correlated by the expression:-

$$Nu = 0.0258\ Re_o^{0.83}$$

This equation resembles closely that for turbulent heat transfer from a flat stationary disc in a transverse air flow.

In the context of a train wheel only average radial heat transfer coefficients are of interest. However to understand the mechanism more fully a thin film sensor has been used to measure the instantaneous heat transfer coefficients. With minimum separation over the disc the variation in the heat transfer is in accordance with the predicted patterns showing the sinusoidal variation with angular position. The relative effects of rotation are shown to be small in comparison with the main air stream effects. Reducing the aspect ratio and thereby increasing the separation alters the pattern considerably and there is a slight tendency for the separation and reattachment zones to be dragged with the rotation.

Smoke visualisation tests have helped to understand the results of the heat transfer tests. However they have not shown what occurs close to disc surface where to a large extent the velocity gradients at the 'wall' determine the level of heat transfer. The velocity distribution has been assessed with the aid of hot wire anemometry. When the disc is rotating in still air the results are in good agreement with the theoretical and experimental published works. When the disc is stationary the effectiveness of the leading edge shroud, used to simulate different aspect ratios, is confirmed. For the rotating disc in the transverse airflow the results qualify the view that the main air stream dominates the boundary layer and thus also the heat transfer coefficient.

In conclusion a study of the heat transfer coefficient variation from a simple wheel shape has been done. The results emphasise the fact that to obtain laboratory measurements which are meaningful in full-scale situations, such as train wheels, full modelling mustbe achieved. The size, shape and thickness of the wheel are important in that they govern the main flow pattern and thus the resulting heat tr.nsfer pattern.

Recommendations

In Chapter 4 the limitations of the thin film sensor were discussed. It is therefore recommended that the results should be repeated with modifications to the sensor design. Although the fluctuating component was considered accurate, the absolute mean level of the heat transfer required adjusting to take into account losses from the Platinum film. The film should be so arranged to cover the whole of the substrate surface. Furthermore, calibration of the sensor would remove the errors and inaccuracies present in the theoretical evaluation of the heat transfer coefficient.

In Chapter 6, the testing of a simple train wheel shape has proved useful. This work should be extended to a more 'adult' level where the wheel is accurately modelled and the thermal gradients present across the diameter are included in the investigation.

Appendix 1

Thermal Design of Heat Flux Sensor

This appendix investigates the thermal design of the heat flux sensor in detail and predicts its accuracy in measuring heat transfer coefficients from a rotating disc.

Figure (A1.1) illustrates the sensor and describes the relevant dimensions. From a thermal aspect the sensor is divided up into twelve component resistances as illustrated by Figure (A1.2). These resistances are determined from standard one dimensional steady state heat conduction and convection analysis, where an engineer's order of magnitude type analysis is done. In determining the convective resistances two extreme conditions of operation are used. The maximum and minimum heat transfer coefficients, h_c are taken as 150 and 15 W/m^2 deg.C.

Referring to Figures (A1.1) and (A1.2) the thermal resistance are determined as follows:-

1) Resistance to heat dissipation from the copper surface A via convection, R_1, is given as

$$R_1 = \frac{1}{h_c A_A} = \frac{10^4 \times 4}{15 \times \pi \times (1.48)^2} = 390 \text{ deg.C/W} \quad (39)$$

the bracketed quantity referring to the maximum heat transfer condition $h = 150$ W/m^2 deg.C.

2) Resistance to flow through copper disc A outwards radially R_2 is given as

$$R_2 = \frac{\log_e \frac{r_2}{r_1}}{2\pi k_c t_A} = \frac{\log_e \frac{0.74}{0.25} \times 10^4}{2\pi \times 386 \times 5} = 0.9 \text{ deg.C/W}$$

3) Resistance to flow through copper axially R_3 is

$$\frac{t_A}{k_c A_A} = \frac{5 \times 10^{-4} \times 10^4 \times 4}{386 \times \pi \times (1.48)^2} = 0.00755 \text{ deg.C/W}$$

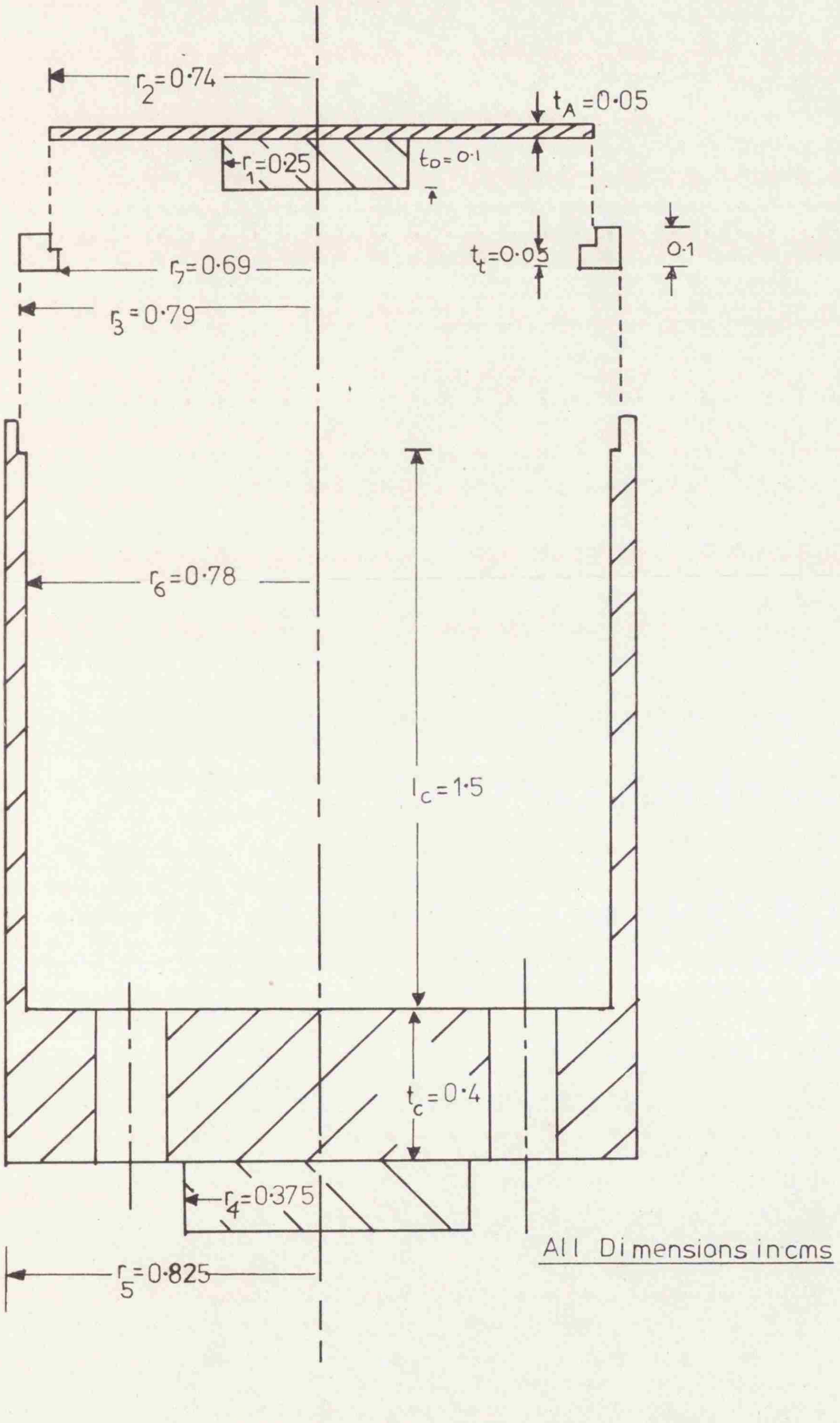

Fig A1.1 The Heat Flux Sensor

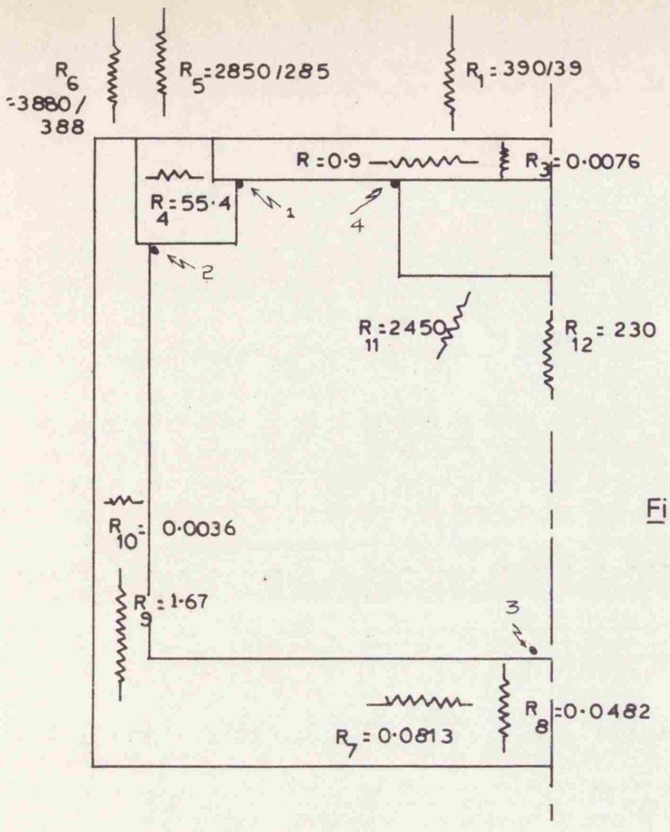

Fig A1.2 Component thermal resistances of sensor

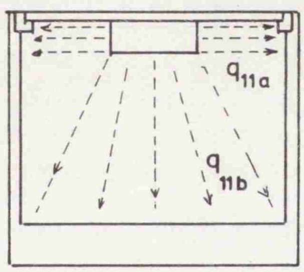

Fig A1·3

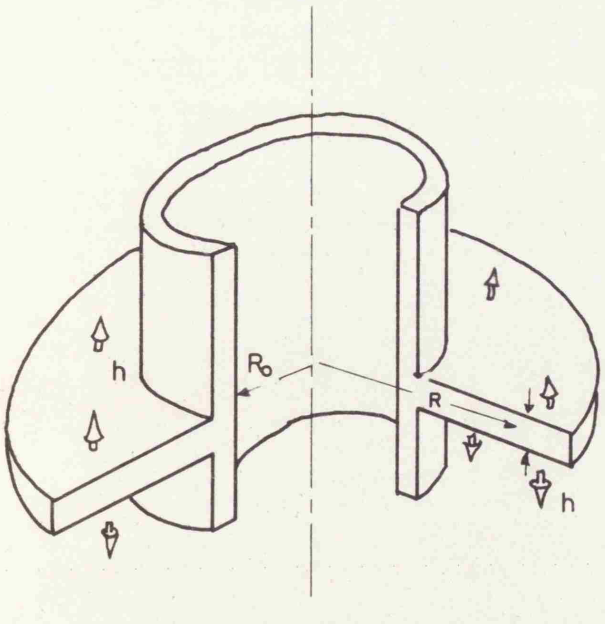

Fig A1·4 Uniform Circular fin

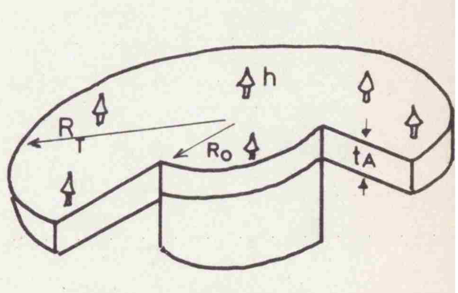

Fig A1·5 Copper Disc A

4) Resistance through Tufnol annular ring R_4. The sizing of this washer is a balance between ensuring that there is small leakage through it radially, maintaining its surface temperature close to the surrounds and reducing leakage from the surface area of the washer.

$$R_4 = \frac{\log_e \frac{r_3}{r_2}}{2\pi k_T t}$$

where t varies between 0.5 mm at radius r_2 and 1 mm at radius r_3. It is therefore taken as a mean of these two values.

$$= \frac{\log_e \frac{0.79}{0.74} \times 10^3}{2\pi \times 0.26 \times 0.75} = 55.4 \text{ deg.C/W}$$

5) The resistance to convective heat dissipation from the insulation surface B, R_5 is given as

$$R_5 = \frac{1}{h_c A_B} = \frac{4 \times 10^4}{15 \times \pi \times (1.58^2 - 1.48^2)} = 2850 \text{ deg.C/W} \quad (285)$$

6) Resistance to convective heat dissipation from the exposed surface of the guard ring C, R_6 is

$$R_6 = \frac{1}{h_c A_C} = \frac{4 \times 10^4}{15 \times \pi \times (1.68^2 - 1.58^2)} = 3880 \text{ deg.C/W} \quad (388)$$

7) Resistance to radial conduction along bottom section of copper cylinder C is

$$R_7 = \frac{\log_e \frac{r_5}{r_4}}{2\pi k_c t_C} = \frac{\log_e \frac{0.825}{0.375} = 10^2}{2\pi \times 386 \times 0.4} = 0.0813 \text{ deg.C/W}$$

8) Resistance to axial conduction in bottom section of C

$$R_8 = \frac{t_c}{k_c A_C} = \frac{0.4 \times 10^{-2} \times 10^4 \times 4}{386 \times \pi \times 1.65^2} = 0.0482 \text{ deg.C/W}$$

9) Resistance to axial conduction up through wall of guard cylinder C

$$R_9 = \frac{\ell_c}{\pi k_c (r_5^2 - r_6^2)} = \frac{1.5 \times 10^{-2} \times 10^4}{386 \times \pi \times (0.825 - 0.78^2)} = 1.67.$$

10) Resistance to radial conduction through wall of cylinder C

$$R_{10} = \frac{\log_e \frac{r_5}{r_6}}{2\pi k_c \ell_c} = \frac{\log_e \frac{1.65}{1.56} \times 10^2}{2\pi x 386 x 1.5} = 0.0036$$

11) Resistance to heat loss from thermistor D by conduction through stationary air to guard ring C is determined by considering both axial and radial losses as illustrated by Figure (A1.3)

The radial resistance $R_{11a} = \dfrac{\log_e \frac{r_6}{r_1}}{2\pi k_a t_D} = \dfrac{\log_e \frac{0.78}{0.25} \times 10^3}{0.0262 x 2\pi x 1.5} = 4550$

The axial resistance R_{11b} is given by

$R_{11b} = \dfrac{\ell_c - t_D}{k_a \times A}$ where A varies between πr_1^2 and πr_6^2 and is approximated to a mean area.

$$= \frac{(1.5-0.15) x 10^4 x 2 x 10^{-2}}{0.0262 x \pi x (0.725^2 + 0.25^2)} = 5600$$

The total resistance R_{11} is given as

$$\left(\frac{1}{R_{11a}} + \frac{1}{R_{11b}}\right)^{-1} = 2450 \text{ deg.C/W}$$

12) The resistance to heat loss through the thermistor D wires

$$R_{12} = \frac{1.5 x 10^{-2} x 10^8 x 4}{386 x \pi x (1.25)^2 x 14} \doteq 230 \text{ deg.C/W}$$

A brief study of these resistances indicates a number of points. Firstly the component resistances of the guard ring C, R_7, R_8, R_9 and R_{10} are such that a uniform temperature distribution can be expected throughout its volume. Secondly the axial resistance R_3 ensures that no appreciable temperature gradient exists between the underside and top surface of copper disc A .

Systematic Errors

a) Heat leakage from the copper disc A through the Tufnol washer B into the neighbouring air

Both A and C contribute to this convective loss from the surface of the washer B , the guard ring C contributing more than half by virtue of its larger area of contact. For the purposes of this analysis an equal share is assumed. The surface areas of A and B are subject to the same convective conditions and it is assumed that they are both at the same temperature. The heat leakage expressed as a percentage of the convective heat transfer from the surface of disc A is therefore given as:-

$$\text{Heat leakage} = \frac{R_1}{2R_5} \times 100$$

$$= \frac{390 \times 100}{2 \times 2850} = 6.8\%$$

This error remains constant irrespective of the convective condition and temperatures prevailing.

b) Temperature variation across the copper disc A

The flow of heat from thermistor D through the disc A via resistance R_2 inevitably causes a temperature gradient between points 1 and 4 . If this difference is large the heat transfer coefficient, computed from $hA(T_1 - T_\infty)$, where T_1 is the thermocouple temperature at position 1, is in error. Furthermore the leakage from the thermistor occurs as a result of its higher temperature than the surrounds. The worst possible condition is when h is large (e.g. 150 W/m^2 deg.C).

Assuming the copper disc can be treated as a circular fin, with the boundary conditions of no heat loss through the fin tip, see Figures (A1.4, A1.5), then the temperature distribution is given by[17]

$$T = T_o \left[\frac{I_o(pR)K_1(pR_t) + I_1(pR_t)K_o(pR)}{I_o(pR_o)K_1(pR_t)+I_1(pR_t)K_o(pR_o)} \right]$$

where $p = \frac{h_c}{k_c t_A}$ and where I_o, K_o and $I_1 K_1$ are the normal Bessel functions of the first and second kind. The boundary condition is not satisfied as there is a certain degree of leakage through into the Tufnol washer B . An approximation is used where the Bessel functions are evaluated at $R_t' = \sqrt{R_t(R_t + t_A)}$. The temperature T_1 at the disc tip is then determined as

$$T_1 = T_4 \left[\frac{I_o(pR_t')K_1(pR_t') + I_1(pR_t')K_o(pR_t')}{I_o(pR_o)K_1(pR_t') + I_1(pR_t')K_o(pR_o)} \right]$$

From Figure(A1.1) $t_A = 0.05$ cm

$R_o = 0.25$ cm

$R_t = 0.74$ cm

and $R_t' = 0.764$ cm

Evaluating the Bessel functions yields $T_1 = 0.9913\ T_4$. Thus when operating at a condition $T_1 = T_2 = T_3 = 100$ deg.C (above ambient) the temperature T_4 is approximately one degree higher. The effect of this discrepancy is two fold. Firstly the surface temperature varies between 100 and 101 deg.C and the error caused by not using thecorrect surface temperature is determined to be no greater than 1%. The value measured in this instance is greater than the true heat transfer coefficient present. The second error is the heat loss to the guard ring from the thermistor D which is at the higher temperature of 101 deg.C. The error expressed as a percentage of the total heat transfer is given as

$$\frac{1(\text{deg.C})}{\left(\frac{1}{R_{11}} + \frac{1}{R_{12}}\right)^{-1}} \Bigg/ \frac{100(\text{deg.C})}{R_1} \times 100$$

and is less than 0.2 per cent. The value measured is greater than the true heat transfer coefficient. The nett effect of these two errors is 1.2%.

c) Heat loss by radiation

The sensor loses heat by radiation. The error resulting from ignoring this loss is largest when low convective condition and high temperatures prevail (ΔT = 100 deg.C).

The radiation exchange Q_R is determined from the equation[11]

$$Q_R = \sigma\, A_A\, \eta(T_1^4 - T_\infty^4)$$

where η is the Hottel factor as is assumed in this instance equal to the emissivity of the copper surface, ε = 0.052 for polished copper.
The Stefan-Boltzman constant σ is 5.663 x 10^{-8} J/m^{2}s (deg.K)^4.

$$\therefore \qquad Q_R = \frac{5.663 \times \pi \times 1.48^2 \times 0.052 \times 10^{-1}}{4} \left[(3.93)^4 - (2.93)^4\right]$$

$$= 8.34 \text{ mW.}$$

[For low temperatures (ΔT = 20 deg.C) this heat loss reduces significantly to 1 mW.]

Expressed as a percentage of the convective heat transfer this radiation loss is 3.25 and 0.325 per cent for h = 15 and 150 W/m^2 deg.C respectively.

Random Errors

If the temperatures at positions 1, 2 and 3 are not equal there is a heat transfer between the guard ring and the thermistor D / copper disc A through the resistances R_4, R_{11} and R_{12} and the calculated heat transfer coefficient is in error. The percentage error is greatest when measuring low convective heat transfer coefficients at small temperature differences.

For h = 15 W/m^2 deg.C and ΔT = 20 degrees the convective heat output is

$$q_c = \frac{\Delta T}{R_1} = 51.4 \text{ mW}$$

A 0.25 degree in balance in temperature gives a loss of

$$\frac{0.25}{\left(\frac{1}{R_4} + \frac{1}{R_{11}} + \frac{1}{R_{12}}\right)^{-1}} = 5.71 \text{ mW}$$

Expressed as a percentage of the output q_c the error is 11.2 per cent. This error is reduced proportionately as the heat transfer coefficient and temperature gradient increase.

Appendix 2

Response Characteristics of the Heat Flux Sensor

The sensor is modelled as a copper disc of mass m, specific heat c_p and face area Y as shown in Figure (A2.1). Heat is applied to the disc at a rate $\dot{q}$ and one face loses heat by forced convection characterized by a time dependent heat transfer coefficient $h(t)$. It is assumed that there is no other heat loss and that the disc's thermal conductivity is infinite. The disc temperature above ambient is θ.

The governing equation is

$$\frac{d\theta}{dt} + \frac{h(t)Y\theta}{mc_p} = \frac{\dot{q}}{mc_p} \tag{A2.1}$$

for a heat transfer variation of the form $A' + B'\sin\omega t$, as shown in Figure (A2.2) equation (A2.1) becomes

$$\frac{d\theta}{dz} + (A + B\sin z)\theta = K \tag{A2.2}$$

where $z = \omega t$, $A = \frac{A'Y}{mc_p\omega}$, $B = \frac{B'Y}{mc_p\omega}$ and $K = \frac{\dot{q}}{mc_p\omega}$ the solution is

$$\theta = e^{-(Az-B\cos z)}\, K \int e^{(Az-B\cos z)}dz + Ce^{-(Az-B\cos z)} \tag{A2.3}$$

The integral is evaluated by expressing $e^{-B\cos z}$ as a series

$$\int e^{Az}\, e^{-B\cos z}dz = \int e^{Az}\left(1 - B\cos z + \frac{B^2\cos^2 z}{2!} - \frac{B^3\cos^3 z}{3!} \;.....\right)dz \tag{A2.4}$$

The general term is $(-1)^N \int e^{Az}\, \frac{B^N\cos^N z}{N!}\, dz$

Integrating by parts

$$\int e^{Az}\cos^N z\,dz = \frac{\cos^N z}{A}e^{Az} + N\cos^{N-1}z\,\frac{\sin z}{A^2}e^{Az} - \frac{N}{A^2}\int e^{Az}\,(\cos^N z-(N-1)\cos^{N-2}z + (N-1)\cos^N z)dz$$

$\therefore$

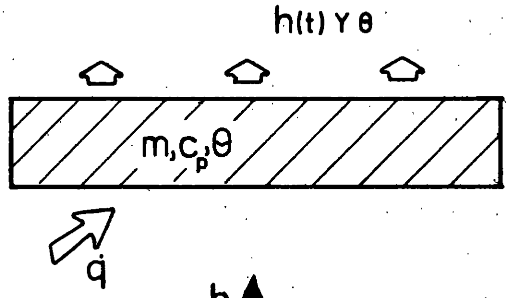

Fig A2·1

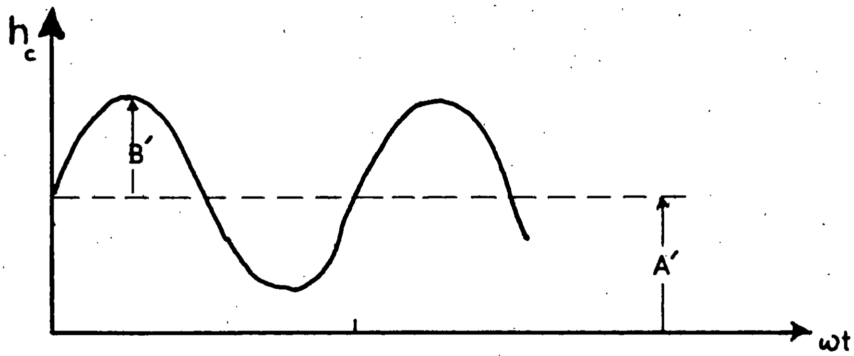

Fig A2·2

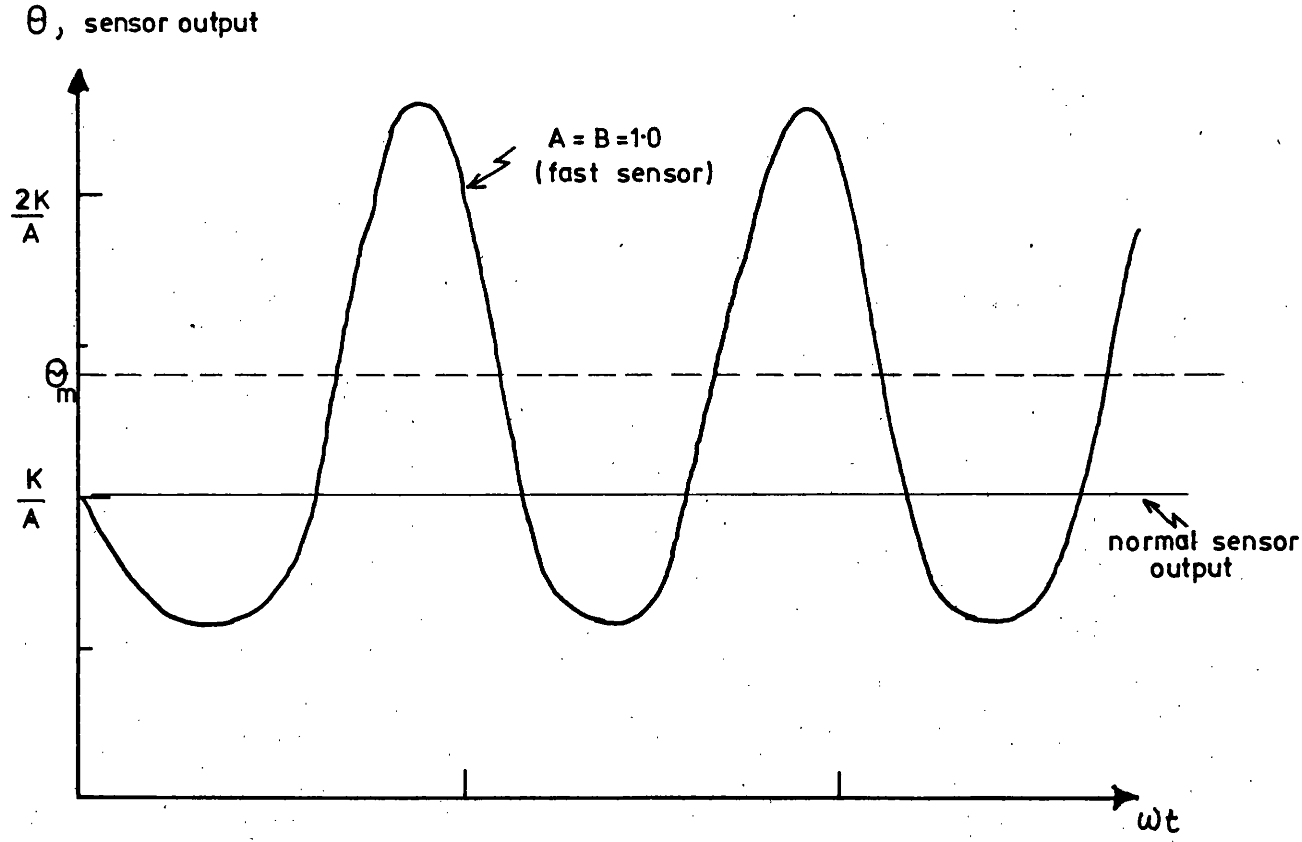

Fig A2·3 Theoretical output, θ, of normal and fast responding sensors

$$\therefore \left(1+\frac{N^2}{A^2}\right)\int e^{Az}\cos^N z\,dz = \frac{\cos^N z}{A}e^{Az} + N\cos^{N-1}z\,\frac{\sin z}{A^2}e^{Az} + \frac{N(N-1)}{A^2}\int e^{Az}\cos^{N-2}z\,dz$$

$$\therefore \int e^{Az}\cos^N z\,dz = \frac{\left(\frac{\cos^N z}{A} + N\frac{\cos^{N-1}z\sin z}{A^2}\right)e^{Az}}{1+\frac{N^2}{A^2}} + \frac{N(N-1)}{A^2\left(1+\frac{N^2}{A^2}\right)}\int e^{Az}\cos^{N-2}z\,dz$$

at $N = 0$ $\quad \int e^{Az}dz = \frac{e^{Az}}{A}$

$$N = 1 \quad \int e^{Az}B\cos z = \frac{B\left(\left(\frac{\cos z}{A} + \frac{\sin z}{A^2}\right)e^{Az}\right)}{1+\frac{1}{A^2}}$$

and so on for $N = 2, 3, 4$ etc.

Thus equation 3 becomes

$$\theta = Ke^{B\cos z}\left[\frac{1}{A} - \frac{\left(B\frac{\cos z}{A} + \frac{\sin z}{A^2}\right)}{1+\frac{1}{A^2}} + \frac{B^2}{2!}\frac{\left(\frac{\cos^2 z}{A} + \frac{\sin 2z}{A^2} + \frac{2}{A^3}\right)}{1+\frac{4}{A^2}} - \right.$$

$$\frac{B^3}{3!}\left(\frac{\cos^3 z}{A} + \frac{3\cos^2 z\sin z}{A^2} + \frac{6}{A^2}\frac{\left(\frac{\cos z}{A} + \frac{\sin z}{A^2}\right)}{1+\frac{1}{A^2}}\right)\Big/\left(1+\frac{9}{A^2}\right) +$$

$$\left.\frac{B^4}{4!}\left(\frac{\cos^4 z}{A} + \frac{4\cos^3 z\sin z}{A^2} + \frac{12}{A^2}\frac{\left(\frac{\cos^2 z}{A} + \frac{\sin^2 z}{A^2}\right)}{1+\frac{4}{A^2}} + \frac{24}{A^4\left(1+\frac{4}{A^2}\right)}\frac{1}{A}\right)\Big/\left(1+\frac{16}{A^2}\right)\right]$$

$$+ \ldots\ldots\ldots\ldots\ldots\ldots\ Ce^{-(Az-B\cos z)} \qquad \text{(A2.5)}$$

The last term $Ce^{-(Az-B\cos z)}$ is the complementary function and goes to zero after steady state conditions are reached.

Consider a variation in the heat transfer coefficient $h(t) = 90 + 90 \sin\omega t$. (These values have been chosen as they represent the level of the measurements. Furthermore it is desirable to investigate the effect of zero heat transfer at the position where the relative velocity is zero.)

Assuming a typical speed of rotation ω = 630 r.p.m.

$$A = \frac{A'Y}{mc_p\omega} = \frac{A'}{\rho c_p t_c \omega}$$ where ρ = density of copper 8954 kg/m^3

t_c = thickness of copper disc 5×10^{-4}m

c_p = 380 J/kg deg.C.

$$= 8 \times 10^{-4}$$

and similarly $B = \frac{B'Y}{mc_p\omega} = 8 \times 10^{-4}$

Thus $\theta = \frac{K}{A} e^{8\times10^{-4}\cos z} (1 - (5.12 \times 10^{-10}\cos z + 6.4 \times 10^{-7}\sin z) + \ldots\ldots$

$\therefore$ $\theta \simeq \frac{K}{A} = \frac{\dot{q}}{A'Y}$, since $e^{8\times10^{-4}\cos z}$ is very close to unity irrespective of values of cosz.

But this is just the value that would be given if the sensor were exposed to a constant heat transfer of A'. The analysis therefore shows that the measured heat flux of the sensor represents a straight average of a sinusoidal varying heat transfer coefficient. It is also expected that similar results will be obtained from other waveforms by virtue of its very slow response.

The above statements do not apply if the thickness of the disc is greatly reduced ($\simeq \times 1000$) so that A = B = 1. The function θ is then

$$\theta = Ke^{\cos z}\left\{1 - \frac{1}{2}(\cos z+\sin z) + \frac{1}{2}\,\frac{\cos^2 z+\sin 2z)}{5} + \frac{1}{5} - \frac{1}{6}\left[\frac{\cos^3 z+\cos^2 z\sin z}{10} + \frac{3}{10}(\cos z\sin z)\right] + \frac{1}{24}\left\{\frac{(\cos^4 z+4\cos^3 z\sin z)}{17} + \frac{12}{17}\,\frac{\cos^2 z+2\cos z\sin z)}{5} + \frac{24}{17 \times 5}\right\} + \ldots\right.$$

and the resulting profile is shown in Figure (A2.3).

It is appreciated that the final output is subject to the characteristics of the measuring device. If the device is too slow to respond to these temperature changes then the mean temperature recorded θ_m will not correspond to the mean heat transfer coefficient as determined by a slow responding sensor.

Appendix 3

Results

Table 1. Rotating Disc in Still Air

Table 2. Rotating Disc in Matched Transverse Air Stream

NB. These tables are representative of all the heat transfer coefficient measurements made with the heat flux sensor. They illustrate the ranges and behaviours of all the variables involved. For this reason all the other results have not been tabulated as they contribute no more than is already available in the graphs.

Table 1

Rotating Disc in Still Air

N rpm	R m	V volts	I mA	T_1 °C	T_∞ °C	h_R W/m^{2}deg.C	Nu	Re x 10^{-4}
296	0.085	2.15	68.0	73.2	16.0	14.5	45.0	1.30 x 10^4
	"	2.25	54.5	53.0	16.0	14.8	46.7	1.37
	0.112	2.15	61.5	67.0	17.0	14.95	61.0	2.30
	"	2.20	46.5	57.0	17.5	14.7	60.6	2.36
	0.13	2.15	65.0	70.0	16.0	14.7	68.0	3.14
	0.159	2.20	38.0	50.3	17.8	14.6	86.2	4.88
	"	2.15	54.5	61.5	18.0	15.2	88.5	4.68
	0.18	2.20	54.7	57.0	18.0	14.8	94.6	6.02
	0.212	2.25	44.5	56.0	18.0	14.55	113.5	8.65
	"	2.10	62.0	67.0	18.5	15.2	117.0	8.36
	0.225	2.15	61.6	68.0	18.0	15.0	124.0	9.15
436	0.085	2.15	58.0	63.0	20.0	16.5	51.0	1.94
	"	2.15	67.0	68.0	20.0	17.0	52.4	1.92
	0.112	2.35	48.0	57.0	19.0	16.8	70.0	3.42
	"	2.20	66.0	67.5	19.5	17.15	69.6	3.34
	0.13	2.15	69.0	69.0	19.0	16.85	78.0	4.63
	0.159	2.25	64.0	65.8	18.0	17.0	98.5	6.80
	"	2.10	83.5	76.0	18.0	17.05	97.0	6.60
	0.18	2.15	69.6	68	18.0	17.0	109	8.9
	0.212	2.10	78.0	73.8	18.0	16.6	127.0	11.95
	"	2.00	96.0	83.0	18.0	16.8	127.0	11.45
	0.225	2.25	60.0	63.2	18.2	17.0	136.0	13.9
530	0.085	2.40	28.5	38.3	18.2	18.9	61.2	2.62
	"	2.45	61.8	64.3	18.5	18.7	58.0	2.42
	0.112	2.35	32.3	42.5	19.5	18.7	80.0	4.50
	"	2.45	48.0	54.5	19.5	18.9	78.1	4.26
	0.13	2.40	48.6	56.0	19.0	18.9	91.5	5.62
	0.159	2.45	67.0	66.9	19.0	19.2	112.5	8.40
	"	2.40	30.0	40.0	19.0	19.2	115.0	8.90
	0.18	2.4	45.0	51.0	19.0	19.2	123.0	10.8
	0.212	2.48	41.5	49.5	19.2	19.2	149.0	15.2
	"	2.48	61.0	63.5	19.5	19.4	148.0	14.6
	0.225	2.45	55.6	59.0	19.0	19.4	163.0	16.9

Table 1 continued

N rpm	R m	V volts	I mA	T_1 ^oC	T_∞ ^oC	h_R $W/m^2 deg.C$	Nu	Re x 10^{-4}
630	0.085	2.40	59.0	62.0	24.8	21.0	65.0	2.76
	0.112	2.4	62.2	62.0	22	21.2	88.0	5.0
	0.13	2.2	82.0	72.2	22.2	21.4	104.0	6.69
	0.159	2.25	77.0	70.0	25.0	21.8	124	9.45
	0.18	2.4	62.0	63.0	23.0	21.0	141	12.8
	"	2.4	64.5	63.0	22.0	21.4	143	12.8
	0.212	2.3	76.5	68	22.2	21.8	171	17.8
	0.225	2.4	65.4	61.0	24.0	24.0	200	20.0
780	0.225	7.4	29.3	49.0	19.6	42.0	350	24.9
	0.212	7.0	27.4	51.0	20.8	36.0	293	22.1
	0.18	6.0	25.6	54.0	19.25	25.0	167	15.9
	0.159	6.0	25.5	54.0	19.0	24.5	143.5	12.45
	0.13	5.95	27.4	57.6	19.9	24.6	118.5	8.3
	0.112	5.85	25.0	53.3	19.1	24.2	100	6.16
	0.085	5.85	23.4	51.4	19.1	24.0	75.5	3.56
910	0.225	9.5	28.4	43.0	16.7	58.0	485	29.1
	0.212	8.4	34.0	49.0	17.8	52.0	408	25.8
	0.18	6.9	25.0	47.0	17.1	30.0	200	18.6
	0.159	6.45	23.0	51.4	19.2	26.2	154	14.6
	0.13	6.5	23.6	50.3	17.2	26.2	120	9.7
	0.112	6.35	24.8	54.9	19.3	25.7	104	7.2
	0.085	6.35	25.5	54.5	19.3	26.0	84	4.15
1120	0.225	9.5	39.6	50.5	20.6	71.0	590	35.4
	0.212	9.45	39.7	51.0	20.6	69.3	545	31.8
	0.18	7.4	25.5	48.0	19.4	37.0	290	22.8
	0.159	6.4	26.4	51.0	19.6	30.6	180	18.0
	0.13	6.35	23.6	50.2	19.5	27.6	133	11.9
	0.112	6.35	23.4	48.8	19.5	28.6	119	8.85
	0.085	6.35	24.7	50.5	19.7	28.6	90	5.1
1200	0.225	9.7	42.0	51.0	20.6	75.0	622	37.1
	0.212	9.65	39.1	50.0	20.8	73.1	574	34.1
	0.18	8.2	32.4	52.3	21.0	48.0	320	24.5
	0.159	7.65	22.2	41.0	15.4	37.4	220	19.3
	0.13	6.5	26.2	52.0	21.0	31.2	150	12.75
	0.112	6.3	25.2	50.2	20.8	30.0	124	9.5
	0.085	6.3	26.0	52.0	21.0	30.0	92	5.46

Table 1 continued

N rpm	R m	V volts	I mA	T_1 °C	T_∞ °C	h_R W/m^{2}deg.C	Nu	Re x 10^{-4}
1650	0.225	11.25	53.0	51.2	17.2	99.5	826	52.0
	0.212	10.7	46.2	50.0	20.8	96.0	755	47.0
	0.18	10.7	47.4	50.5	17.5	85.0	565	33.6
	0.159	10.05	42.5	48.9	15.4	73.0	430	26.5
	0.13	7.75	30.0	48.0	15.4	40.5	170	17.5
	0.112	7.4	26.8	47.5	15.4	34.8	144	13.0
	0.085	7.3	27.2	49.5	15.5	33.0	105	7.5

Table 2

Rotating disc in matched transverse air stream

N rpm	U m/s	R m	V volts	I amps	T_1 °C	T_∞ °C	h $W/m^2 °C$	Nu	Re x 10^{-4}
1120	29.5	0.085	13.0	57.7	49.2	20.8	150.0		
		0.112	12.5	59.7	51.0	23.2	152.0		
		0.13	11.55	50.2	46.0	24.5	153.0		
		0.159	11.8	50.8	48.2	26.9	159.0		
		0.18	11.45	63.6	51.0	23.9	153.0		
		0.212	11.6	61.5	53.0	25.1	145.0		
		0.225	11.0	58.5	50.1	22.1	131.0		
910	24	0.085	12.5	54.5	49.4	19.4	128.5		
		0.112	12.3	59.4	52.1	20.5	132.0		
		0.13	11.25	45.1	45.1	23.3	132.5		
		0.159	11.4	54.6	51.2	25.2	136.0		
		0.18	10.55	62.3	53.1	23.8	127.5		
		0.212	11.05	57.2	53.9	23.9	120.0		
		0.225	10.85	51.2	48.8	20.2	110.0		
780	20.6	0.085	12.2	50.2	49.0	18.0	112.0		
		0.112	11.9	58.7	53.8	19.0	114.0		
		0.13	10.85	46.2	47.3	22.8	116.0		
		0.159	11.0	52.8	52.5	24.7	118.0		
		0.18	10.3	57.5	53.0	23.2	113.0		
		0.212	10.6	55.7	55.0	22.8	104.0		
		0.225	10.55	48.4	49.0	19.4	98.0		
630	16.7	0.085	5.4	126.0	58.0	19.0	99.0		
			5.5	66.0	40.0	19.0	98.0	315	2.99
		0.112	5.5	122.0	56.0	19.1	103.2	429	4.96
			5.6	88.0	46.0	19.4	105.0	443	5.10
		0.13	5.6	105.0	49.5	18.0	106.0	516	6.83
			5.75	77.0	41.8	18.0	105.0	520	6.99
			11.45	57.1	53.6	18.3	105.0	506	6.75
		0.159	5.35	122.0	55.1	21.0	108.0	638	10.05
			5.55	113.0	52.5	19.6	108.0	639	10.12
		0.181	5.45	130.0	57.5	18.0	102.5	680	12.94
			5.60	88.0	45.8	18.5	102.2	694	13.4
			11.00	60.8	56.2	19.0	102.0	685	12.95

Table 2 continued

N rpm	U m/s	R m	V volts	I amps	T_1 ^oC	T_∞ ^oC	h $W/m^2 {}^oC$	Nu	Re x 10^4
630	16.7	0.212	5.05	138.0	61.2	19.8	95.5	746	17.5
			5.40	88.0	47.3	20.0	98.0	777	18.25
		0.225	5.15	124.0	58.5	18.9	92.0	764	20.0
			5.35	89.5	48.2	19.0	93.4	786	20.6
530	14.5	0.085	10.5	59.7	57.8	17.1	88.5	279	2.40
			11.0	40.3	45.5	17.9	88.3	282	2.48
		0.112	11.0	59.0	56.5	17.0	95.6	398	4.18
			11.9	38.0	43.2	17.0	98.0	416	4.35
		0.13	10.4	61.7	57.1	19.5	97.0	467	5.60
			10.95	44.9	48.0	20.0	99.0	481	5.75
		0.159	10.55	64.9	58.5	19.2	98.0	575	8.40
			11.25	41.0	45.5	19.8	100.0	594	8.70
		0.181	9.95	63.8	58.8	19.0	90.4	603	10.82
			10.5	42.9	47.0	19.2	91.5	620	11.20
		0.212	9.55	65.3	61.6	20.1	85.0	664	14.72
			10.05	47.5	52.0	20.5	86.0	680	15.10
		0.225	9.42	65.5	63.5	1810	77.0	638	16.6
			10.00	48.7	52.9	18.2	79.5	674	17.1
			10.25	40.0	46.8	18.0	80.7	682	17.35
436	11.1	0.085	9.00	57.8	60.8	21.8	75.5	236	1.95
			9.20	43.0	51.2	22.0	77.0	253	2.00
		0.112	9.20	66.0	63.9	22.0	82.0	337	2.98
			9.50	50.0	54.6	22.6	84.0	348	3.06
		0.159	9.15	70.7	64.9	21.9	85.2	496	6.76
			9.75	48.5	53.0	22.0	86.5	510	7.00
		0.181	8.85	70.3	65.1	19.0	76.4	504	8.75
			9.6	47.5	52.8	19.0	76.4	515	9.05
			9.95	36.6	45.2	19.1	79.0	538	9.28
		0.13	9.5	59.6	58.3	20.9	86.0	413	4.58
			10.00	43.2	49.0	21.0	87.5	425	4.70
			10.5	48.9	52.0	17.4	84.0	406	4.58
		0.212	8.95	58.4	61.3	21.0	73.5	574	12.1
			9.35	42.1	51.8	21.2	73.0	576	12.4
		0.225	8.55	67.5	65.9	19.6	70.5	581	13.5
			9.00	46.5	54.9	19.9	68.0	568	13.9

Table 2 continued

N rpm	U m/s	R m	V volts	I amps	T_1 ^oC	T_∞ ^oC	h $W/m^{2o}C$	Nu	Re x 10^4
296	7.8	0.085	8.00	63.5	72.0	17.8	52.5	162	1.28
			8.35	40.3	54.0	17.9	52.8	168	1.35
		0.112	8.42	63.0	67.8	18.0	60.5	247	2.26
			8.55	51.7	60.3	18.3	60.0	249	2.30
			9.10	38.4	51.3	18.7	60.8	254	2.36
		0.13	8.6	49.6	59.9	21.0	62.5	300	3.10
			9.05	36.9	51.0	21.0	63.0	306	3.18
		0.159	8.55	56.8	64.0	19.0	61.3	358	4.63
			9.00	40.8	53.3	19.3	61.4	362	4.76
		0.181	8.05	57.9	66.4	20.6	57.8	381	5.92
			8.55	39.1	53.7	20.9	57.6	386	6.14
		0.212	7.95	50.8	63.6	19.3	51.6	402	8.18
			8.50	35.9	52.7	19.3	52.4	414	8.44
		0.225	7.6	46.3	62.8	20.0	46.5	384	9.24
			8.00	36.2	54.1	20.1	48.0	404	9.46

References

1. Dorfman, L.A. "Hydrodynamic Resistance and Heat Loss from Rotating Solids" (Transl. by N. Kemmer). Oliver and Boyd, Edinburgh and London (1963).

2. Kreith, F. "Advances in Heat Transfer", 5, 129, (1968).

3. Cobb, E.C. and Saunders, O.A. Proc. Roy. Soc. A., 236, 343, (1956).

4. Owen, J.M., Haynes, C.M., and Bayley, F.J. "Heat Transfer from an Air Cooled Rotating Disc", Mech. Eng. Rep. 72/Me/43 School of Applied Sciences, University of Sussex (1972). * updated see p. 83B.

5. Chilton, T.H. and Colburn, A.P. Ind. Eng. Chem. 26, 1183 (1934).

6. Nash, K.L. and Maxwell, R.W. "Convective Mass Transfer from Stationary Cylinders and Spherical Surfaces", University of Leicester Engineering Report 69-26 Oct. (1969).

7. Nash, K.L. and Maxwell, R.W. "Convective Mass Transfer from Stationary and Moving Surfaces", University of Leicester Engineering Report 70-13 April (1970).

8. Gregory, N., Stuart, J.T. and Walker, W.S. "On the stability of three dimensional boundary layers with application to the flow due to a rotating disc", Phil. Trans. Roy. Soc. London, A248, 155-199 (1955).

9. Cobb, E.C. and Saunders, O.A. "Heat Transfer from a Rotating Disc", Proc. Roy. Soc. A., 236, 343, 1956.

10. Goldstein, S. Proc. Cambridge Phil. Soc., 31, 232, 1935.

11. Kreith, F. "Principles of Heat Transfer", 2nd Edition, Intern. Text Book Co., 1965.

12. Gardon, R. "An instrument for the direct measurement of intense thermal radiation", The Review of Sc. Instruments, 24, 5, p.366, May 1953.

13. Schultz, D.L. and Jones, T.C. "Heat Transfer Measurements in Short-duration Hypersonic Facilities", Advisory Group for Aerospace Research and Development Agard No. 165.

14. Cook, W.J. and Felderman, E.J. Reduction of Data fror Thin film heat transfer gauges. A concise numerical technique. AIAA J. 4, 3, 1966, p.561.

15. Hartunian, R.A. and Varwig, R.L. "On Thin Film Heat Transfer Measurements in Shock Tubes and Shock Tunnels", Phys. Fluids, 5, 2, 1962, p.169.

16. Cochran, W.G. The Flow due to a Rotating Disc. Proc. Cambridge Phil. Soc. 30, 365, (1934).

17. Bayley, F.J., Owen, J.M. and Turner, A.B. "Heat Transfer" Nelson 1972.

18. Hinze, J.O. Turbulence. McGraw-Hill, 1959.

19. Schlichting, H. "Boundary Layer Theory", (Transl. by J. Kestin) Fourth edition, McGraw-Hill.

20. Kay, J.M. An Introduction to Fluid Mechanics and Heat Transfer. Second edition, C.U.P.

21. Dennis, R.W.,Newstead, C, and Ede, A.J. The Heat Transfer from a Rotating Disc in an Air Crossflow. 4th International Heat Transfe. Conference 1971 - Versailles.

22. Hartnett, J.P "Heat Transfer from a Non-Isothermal Disc Rotating in Still Air." J. Appl. Mech., 26 , 672, (1959)

23. Wagner, C. "Heat Transfer from a Heated Disc to Ambient Air", J. Appl. Phys. 19 , 837, (1948).

24. Millsaps, K. and Pohlhausen, K., "Heat Transfer by Laminar Flow from a Rotating Plate", J. Aero. Sc. 19 ,2, 120, (1952).

25 Young, R.L. "Heat Transfer from a Rotating Plate", Trans ASME., 78 , 1163, (1956).

26. Kreith F, Taylor J.H., and Chang J.P., "Heat and Mass Transfer from a Rotating Disc ", J. Heat Transfer., 81 95, (1959).

27. Richardson P.D. and Saunders C.A., "Studies of Flow and Heat Transfer associated with a Rotating Disc." J. Mech. Eng. Sc. 5, 4, 336, (1963).

28. Mc Comas S.J and Hartnett J.P. "Temperature Profiles and Heat Transfer associated with a Single Disc Rotating in Still Air", 4th Int. Heat Transfer Conf. Versailles, 111 FC7.7 , (1970)

29. Ostrach S. and Thornton P.R. " Compressible Laminar Flow and Heat Transfer about a Rotating Isothermal Disc," NACA TN 4320 (1958).

****

4. Owen J.M., Haynes, C.M., and Bayley, F.J. " Heat Transfer from an Air Cooled Rotating Disc. " Proc.Roy. Soc. Lond. A 336 , 453 -474. 1974

Acknowledgement

The author wishes to thank the many members of the staff of the Department of Engineering, University of Leicester, who have given advice and help during this work. In particular the author wishes to express his gratitude to Messrs. J. Cooke, J. Donisthorpe, C. Harris and R.V. Sexton.

The author would also like to thank the Royal Aircraft Establishment, Farnborough, who very kindly supplied the Platinum film substrate and gave helpful advice and direction.

Finally, the author wishes to thank Dr. G.L. Booth who supervised the work throughout its period and gave encouragement and guidance whenever it was needed, and to Mr. Douglas Pratt, Mr. John Pearson and Mrs. Helen Sheppard for their help in the preparation of the drawings, photographs and typing of the thesis.

Reprint of a paper

presented at the

5th International Heat Transfer Conference

September 3 – September 7, 1974

at

Keidanrenkaikan Building, Tokyo

REFERENCES

/1/ Tetervin, N.: NACA TN 1644, 1948

/2/ Glauert, M.B.: Journal of Fluid Mechanics, 1, 625 (1956)

/3/ Bajura, R.A. and A.A. Szewczyk.: Technical Report No. 67-17, University of Notre Dame (1967)

/4/ Gorla, R.S.R. and D.R. Jeng.: Developments in Mechanics, 6, 137 (1971)

/5/ Rarity, B.S.H.: Quart. Journal of Mechanics and Applied Mathematics, 18, 455 (1965)

/6/ Schwarz, W.H. and B. Casewell.: Chemical Engineering Science, 16, 338 (1961)

/7/ Abramowitz, M. and I.A. Stegun.: "Handbook of Mathematical Functions", National Bereau of Standards, Applied Mathematics Series 55 (1964)

/8/ Erdelyi, A.: "Higher Transcendental Functions:, Vol. 1, McGraw - Hill Publishers, New York (1953)

APPENDIX

Table I. ISOTHERMAL SERIES WALL VALUES

P_r	$\theta_0'(o)$	$\theta_1'(o)$	$\theta_2'(o)$
0.01	-0.00975	-0.00472069	0.0297832
0.1	-0.080190	-0.0490665	0.163431
0.73	-0.288000	-0.295591	0.833845
1.0	-0.333300	-0.367727	1.02546
10.0	-0.78860	-1.29405	3.48927
50.0	-1.36900	-2.65265	7.22528
100.0	-1.72800	-3.52286	9.66430
1000.0	-3.71700	-8.25715	23.5268

Table II. WALL VALUES FOR CONSTANT SURFACE HEAT FLUX SERIES

P_r	$\theta_0(o)$	$\theta_1(o)$	$\theta_2(o)$
0.01	31.8081	-4.48627	17.0210
0.1	5.67717	-1.57808	4.82134
0.73	2.04932	-1.25491	4.05757
1.0	1.81485	-1.20139	3.93128
10.0	0.811090	-0.782042	2.80471
50.0	0.472765	-0.525866	1.99075
100.0	0.375147	-0.435095	1.67857
1000.0	0.174379	-0.214415	0.861139

FC1.7 CONVECTIVE HEAT TRANSFER FROM A ROTATING DISC IN A TRANSVERSE AIR STREAM

G. L. Booth and A. P. C. De Vere
University of Leicester, England

Abstract

Radial variation of heat transfer coefficient is reported for a disc rotating at speeds up to 1650 r.p.m. in still air and in transverse air streams of speeds up to 33 m/s. A sensor for local heat transfer coefficient, with thermistors as heating elements, is described. The size of the coefficient is governed by the main air stream, the rotating boundary layer on the disc giving small perturbations. Experiments with discs of different aspect ratios (simulated by the test disc protruding from a shroud) show the radial variations can be explained in terms of flow separation at the disc leading edge followed by reattachment to the face. At large aspect ratio the heat transfer coefficient increases with radius but at smaller aspect ratio it passes through a maximum.

NOMENCLATURE

h : local heat transfer coefficient, W/m^2deg.C.
k : thermal conductivity, W/m deg.C.
N : disc rotational speed, r.p.m.
R : radial position on disc, cm.
t : shroud set back, cm.
U : transverse air stream velocity, m/s.
ν : kinematic viscosity, m^2/s.
Re : rotational Reynolds Number, NR^2/ν.
Nu : Nusselt Number, hR/k.

1. INTRODUCTION

This work arose from an interest in the temperature distribution and the consequent stress distribution in train wheels resulting from a continued braking condition. To calculate such a temperature distribution for a new proposed wheel shape a knowledge of the surface heat transfer coefficient is necessary. The geometry under investigation, a plane rotating disc in a free air jet, is idealised from the train situation. There the wheel shape is not a plane disc and the surrounding suspension gear, the track and the ground causes considerable shrouding around the wheel. Nevertheless the present idealised geometry is an obvious starting point from which to build experience in this field.

Measurements of heat transfer from a rotating disc in still air and in an air stream normal to the disc surface have been reported. However little work seems to have been done measuring heat transfer coefficients for a rotating disc in an air stream parallel to the disc surface (herein referred to as transverse air flow).

For a disc rotating in still air, the tangential friction drag at the surface imparts a circumferential velocity to the air and, due to centrifugal forces, an outward radial flow occurs. At high disc speeds there is a transition in the resultant spiral flow from laminar to turbulent. For the laminar case analytic solutions have been produced and with suitable assumptions predictions have been made for the fully turbulent case. Comprehensive surveys of work in this field have been published by Dorfman |1| and Kreith |2|.

In the case of a rotating disc in a transverse air flow, the flow pattern is of a complex three dimensional nature giving little hope for an analytic solution at present. Thus the emphasis in this work is experimental.

The paper reports measurements of heat transfer from a heated isothermal disc rotating in still air and in a transverse air flow. To enable local heat transfer coefficients to be measured a small heat flux sensor has been used in which a thermistor provides a localised energy source. Measurements on the disc rotating in still air have been used to prove the sensor, comparison of the results being made with published data.

For the disc rotating in a transverse air flow measurements have been taken over a range of air jet speeds. Speeds both below and above the disc peripheral speed have been investigated and particular attention paid to the condition where air speed and disc peripheral speed are matched.

In reaching an understanding of the measurements further tests on the disc stationary in the transverse air stream together with flow visualisation using smoke have been useful. All the results suggest that the heat transfer process is dominated by the main air flow, the secondary flow caused by the disc rotation having a minor effect. In particular flow separation at the disc leading edge followed by reattachment to the disc face is important. The extent of the separation, reattachment zone is determined by the aspect ratio of the disc (disc radius/disc thickness). So further measurements have been made for a range of disc aspect ratios. These have been simulated using a single disc by rotating the disc within a shroud. By allowing the disc to protrude from the shroud into the transverse air stream any desired aspect ratio is set up.

2. EXPERIMENTAL ARRANGEMENT

The apparatus used consists of a heated composite disc carried overhung at one end of a shaft mounted in self aligning ball bearings. Lead wires from heaters, thermocouples and a heat transfer sensor mounted in the aluminium disc are brought out through slip rings mounted on the shaft. The shaft can be belt driven from an electric motor at a number of speeds up to 1650 r.p.m.

The structure is placed with the disc central in the neck of an open jet wind tunnel, with the disc face aligned with the direction of flow of the air jet. To avoid any vibrations which could affect the laminar - turbulent transition in the boundary layers formed on the disc the system is mechanically balanced.

2.1. The disc.

The disc is a composite structure. Two aluminium plates, 50cm diameter and 1.25cm thick sandwich electric heaters located in five annular grooves. This metal pair is made massive to even out the energy distribution from the heaters and ensure a uniform surface temperature. The back face is covered by an asbestos board to reduce heat loss from that surface, followed by a wooden backing board. The composite, 5cm thick, is clamped together by twelve bolts.

The front surface temperature is measured by seven thermocouples distributed across a diameter. The thermocouples are pushed into blind holes with the junction located just below the metal surface and pressed hard against the bottom of the hole. In practice the composite described gives a uniform surface temperature. Thermocouples located near the edge and near the centre of the disc show the largest variations from the mean of all the surface temperature values. At most this variation is four per cent of the temperature difference between the disc face and the ambient air.

The composite disc carries holes to allow mounting of a heat flux sensor in any one of seven radial positions, with the sensor face flush with the front face of the aluminium. The holes not in use are filled with dummy aluminium plugs.

2.2. The heat flux sensor.

The heat flux sensor, shown in Figure 1, is a small heated disc surrounded by a guard ring to ensure that all the measured energy input to this disc passes through the front face into the neighbouring air.

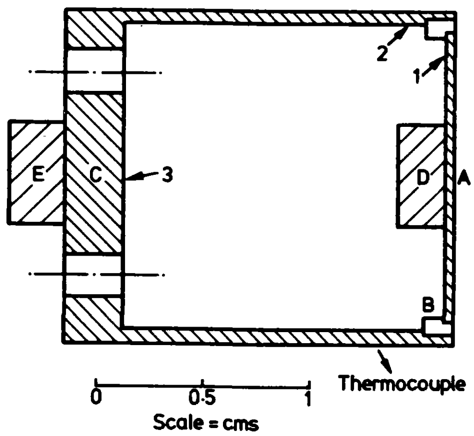

Fig. 1. HEAT FLUX SENSOR.

A thin copper disc, A, is mounted on a Tufnol washer, B, which is seated flush across the mouth of a hollow cylinder, C. Small heating elements, D,E, are attached to the undersides of A,C respectively. Disc thermistors have proved ideal for this purpose. They give uniform energy generation throughout their volume and avoid winding small heating coils. Three thermocouples are attached at the positions shown. They are used to indicate equality of temperature between the guard ring, C, and the front disc, A. The sizing of the Tufnol washer B is a compromise between mechanical strength and minimising heat loss from the disc, A, through the Tufnol to the air and surrounding metal. In measurement of heat transfer coefficient the cylindrical guard ring and the front disc are brought to the same temperature as the front face of the heated aluminium disc.

This heat flux sensor allows a determination of local heat transfer coefficient when the main disc is stationary. When the disc is rotating the time response is too slow for variations in heat transfer coefficient along the circular paths traversed to be followed. An average value is obtained. In the context of the train wheel this is appropriate for a massive train wheel can be regarded as a device with a very long time constant.

2.3. The wind tunnel.

The open jet wind tunnel gives a circular jet of 61cm diameter with air speed variable up to 33m/s. Pitot-static traverses at the tunnel mouth across both horizontal and vertical diameters show the jet to have a square profile. With the disc shaft centered on the tunnel axis, the maximum variation in air velocity from the mean velocity over the disc diameter is four per cent. Further pitot-static traverses around the disc confirm that the disc can be considered to be in a uniform air stream.

3. EXPERIMENTAL RESULTS.

3.1. Isothermal disc rotating in still air.

These tests over a range of disc speeds were carried out to provide a check on the efficiency of the heat flux sensor in measuring heat transfer coefficients by making comparisons with published data. The disc surface temperature was varied between 20 and 60 deg. C. above ambient with no effect on the measured heat transfer coefficient. The results are plotted in non dimensional form in Figure 2, physical properties being evaluated at film temperature.

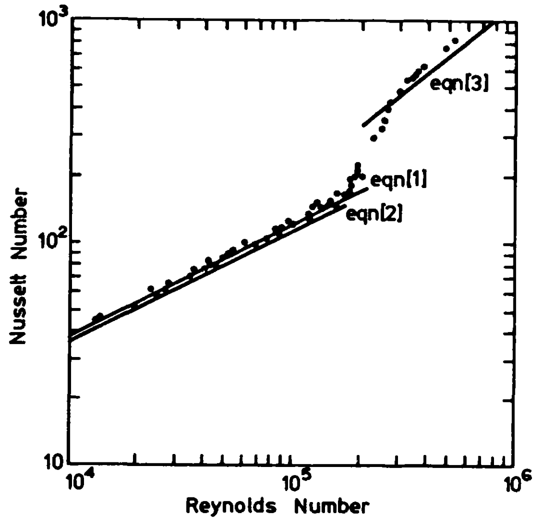

Fig.2.ROTATING DISC IN STILL AIR-DIMENSIONLESS PLOT.

The experimental data of Cobb and Saunders |3| for laminar flow is correlated by the expression

$$Nu = 0.36\ Re^{0.5} \tag{1}$$

and that of Goldstein |4| by

$$Nu = 0.38\ Re^{0.5} \tag{2}$$

Dorfman suggests that results in the turbulent region can be correlated by

$$Nu = 0.0194\ Re^{0.8} \tag{3}$$

for a Prandtl Number of 0.7.

These correlations are shown by the solid lines in Figure 2.

The present work shows good agreement with that of Goldstein although it is a few per cent higher than that of Cobb and Saunders. In the turbulent region the measured values are some ten per cent higher than the predictions of Dorfman. In view of the assumptions inherent in this prediction the agreement is considered to be reasonable. On the evidence of the information presented in Figure 2 the heat flux sensor is regarded as a viable instrument.

For a sample of speeds from the whole range of measurements Figure 3 shows how the local heat transfer coefficient varies along a radius. In the laminar region (296, 530 r.p.m.) the heat transfer coefficient is seen to be independent of radial position as predicted by theory and is evident in equations (1), (2). At higher speeds (780, 1120, 1650 r.p.m.) the radial variation shows the flow to be laminar near the centre becoming turbulent at larger radii. As the speed increases the transition point moves towards the centre.

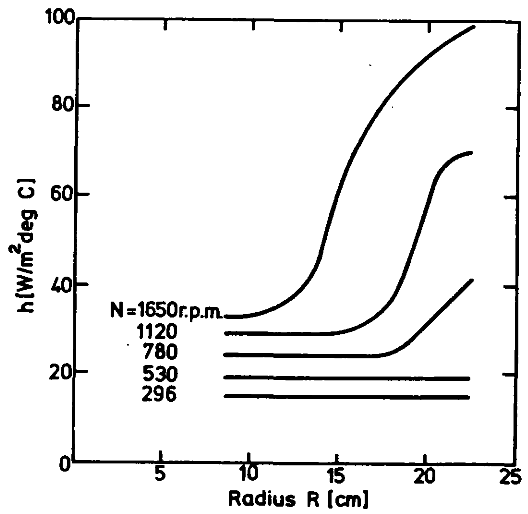

Fig.3. ROTATING DISC IN STILL AIR-RADIAL VARIATION.

3.2. Isothermal disc rotating in a transverse air stream

Considerable testing has been done over a range of disc rotational speeds from 296 to 1120 r.p.m. and at each speed for a range of main stream air speeds from 0 to 33m/s. As yet no single correlation has been ascertained that summarises all these results. To show the type of results that are obtained a selection is presented.

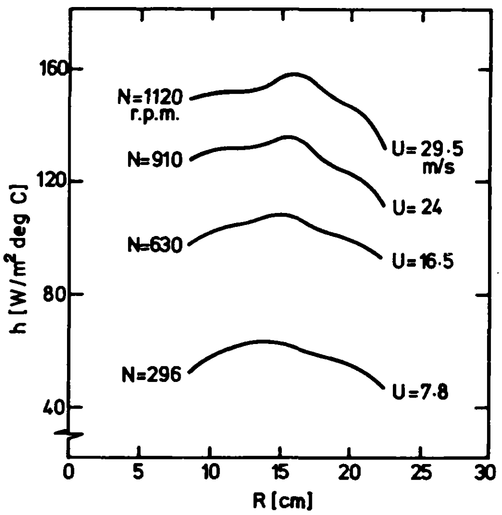

Fig. 4. ROTATING DISC IN MATCHED AIRSTREAM.

Of particular interest (from the train wheel point of view) is the condition where the air jet speed is matched to the disc peripheral speed. For this case the radial variation in heat transfer coefficient is shown in Figure 4. In Figure 5 (a) and (b) radial variations of heat transfer coefficients are shown for a selection of unmatched flows for two disc speeds.

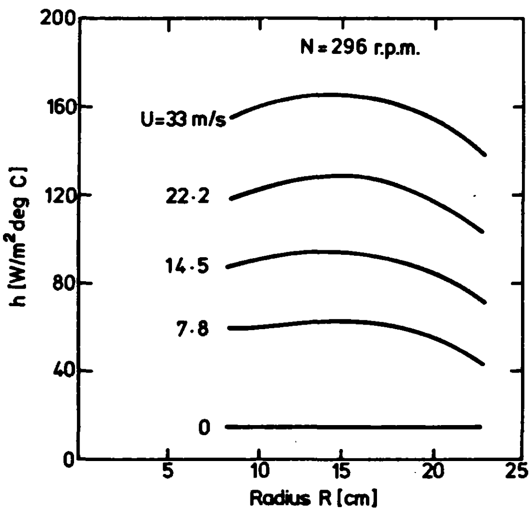

Fig. 5(a). EFFECT OF UNMATCHED AIR SPEED - DISC SPEED 296 R.P.M.

4. DISCUSSION

Two main observations can be made from the information presented.

1. The magnitude of the heat transfer coefficient is dominated by the main air stream flow. For

instance at a disc speed of 1120 r.p.m. changes in air speed from 0 to 33m/s causes some four fold increase in heat transfer coefficient (Figure 5(b)). At an air speed of 33m/s a change in disc speed from 296 to 1120 r.p.m. only causes a 10 per cent variation (Figures 5(a) and (b)).

2. The radial variation is considerably altered from the still air case. At low rotational speeds the heat transfer coefficient is no longer independent of radius but shows a peak value at approximately half radius (Figure 5(a)). At high rotational speeds the marked radial change in heat transfer coefficient due to the laminar-turbulent transition becomes smoothed out (Figure 5(b)). This set of curves again demonstrates how the flow regime and hence the heat transfer process rapidly becomes dominated by the main stream flow rather than the secondary rotational flow.

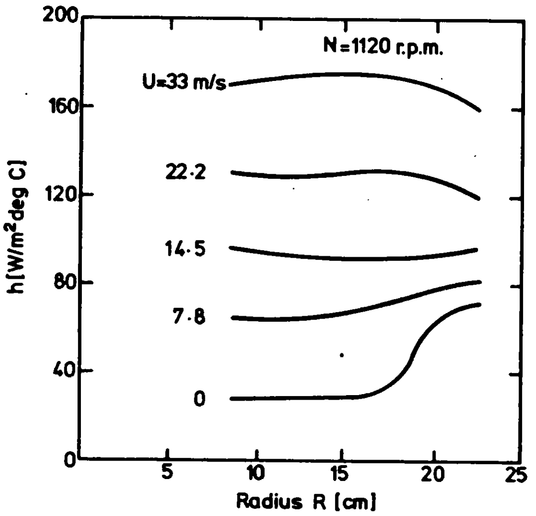

Fig. 5(b). EFFECT OF UNMATCHED AIR SPEED - DISC SPEED 1120 R.P.M.

To strengthen this view of main stream dominance a series of tests were made with the disc stationary in the transverse air flow. The sensor, when rotating, gives an average heat transfer coefficient over the circular path traversed. For the stationary disc local heat transfer coefficients were measured at each radial position for five different angular positions, 0, 45, 90, 135, 180 degrees, 0 corresponding to the leading edge of the disc on the centre line of the tunnel. Since in this case the flow is symmetrical above and below the tunnel centre line it was assumed that similar values hold for the bottom half of the disc. At each radius a straight average of the eight values obtained was computed. These average values are shown in Figure 6 in comparison with curves taken from Figure 4. This gives added weight to the view that the level of the heat transfer coefficient is determined by the main flow with the rotation having a small second order effect.

Flow visualisation using smoke shows that the flow separates from the disc face at the leading edge and reattaches to the disc face further downstream. At a given air speed the details of this separation/reattachment process are unaffected by the disc rotational speed. A low heat transfer coefficient is to be expected in the separated region. A high value is expected at the reattachment point followed by a slow fall off as the flow moves over the face in much the manner of the heat transfer variation in the starting length of flow over a heated flat plate. The local heat transfer coefficients taken across the 0 - 180° diameter and lines parallel to it confirm this picture.

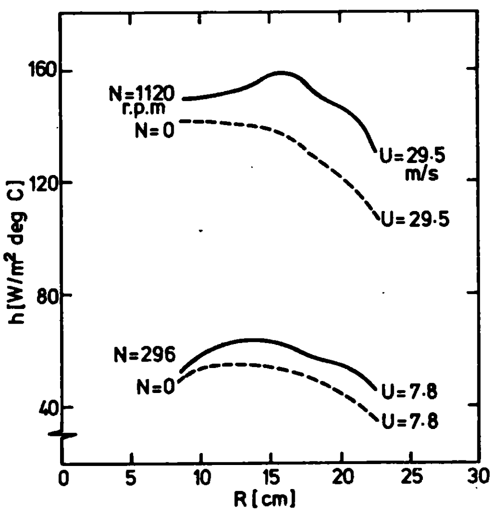

Fig. 6. EFFECT OF DISC ROTATION.

This flow separation and reattachment explains the maximum observed in the radial heat transfer coefficients shown in Figure 5. The sensor gives an average value over the path it traverses. At the outer radius a large proportion of that path lies in the low heat transfer separation region. At a medium radial position a large proportion of the path lies in the first part of the reattachment with consequent high heat transfer.

5. EFFECT OF ASPECT RATIO

In section 4 the radial variation of heat transfer coefficient is explained in terms of flow separation and reattachment. The experimental disc is a bluff body and the degree of separation is dependent on its aspect ratio. To use the existing disc to simulate larger aspect ratios an annular shroud of triangular cross section was held just upstream of the front half of the disc. This shroud could be positioned at any point across the width of the disc, the configuration being shown in Figure 7.

The whole range of tests was repeated for a number of positions of the shroud. Figure 7 also shows the radial heat transfer variations for one disc speed and the matched air speed. This set is typical.

At very large effective aspect ratios (very little separation) the picture is consistent with the starting length for flow over a flat plate. Remembering the heat transfer coefficient is an average value over the path traversed, at large radii a large proportion of the path lies in the region of very high heat transfer coefficient. Coming into the centre more and more of the path lies in the region of lower, more slowly varying heat transfer coefficient. Thus the steady increase in heat transfer coefficient with radius. As the effective aspect ratio is decreased the radial pattern gradually changes, as the separation region grows, to the peaked distribution discussed in section 4.

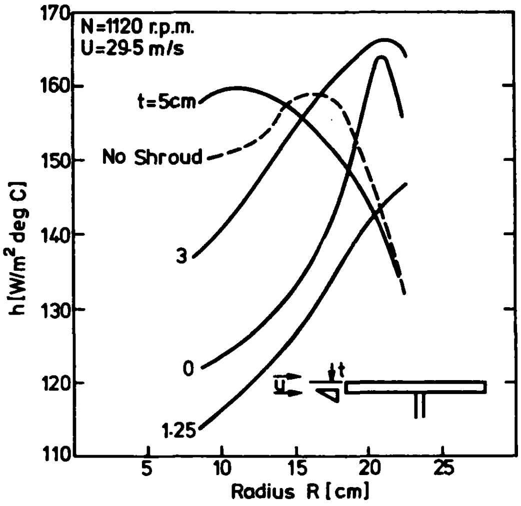

Fig. 7. EFFECT OF VARYING ASPECT RATIO.

Figure 8 shows the variation in heat transfer coefficient across the 0 - 180° diameter of the disc when held stationary in the transverse air flow, with and without the shroud. This confirms the view of the "starting length variation" moving across the face of the disc, preceded by a region of lower heat transfer, as the aspect ratio decreases.

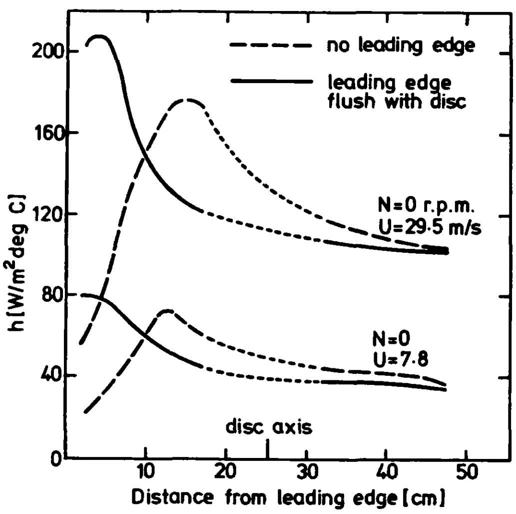

Fig.8.HEAT TRANSFER ACROSS FACE OF STATIONARY DISC.

Smoke flow visualisation tests indicate that the shroud is a fair simulation of discs of varying aspect ratio. However with the face of the shroud flush with the front face of the disc there is a small separation zone. Complete attachment of the flow over the whole of the disc face occurs when the shroud is set back 1.25cm. This accounts for the initial drop in heat transfer coefficients as the set back increases from zero.

6. CONCLUSIONS

From a comprehensive set of measurements of the radial variation of heat transfer coefficients for a disc rotating in a transverse air stream two dominant conclusions emerge.

1. In any situation the level of the heat transfer coefficient is determined in the main by the speed of the transverse air flow. The rotation of the disc results in a small upward perturbation on this level.

2. The aspect ratio of the disc greatly modifies the radial distribution of the heat transfer coefficient, but again the main airstream speed is dominant in determining the level of the heat transfer coefficient.

REFERENCES

|1| Dorfman, L.A. : "Hydrodynamic Resistance and the Heat Loss of Rotating Solids". (Transl. by N. Kemmer). Oliver and Boyd, Edinburgh and London, (1963)

|2| Kreith, F. : "Advances in Heat Transfer", 5, 129, (1968)

|3| Cobb, E.C. and Saunders, O.A. Proc. Roy. Soc. A., 236, 343, (1956)

|4| Goldstein, S. Proc. Cambridge Phil. Soc., 31, 232, (1935)

ACKNOWLEDGEMENTS

The authors wish to thank the Department of Engineering, University of Leicester, for providing the facilities which made this work possible.

Mr. de Vere is in receipt of a studentship from the Science Research Council.